2015

Design and Validation of a Prototype Collimation System with Reduced Applicator Weights for Elekta Electron Therapy Beams

Garrett Michael Pitcher
Louisiana State University and Agricultural and Mechanical College, garrettp17@gmail.com

DESIGN AND VALIDATION OF A PROTOTYPE COLLIMATION SYSTEM WITH REDUCED APPLICATOR WEIGHTS FOR ELEKTA ELECTRON THERAPY BEAMS

A Dissertation

Submitted to the Graduate Faculty of the
Louisiana State University and
Agricultural and Mechanical College
in partial fulfillment of the
requirements for the degree of
Doctor of Philosophy

in

The Department of Physics and Astronomy

by
Garrett Michael Pitcher
B.S., University of Tennessee, 2008
M.S., University of Tennessee, 2009
December 2015

Acknowledgements

I acknowledge my supervisory committee members, Drs. Kenneth Hogstrom, Bobby Carver, Wayne Newhauser, and William Metcalf, for their advisement throughout my project. In particular, I thank Dr. Hogstrom for his invaluable expertise, insight, and guidance, without whose help, I could not have completed my work, and Dr. Carver for his assistance in MC calculations and other technical problems throughout my project. I express my appreciation to Susan Hammond for her administrative assistance in navigating the deadlines and requirements of completing my degree. I also thank Mary Bird Perkins Cancer Center and its clinical staff for providing resources, facilities, and instruction during my investigations.

I am extremely grateful for my family and friends, particularly my mother and father for their support throughout my time in Baton Rouge and before. Lastly, and most importantly, I thank my wife, Maria, whose reassurance, understanding, and encouragement sustained me through the most difficult times of my work.

This research was funded in part through a research agreement with Elekta Limited, who also provided applicators, technical information, and accelerator support necessary to complete the project. Portions of this research were conducted with high-performance computational resources provided by Louisiana State University (http://www.hpc.lsu.edu). Lastly, thanks to Vincent Vaughn of the Physics machine shop for the fabrication of the prototype applicators.

Table of Contents

Acknowledgements ii

List of Tables vii

List of Figures ix

Abstract xx

Chapter 1 - Introduction 1
1.1. Background and Significance 1
1.1.1. Fundamental Properties and Advantages of Electron Therapy 1
1.1.2. Purposes of Accelerator Head and Collimation System 3
1.1.3. Dose Components to Account for in Collimation Design 7
1.1.4. Previous Work on Collimation Design Issues 8
1.1.5. Electron Collimation System Acceptance Criteria 9
1.2. Purpose of Study 12
1.2.1. Elekta Infinity Electron Collimation System Design Description and Potential Areas for Enhancement 12
1.2.2. Purpose and Description of Investigation 19
1.3. Hypothesis 20
1.4. Specific Aims 20
1.4.1. Aim 1 - Evaluation of the Current Collimation Design and MC Model Using Measurement 20
1.4.2. Aim 2 - Develop and Validate an Analytical Radiation Transport Code for Optimizing Trimmer Design 20
1.4.3. Aim 3 - Perform Material and Range Analysis to Determine the Best Trimmer Material and Thickness 21
1.4.4. Aim 4 - Determine Inner Edge Divergence Angles for Each Trimmer 21
1.4.5. Aim 5 - Determine Optimal Applicator Geometry 21
1.4.6. Aim 6 - Construct Prototype Applicators and Evaluate Prototype Collimating System 21

Chapter 2 - Aim 1 - Evaluation of the Current Collimation Design and MC Model Using Measurement 22
2.1. Aim 1 - Introduction 22
2.2. Aim 1 - Methods 23
2.2.1. Measurements 23
2.2.2. Monte Carlo Model of Elekta Infinity 29
2.3. Aim 1 - Results and Discussion 33
2.3.1. Quality of Measured Data 33
2.3.2. In-Field Results 34
2.3.3. Out-of-Field Results 40
2.3.4. Leakage Dose Component Analysis 47
2.4. Aim 1 - Conclusions 53

Chapter 3 - Aim 2 - Develop and Validate an Analytical Radiation Transport Code for Optimizing Trimmer Designs 55
3.1. Aim 2 - Introduction 55
3.2. Aim 2 - Methods 57

3.2.1. Analytical Model 57
3.2.2. MC Simulations for Model Evaluation 69
3.3. Aim 2 - Results and Discussion 71
3.3.1. Comparison of Analytical Primary Electron Model with MC 71
3.3.2. Comparison of Analytical Photon Model with MC 77
3.4. Aim 2 - Conclusions 79

Chapter 4 - Aim 3 - Perform Material and Range Analysis to Determine the Best Trimmer Material and Thickness 81
4.1. Aim 3 - Introduction 81
4.2. Aim 3 - Methods 83
4.2.1. Determination of Energy-Range Relation 83
4.2.2. Effects of Trimmer Material on Leakage Dose 88
4.3. Aim 3 - Results and Discussion 90
4.3.1. Determination of Energy-Range Relation 90
4.3.2. Effects of Trimmer Material on Leakage Dose 92
4.4. Aim 3 - Conclusions 96
4.4.1. Determination of Energy-Range Relation Equation 96
4.4.2. Effects of Trimmer Material on Leakage Dose 97

Chapter 5 - Aim 4 - Determine Inner Edge Divergence Angles for Each Trimmer 98
5.1. Aim 4 - Introduction 98
5.2. Aim 4 - Methods 99
5.3. Aim 4 - Results and Discussion 102
5.4. Aim 4 - Conclusions 107

Chapter 6 - Aim 5 - Determine Optimal Applicator Geometry 108
6.1. Aim 5 - Introduction 108
6.2. Aim 5 - Design Step 1 - Initial Collimation System Design 109
6.2.1. Methods 109
6.2.2. Results and Discussion 114
6.3. Aim 5 - Design Step 2 - Specify Applicator Field Size at Isocenter 114
6.3.1. Methods 117
6.3.2. Results and Discussion 117
6.4. Aim 5 - Design Step 3 - Beveling Outer Trimmer Edges 118
6.4.1. Methods 118
6.4.2. Results and Discussion 120
6.5. Aim 5 - Design Step 4 - Optimization of Upper and Middle Trimmer *z*-Positions 120
6.5.1. Methods 121
6.5.2. Results and Discussion 121
6.6. Aim 5 - Design Step 5 - Inner Trimmer Edge Fluence Matching OAR Determination 122
6.6.1. Methods 123
6.6.2. Results and Discussion 127
6.7. Aim 5 - Design Step 6 - Jaw Position Variation with Beam Energy 132
6.7.1. Methods 133
6.7.2. Results and Discussion 137
6.8. Aim 5 - Design Step 7 - Trimmer Thickness and Outer Bevel Shape Adjustments 143
6.8.1. Methods 144
6.8.2. Results and Discussion 148
6.9. Aim 5 - Evaluation of Final Design 153
6.9.1. Methods 153

6.9.2. Results and Discussion 153
6.10. Aim 5 - Summary and Conclusions 157
6.10.1. Summary of Weight Reduction in Design Process 157
6.10.2. Conclusions 158

Chapter 7 - Aim 6 - Construct Prototype Applicator and Evaluate Prototype Collimating System 159
7.1. Aim 6 - Introduction 159
7.2. Aim 6 - Methods 160
7.2.1. Trimmer Modifications for Fabrication 160
7.2.2. Evaluation of Prototype Collimation System 164
7.2.3. Lateral Leakage Analysis 167
7.2.4. Jaw Position Error Analysis 168
7.3. Aim 6 - Results and Discussion 169
7.3.1. Fabricated Applicator 169
7.3.2. Evaluation of Prototype Collimation System 175
7.3.3. Lateral Leakage Analysis 186
7.3.4. Jaw Position Error Analysis 189
7.4. Aim 6 - Conclusions 195

Chapter 8 - Summary of Results and Conclusions 197
8.1. Introduction 197
8.1.1. Purpose 197
8.1.2. Hypothesis 197
8.1.3. Approach 197
8.2. Aim 1 - Evaluation of the Current Collimation Design and MC Model Using Measurement 198
8.2.1. Summary of Results 198
8.2.2. Conclusions 199
8.3. Aim 2 - Develop and Validate an Analytical Radiation Transport Code for Optimizing Trimmer Design 200
8.3.1. Summary of Results 200
8.3.2. Conclusions 201
8.4. Aim 3 - Perform Material and Range Analysis to Determine the Best Trimmer Material and Thickness 202
8.4.1. Summary of Results 202
8.4.2. Conclusions 203
8.5. Aim 4 - Determine Inner Edge Divergence Angles for Each Trimmer 203
8.5.1. Summary of Results 203
8.5.2. Conclusions 204
8.6. Aim 5 - Determine Optimal Applicator Geometry 204
8.6.1. Summary of Results 204
8.6.2. Conclusions 206
8.7. Aim 6 - Construct Prototype Applicator and Evaluate Prototype Collimating System 206
8.7.1. Summary of Results 206
8.7.2. Conclusions 207
8.8. Overall Conclusions and Recommendations for Future Work 208
8.8.1. Response to Hypothesis 208
8.8.2. Recommendations for New Electron Collimation System 208
8.8.3. Recommendations for Additional Physics Studies 209

References 212

Appendix A - Supplemental Figures for Aim 2 216

Appendix B - Supplemental Figures for Aim 3 225

Appendix C - Supplemental Figures for Aim 5 231

Appendix D - Supplemental Figures for Aim 6 235

Appendix E - Prototype Applicator Dimensions and Images 241
E.1. 10x10 cm^2 Applicator 241
E.1.1. Full Applicator 241
E.1.2. Upper Trimmer - Lead 242
E.1.3. Middle Trimmer - Lead 245
E.1.4. Lower Trimmer - Lead 248
E.1.5. Upper Trimmer - Aluminum 251
E.1.6. Middle Trimmer - Aluminum 254
E.1.7. Lower Trimmer - Aluminum 256
E.1.8. Aluminum Spacer Tubers 259
E.2. 20x20 cm^2 Applicator 261
E.2.1. Full Applicator 261
E.2.2. Upper Trimmer - Lead 262
E.2.3. Middle Trimmer - Lead 265
E.2.4. Lower Trimmer - Lead 269
E.2.5. Upper Trimmer - Aluminum 272
E.2.6. Middle Trimmer - Aluminum 274
E.2.7. Lower Trimmer - Aluminum 277
E.2.8. Aluminum Spacer Tubers 279

Vita 281

List of Tables

Table 1-1. Applicator weights for the Elekta Infinity and Varian 21EX accelerators 16

Table 2-1. Beam characteristics and machine settings for each nominal beam energy available on the MBPCC Elekta Infinity accelerator used in this study. 26

Table 2-2. Number of measurement scans performed for each profile on each day. 28

Table 2-3. Incident particle energy spectra used for BEAMnrc MC calculations 31

Table 2-4. MC calculated minus measured percent dose differences calculated at the edge of the uniformity region. 39

Table 2-5. Minimum and maximum differences of the MC-calculated minus measured relative dose for each off-axis profile in the leakage region 45

Table 2-6. Mean percent leakage doses calculated per IEC specifications for MC-calculated and measured off-axis profiles 46

Table 2-7. Maximum percent leakage doses calculated per IEC specifications for MC-calculated and measured off-axis profiles. 46

Table 2-8. Contributions to mean leakage dose for the 20x20 cm^2 applicator. 53

Table 4-1. Full trimmer thicknesses as calculated by each range-energy relation method. 91

Table 4-2. Mean percent leakage for each dose component for each applicator material. 94

Table 5-1. Mean percent leakage dose calculated per IEC specifications for 20x20 cm^2 applicators designed with varying inner trimmer edge divergence angles at 7, 13, and 20 MeV. 106

Table 6-1. Example of potential upper and lower boundaries and grid step sizes of each of the five parameters for each of the three iterations of the search grid optimization 124

Table 6-2. Fluence matching OARs for the inner edges of each trimmer of each 10x10 and 20x20 cm^2 applicator modeled for the MC inner edge adjustment analysis. 126

Table 6-3. Results of jaw position variation with beam energy analysis. 141

Table 6-4. Results of the trimmer thickness reduction and bevel shape analyses. 150

Table 6-5. Summary of design progression and weight reduction results. 157

Table 7-1. Trimmer inner edge fluence matching OARs for the design of each prototype applicator 165

Table 7-2. Weight comparison of prototype applicators with current clinical Elekta and Varian applicators. 170

Table 7-3. Mean and maximum percent leakage dose for the MC-calculated and measured dose distributions for the nominal 7, 13, and 20 MeV beams with the prototype collimation system. 184

Table 7-4. Comparison of mean and maximum percent leakage doses of the prototype applicators with the current clinical Elekta applicators for both the MC-calculated and measured dose distributions..... 186

Table 7-5. Mean percent leakage dose values for each 20x20 cm^2 collimation system modeled in the jaw position error analysis for the 7, 13, and 20 MeV beams. 194

List of Figures

Figure 1-1. PDD for a 13 MeV electron beam measured in water. 1

Figure 1-2. Depth dose curves in water for each nominal beam energy available on the Elekta Infinity linear accelerator. 2

Figure 1-3. Cross-sectional view of the Elekta Infinity treatment head (MLCi2) components and electron applicator 5

Figure 1-4. The five electron applicators of the Elekta Infinity accelerator. 6

Figure 1-5. Elekta Infinity accelerator with the 14x14 cm^2 applicator attached to the treatment head 6

Figure 1-6. IEC specified geometry for measurements to obtain mean and maximum leakage in the patient plane. 11

Figure 1-7. Beam flatness specifications within the field along the major axes. 13

Figure 1-8. Comparison of the current clinical Elekta and Varian applicator designs for the 10x10 and 20x20 cm^2 sizes. 15

Figure 1-9. Comparison of photon and electron treatment setup causing ODI light beam to be blocked by the applicator 17

Figure 1-10. Attachment plate of the Elekta Infinity accelerator with the prongs, alignment pin, and latch labelled. 18

Figure 1-11. Comparison of the latching attachment mechanism used by Elekta with the sliding mechanism used by Varian. 19

Figure 2-1. Cross-plane cross sectional view of the Elekta Infinity (MLCi2) accelerator modeled in BEAMnrc. 24

Figure 2-2. Comparison of measured and MC calculated major axes profiles of relative dose versus off-axis position in the field for the 20x20 cm^2 applicator. 35

Figure 2-3. Comparison of measured and MC calculated major axes profiles of relative dose versus off-axis position in the field for the 10x10 cm^2 applicator. 36

Figure 2-4. Comparison of measured and MC calculated diagonal profiles of relative dose versus off-axis position in the field for the 20x20 cm^2 applicator. 37

Figure 2-5. Comparison of measured and MC calculated diagonal profiles of relative dose versus off-axis position in the field for the 10x10 cm^2 applicator. 38

Figure 2-6. Comparison of measured and MC calculated major axes profiles of relative dose versus off-axis position in the out-of-field region for the 20x20 cm^2 applicator. 41

Figure 2-7. Comparison of measured and MC calculated major axes profiles of relative dose versus off-axis position in the out-of-field region for the 10x10 cm^2 applicator. 42

Figure 2-8. Comparison of measured and MC calculated major axes profiles of relative dose versus off-axis position in the out-of-field region for the 20x20 cm^2 applicator. 43

Figure 2-9. Comparison of measured and MC calculated major axes profiles of relative dose versus off-axis position in the out-of-field region for the 10x10 cm^2 applicator. 44

Figure 2-10. Cross-plane leakage dose component profiles for the 20x20 cm^2 applicator. 49

Figure 2-11. In-plane leakage dose component profiles for the 20x20 cm^2 applicator 50

Figure 2-12. Effects of jaw position on collimator scatter. 52

Figure 3-1. Propagation of the primary electron fluence to the subsequent calculation planes. 61

Figure 3-2. Electron pencil-beam fluence propagation and depiction of terms for the primary electron model. 63

Figure 3-3. Photon ray tracing and attenuation within the collimation system. 67

Figure 3-4. Full cross-plane primary electron dose profile comparisons of analytical and MC calculations for the 20x20 cm^2 applicator with a monoenergetic 7 MeV beam. 72

Figure 3-5. Cross-plane primary electron dose profile comparisons of analytical and MC calculations for the 20x20 cm^2 applicator with a monoenergetic 7 MeV beam in the penumbral fall-off region. 73

Figure 3-6. Cross-plane primary electron dose profile comparisons of analytical and MC calculations for the 20x20 cm^2 applicator with a monoenergetic 7 MeV beam in the low dose leakage region 74

Figure 3-7. Comparison of MC and analytically calculated bremsstrahlung profiles. 78

Figure 4-1. Linear fit of lead thickness required to stop electron beams as a function of beam energy. 84

Figure 4-2. Beam's-eye view of metal slab divided into 25 subsections of different thicknesses for MC calculations. 86

Figure 4-3. Comparison of relative dose calculated versus material thickness in the low dose region. 87

Figure 4-4. Comparison of methods for determining the energy-range relation for each material. 90

Figure 4-5. Cross-plane leakage dose component profiles for copper, lead and tungsten 20x20 cm^2 applicators for the 20 MeV beam. 93

Figure 5-1. Depiction of trimmer inner edge angled to be fully-divergent, semi-divergent, or non-divergent. 100

Figure 5-2. Leakage dose component profiles plotted versus off-axis position for 20x20 cm^2 applicators designed with non-divergent, semi-divergent, and fully-divergent inner edges for the 7 MeV beam. 103

Figure 5-3. Leakage dose component profiles plotted versus off-axis position for 20x20 cm^2 applicators designed with non-divergent, semi-divergent, and fully-divergent inner edges for the 13 MeV beam. 104

Figure 5-4. Leakage dose component profiles plotted versus off-axis position for 20x20 cm^2 applicators designed with non-divergent, semi-divergent, and fully-divergent inner edges for the 20 MeV beam. 105

Figure 6-1. Schematic illustrating the basis for designing location of inner and outer edges of downstream trimmer. 112

Figure 6-2. Schematic cross sectional view of the right half of the collimation system 113

Figure 6-3. In-plane cross sectional view of the design progression of the 10x10 cm^2 applicator trimmers in Design Steps 1 through 4. 115

Figure 6-4. In-plane cross sectional view of the design progression of the 20x20 cm^2 applicator trimmers in Design Steps 1 through 4. 116

Figure 6-5. Bevel shape calculation method for outer trimmer edge. 119

Figure 6-6. Cross sectional view of trimmer with outer edge bevel. 120

Figure 6-7. Calculated isomass plots applicators as a function of middle and upper trimmer *z*-positions optimization results. 122

Figure 6-8. In-plane cross sectional view of the design progression of the 10x10 cm^2 applicator trimmers in Design Steps 4 and 5. 128

Figure 6-9. In-plane cross sectional view of the design progression of the 20x20 cm^2 applicator trimmers in Design Steps 4 and 5. 129

Figure 6-10. In-field off-axis dose profiles for the analysis to determine the inner trimmer edge positions. 131

Figure 6-11. Effect of jaw position adjustments for high energy beams on the upper trimmer shape 135

Figure 6-12. In-field diagonal dose profiles for the analysis of jaw position dependence on energy. 138

Figure 6-13. Cross-plane total dose profiles plotted versus off-axis position in the leakage region for the analysis of jaw position variation with beam energy. 140

Figure 6-14. Cross-plane leakage component profiles for analysis of jaw position variation with beam energy. 142

Figure 6-15. Effect of thickness reduction on trimmer cross sectional shape 145

Figure 6-16. Effect of bevel shape adjustment on trimmer cross sectional shape. 147

Figure 6-17. 20 MeV cross-plane leakage dose profiles plotted versus off-axis position for the trimmer thickness reduction and bevel shape analyses. 149

Figure 6-18. Mean percent leakage dose plotted versus applicator weight for the applicator designs produced in the trimmer thickness reduction and bevel shape analyses. 151

Figure 6-19. In-field diagonal dose profiles plotted versus off-axis position for the selected 10x10 and 20x20 cm^2 collimation designs. 154

Figure 6-20. Leakage dose profiles plotted versus off-axis position for the selected 10x10 and 20x20 cm^2 collimation designs. 156

Figure 7-1. Cross sectional view of a trimmer designed with modifications for fabrication. 162

Figure 7-2. Fabricated 10x10 cm^2 applicator prototype. 163

Figure 7-3. Fabricated 20x20 cm^2 applicator prototype. 164

Figure 7-4. Cross sectional views of the prototype and current clinical Elekta 10x10 cm^2 applicator models. 171

Figure 7-5. Cross sectional views of the prototype and current clinical Elekta 20x20 cm^2 applicator models. 172

Figure 7-6. Jaw position comparison for the prototype and current Elekta collimation systems for all beam energies. 174

Figure 7-7. Comparison of measured and MC calculated in-plane profiles of relative dose versus off-axis position in the field. 176

Figure 7-8. Comparison of measured and MC calculated cross-plane profiles of relative dose versus off-axis position in the field. 177

Figure 7-9. Comparison of measured and MC calculated diagonal profiles of relative dose versus off-axis position in the field. 178

Figure 7-10. Comparison of measured and MC-calculated major axes relative dose profiles versus off-axis position outside the field for the prototype 10x10 cm^2 applicator. 180

Figure 7-11. Comparison of measured and MC-calculated major axes relative dose profiles versus off-axis position outside the field for the prototype 20x20 cm^2 applicator. 181

Figure 7-12. Comparison of measured and MC-calculated diagonal relative dose profiles versus off-axis position outside the field for the prototype 10x10 cm^2 applicator. 182

Figure 7-13. Comparison of measured and MC-calculated diagonal relative dose profiles versus off-axis position outside the field for the prototype 20x20 cm^2 applicator. 183

Figure 7-14. Leakage dose profiles MC-calculated at various *z*-positions along the side of the 10x10 cm^2 prototype applicators. 187

Figure 7-15. Leakage dose profiles MC-calculated at various *z*-positions along the side of the 20x20 cm^2 prototype applicators. 188

Figure 7-16. Profiles of MC-calculated relative dose versus off-axis position for the 7 MeV beam, 20x20 cm^2 prototype applicator. 190

Figure 7-17. Profiles of MC-calculated relative dose versus off-axis position for the 13 MeV beam, 20x20 cm^2 prototype applicator. 191

Figure 7-18. Profiles of MC-calculated relative dose versus off-axis position for the 20 MeV beam, 20x20 cm^2 prototype applicator. 192

Figure A-1. Full in-plane primary electron dose profile comparisons of analytical and MC calculations for the 20x20 cm^2 applicator with a monoenergetic 7 MeV beam. 216

Figure A-2. In-plane primary electron dose profile comparisons of analytical and MC calculations for the 20x20 cm^2 applicator with a monoenergetic 7 MeV beam in the penumbral fall-off region. 217

Figure A-3. In-plane primary electron dose profile comparisons of analytical and MC calculations for the 20x20 cm^2 applicator with a monoenergetic 7 MeV beam in the low dose leakage region 218

Figure A-4. Full cross-plane primary electron dose profile comparisons of analytical and MC calculations for the 10x10 cm^2 applicator with a monoenergetic 7 MeV beam. 219

Figure A-5. Cross-plane primary electron dose profile comparisons of analytical and MC calculations for the 10x10 cm^2 applicator with a monoenergetic 7 MeV beam in the penumbral fall-off region. 220

Figure A-6. Cross-plane primary electron dose profile comparisons of analytical and MC calculations for the 10x10 cm^2 applicator with a monoenergetic 7 MeV beam in the low dose leakage region 221

Figure A-7. Full in-plane primary electron dose profile comparisons of analytical and MC calculations for the 10x10 cm^2 applicator with a monoenergetic 7 MeV beam. 222

Figure A-8. In-plane primary electron dose profile comparisons of analytical and MC calculations for the 10x10 cm^2 applicator with a monoenergetic 7 MeV beam in the penumbral fall-off region. 223

Figure A-9. In-plane primary electron dose profile comparisons of analytical and MC calculations for the 10x10 cm^2 applicator with a monoenergetic 7 MeV beam in the low dose leakage region. 224

Figure B-1. Comparison of calculated relative dose (% of D_{max}) versus material thickness in the low dose region. 225

Figure B-2. Cross-plane leakage dose component profiles for copper, lead and tungsten 20x20 cm^2 applicators for the 7 MeV beam. 226

Figure B-3. Cross-plane leakage dose component profiles for copper, lead and tungsten 20x20 cm^2 applicators for the 13 MeV beam. 227

Figure B-4. In-plane leakage dose component profiles for copper, lead and tungsten 20x20 cm^2 applicators for the 7 MeV beam. 228

Figure B-5. In-plane leakage dose component profiles for copper, lead and tungsten 20x20 cm^2 applicators for the 13 MeV beam. 229

Figure B-6. In-plane leakage dose component profiles for copper, lead and tungsten 20x20 cm^2 applicators for the 20 MeV beam. 230

Figure C-1. In-plane total dose profiles plotted versus off-axis position in the leakage region for the analysis of jaw position variation with beam energy. 231

Figure C-2. In-plane leakage component profiles for analysis of jaw position variation with beam energy. 232

Figure C-3. In-field in-plane and cross-plane dose profiles plotted verses off-axis position for the selected 10x10 cm^2 collimation design. 233

Figure C-4. In-field in-plane and cross-plane dose profiles plotted verses off-axis position for the selected 20x20 cm^2 collimation design. 234

Figure D-1. Cross sectional views of the prototype and current clinical Elekta 6x6 cm^2 applicator models. 235

Figure D-2. Cross sectional views of the prototype and current clinical Elekta 14x14 cm^2 applicator models. 236

Figure D-3. Cross sectional views of the prototype and current clinical Elekta 25x25 cm^2 applicator models. 237

Figure D-4. MC calculated dose profiles plotted versus off-axis position for the prototype 6x6 cm^2 applicator. 238

Figure D-5. MC calculated dose profiles plotted versus off-axis position for the prototype 14x14 cm^2 applicator. 239

Figure D-6. MC calculated dose profiles plotted versus off-axis position for the prototype 25x25 cm^2 applicator. 240

Figure E-1. Orthogonal view of the full 10x10 cm^2 applicator. 241

Figure E-2. Top orthogonal view of the 10x10 cm^2 upper trimmer lead plate. 242

Figure E-3. Bottom orthogonal view of the 10x10 cm^2 upper trimmer lead plate. 242

Figure E-4. Top view of the 10x10 cm^2 upper trimmer lead plate illustrating the cross-plane dimensions. 242

Figure E-5. Top view of the 10x10 cm^2 upper trimmer lead plate illustrating the in-plane dimensions. 243

Figure E-6. Cross sectional view of the 10x10 cm^2 upper trimmer lead plate in the in-plane dimension illustrating the lateral dimensions of the plate. 243

Figure E-7. Cross sectional view of the 10x10 cm^2 upper trimmer lead plate in the in-plane dimension illustrating the thickness values of the plate. 243

Figure E-8. Cross sectional view of the 10x10 cm^2 upper trimmer lead plate in the cross-plane dimension illustrating the lateral dimensions of the plate. 244

Figure E-9. Cross sectional view of the 10x10 cm^2 upper trimmer lead plate in the cross-plane dimension illustrating the thickness values of the plate. 244

Figure E-10. Orthogonal view of the 10x10 cm^2 upper trimmer lead plate illustrating hole dimensions. 244

Figure E-11. Top orthogonal view of the 10x10 cm^2 middle trimmer lead plate. 245

Figure E-12. Bottom orthogonal view of the 10x10 cm^2 middle trimmer lead plate. 245

Figure E-13. Top view of the 10x10 cm^2 middle trimmer lead plate illustrating the in-plane and cross-plane dimensions. 246

Figure E-14. Cross sectional view of the 10x10 cm^2 middle trimmer lead plate illustrating the in-plane and cross-plane lateral dimensions of the plate. 247

Figure E-15. Cross sectional view of the 10x10 cm^2 middle trimmer lead plate illustrating the thickness values of the plate. 247

Figure E-16. Orthogonal view of the 10x10 cm^2 middle trimmer lead plate illustrating hole dimensions. 247

Figure E-17. Top orthogonal view of the 10x10 cm^2 lower trimmer lead plate. 248

Figure E-18. Bottom orthogonal view of the 10x10 cm^2 lower trimmer lead plate. 248

Figure E-19. Top view of the 10x10 cm^2 lower trimmer lead plate illustrating the in-plane and cross-plane dimensions. 249

Figure E-20. Cross sectional view of the 10x10 cm^2 lower trimmer lead plate illustrating the in-plane and cross-plane lateral dimensions of the plate. 250

Figure E-21. Cross sectional view of the 10x10 cm^2 lower trimmer lead plate in the cross-plane dimension illustrating the thickness values of the plate. 250

Figure E-22. Orthogonal view of the 10x10 cm^2 lower trimmer lead plate illustrating hole dimensions. 250

Figure E-23. Top orthogonal view of the 10x10 cm^2 upper trimmer aluminum plate. 251

Figure E-24. Bottom orthogonal view of the 10x10 cm^2 upper trimmer aluminum plate. 251

Figure E-25. Top view of the 10x10 cm^2 upper trimmer aluminum plate illustrating the in-plane and cross-plane dimensions. 252

Figure E-26. Cross sectional view of the 10x10 cm^2 upper trimmer aluminum plate in the cross-plane dimension illustrating the thickness and lateral dimensions of the plate. 252

Figure E-27. Cross sectional view of the 10x10 cm^2 upper trimmer aluminum plate in the in-plane dimension illustrating the thickness and lateral dimensions of the plate. 253

Figure E-28. Orthogonal view of the 10x10 cm^2 upper trimmer aluminum plate illustrating hole dimensions. 253

Figure E-29. Top view of the 10x10 cm^2 upper trimmer aluminum plate illustrating hole dimensions. 253

Figure E-30. Orthogonal view of the 10x10 cm^2 middle trimmer aluminum plate. 254

Figure E-31. Top view of the 10x10 cm^2 middle trimmer aluminum plate illustrating the in-plane and cross-plane dimensions. 254

Figure E-32. Cross sectional view of the 10x10 cm^2 middle trimmer aluminum plate illustrating the thickness and lateral in-plane and cross-plane dimensions of the plate. 255

Figure E-33. Orthogonal view of the 10x10 cm^2 middle trimmer aluminum plate illustrating hole dimensions. 255

Figure E-34. Top view of the 10x10 cm^2 middle trimmer aluminum plate illustrating hole dimensions. 256

Figure E-35. Orthogonal view of the 10x10 cm^2 lower trimmer aluminum plate. 256

Figure E-36. Top view of the 10x10 cm^2 lower trimmer aluminum plate illustrating the in-plane and cross-plane dimensions. 257

Figure E-37. Cross sectional view of the 10x10 cm^2 lower trimmer aluminum plate illustrating the thickness and lateral in-plane and cross-plane dimensions of the plate. 257

Figure E-38. Top view of the 10x10 cm^2 lower trimmer aluminum plate illustrating hole dimensions. 258

Figure E-39. Orthogonal view of the 10x10 cm^2 lower trimmer aluminum plate illustrating hole dimensions. 258

Figure E-40. Upper aluminum spacer tubes which connect the upper trimmer and the attachment plate. 259

Figure E-41. Middle aluminum spacer tubes which connect the middle and upper trimmers. 259

Figure E-42. Lower aluminum spacer tubes which connect the lower and middle trimmers. 260

Figure E-43. Orthogonal view of the full 20x20 cm^2 applicator. 261

Figure E-44. Top orthogonal view of the 20x20 cm^2 upper trimmer lead plate. 262

Figure E-45. Bottom orthogonal view of the 20x20 cm^2 upper trimmer lead plate. 262

Figure E-46. Top view of the 20x20 cm^2 upper trimmer lead plate illustrating the cross-plane dimensions. 263

Figure E-47. Top view of the 20x20 cm^2 upper trimmer lead plate illustrating the in-plane dimensions. 263

Figure E-48. Cross sectional view of the 20x20 cm^2 upper trimmer lead plate in the in-plane dimension illustrating the lateral dimensions of the plate. 264

Figure E-49. Cross sectional view of the 20x20 cm^2 upper trimmer lead plate in the in-plane dimension illustrating the thickness values of the plate. 264

Figure E-50. Cross sectional view of the 20x20 cm^2 upper trimmer lead plate in the cross-plane dimension illustrating the lateral dimensions of the plate. 264

Figure E-51. Cross sectional view of the 20x20 cm^2 upper trimmer lead plate in the cross-plane dimension illustrating the thickness values of the plate. 264

Figure E-52. Inner edge divergence of the 20x20 cm^2 upper trimmer lead plate. 265

Figure E-53. Orthogonal view of the 20x20 cm^2 upper trimmer lead plate illustrating hole dimensions. 265

Figure E-54. Top orthogonal view of the 20x20 cm^2 middle trimmer lead plate. 265

Figure E-55. Bottom orthogonal view of the 20x20 cm^2 middle trimmer lead plate. 266

Figure E-56. Top view of the 20x20 cm^2 middle trimmer lead plate illustrating the cross-plane dimension. 266

Figure E-57. Top view of the 20x20 cm^2 middle trimmer lead plate illustrating the in-plane dimension. 267

Figure E-58. . Cross sectional view of the 20x20 cm^2 middle trimmer lead plate illustrating the in-plane and cross-plane lateral dimensions of the plate. 267

Figure E-59. Cross sectional view of the 20x20 cm^2 middle trimmer lead plate illustrating the thickness values of the plate. 268

Figure E-60. Orthogonal view of the 20x20 cm^2 middle trimmer lead plate illustrating hole dimensions. 268

Figure E-61. Top orthogonal view of the 20x20 cm^2 lower trimmer lead plate. 269

Figure E-62. Bottom orthogonal view of the 20x20 cm^2 lower trimmer lead plate. 269

Figure E-63. Top view of the 20x20 cm^2 lower trimmer lead plate illustrating the cross-plane dimensions. 270

Figure E-64. Top view of the 20x20 cm^2 lower trimmer lead plate illustrating the in-plane dimensions. 270

Figure E-65. Cross sectional view of the 20x20 cm^2 lower trimmer lead plate illustrating the in-plane and cross-plane lateral dimensions of the plate. 271

Figure E-66. Cross sectional view of the 20x20 cm^2 lower trimmer lead plate in the cross-plane dimension illustrating the thickness values of the plate. 271

Figure E-67. Orthogonal view of the 20x20 cm^2 lower trimmer lead plate illustrating hole dimensions. 271

Figure E-68. Top orthogonal view of the 20x20 cm^2 upper trimmer aluminum plate. 272

Figure E-69. Top view of the 20x20 cm^2 upper trimmer aluminum plate illustrating the in-plane and cross-plane dimensions. 272

Figure E-70. Cross sectional view of the 20x20 cm^2 upper trimmer aluminum plate in the cross-plane dimension illustrating the thickness and lateral dimensions of the plate. 273

Figure E-71. Cross sectional view of the 20x20 cm^2 upper trimmer aluminum plate in the in-plane dimension illustrating the thickness and lateral dimensions of the plate. 273

Figure E-72. Orthogonal view of the 20x20 cm^2 upper trimmer aluminum plate illustrating hole dimensions. 273

Figure E-73. Top view of the 20x20 cm^2 upper trimmer aluminum plate illustrating hole dimensions. 274

Figure E-74. Orthogonal view of the 20x20 cm^2 middle trimmer aluminum plate. 274

Figure E-75. Top view of the 20x20 cm^2 middle trimmer aluminum plate illustrating the in-plane and cross-plane dimensions. 275

Figure E-76. Cross sectional view of the 20x20 cm^2 middle trimmer aluminum plate illustrating the thickness and lateral in-plane and cross-plane dimensions of the plate. 275

Figure E-77. Orthogonal view of the 20x20 cm^2 middle trimmer aluminum plate illustrating hole dimensions. 276

Figure E-78. Top view of the 20x20 cm^2 middle trimmer aluminum plate illustrating hole dimensions. 276

Figure E-79. Orthogonal view of the 20x20 cm^2 lower trimmer aluminum plate. 277

Figure E-80. Top view of the 20x20 cm^2 lower trimmer aluminum plate illustrating the in-plane and cross-plane dimensions. 277

Figure E-81. Cross sectional view of the 20x20 cm^2 lower trimmer aluminum plate illustrating the thickness and lateral in-plane and cross-plane dimensions of the plate. 278

Figure E-82. Top view of the 20x20 cm^2 lower trimmer aluminum plate illustrating hole dimensions. 278

Figure E-83. Upper aluminum spacer tubes which connect the upper trimmer and the attachment plate. 279

Figure E-84. Middle aluminum spacer tubes which connect the middle and upper trimmers. 279

Figure E-85. Lower aluminum spacer tubes which connect the lower and middle trimmers. 280

Abstract

The objective of this study was to design an electron collimation system for Elekta Infinity accelerators with significantly reduced applicator weights, while maintaining acceptable in-field beam flatness and out-of-field leakage dose. The design was restricted to 6-20 MeV beams for 6x6 to 25x25 cm^2 applicators at 100 cm SSD with the MLCi2 treatment head. In Aim1, measured off-axis profiles showed that the current Elekta collimation system met dose flatness (±4%) and IEC leakage dose specifications in the patient plane for custom 7, 13, and 20 MeV beams at MBPCC. Also, Monte Carlo (MC) calculations based on MBPCC beam models sufficiently agreed with measured doses to be useful for collimation design. In Aim 2, fast, analytical models for the electron and photon dose components were developed for calculating dose inside the field and its penumbra during trimmer weight optimization. In Aim 3, 1% electron ranges and out-of-field leakage doses were both computed using MC for copper, lead, and tungsten. At 20 MeV tungsten and lead had comparable ranges (g cm^{-2}), both lower than copper. However, tungsten had lower out-of-field dose, making it the preferred trimmer material. In Aim 4, MC calculations evaluated the effect of diverging the trimmer inner edges on out-of-field dose. Results showed that edges diverging from the virtual source for the upper and middle trimmers gave the least out-of-field dose; the divergence of the lower trimmers edges made little difference. In Aim 5, off-axis positions of the inner and outer trimmer edges computed by a simple model resulted in initial 10x10 and 20x20 cm^2 applicator designs having excessive trimmer weights of 7.06 and 10.87 kg, respectively. Trimmer modifications (beveling outer edges, optimizing *z*-positions, optimizing edge positions, reducing photon jaw positions, and adjusting trimmer thicknesses and bevel shapes) reduced trimmer weights to 3.73 and 5.09 kg, well below the objectives (5.00 and 7.10 kg, respectively). In Aim 6, dose measurements with fabricated 10x10 and 20x20 cm^2 prototype applicators confirmed acceptable in-field flatness and out-of-field leakage dose at 7, 13, and 20 MeV, achieving the objective. Also, photon jaw inner edges should be within 1 cm of the optimized locations.

Chapter 1 - Introduction

1.1. Background and Significance

1.1.1. Fundamental Properties and Advantages of Electron Therapy

Electron beams deliver an approximately uniform dose from the patient surface to a therapeutic depth. Beyond this therapeutic depth the dose distribution falls off rapidly to the depth corresponding to the practical range of the electrons. Figure 1-1 shows the percent depth dose (PDD) curve of a 13 MeV electron beam from the Elekta Infinity accelerator. The measurements were taken in a water phantom with a source to surface distance (SSD) of 100 cm. The depth of maximum dose (R_{100}), the maximum depth of the therapeutic range, which corresponds to the depth of 90% of the maximum dose (R_{90}), and the practical range of the electrons (R_p) are labelled. The uniform dose within the treatment region and the sharp distal fall-off make electrons well suited for treating shallow tumors ($\leq$ 6cm). The uniform dose region allows for the delivery of a relatively uniform dose to the tumor, and the rapid dose fall-off beyond R_{90} is beneficial for sparing distal critical structures.

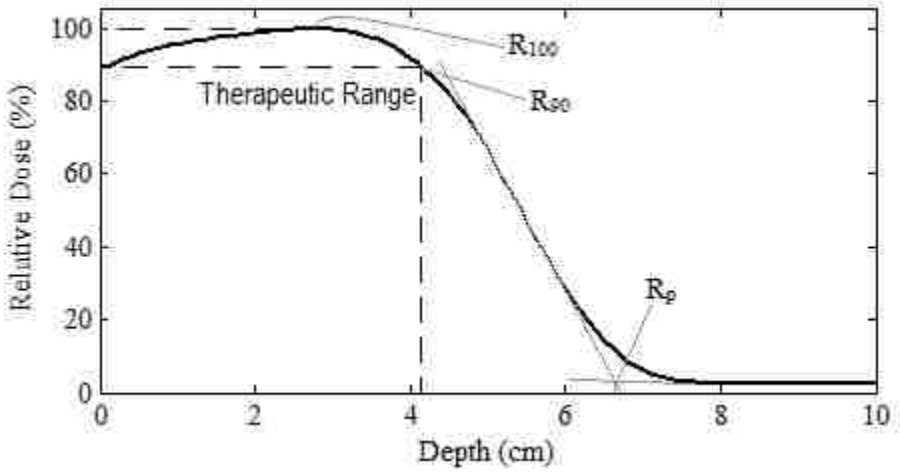

Figure 1-1. PDD for a 13 MeV electron beam measured in water. The dose is plotted versus depth with the depth of maximum dose (R_{100}), depth of 90% dose (R_{90}), which corresponds to the therapeutic range of the beam, and the practical range of the electrons (R_p) labelled.

In electron therapy, the beam energy is selected based on the depth of the tumor. As the beam energy increases, both R_{90} and R_p increase. Figure 1-2 shows PDD curves for the seven beam energies available with the Elekta Infinity linear accelerator at Mary Bird Perkins Cancer Center (MBPCC),

nominally listed as 7, 9, 10, 11, 13, 16, and 20 MeV, which are non-standard energies uniquely configured for our accelerator. The PDDs of the nominal beam energies used most throughout this project, 7, 13, and 20 MeV, are shown as solid curves, and the other beam energies are shown as dotted curves. The table in the upper right portion of the figure lists the most probable electron energy ($E_{p,0}$) and R_{90} for each nominal beam energy. The figure also illustrates the increase in R_p with increasing energy. Additionally, increasing the beam energy also increases the relative surface dose, as shown in the figure. The beam energy should be selected such that it provides sufficient dose coverage over the full extent of the tumor (i.e. R_{90} greater than the depth of the distal surface of the treatment volume), but spares distal critical structures (i.e. R_p less than the depth of the proximal surface of any critical structures). Electron beams are typically approximately monoenergetic, with a full-width-half-maximum (FWHM) energy

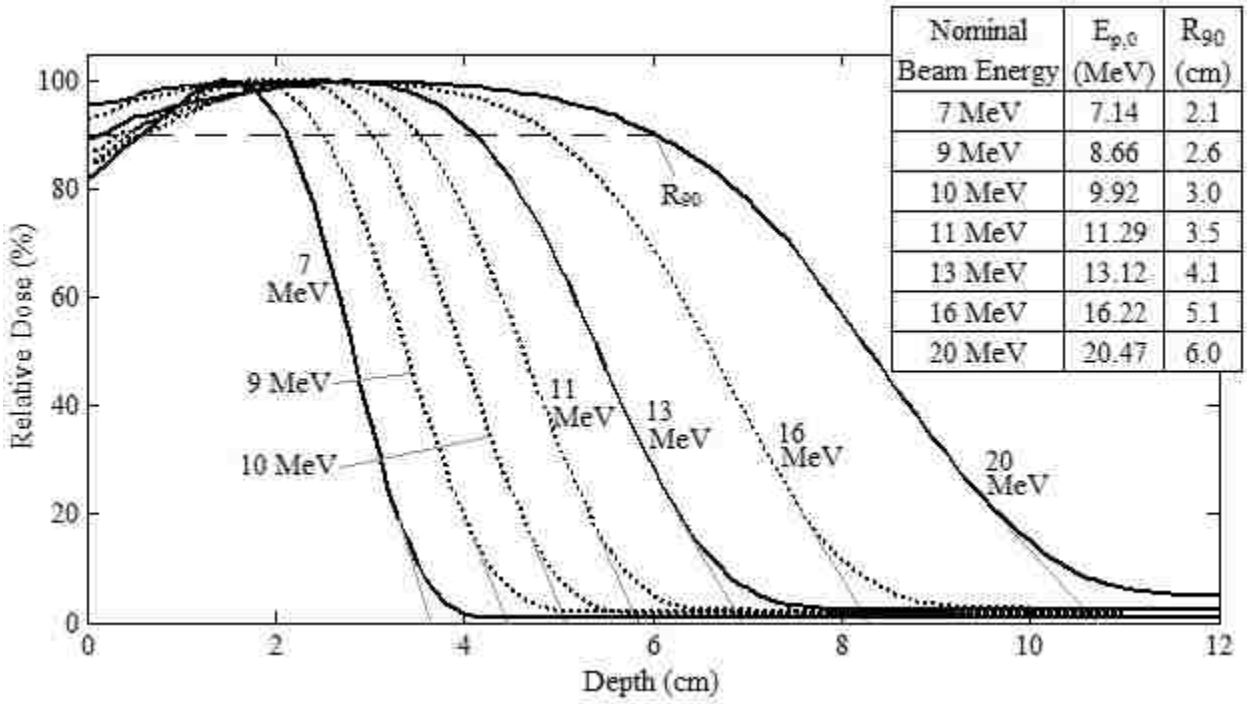

Figure 1-2. Depth dose curves in water for each nominal beam energy available on the Elekta Infinity linear accelerator. The PDDs of the nominal beam energies used most throughout this project, 7, 13, and 20 MeV, are shown as solid curves, and the other beam energies are shown as dotted curves. The table in the upper right portion lists the $E_{p,0}$ and R_{90} values for each nominal beam energy.

spread ranging from approximately 5% to 22% of the mean energy, depending on accelerator (Deasy *et al.*, 1996). The Elekta Infinity is a standing wave accelerator with recirculating power and a ±9% energy slot, which gives it a FWHM energy spread of approximately 20% of the mean energy (McLaughlin, 2013).

Electron beam therapy has been utilized for numerous patient sites within 6 cm of the surface (Tapley, 1976; Hogstrom, 1991b; Hogstrom, 2004; Gerbi *et al.*, 2009). These sites include the scalp, lips, ear, nose, salivary glands, cervical lymph nodes, post-lumpectomy tumor bed, internal mammary chain lymph nodes, post-mastectomy chest wall, and digestive tract. It has also been used to treat more widely spread diseases of the limbs, such as sarcoma, lymphoma, and melanoma, and mycosis fungoides (total skin irradiation), and intraoperative sites of the abdomen, chest, and head.

1.1.2. Purposes of Accelerator Head and Collimation System

Electron radiotherapy treatments are delivered using an electron linear accelerator. In these accelerators, electrons are emitted from a heated filament and injected into an accelerator chamber. The electrons are then accelerated using microwaves produced by either a magnetron or klystron with either a traveling wave or standing wave guide (Khan, 2003). The Elekta Infinity accelerator uses a magnetron with a traveling wave guide.

The accelerated electrons exit the accelerating components and enter the treatment head as an approximately monoenergetic, monodirectional, horizontal beam. The treatment head of the accelerator monitors and modifies the beam to be useful for patient treatment. The treatment head accomplishes this by serving four main purposes:

1. Redirect: The direction of the electrons exiting the accelerating components is approximately horizontal. In order for the beam to be made useful for treating a patient lying horizontally on a treatment couch, the beam must be redirected such that it is perpendicular to the patient (e.g. vertical). This is accomplished using a bending magnet system which redirects the beam either 270˚ or 90˚ downward toward the patient (isocenter). These magnet systems are achromatic, maintaining a focused, approximately monodirectional beam after the bend. A depiction of the 90˚ slalom-type magnet used in

the Elekta Infinity accelerator is shown in Figure 1-3. This figure shows a cross-sectional view of the Elekta Infinity treatment head components in electron mode.

2. Broaden and Flatten: After the beam is redirected toward the patient, it is necessary to broaden the beam to encompass the full width of the largest field size used clinically, typically on the order of 30x30 cm^2. This is performed using a dual foil scattering system consisting of two separate foils. The first foil, a thin high atomic number primary scattering foil, broadens the beam into an approximately Gaussian shape. A secondary flattening foil is then used to flatten the beam by preferentially scattering electrons in the central portion of the beam outward, thereby making it uniform. Each of these foils is labelled in Figure 1-3.

3. Monitor: The flatness, symmetry, and output of the beam should be monitored throughout the treatment. This is performed using a pair of segmented, parallel plate ionization chambers within the treatment head. These chambers monitor these three parameters during the treatment, and signal the interlock systems to shut off the beam if any parameters are outside tolerance. The location of these chambers is shown in Figure 1-3.

4. Collimate: The electron collimation system is used to shape the beam to the projection of the planning target volume (PTV) plus a small margin. This is performed using three separate collimation component levels, each labelled in Figure 1-3. 1) The primary collimator, located between the primary and secondary scattering foils, reduces bremsstrahlung photon leakage well outside the field. 2) The photon or x-ray diaphragms (jaws), located just above the Mylar treatment head exit window, provides initial collimation of the external beam. The off-axis positions of the jaws are dependent on the applicator size and beam energy combination. 3) The electron applicator, which is attached externally to the treatment head, further collimates the beam close to the patient surface. Presently, there are five commercially available Elekta electron applicators at MBPCC that form square fields of 6x6, 10x10, 14x14, 20x20, and 25x25 cm^2 at 95 cm SSD or 1.05 times that size at isocenter. These applicators are shown in Figure 1-4 in ascending order of field size. Because treatment volumes are irregularly shaped and vary from patient to patient, the collimation system must be able to conform the beam to any arbitrary

shape. This is typically performed using a custom made Lipowitz metal (Cerrobend) insert, which is uniquely designed to match the shape of each individual PTV.

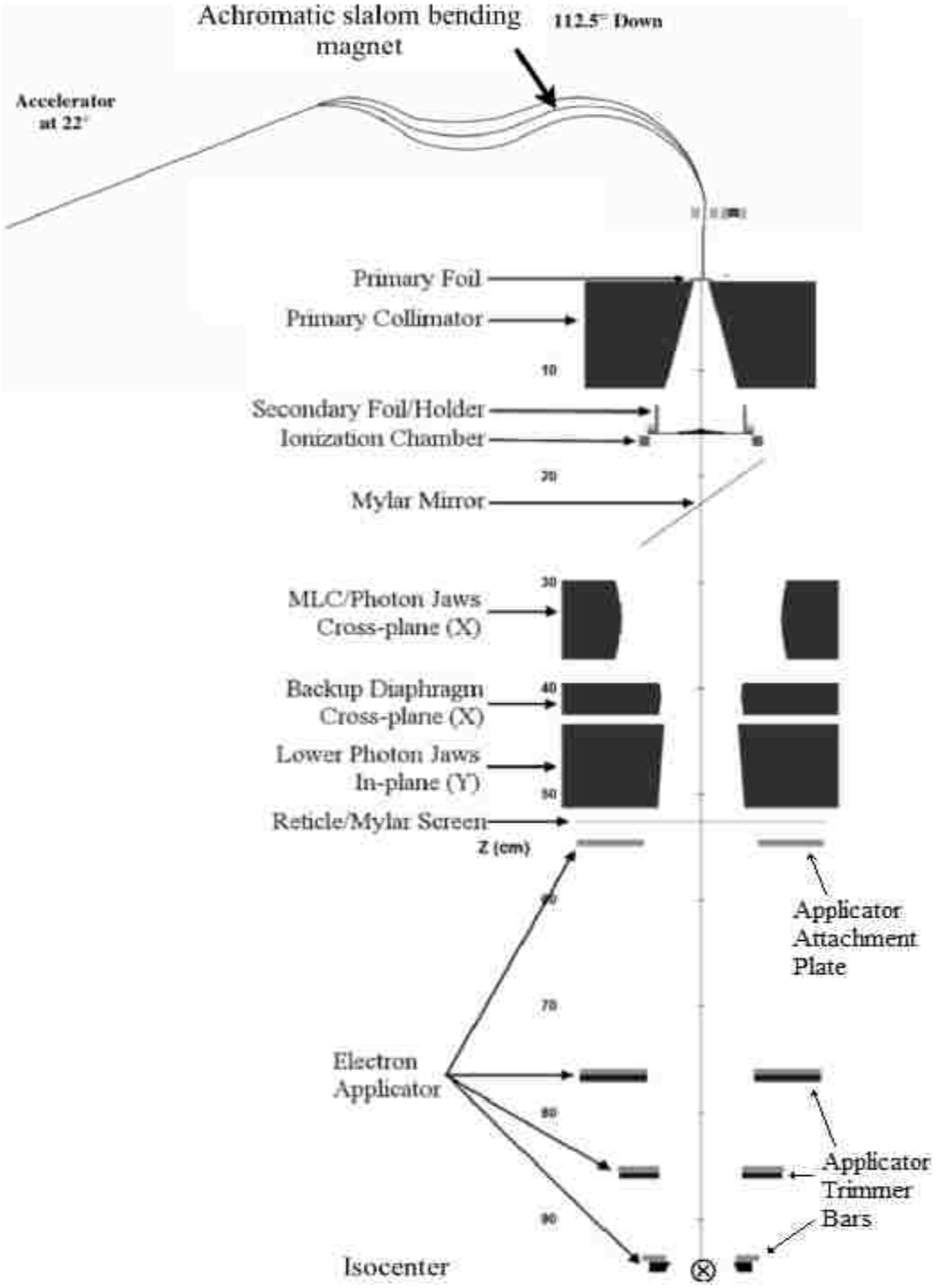

Figure 1-3. Cross-sectional view of the Elekta Infinity treatment head (MLCi2) components and electron applicator (from LeBlanc, 2012). The MLC/photon jaws and backup diaphragm collimate in the cross-plane dimension, and the lower photon jaws collimate in the in-plane dimension.

The Elekta Infinity accelerator's electron collimation system was the focus of this investigation. A picture of this accelerator with the 14x14 cm^2 applicator attached to the treatment head is shown in Figure 1-5.

Figure 1-4. The five electron applicators of the Elekta Infinity accelerator. These applicators have field sizes of (as shown left to right) 6x6, 10x10, 14x14, 20x20, and 25x25 cm^2 at 95 cm SSD.

Figure 1-5. Elekta Infinity accelerator with the 14x14 cm^2 applicator attached to the treatment head (from Harris, 2012).

1.1.3. Dose Components to Account for in Collimation Design

In electron therapy, multiple dose components (primary electrons, bremsstrahlung photons, and collimation scattered electrons) contribute to the dose delivered to the patient both within and outside the field. Each of these components must be taken into account for in the design process.

1.1.3.1. Primary Electrons

Primary electrons are those electrons which interact only with air (i.e. no collimation components) after exiting the secondary flattening foil. While this component is the main contributor to the dose within the field (approximately 92% at the surface), it is much less so outside the field. The contribution of these particles to the out-of-field dose increases with decreasing energy, due to the increased scattering power of the low energy electrons. The distribution of these electrons is primarily affected by multiple Coulomb scattering (MCS), the elastic scattering of the electrons off atomic nuclei, in air in route to the patient. The effect of this scattering on the distribution of electrons traversing a collimation system has been described mathematically by Hogstrom *et al.* (1985) and Huizenga and Storchi (1987).

1.1.3.2. Bremsstrahlung Photons

Bremsstrahlung photons are created when electrons are strongly deflected by an atomic nucleus. The rate of energy loss in the creation of these photons, known as radiative energy loss, increases with increasing energy and atomic number of the material. For this reason, the large majority of these bremsstrahlung photons are created in the scattering foils and the applicator trimmer bars. These photons are responsible for the formation a bremsstrahlung "tail" region of the depth dose curve at depths beyond R_p, as can be seen in Figure 1-2. Additionally, these photons constitute a significant portion of the out-of-field dose, particularly at the higher beam energies.

1.1.3.3. Collimation Scattered Electrons

In the process of collimating the beam, a portion of the electrons will inevitably not be absorbed (stopped) in the collimation, but rather scatter through the collimation edges back into the field and into the leakage region. These electrons have the effect of increasing the surface dose within the field due to

their decreased energies and increased angle. According to Lax and Brahme (1980) the energy of these particles is reduced to an average of 40% of the primary electron energy. Additionally, these particles can negatively impact the field flatness at depths beyond R_{100}, if they are used to maintain field flatness near the surface (Lax and Brahme, 1980), due to the reduced range of these lower energy scattered electrons compared with the primary electrons. These scattered electrons also constitute a significant portion of the out-of-field dose, particularly at higher beam energies.

1.1.4. Previous Work on Collimation Design Issues

Several studies have been performed analyzing the out-of-field dose from older electron collimation systems for Varian accelerators. Many of these studies noted excessive leakage both along the side of the applicator (Schneider, 1982; Pennington *et al.*, 1988; Das *et al.*, 1990), and at 100 cm SSD (Keys and Purdy, 1984; Pennington *et al.*, 1988; Das *et al.*, 1990). These studies found leakage values as high as 24% of D_{max} (the central axis measured at R_{100}, 100 cm SSD) at a point 2 cm from the side of the applicator (Pennington *et al.*, 1988), and 9% at 100 cm SSD (Keys and Purdy, 1984). A variety of techniques were studied to reduce these leakage levels, including placing lead plates along the applicator housing walls (Das *et al.*, 1990) and covering holes in the collimation material through which leakage radiation was transmitted (Keys and Purdy, 1984). However, these modifications had the adverse effect of adding to the applicator weight and were never adopted. Additionally, a study conducted by Yeboah *et al.* (2010) noted excessive leakage from the electron collimation system of a Siemens Primus accelerator both at 100 cm SSD and along the side of the applicator.

The older Varian applicator models were typically designed with thin upper and middle collimation trimmers and enclosed within a wall of housing material (Kassaee *et al.*, 1994). This design impacted the in-field dose distribution by contributing a large number of applicator scattered electrons with reduced energies to the in-field dose distribution. In some cases, these applicator scattered electrons were used to increase the dose at the corners of the field to improve field flatness. These electrons had the additional effect of increasing the surface dose within the field. This method for improving off-axis

dose flatness at the surface adversely affected the off-axis dose flatness at depths beyond R_{100}. (Lax and Brahme, 1980).

To remedy these issues, modern applicators are typically designed with more robust, thicker trimmer bars and to be "open", i.e. unenclosed such that only the trimmers are used for collimation and no significant amount of material separates the in-field from the out-of-field space. By increasing the thickness of the collimation trimmers and removing the applicator housing walls, the impact of degraded energy scattered electrons to the in-field dose distribution was decreased. Investigators have compared these designs, noting the benefits of this enhancement (Kassaee *et al.*, 1994; Shiu *et al.*, 1994; Klein *et al.*, 1995). According to Klein *et al.* (1995), by making this adjustment to the Varian accelerator collimation systems, the leakage dose was reduced, the surface dose was increased, and off-axis dose flatness at R_{100} was improved.

Older Siemens applicator models were designed with the lower trimmer situated at 100 cm SSD, such that it was designed to come in contact with the patient during treatment. This caused issues with patient setup since the surface of the patient is seldom flat. To remedy this issue, a 5 cm air gap was added between the lower trimmer and the patient to allow flexibility in the setup (Meyer *et al.*, 1984). Additionally, in the old design, the inner edges of the lower trimmer were situated to directly align with the projection of the upper trimmer from the virtual source. This caused a broadening of the penumbra at the edge of the beam when the lower trimmer was moved away from the patient surface. To account for this, the lower trimmer was moved inward relative to the projection of the upper trimmer to sharpen the penumbra at the edge of the beam (Meyer *et al.*, 1984).

1.1.5. Electron Collimation System Acceptance Criteria

In the process of shaping the beam to conform to the projection of the PTV, the electron collimation system must meet certain criteria in order to be deemed acceptable. Outside the field, the leakage dose should be kept as low as possible to minimize the effects of stray radiation (i.e. radiation from particles with trajectories such that they would not contribute to the treatment field dose) delivered to normal tissue. Within the field, the off-axis distribution of the beam must be uniform in order to

deliver a uniform dose to the PTV. For this study, the guidelines for leakage dose requirements are outlined in IEC Report 60601-2-1 (1998), and the guidelines for in-field flatness requirements are outlined in *Principals and Practices of Radiation Oncology* (Hogstrom, 2004) and consistent with the recommendations of AAPM Task Group 25 (Khan *et al.*, 1991).

1.1.5.1. Leakage Dose Criteria

Investigations have been performed to develop a set of quantified limits to the leakage dose. These limits should be set high enough that they are reasonably achievable without an excessive amount of shielding, but low enough that the adverse effects from leakage radiation are minimized. Morgan *et al.* (1993) used a secondary cancer risk assessment model to evaluate a set of proposed limits, noting that these limits were comparable to leakage levels measured from a Varian 2500 accelerator. Ultimately, it is the responsibility of the International Electrotechnical Commission (IEC) to specify these limits.

The IEC mandates that measurements for determining the mean and maximum percent leakage dose be taken within an area M or area M_{10} at the normal treatment distance, which we selected as the patient plane (the plane perpendicular to beam central axis at 100 cm SSD plus 1 cm depth). These measured off-axis profiles should extend along the in-plane (parallel and coincident to the plane of electron trajectory exiting the accelerating components and within the bending magnets) and cross-plane (perpendicular to in-plane and including isocenter) axes, as well as both diagonal axes as depicted in Figure 1-6, which shows a beam's-eye view of the patient plane with the central shaded square representing a 20x20 cm^2 radiation field. Measured profiles should extend laterally out to the edge of area M or M_{10}, whichever extent is applicable. Area M, defined as the geometric projection at isocenter of the primary collimator within the treatment head from the nominal source position (100 cm upstream of isocenter along central axis), has a radius of 24.8 cm for the Elekta Infinity accelerator. Area M_{10} is defined as the union of area M and a square with edges 10 cm outside the radiation field edges at isocenter. As the figure shows, for larger field size (e.g. the 20x20 and 25x25 cm^2 Elekta applicator), measured profiles extend to the edge of area M_{10}. For small field sizes, such that a square with edges 10

cm outside the radiation field is completely contained within area M (e.g. the 6x6, 10x10, and 14x14 cm^2 Elekta applicators), the edge of area M defines the outer boundary of the measured profiles.

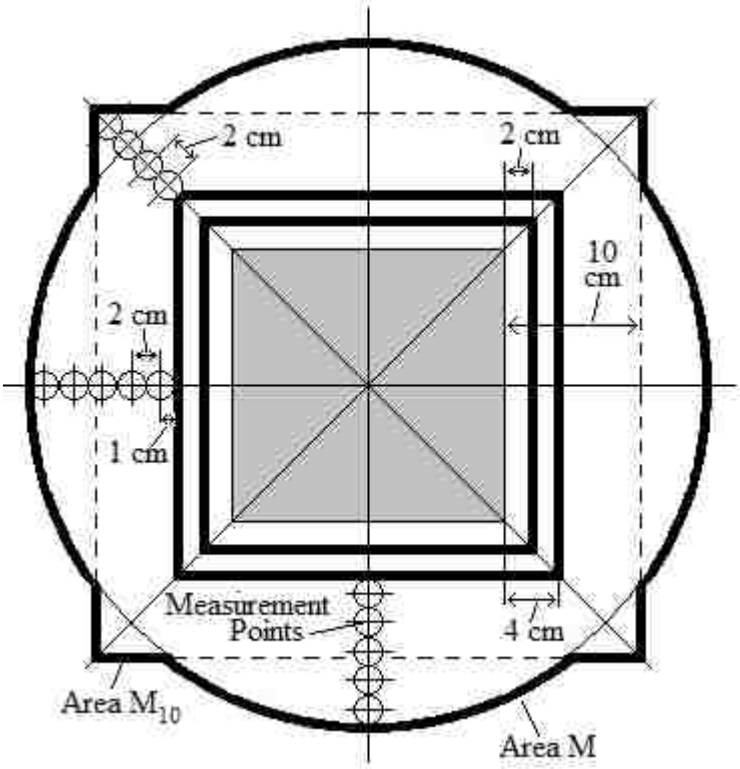

Figure 1-6. IEC specified geometry for measurements to obtain mean and maximum leakage in the patient plane. The image shows a beam's-eye view of the projected radiation field (shaded square) with the surrounding leakage region as defined by the IEC for a 20x20 cm^2 beam. The small circles with 2 cm spacing represent the points of measurement within the leakage region. These points extend from the inner boundary of the leakage region to the periphery of area M (outer black circle) or M_{10} (union of outer circle and outer dashed square, indicated by the thick black curve along the outer boundary) along the in-plane, cross-plane and both diagonal axes. The inner boundary for determining mean leakage (outer solid black square) is 4 cm outside the radiation field. The inner boundary for determining maximum leakage (inner solid black square) is 2 cm outside the radiation field. The figure is adapted from IEC Report 60601-2-1 (1998).

For calculation of the mean leakage dose, the inner boundary of the leakage region is defined by a square with edges located 4 cm outside the geometric edge of the radiation field, indicated in Figure 1-6 as the outer solid black square. For calculation of the maximum leakage dose, the inner boundary of the leakage region is defined by a square with edges located 2 cm outside the radiation field, shown as the inner solid black square in the figure. For both mean and maximum leakage dose, measurements are to be taken with 2 cm spacing from the inner boundary to the border of area M or M_{10}, whichever is greater,

along the in-plane, cross-plane and both diagonal axes with 1 cm buildup. The IEC mandates that the mean value of these points not exceed a value in the range of 1% to 1.8%, which varies according to beam energy, of D_{max} (the central axis dose in water at R_{100}, 100 cm SSD). The nominal beam energies most used throughout this study, 7, 13, and 20 MeV, have specified mean leakage limits of 1.00%, 1.10%, and 1.34%, respectively (calculated using their $E_{p,0}$ values of 7.14, 13.12, and 20.47 MeV, respectively). The report also mandates that the maximum dose of these measurement points not exceed 10% of maximum dose at depth on central axis. Additionally, the report specifies that the maximum leakage alongside the applicator at a position 2 cm outside the volume contained by the applicator not exceed 10% of D_{max}.

1.1.5.2. In-Field Beam Flatness Criteria

Hogstrom (2004) states that field flatness should not differ from the central-axis dose by more than ±3% along the major axes (in-plane and cross-plane), and ±4% along the diagonal axes. These criteria should be evaluated within a region 2 cm inside the edge of the field for the major axes, and $2\sqrt{2}$ cm inside the edge of the field for the diagonal axes. These specifications are to be assessed at a depth of 1 cm for energies of 9 MeV or less, and 2 cm for energies greater than 9 MeV. Figure 1-7 illustrates these criteria for the major axes, showing a lateral measured dose profile. In this figure the shaded box represents the uniformity region, the region over which the dose should be flat such that the profile does not escape the upper or lower boundaries of the box. These recommendations (Hogstrom, 2004), which differ slightly from those of Task Group 25 (Khan *et al.*, 1991), i.e. that flatness should be evaluated both near the surface and near the therapeutic depth, are those used at our and other institutions.

1.2. Purpose of Study

1.2.1. Elekta Infinity Electron Collimation System Design Description and Potential Areas for Enhancement

The Elekta Infinity electron collimation system consists of five electron applicators, ranging in size from 6x6 to 25x25 cm^2 (specified at 95 cm SSD), each of which has its own unique photon jaw position setting for each beam energy. The applicators consist of three trimmer bars, comprised of a

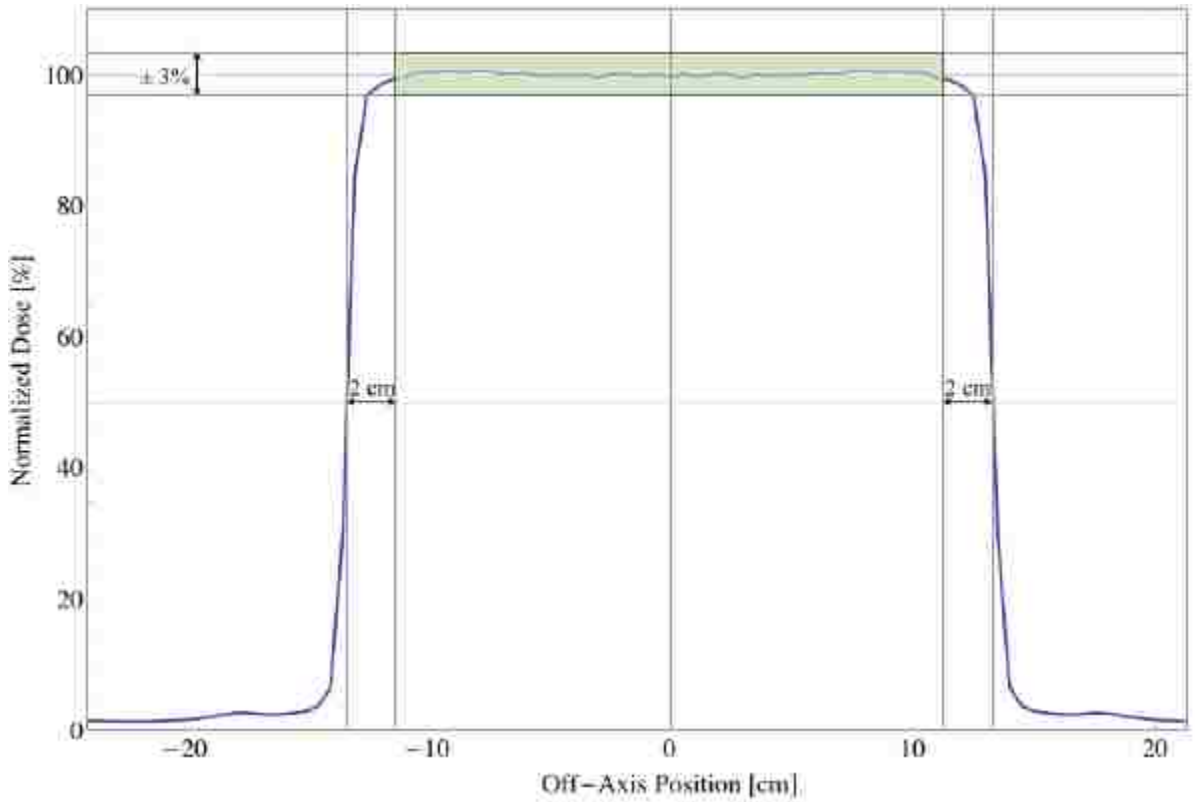

Figure 1-7. Beam flatness specifications within the field along the major axes. Dose relative to central axis value (off-axis ratio, OAR) is plotted versus off-axis position along one of the major axes for the Elekta Infinity at MBPCC with the 25x25 cm^2 applicator. The shaded box represents the region over which the in-field beam flatness is evaluated. The dose profile should not escape the upper or lower boundaries (±3%) of this box (from LeBlanc, 2012).

combination of aluminum and lead. These applicators are attached externally to the treatment head via an attachment plate with a latching mechanism.

The MBPCC clinical staff has found Elekta electron applicators to meet well our clinical needs from a perspective of dose distributions and out-of-field leakage dose. However, the MBPCC staff has identified three potential areas for enhancement: 1) the applicators are excessively heavy, causing difficulty in handling by the radiation therapists, 2) the positioning of the optical distance indicator (ODI) relative to the applicator makes it impossible to read the SSD with the applicator inserted, and 3) the latching mechanism for attaching the applicator to the treatment head could be less cumbersome. Also, less of a functional and more of an aesthetics issue is that the field sizes at isocenter (100 cm SSD), the

nominal treatment SSD, are not standard sizes, i.e. they are 6.3x6.3, 10.5x10.5, 14.7x14.7, 21.1x21.1, and 26.3x26.3 cm^2 for the 6x6, 10x10, 14x14, 20x20, and 25x25 cm^2 applicators, respectively.

1.2.1.1. Potential Area of Enhancement 1: Excessive Weight

The first potential area of enhancement with the Elekta Infinity electron collimation system is its excessive applicator weights. When compared against the Varian applicators for approximately the same field size, the Elekta applicators weigh significantly more. Figure 1-8 shows pictures comparing the Elekta and Varian 21EX applicators for the 10x10 and 20x20 cm^2 sizes. The field insert, the upper, middle, and lower trimmers, and the attachment plate are labelled for each applicator. For the Varian designs, the upper trimmer and attachment plate are joined, such that they can be considered one component. The pictures show that the Elekta applicators are longer (i.e. have a greater distance from the attachment plate to the field insert). This is due to the positioning of the bottom of the Elekta treatment head further from isocenter. The figure also shows that the Elekta upper, middle, and lower trimmers are positioned closer to one another than the Varian trimmers. Additionally, the images show the difference in trimmer shape. The Varian trimmers are designed with the inner portion of the trimmers much thicker than the outer portion of the trimmers, whereas the Elekta trimmer thickness is uniform across the width of the trimmer.

The weights of the Elekta and Varian applicators are compared in Table 1-1 for the five available applicator sizes, ranging from 6x6 to 25x25 cm^2. This table outlines both the full applicator weight (including the weight from all structural and electronic components) and the weight of only the trimmer material for both the Elekta and Varian collimation systems. The "trimmer only" weight for the Varian applicators was approximated as the full applicator weight minus 1.5 kg. This 1.5 kg value was obtained by disassembling a 15x15 cm^2 Varian applicator and weighing the separate applicator components individually, revealing that the non-trimmer material (structural and electrical components) comprised approximately 1.5 kg of the of the total applicator weight. This non-trimmer weight was assumed

Figure 1-8. Comparison of the current clinical Elekta and Varian applicator designs for the 10x10 and 20x20 cm^2 sizes. The locations of the field insert, the upper, middle and lower trimmers, and the attachment plate are labelled for each applicator.

Table 1-1. Applicator weights for the Elekta Infinity and Varian 21EX accelerators listed in kg.

Applicator Size (cm x cm)	Elekta Weight (kg)		Varian Weight (kg)	
	Full Applicator	Trimmers Only	Full Applicator	Trimmers Only
6 x 6	7	4.75	5.7	4.20[b]
10 x 10	7.7	5.52	6.5	5.00[b]
14 x 14	9.1	6.71	7.6[a]	6.10[ab]
20 x 20	10.9	8.36	8.6	7.10[b]
25 x 25	13.4	10.00	9.5	8.00[b]

[a]Weights are for 15x15 cm^2 applicator

[b]Varian trimmer weights were estimated as the measured full applicator weight minus 1.5 kg

constant for the other applicator sizes, which were not available for disassembly. It should also be noted that the Varian accelerator uses a 15x15 cm^2 applicator, rather than the 14x14 cm^2 size used by Elekta. Therefore, the Varian weights listed in the 14x14 cm^2 row of the table actually apply to the 15x15 cm^2 applicator.

The data in this table shows that for all applicator sizes the Elekta applicators outweigh the Varian applicators of the same size. This is true for both the "full applicator" weights, and the "trimmers only" weights. Furthermore, the data show that the discrepancy is more severe for the heavier applicators. For instance the 25x25 cm^2 Elekta applicator weighs 41% (3.9 kg) more than the Varian model, while the 10x10 cm^2 Elekta model only weighs 18% (1.2 kg) more than Varian model.

The greater weight of these applicators makes lifting and attaching them to the accelerator a more burdensome task for the MBPCC clinical therapy staff. This is especially true when taking into account the current attachment mechanism, which requires an awkward maneuver for applicator attachment. Hence, reducing applicator weight is the focus of this investigation.

1.2.1.2. Potential Area of Enhancement 2: Blocking of Optical Distance Indicator

The ODI is used to determine the SSD of a patient setup. When the electron applicator is inserted into the treatment head of the Elekta Infinity accelerator, the ODI light beam is blocked by the applicator from reaching the patient surface. This makes it difficult for the therapist to ensure the patient is being positioned properly. Figure 1-9 illustrates this setup deficiency. When no applicator is attached (e.g.

photon mode) the ODI light beam has a clear path to show the patient SSD, as shown on the left side of the figure. When the applicator is attached, as shown on the right, the ODI light beam is blocked from reaching the patient.

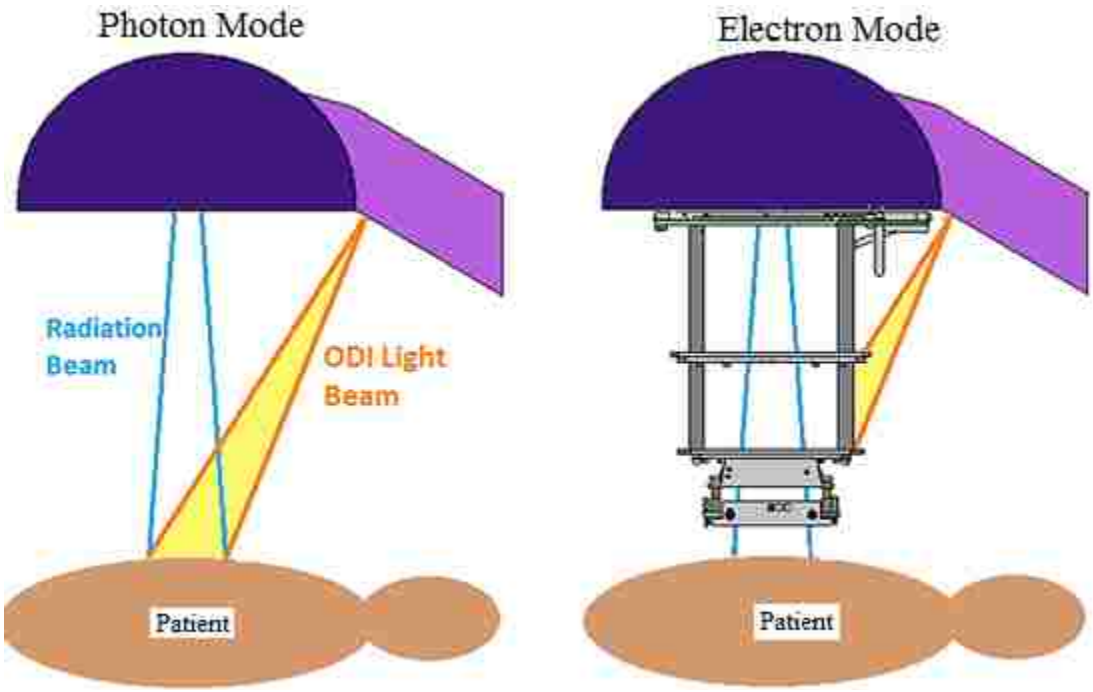

Figure 1-9. Comparison of photon and electron treatment setup causing ODI light beam to be blocked by the applicator when inserted.

1.2.1.3. Potential Area of Enhancement 3: Cumbersome Latching Mechanism

The current clinical Elekta Infinity applicators use a latching mechanism on an attachment plate to attach the applicator to the treatment head (Figure 1-10). This requires sliding a set of prongs into a placeholder on the treatment head, and pushing the entire applicator upward to secure a latch on the attachment plate, while simultaneously positioning an alignment pin on the attachment plate to align with an insert hole on the treatment head. Each of these attachment components is labelled in Figure 1-10, which shows an image of the attachment plate. This attachment process must be performed while the applicator is suspended at arm's length over the treatment couch, creating a difficult maneuver for the radiation therapist or medical physicist to perform. Alternatively, the couch can be rotated, which can be time consuming. Also, rotating the gantry to 180˚ for ease of attachment may be recommended; however,

this is very time consuming both during patient treatment and beam commissioning, and is not a common practice at MBPCC and in the United States. This method for applicator attachment is depicted in the image on the left in Figure 1-11, which compares the Elekta (left) and Varian (right) applicator attachment methods. This image shows that the Elekta applicator must be thrust upward while suspended over the table in order to secure the latch. For comparison, the Varian 21EX applicators use a sliding mechanism to attach the applicator to the accelerator head. In the Varian design, the applicator is slid horizontally into an insert tray, eliminating any maneuver requiring the applicator to be thrust upward while held at a distance away from the body.

Figure 1-10. Attachment plate of the Elekta Infinity accelerator with the prongs, alignment pin, and latch labelled.

1.2.1.4. Aesthetics: Field Size Specified at 95 cm SSD rather than 100 cm SSD

The field size of the current Elekta applicators is specified at 95 cm SSD. This results in the current nominal 6x6, 10x10, 14x14, 20x20, and 25x25 cm^2 applicators having non-standard field sizes at isocenter of 6.3x6.3, 10.5x10.5, 14.7x14.7, 21.1x21.1, and 26.3x26.3 cm^2, respectively. For most other manufacturers, including Varian, it is standard practice to define the field sizes at isocenter, i.e. a nominal 10x10 cm^2 applicator would have a field size of 10x10 cm^2 at 100 cm SSD. Designing the applicators in this way has the benefit of making them somewhat lighter, since the side length of each trimmer is reduced. This enhancement will be addressed in the new collimation system design process.

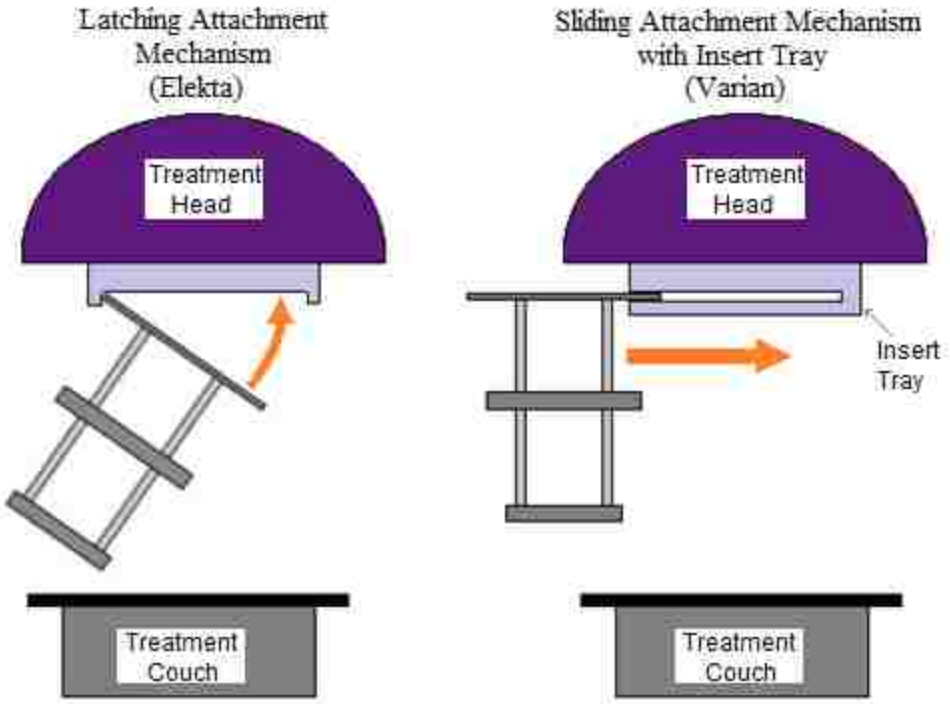

Figure 1-11. Comparison of the latching attachment mechanism used by Elekta with the sliding mechanism used by Varian.

1.2.2. Purpose and Description of Investigation

The purpose of this investigation is to redesign the Elekta Infinity electron collimation system to allow for new prototype applicators designed at reduced weights. Within this process, care has been taken to ensure that acceptable levels of in-field dose flatness and out-of-field leakage dose are maintained. This redesign focuses on the collimation components, including all trimmer specifications and the photon jaw positions. Design of the structural, electrical, collision protection, and other non-collimating components of the applicator will not be within the scope of this project. This includes the interference of the applicator with the ODI light beam and the cumbersome latching mechanism, as well as the mechanism for accommodating irregular field inserts.

Because the Varian 21EX applicators have been shown to perform adequately, new applicator designs that meet field flatness and leakage level criteria with weights equivalent to the Varian applicators should be obtainable. For this reason, the Varian applicator weights are used as a basis of comparison in

this study. Specifically, for the 10x10 and 20x20 cm^2 sizes, the goals of this study are for weight reduction that matches or is less than the weights of the Varian 10x10 and 20x20 cm^2 applicators. Because this redesign focuses only on the collimation (trimmer) material, rather than the structural, electrical, collision protection, and other non-collimating components, the "trimmer only" Varian applicator weights are used for comparison (i.e. 5.00 and 7.10 kg for the 10x10 and 20x20 cm^2 applicators, respectively).

1.3. Hypothesis

It is hypothesized that using a sound understanding of how radiation transport impacts the design of the Elekta electron collimating system, it is possible to design prototype 10x10 and 20x20 cm^2 applicators whose collimating components (trimmers) will (1) total less than 5.00 and 7.10 kg, respectively, (2) meet IEC radiation leakage dose specifications outside the field, and (3) achieve beam flatness inside the field as specified by Hogstrom (2004).

1.4. Specific Aims

This hypothesis will be tested by completing the following specific aims:

1.4.1. Aim 1 - Evaluation of the Current Collimation Design and MC Model Using Measurement

Measure off-axis dose profiles in a water phantom (100 cm SSD) at prescribed depths to document the beam flatness and leakage dose for the current clinical applicator design. Also, use that measured data to assess the accuracy of the electron MC model developed by Harris (2012) for the Elekta Infinity accelerator both in the field and in the leakage region.

1.4.2. Aim 2 - Develop and Validate an Analytical Radiation Transport Code for Optimizing Trimmer Design

Develop an analytical electron transport model based on pencil-beam theory to use in collimation system design. The model will incorporate both a primary electron and photon component, and its accuracy will be assessed. The impetus for creating this analytical model is to evaluate new collimation designs created within the design process for both in-field flatness and out-of-field leakage dose.

1.4.3. Aim 3 - Perform Material and Range Analysis to Determine the Best Trimmer Material and Thickness

Determine the optimal high-density material and thickness for the applicator trimmer bars, i.e. the material and range combination which produces the least amount of leakage dose while allowing the applicator to be designed with minimal weight.

1.4.4. Aim 4 - Determine Inner Edge Divergence Angles for Each Trimmer

Determine whether it is more suitable for the inner edge of each trimmer to be situated parallel to central axis or divergent such that it is emanating from the virtual source of the beam. The divergence angles that minimize out-of-field leakage dose are more suitable.

1.4.5. Aim 5 - Determine Optimal Applicator Geometry

Determine the optimal thickness, shape, and position of each trimmer bar, along with the photon jaw positions for each beam energy. These specifications will be selected such that the applicator weight is minimized while meeting leakage dose and beam flatness criteria.

1.4.6. Aim 6 - Construct Prototype Applicators and Evaluate Prototype Collimating System

Fabricate prototypes of the newly designed 10x10 and 20x20 cm^2 applicators in order to evaluate the prototype collimation system. Off-axis profiles will be measured in a water phantom to evaluate the in-field beam flatness and leakage dose of the prototype collimation system, and the prototype applicators will be weighed to determine the reduction in weight from the current clinical applicator designs. Additionally, MC calculations will be performed to evaluate the leakage dose along the side of the applicator and to investigate the effects of altering the designated photon jaw positions on the patient plane dose distribution.

Chapter 2 - Aim 1 - Evaluation of the Current Collimation Design and MC Model Using Measurement

Aim 1: Measure off-axis dose profiles in a water phantom (100 cm SSD) at prescribed depths to document the beam flatness and leakage dose for the current clinical applicator design. Also, use that measured data to assess the accuracy of the electron MC model developed by Harris (2012) for the Elekta Infinity accelerator both in the field and in the leakage region.

2.1. Aim 1 - Introduction

In electron radiotherapy a collimation system is used to shape the beam to conform to the profile of the PTV. The purpose of the collimation system, in conjunction with the dual scattering foils, is to ensure that the beam is suitably flat over the full extent of the field, while leakage dose outside the field is kept acceptably low. This is normally accomplished using an electron applicator attached externally to the treatment head. Current applicators typically consist of a series of shielding trimmers which continually shape the beam penumbra while maintaining acceptable in-field beam flatness and reducing stray radiation dose to acceptable levels. Various collimation system design features, including material, position, thickness, width, and shape, of the trimmers and photon jaws, can impact the system's ability to meet these criteria. These design features can vary significantly between different accelerators and manufacturers.

While the collimation system should absorb the large majority of the stray electrons, inevitably some remain, contributing to the leakage radiation. Several investigations have been performed to quantify this leakage for multiple collimation systems designed by different manufacturers, including Varian (Schneider, 1982; Pennington *et al.*, 1988; Das *et al.*, 1990; Perec and Kubo, 1990; Chow and Grigorov, 2006; Shimozato *et al.*, 2012) and Siemens (Ebert and Hoban, 1995a; Yeboah *et al.*, 2010). These studies utilized various techniques to measure the dose outside the field, including film (Keys and Purdy, 1984; Perec and Kubo, 1990; Chow and Grigorov, 2006) , diodes (Pennington *et al.*, 1988; Yeboah *et al.*, 2010) and ionization chambers (Keys and Purdy, 1984; Shimozato *et al.*, 2012). Additionally, MC models have been used to analyze the leakage dose. Shimozato (2012) used ionization

chamber measurements to validate a MC model built for the Varian Clinac 2100CD using EGSnrc (Kawrakow *et al.*, 2011). The model was then used to determine the energy spectrum and fluence profiles for different radiation components both within the field and in the leakage region.

To the knowledge of this investigator, only a limited study analyzing the electron collimation system of Elekta Infinity accelerators has been performed to date (Olsson, 2003). It was the purpose of the current study to evaluate the Elekta Infinity system (configured with the MLCi2 treatment head) using both measurement and MC techniques. Both the in-field and out-of-field regions were investigated to determine if criteria for in-field beam flatness and patient plane leakage dose levels, respectively, were met. The accuracy of the MC calculations was also evaluated by comparison with measured data. Additionally, the MC calculations were separated into dose components for further analysis, and the mean leakage from each component was independently calculated. These dose components included photons, primary electrons, and electrons scattered from various collimation components. This was done to gain insight into how different aspects of collimation design affect the leakage dose distribution.

2.2. Aim 1 - Methods

2.2.1. Measurements

2.2.1.1. Purpose of Measurements

Measurements were taken on the Elekta Infinity accelerator with the MLCi2 treatment head to serve two purposes. First, the measurements were used to evaluate both the in-field flatness and out-of-field leakage levels for combinations of three beam energies and two applicators. The beam flatness was evaluated using criteria specified by Hogstrom (2004) and the leakage levels were evaluated according to the regulations outlined by the IEC (1998). Second, the measurements were used to assess the accuracy of a MC model created by Harris (2012). Specifically, this was performed at shallow depths near the phantom surface where both the beam flatness and patient plane leakage levels are evaluated.

2.2.1.2. Configuration of Elekta Infinity Accelerator

The Elekta Infinity electron beam collimating system with the MLCi2 treatment head uses the in-plane and cross-plane photon diaphragms, and an attachable electron applicator to collimate the beam.

Figure 2-1 shows a cross sectional view of the accelerator and collimation system created in BEAMnrc with the 10x10 cm^2 applicator, with each collimating structure labelled. The stationary tungsten primary collimator, positioned between the primary and secondary scattering foils, has little effect on electron beams. The primary scattering foils serve to broaden the beam, and the secondary foils serve to flatten the beam (LeBlanc, 2012). The secondary foils in the accelerator used in this study were uniquely designed for the non-standard beam energies of the Elekta radiotherapy accelerators at MBPCC. The

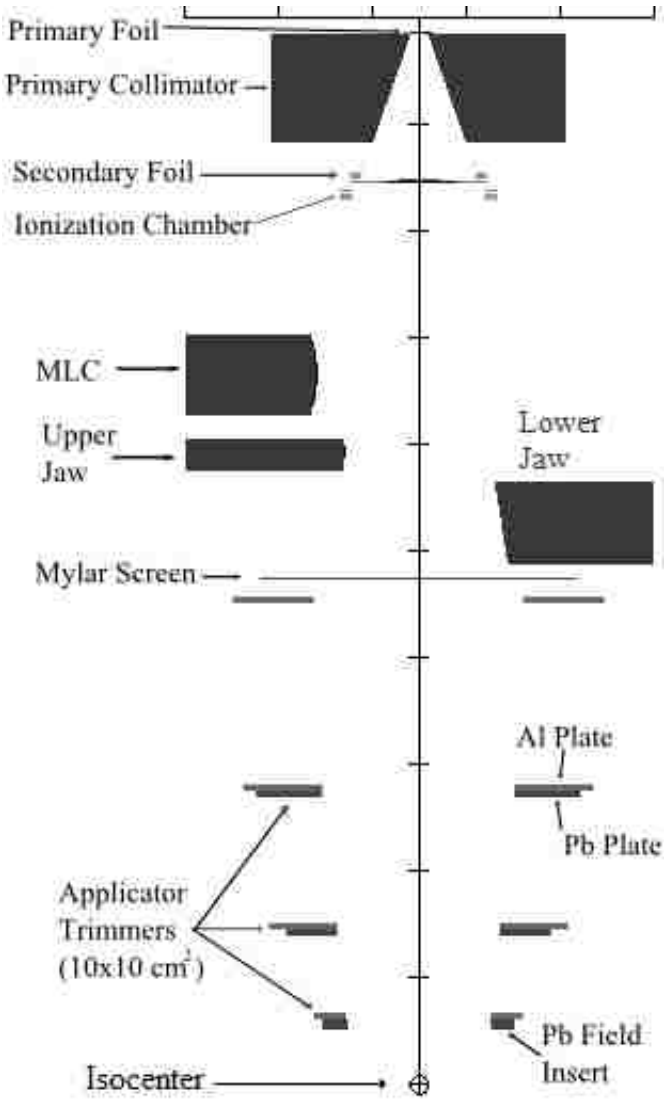

Figure 2-1. Cross-plane cross sectional view of the Elekta Infinity (MLCi2) accelerator modeled in BEAMnrc. The left side of the image demarcates the cross-plane components (MLC and upper jaw); the right side of the image demarcates the in-plane components (lower jaw). Tick marks have 10 cm spacing.

tungsten cross-plane (upper) and in-plane (lower) photon diaphragms, or jaws, are used to collimate the beam as it exits the treatment head. Both the tungsten multi-leaf collimator (MLC) and upper jaws are designed with curved inner edges, whereas the lower jaws have divergent inner edges. In electron mode the MLC leaves are parked in their furthest possible position off-axis (±20 cm off central axis projected to isocenter in the cross-plane dimension with the treatment head at 0˚) for all energies and applicators, and only the underlying photon jaws are used for collimation.

The accelerator used for this study had seven beam energies, nominally listed as: 7, 9, 10, 11, 13, 16, and 20 MeV. These beam energies, different (by as much as 0.5 cm change in R_{90}) from the standard energies offered with the Elekta infinity accelerator, were modified to fit the clinical needs of MBPCC and were selected for R_{90} values with 0.5 cm (±0.1 cm) spacings of 2.0, 2.5, 3.0, 3.5, and 4.0 cm for 7-13 MeV beams and 1.0 cm spacings of 4.0, 5.0, and 6.0 cm for 13-20 MeV beams. For each nominal beam energy, $E_{p,0}$ and R_{90} values are shown in Table 2-1. The beams utilize three different primary foils and three different secondary foils, with each energy beam using a unique primary-secondary foil combination. The foils used for each energy are displayed in Table 2-1. In this table, the primary foils are labelled as #3, #4, or #5 and the secondary foils are labelled as #1, #3, or #4. These numbers refer to the position in the tray within the accelerator head that each foil is placed. The secondary foils in the MBPCC Elekta accelerators used in this study were unique modifications of standard Elekta foils, designed to achieve in-field flatness for the non-standard beam energies used at MBPCC. For more information on the design of these foils or the head geometry, refer to Harris (2012).

The accelerator uses five different applicator sizes: 6x6, 10x10, 14x14, 20x20, and 25x25 cm^2, specified at 95 cm SSD. Each applicator-energy combination has a unique in-plane and cross-plane jaw setting. These settings, listed in Table 2-1 as the off-axis position of each jaw projected to isocenter from the nominal source position, are non-standard and specified to account for the non-standard energies and scattering foils on this accelerator; however, it is understood that they fall within the range of photon jaw settings specified by Elekta. The applicators utilize three trimmer levels. The upper two trimmers consist of a 0.6 cm thick layer of lead situated immediately beneath a 0.6 cm thick layer of aluminum. The lower

trimmer consists of a 1 cm thick lead "open field" insert situated immediately beneath a 0.6 cm thick layer of aluminum. The lower face of the upper trimmer has a *z*-position of 73.3 cm for the four largest applicators, and 77.2 cm for the 6x6 cm^2 applicator. The *z*-position is defined in this report as the distance along central axis from the nominal source position (i.e. 100 cm minus the distance along central axis to isocenter). The lower faces of the middle trimmer and field insert are located at *z*-positions of 86.2 and 95.0 cm, respectively, for all applicator sizes. The inner edges of all trimmer plates are vertical, except for the field insert, which is divergent at an angle of 10˚ from vertical for all field sizes.

Table 2-1. Beam characteristics and machine settings for each nominal beam energy available on the MBPCC Elekta Infinity accelerator used in this study. The jaw positions are listed as the off-axis position of the jaw projected to isocenter from the nominal source. The labels for each foil refer to the position in the tray within the accelerator head in which each foil was located (Harris, 2012).

		7 MeV	9 MeV	10 MeV	11 MeV	13 MeV	16 MeV	20 MeV
$E_{p,0}$ (MeV)		7.14	8.66	9.92	11.29	13.12	16.22	20.47
R_{90} (cm)		2.1	2.6	3.0	3.5	4.1	5.1	6.0
Primary Scattering Foil		#3	#5	#3	#4	#5	#3	#5
Secondary Flattening Foil		#3	#3	#4	#4	#4	#1	#1
In-Plane Jaw Position (cm)	6x6 cm^2	7.4	7.3	7.0	7.0	7.0	7.0	7.0
	10x10 cm^2	11.2	10.6	10.0	10.0	8.9	8.5	8.0
	14x14 cm^2	12.3	11.9	10.7	10.5	9.9	9.2	8.7
	20x20 cm^2	14.3	14.4	13.0	12.8	12.7	12.2	11.7
	25x25 cm^2	17.0	18.4	16.8	16.3	17.0	15.8	16.8
Cross-Plane Jaw Position (cm)	6x6 cm^2	8.3	8.2	8.2	7.9	7.9	7.9	7.7
	10x10 cm^2	12.1	11.5	11.2	11.2	9.8	9.7	9.0
	14x14 cm^2	13.1	12.8	11.9	11.5	10.8	10.0	9.8
	20x20 cm^2	15.3	15.4	14.2	13.6	13.5	13.0	12.8
	25x25 cm^2	18.2	19.7	18.2	17.7	18.2	17.0	17.5

2.2.1.3. Scope of Measurements

To limit the number of measurements and calculations, the present study focused on two applicators, 10x10 and 20x20 cm^2, and three beam energies, 7, 13, and 20 MeV. The 10x10 and 20x20

cm^2 applicator sizes were selected to study one small and one large applicator size, and the 7, 13, and 20 MeV beams were selected to span the range of available energies and to include a beam using each of the three secondary scattering foils. This exceeds the IEC specification that the mean and maximum percent leakage be tested for the lowest and highest available beam energies on each accelerator (1998). Therefore, the 7 and 20 MeV beams were of special interest to this investigation. Several scans were taken for both applicator sizes with each beam energy in the in-plane, cross-plane, and both diagonal directions.

2.2.1.4. Methods of Measurement

Measurements were taken to comply with guidelines for determining in-field beam flatness according to Hogstrom (1980) and patient plane leakage dose levels according to the IEC (1998). Scanned off-axis ionization profiles were measured using an OmniPro two-dimensional scanning tank with OmniPro (v.6.2) scanning software package (Scanditronix Wellhofer AB RFA 20-SERVO, Uppsala, Sweden) at depths of 1 and 2 cm in water. Two N31011 cylindrical ionization chambers (PTW, Freiburg, Germany) were used for measurement, one for scanning and one for reference. These chambers have a 0.125 cm^3 active volume with a length of 0.65 cm and an air cavity diameter of 0.55 cm. The scanning chamber was oriented with the stem situated perpendicular to both the central axis of the beam and the scanning direction. The reference chamber was attached to the applicator in the corner of the field. For the diagonal scans the reference chamber was moved to a field corner not coinciding with the scanned profile. The beam scanning system was rotated 0˚, 90˚, and ±45˚ by rotating the treatment couch to measure the in-plane, cross-plane, and diagonal profiles, respectively. Several scans of each off-axis profile were taken on several different days. The number of scans performed for each profile taken on each day is displayed in Table 2-2, with a total of 3 to 9 scans performed for each profile. The numbers in the diagonal profiles columns in this table indicate that scans were performed in both diagonal directions on that day.

Additionally, for cross-plane profiles with the 20x20 cm^2 applicator, the scans were validated by an independent measurement using a parallel plate chamber at multiple positions. Measurements were

taken at points 16 and 22 cm off-axis and 1 cm depth in solid water. The values were normalized to a central axis measurement taken at 1 cm depth for energies of 7, 13, and 20 MeV. A PTW Roos Model N34001 plane-parallel chamber (PTW, Freiburg, Germany) was used for these measurements with a Keithley model 614 electrometer (Keithley Instruments, Inc.). This chamber has an active volume of 0.35 cm^3 (1.5 cm diameter collector and 0.2 cm electrode separation).

Table 2-2. Number of measurement scans performed for each profile on each day. The total number of scans for each profile is listed on the bottom row. The numbers in the diagonal profiles columns indicate that scans were performed in both diagonal directions on that day.

	10x10 cm^2 Applicator Measurements								
	In-Plane Profile			Cross-Plane Profile			Diagonal Profiles		
	7 MeV	13 MeV	20 MeV	7 MeV	13 MeV	20 MeV	7 MeV	13 MeV	20 MeV
Jan. 18	1	1	1	1	1	1	1	1	1
Feb. 16	1	1	0	1	1	0	0	0	0
Feb. 23	1	1	1	1	1	1	0	0	0
Mar. 1	2	2	1	2	2	1	1	1	1
Aug. 2	0	0	0	0	0	0	0	0	0
Oct. 19	1	1	1	1	1	1	1	1	1
Total	6	6	4	6	6	4	3	3	3

	20x20 cm^2 Applicator Measurements								
	In-Plane Profile			Cross-Plane Profile			Diagonal Profiles		
	7 MeV	13 MeV	20 MeV	7 MeV	13 MeV	20 MeV	7 MeV	13 MeV	20 MeV
Jan. 18	1	1	1	1	1	1	1	1	1
Feb. 16	2	2	0	2	2	1	0	0	0
Feb. 23	1	1	1	1	1	1	0	0	0
Mar. 1	4	4	3	2	2	1	1	1	1
Aug. 2	1	1	1	1	1	1	1	1	1
Oct. 19	0	0	0	0	0	0	0	0	0
Total	9	9	6	7	7	5	3	3	3

2.2.1.5. Data Processing

The large number of scanned profile measurements was obtained in order to estimate the measurement error due to setup inconsistencies, detector noise, and delivered beam irregularities. The profiles were centered by shifting them such that the 50% ionization levels were equal distances from the

central axis. Each profile was normalized to the central axis ionization value at the depth of the scan. Relative dose was assumed equal to relative ionization, i.e. conversion factors from ionization to dose were assumed identical for central axis and all off-axis positions.

These multiple measurement sets were used to calculate a mean, standard deviation, and standard error of the mean value for each measurement point. For the in-field results, the mean measurement profiles were determined by averaging the measurement values at each off-axis position from all scans. These mean profiles were then symmetrized about central axis by averaging the mean profile values at each negative and positive off-axis value, i.e. averaging each measured profile with the corresponding "mirrored" profile reflected about central axis, to minimize any errors caused by beam asymmetry unrelated to the collimation system. The standard deviation and standard error of the mean (calculated as the standard deviation at each point divided by the square root of the number of scans) were obtained for the symmetrized profile at each measurement point. This was performed by first determining the standard deviation and standard error of the mean at each point from all scans before symmetrization. These pre-symmetrization standard deviation and standard error of the mean values were then summed in quadrature with the values at their corresponding mirrored positions (i.e. negative off-axis positions) to obtain the standard deviation and standard error of the mean of each point in the symmetrized profile.

For the out-of-field results, no symmetrization was performed. The mean profiles were determined by averaging the measurement values at each off-axis position from all scans. The standard deviation and standard error of the mean values were also calculated from all measurements taken at each off-axis position.

2.2.2. Monte Carlo Model of Elekta Infinity

A MC model was created by Harris (2012) to model the electron therapy beams of the MBPCC configuration of its Elekta Infinity accelerators. The treatment head was modeled using BEAMnrc (Rogers *et al.*, 2011), based on manufacturer schematics of component geometries and materials, provided under a non-disclosure agreement. Simulations were performed using EGSnrc (Kawrakow *et*

al., 2011), and dose calculations were performed using DOSXYZnrc (Walters *et al.*, 2011). A cross-sectional image of the accelerator is shown in Figure 2-1, with the collimation components labelled.

Harris previously validated the model versus measurement for in-field dose calculations for all beam energies and applicators. Results were reported for cross-plane profiles taken at various depths for the 6x6, 14x14, and 25x25 cm^2 applicators, as well as in-plane results for the 25x25 cm^2 applicator. The depths selected for reporting results varied with applicator size, but ranged from 0.5 to 5.5 cm for the 7 MeV beam, from 0.5 cm to 8.5 cm for the 13 MeV beam, and from 0.5 to 12.1 cm for the 20 MeV beam. Additionally, results for the diagonal profiles were reported for the 25x25 cm^2 applicator at depths of 1 cm for the 7 MeV beam and 2 cm for the 13 and 20 MeV beams.

Harris initially tested the accuracy of the MC calculations at each calculation point using a specified distance to agreement criteria of 3mm and 3% (written as 3 mm/3%). According to this criterion for each calculation point position, if the measured dose falls within ±3% of the calculated dose at that position, the calculation point is deemed to pass criteria. Additionally, if any point within ±3 mm of the calculation point along the measured dose profile has the same dose as the calculation point, the calculation point is deemed to pass criteria. If neither of these scenarios is true, the calculation point fails the distance to agreement criteria. Using this criteria Harris was able to achieve 100% of points passing for all in-plane and cross-plane profiles for the 7, 13, and 20 MeV beams with the 25x25 cm^2 applicator. When the distance to agreement criteria was tightened to 2 mm/2%, at least 93% of points passed criteria for all profiles (93.1% of point passed for the 7 MeV cross-plane profile at 1 cm depth), and 24 of the 30 profiles maintained greater than 99% of points passing. For diagonal profiles the reported accuracy was somewhat diminished, with 100.0%, 96.5%, and 92.3% of points passing a distance to agreement criteria of 3 mm/3% for the 7, 13, and 20 MeV beams, respectively. The accuracy was reported to only improve with smaller field sizes. For the 6x6 and 14x14 cm^2 applicators, 100.0% of points passed a 1 mm/2% criteria for all profiles near the surface and 100.0% of points passed a 2 mm/2% criteria for all profiles at all depths (Harris, 2012).

2.2.2.1. BEAMnrc Model and Source Parameters

The treatment head components incorporated into the model (geometry and material composition) include the: nickel vacuum exit window, primary scattering foil, primary collimator, secondary flattening foil, ionization monitor chambers, light field mirror, MLC, upper and lower photon jaws, Mylar exit window, attachment base plate, applicator trimmer bars, and the applicator field insert. The locations of many of these components can be seen in Figure 2-1. Due to lack of information of their specifications and/or complex geometries, some components were neglected from the model, most notably the structural components of the applicator which attach the lower and upper trimmers and the electrical components which serve to trigger the beam interlock system if the applicator is interfered with during treatment. Because these materials are mostly present between the middle and lower trimmers in the in-plane dimension, omitting them from the model may cause an over-prediction in dose in the in-plane profiles from electrons scattered between these two trimmers.

The source was modeled as an elliptical beam with a Gaussian spatial distribution with a FWHM of 0.2 cm in the in-plane direction and 0.1 cm in the cross-plane direction. The beam was assumed perpendicularly incident on the vacuum exit window with no angular spread. The energy spectrum of the incident beam was assumed to be Gaussian in shape, with the peak energy, FWHM of the energy, and the energy distribution limits being unique for each beam. These source parameters are shown in Table 2-3 for each of the three energy beams studied (Harris, 2012). For the nominal 7, 13, and 20 MeV beams, the simulations were performed with $9x10^8$, $4.5x10^8$, and $3x10^8$ histories, respectively, for the calculations.

Table 2-3. Incident particle energy spectra used for BEAMnrc MC calculations from Harris (2012).

Beam Energy (MeV)	Peak Spectrum Energy (MeV)	Spectrum FWHM (% of Peak Energy)	Limits of Distribution (FWHM = 2.355σ)
7	7.8	20	-3.0σ to +3.0σ
13	14	15	-3.0σ to +3.0σ
20	22	15	-3.0σ to +1.5σ

2.2.2.2. Transport Parameters and Dose Calculation

For these MC calculations, the boundary crossing algorithm was set to PRESTA-I and the electron step algorithm was set to PRESTA-II within BEAMnrc. Spin effects were turned on and the maximum fractional energy loss was set to 0.25. The global cutoff energy was set to 0.521 MeV for electrons and 0.01 MeV for photons.

Data were scored at a *z*-position of 99 cm to create a phase space file. The phase space file stores the particle type, position, trajectory, and energy information of every particle which reaches the *z* planar height at which the phase space is scored. To calculate the dose, this phase space file was used as input to DOSXYZnrc, which samples the particles in the phase space file as a source. 10^9 particles were sampled for each of these dose calculations and transported through 1 cm of air into a water tank at 100 cm SSD. Dose was calculated in voxels within the water tank centered at depths of 1 cm (extending from 0.75 cm to 1.25 cm depth) and 2 cm (extending from 1.75 to 2.25 cm depth) with dimensions of 0.5x0.5x0.5 cm^3. At each of these depths, a horizontal voxel matrix was created in which the centers of the voxels spanned from -24.5 to 24.5 cm off-axis in both the in-plane and cross-plane dimensions. In the DOSXYZnrc model, all transport parameters were maintained from the BEAMnrc model, including the boundary crossing algorithm, electron step algorithm, spin effects setting, fractional energy loss, and global energy cutoffs. To reduce statistical uncertainty, the dose distributions were symmetrized in both the in-plane and cross-plane dimensions by reflecting them about central axis. Each profile was normalized to the mean dose calculated within a 3x3 set of voxels centered at central axis at the calculation depth of the profile.

2.2.2.3. Bit Filtering

To gain further insight into the sources of the leakage dose, the LATCH bit filtering feature in EGSnrc was used to calculate dose from particles which interacted within various components of interest. This bit filtering feature allows a particle to be tagged with a particular component's LATCH bit if the particle interacts with that component. This enables the user to distinguish particles scattered from "latched" beam components and calculate their dose independently. Additionally, this feature allows

electron dose to be distinguished from photon dose. Bit filtering was used to analyze the dose due to electrons scattered from particular collimation components, including the: MLC, cross-plane jaw, in-plane jaw, and upper, middle, and lower trimmers. Additionally, the total photon dose, total electron dose, and primary electron dose were independently calculated. Dose components were calculated using DOSXYZnrc using the same phantom setup and phase space file inputs as the total dose calculation. Due to the large number of dose calculations performed, the number of particles used in the LATCH bit dose calculations was reduced from 10^9 to $2.5x10^8$.

These bit filtered calculations were performed for the 20x20 cm^2 applicator at energies of 7, 13, and 20 MeV. Mean percent leakage dose values were calculated for each component based on IEC specifications. This LATCH bit filtering methodology is similar to that used by Ebert and Hoban (1995a), though that study focused primarily on the effects of scattered electrons on the in-field distribution.

2.3. Aim 1 - Results and Discussion

2.3.1. Quality of Measured Data

Between three and nine scanned profiles were measured for each energy applicator combination in the in-plane, cross-plane, and both diagonal directions (c.f. Table 2-2). Both the standard deviation and standard error of the mean were calculated at each measurement point. The standard deviation was found to vary between roughly 0.07% and 0.15% both within the field and in the out-of-field leakage region. The standard deviation values for measurement points within the field for all scans were found to have a mean value of 0.157% and a standard deviation of 0.047%. Outside the field, the standard deviation values for all measurement points were found to have a mean value of 0.111% and a standard deviation of 0.020%.

The standard error of the mean was also determined for each measurement point and was found to vary between roughly 0.04% and 0.09%. The standard error of the mean values for measurement points within the field for all scans had a mean value of 0.066% and a standard deviation of 0.020%. Outside the field, the standard deviation values for all measurement points had a mean value of 0.037% and a

standard deviation of 0.009%. These small errors were assumed to be due to measurement system noise and beam variation between scans.

These variations were much larger in the steep penumbral region, where the standard deviation values were found to be as high as 2% and the standard error of the mean values as high as 0.6%. These large standard deviations and standard error of the mean values in the penumbral region were attributed to alignment error.

2.3.2. In-Field Results

2.3.2.1. Comparison of In-Field MC-Calculated and Measured Data

The measured and MC-calculated major axes profiles are plotted versus off-axis position within the field in Figures 2-2 and 2-3 for the 20x20 and 10x10 cm^2 applicators, respectively. The cross-plane profiles are shown in the left column, and the in-plane profiles are shown in the right column for the 7, 13 and 20 MeV beams. Additionally, the in-field diagonal profiles are shown in Figures 2-4 and 2-5 for the 20x20 and 10x10 cm^2 applicators, respectively, for the 7, 13, and 20 MeV beams. In Figures 2-4 and 2-5 the positive diagonal profiles, shown in the left column of plots, refer to measurement scans taken in the diagonal direction which extends from the negative in-plane (towards gantry) and negative cross-plane (to the left when facing the gantry) quadrant to the positive in-plane (away from gantry) and positive cross-plane (to the right when facing the gantry) quadrant. The negative diagonal profiles, shown in the right column, refer to measurements scans which run perpendicular to the positive diagonal profiles. These scans extend from the positive in-plane and negative cross-plane quadrant, to the negative in-plane and positive cross-plane quadrant. The 7 MeV profiles in these figures were measured at 1 cm depth, and the 13 and 20 MeV profiles were measured at 2 cm depth. These depths were selected for plotting for each beam energy to be consistent with the criteria for evaluating in-field beam flatness (Hogstrom, 2004). The error bars show the standard error of the mean calculated at each measurement point. The MC profiles in these figures have uncertainty values of roughly 0.09% of central-axis dose.

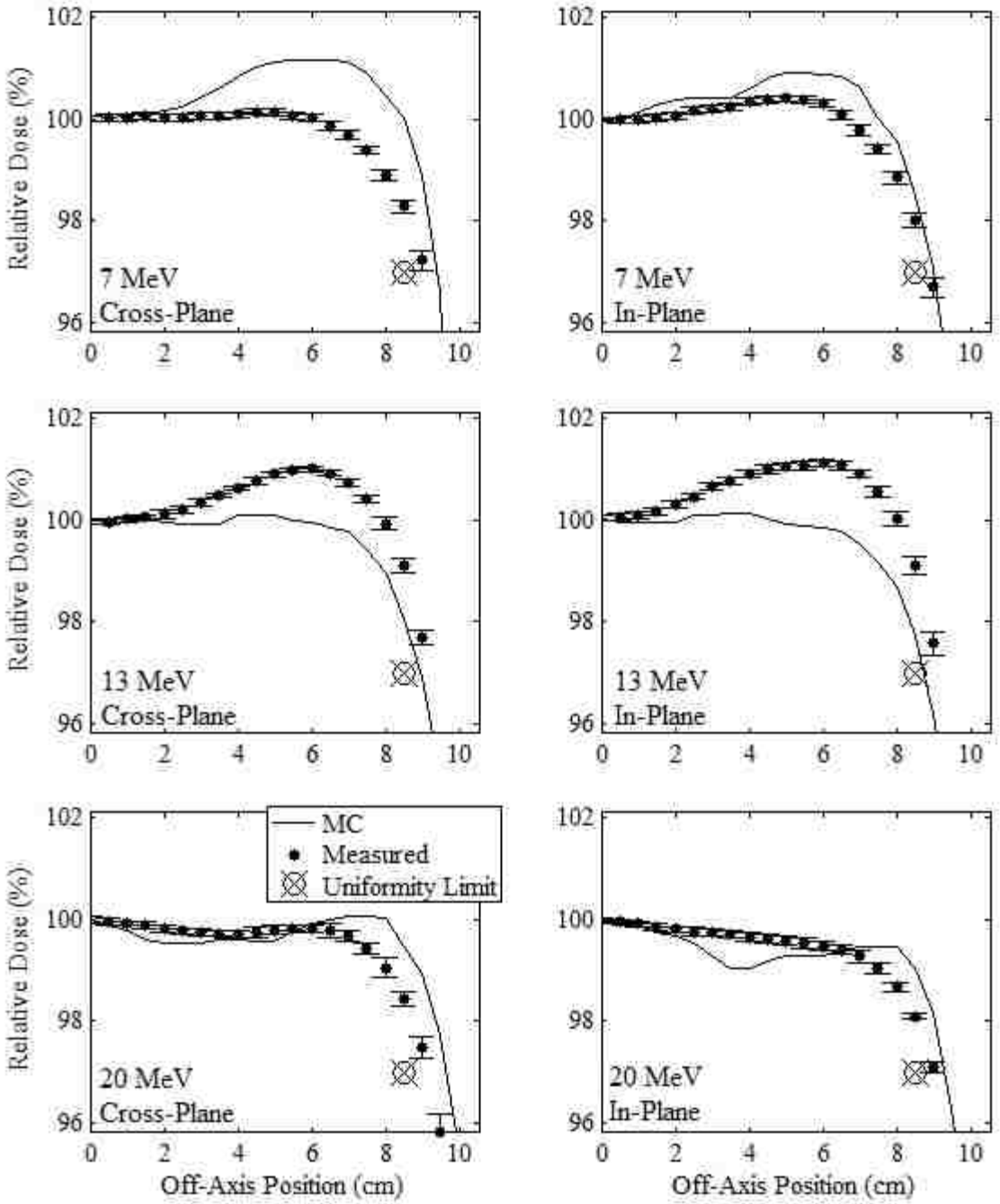

Figure 2-2. Comparison of measured and MC calculated major axes profiles of relative dose versus off-axis position in the field for the 20x20 cm^2 applicator. Cross-plane and in-plane profiles are compared at beam energies of 7 (upper row), 13 (middle row), and 20 MeV (lower row). The solid circular markers represent the measured profiles. The error bars indicate the standard error of the mean for each measurement point. The uniformity limit marker (⊗) represents the minimum value that the profile can have at the edge of the field in order to pass the flatness criteria. The 7 MeV beam profiles were measured at 1 cm depth in water, and the 13 and 20 MeV profiles were measured at 2 cm depth.

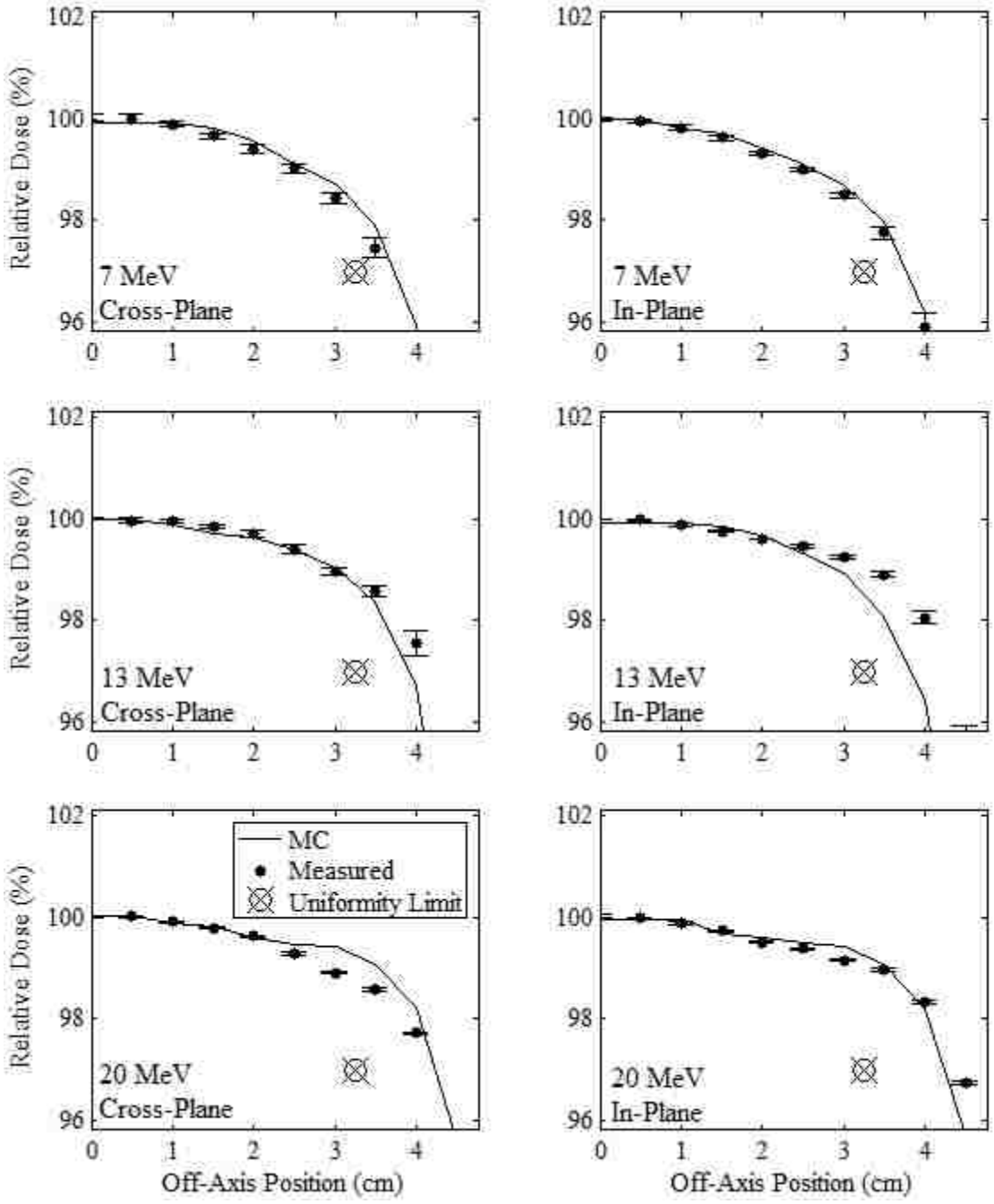

Figure 2-3. Comparison of measured and MC calculated major axes profiles of relative dose versus off-axis position in the field for the 10x10 cm^2 applicator. Cross-plane and in-plane profiles are compared at beam energies of 7 (upper row), 13 (middle row), and 20 MeV (lower row). The solid circular markers represent the measured profiles. The error bars indicate the standard error of the mean for each measurement point. The uniformity limit marker represents (⊗) the minimum value that the profile can have at the edge of the field in order to pass the flatness criteria. The 7 MeV beam profiles were measured at 1 cm depth in water, and the 13 and 20 MeV profiles were measured at 2 cm depth.

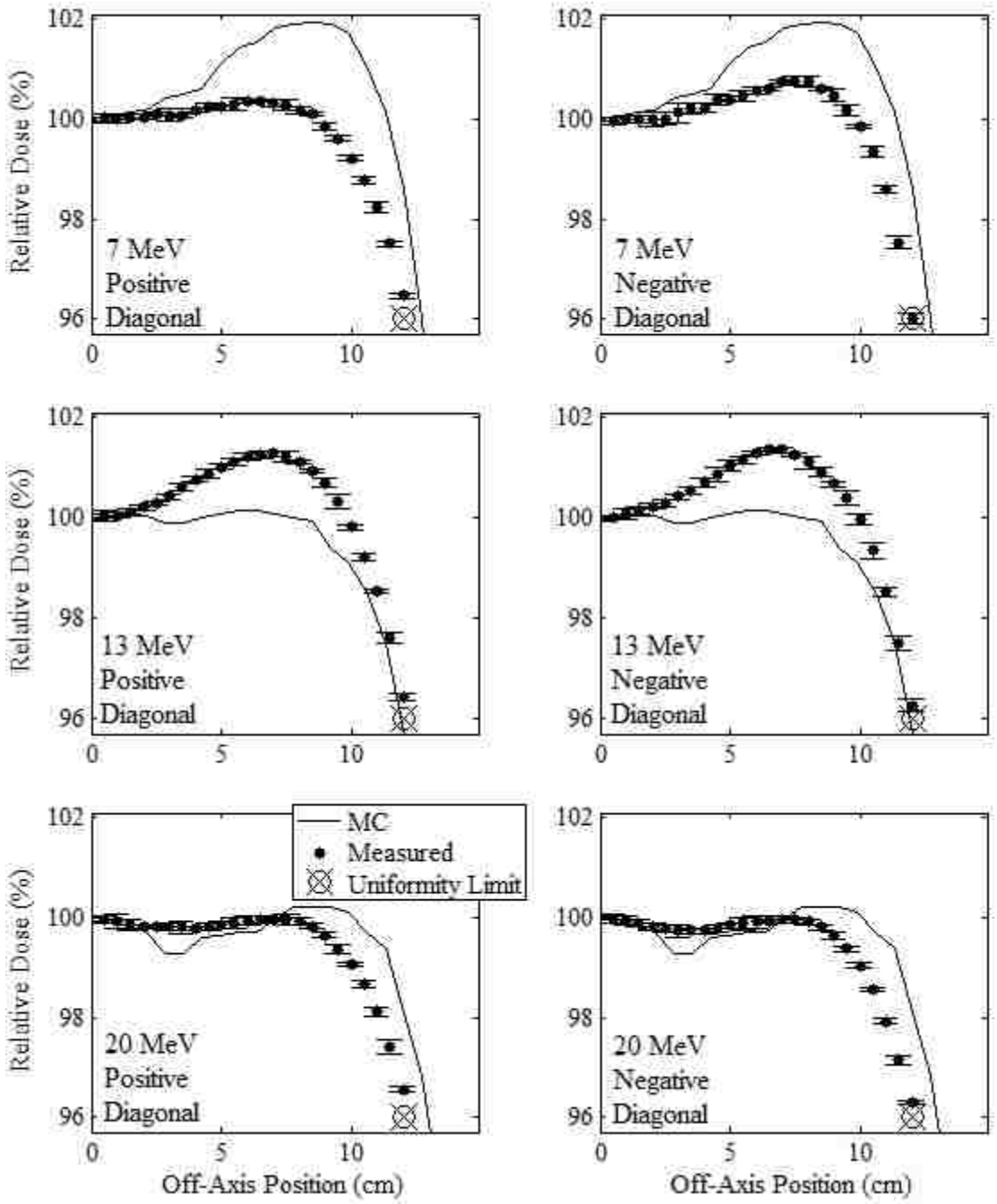

Figure 2-4. Comparison of measured and MC calculated diagonal profiles of relative dose versus off-axis position in the field for the 20x20 cm^2 applicator. Positive and negative diagonal profiles are compared at beam energies of 7 (upper row), 13 (middle row), and 20 MeV (lower row). The solid circular markers represent the measured profiles. The error bars indicate the standard error of the mean for each measurement point. The uniformity limit marker (⊠) represents the minimum value that the profile can have at the edge of the field in order to pass the flatness criteria. The 7 MeV beam profiles were measured at 1 cm depth in water, and the 13 and 20 MeV profiles were measured at 2 cm depth.

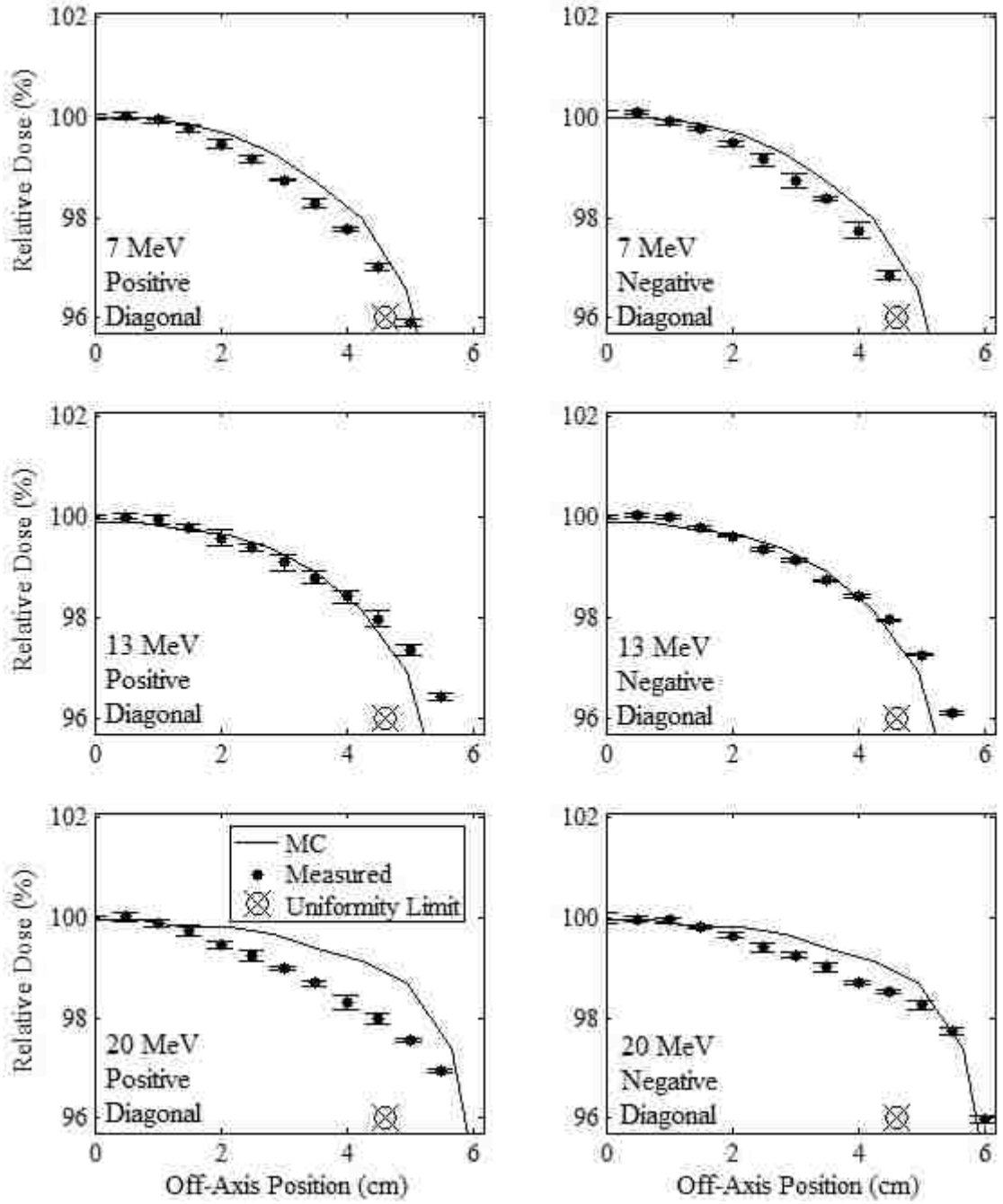

Figure 2-5. Comparison of measured and MC calculated diagonal profiles of relative dose versus off-axis position in the field for the 10x10 cm^2 applicator. Positive and negative diagonal profiles are compared at beam energies of 7 (upper row), 13 (middle row), and 20 MeV (lower row). The solid circular markers represent the measured profiles. The error bars indicate the standard error of the mean for each measurement point. The uniformity limit marker (⊠) represents the minimum value that the profile can have at the edge of the field in order to pass the flatness criteria. The 7 MeV beam profiles were measured at 1 cm depth in water, and the 13 and 20 MeV profiles were measured at 2 cm depth.

The figures show that the MC calculations over-predict the in-field measured dose at the field edge for both the 7 and 20 MeV beams, with the 7 MeV beam having the greater discrepancy, being as great as 2.59% at the edge of the uniformity region (i.e. the region over which field flatness is evaluated). For the 13 MeV beam, the MC calculations under-predict the measured dose, with a maximum discrepancy of 1.60% at the edge of the uniformity region. These results are consistent with the findings of Harris (2012) for the in-field matching of MC-calculated and measured data near the surface.

The percentage differences in the MC minus measured data are shown in Table 2-4, calculated at the outermost boundary of the uniformity region per criteria outlined by Hogstrom (2004) and AAPM Task Group 25 (Khan *et al.*, 1991) (2 cm inside the edge of the field for the major axes and $2\sqrt{2}$ cm for the diagonals). These values will be used in Aim 5 to account for inaccuracies in the MC calculations performed during the design of the prototype collimation system. The values in this table confirm that the MC data over-predicts the measured data for the 7 and 20 MeV beams, and under-predicts the measured data for the 13 MeV beam. The diagonal profile difference values were calculated as the mean of the differences in the negative diagonal measured profile with MC data and the positive diagonal measured profile with MC data.

Table 2-4. MC calculated minus measured percent dose differences calculated at the edge of the uniformity region. The percent differences were calculated at an off-axis position 2 cm inside the edge of the field for the in-plane and cross-plane profiles, and $2\sqrt{2}$ cm for the diagonal profiles. The diagonal profile values shown are the means of the differences in the negative diagonal measured profile with MC and the positive diagonal measured profile with MC.

	Beam Energy	In-Plane Profiles	Cross-Plane Profiles	Diagonal Profiles
10x10 cm^2 Applicator	7 MeV	0.21	0.37	0.77
	13 MeV	-0.57	-0.09	-0.31
	20 MeV	0.19	0.50	1.14
20x20 cm^2 Applicator	7 MeV	0.51	1.74	2.59
	13 MeV	-1.40	-1.06	-0.60
	20 MeV	0.93	1.40	2.20

2.3.2.2. Evaluation of Collimation System Field Flatness

Figures 2-2 through 2-5, show the flatness of the beam within the field. In these figures, the uniformity limit marker represents the minimum value that the profile can have at the edge of the uniformity region in order to pass the flatness criteria as outlined by Hogstrom (2004). These markers are positioned at the edge of the uniformity region (2 cm inside the edge of the field for the major axes and $2\sqrt{2}$ cm for the diagonals) and at relative dose values of 3% and 4% less than the central-axis dose for the major axes and diagonal axes, respectively (i.e. relative dose values of 97% and 96%, respectively). These 3% and 4% variations are obtained from the maximum allowed variations from central-axis dose for the major axes and diagonal profiles, respectively. Profiles which pass above and outside this marker are deemed acceptably flat with respect to the minimum dose specification in the uniformity region. Figures 2-2 through 2-5 show that this is true for all measured profiles, indicating that all investigated measured beams passed beam flatness minimum dose criteria at this off-axis position. Also, the plots show the maximum off-axis relative doses are less than 101.5% for all measured profiles, well within the major axes flatness maximum dose of 103%, indicating that all investigated measured beams passed flatness maximum dose criteria.

2.3.3. Out-of-Field Results

2.3.3.1. Comparison of Out-of-Field MC-calculated and Measured Data

The measured and MC-calculated major axes profiles are plotted versus off-axis position in the leakage region for comparison in Figures 2-6 and 2-7 for the 20x20 and 10x10 cm^2 applicators, respectively. The parallel plate ionization chamber spot measurements for the 20x20 cm^2 applicator in the cross-plane dimension are also plotted versus position in Figure 2-6 and are shown to agree well with the cylindrical ionization chamber measurements. Additionally, the measured and calculated diagonal dose profiles are plotted versus off-axis position and compared shown in Figures 2-8 and 2-9 for the 20x20 cm^2 and 10x10 cm^2 applicators, respectively. The MC-calculated data agree well with the

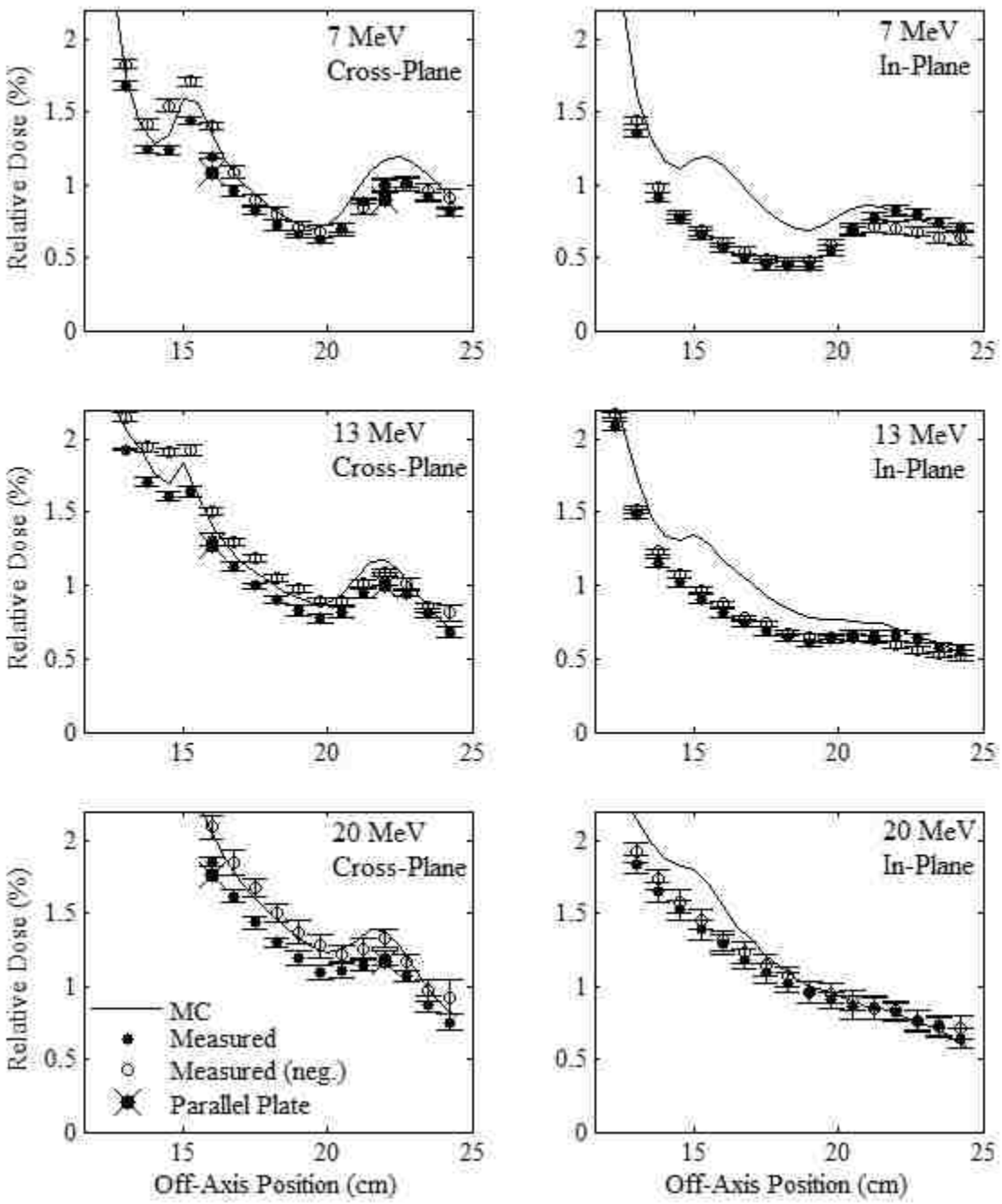

Figure 2-6. Comparison of measured and MC calculated major axes profiles of relative dose versus off-axis position in the out-of-field region for the 20x20 cm^2 applicator. In-plane and cross-plane profiles are compared at beam energies of 7 (upper row), 13 (middle row), and 20 MeV (lower row). The solid circular markers, ●, represent the profiles measured with the cylindrical ionization chamber. The open circular markers, ○, represent the same profiles, mirrored about central axis, such that each point is plotted against its negative off-axis position. The error bars indicate the standard error of the mean for each measurement point. The parallel plate validation measurements are shown for the cross-plane profiles.

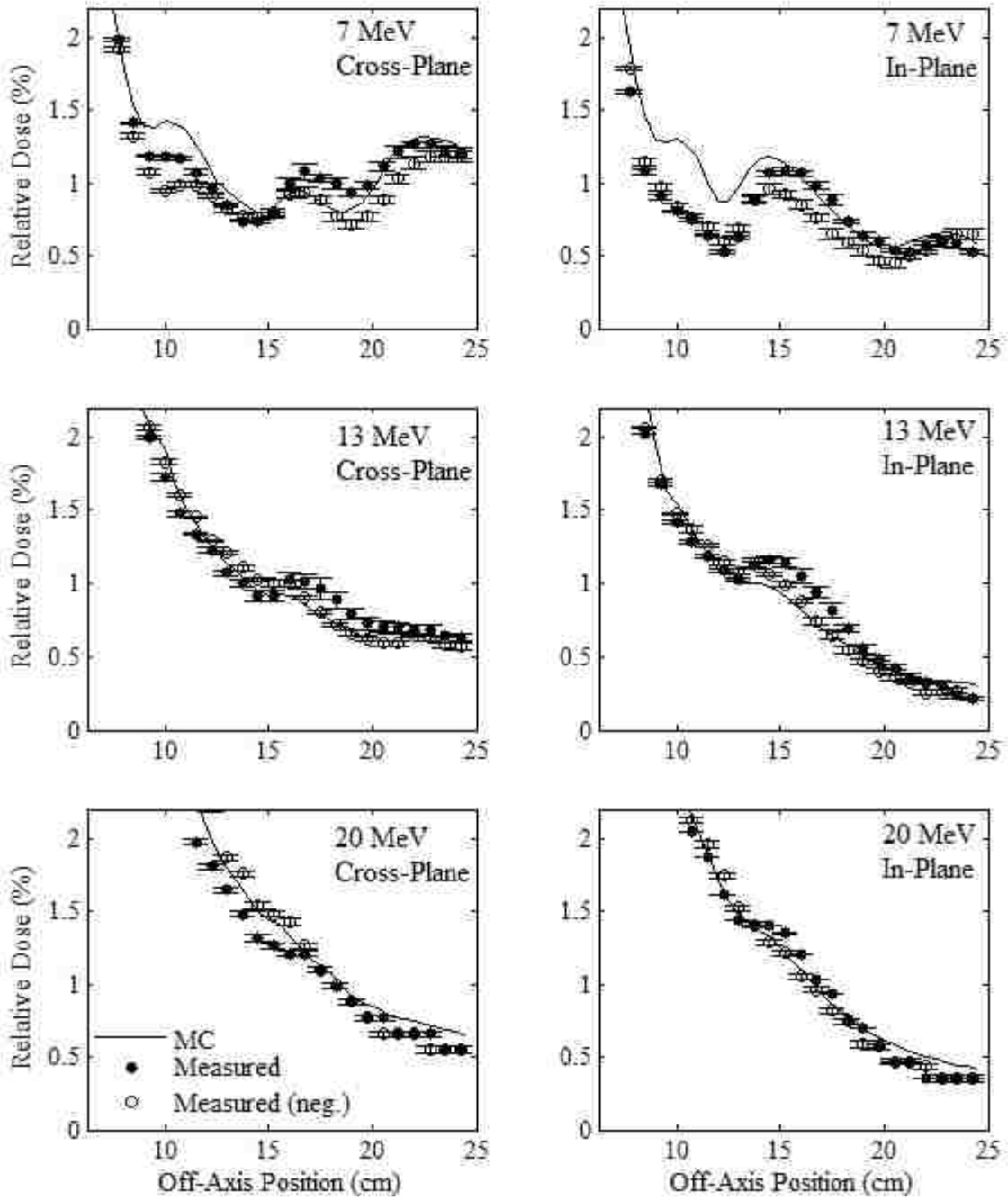

Figure 2-7. Comparison of measured and MC calculated major axes profiles of relative dose versus off-axis position in the out-of-field region for the 10x10 cm^2 applicator. In-plane and cross-plane profiles are compared at beam energies of 7 (upper row), 13 (middle row), and 20 MeV (lower row). The solid circular markers, ●, represent the measured profiles. The open circular markers, ○, represent the same profiles, mirrored about central axis, such that each point is plotted against its negative off-axis position. The error bars indicate the standard error of the mean for each measurement point.

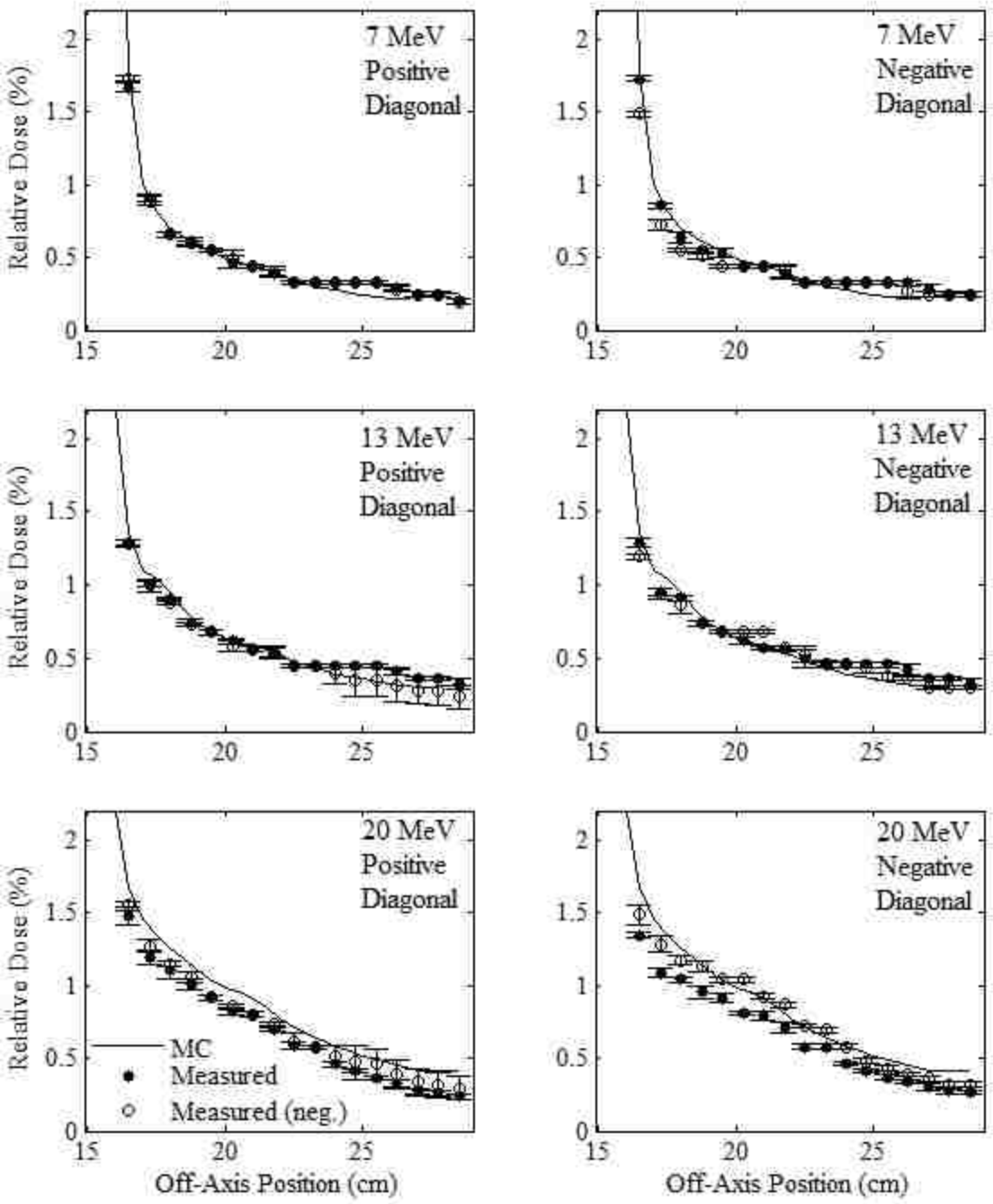

Figure 2-8. Comparison of measured and MC calculated major axes profiles of relative dose versus off-axis position in the out-of-field region for the 20x20 cm^2 applicator. Positive diagonal and negative diagonal profiles are compared at beam energies of 7 (upper row), 13 (middle row), and 20 MeV (lower row). The solid circular markers, ●, represent the measured profiles. The open circular markers, ○, represent the same profiles, mirrored about central axis, such that each point is plotted against its negative off-axis position. The error bars indicate the standard error of the mean for each measurement point.

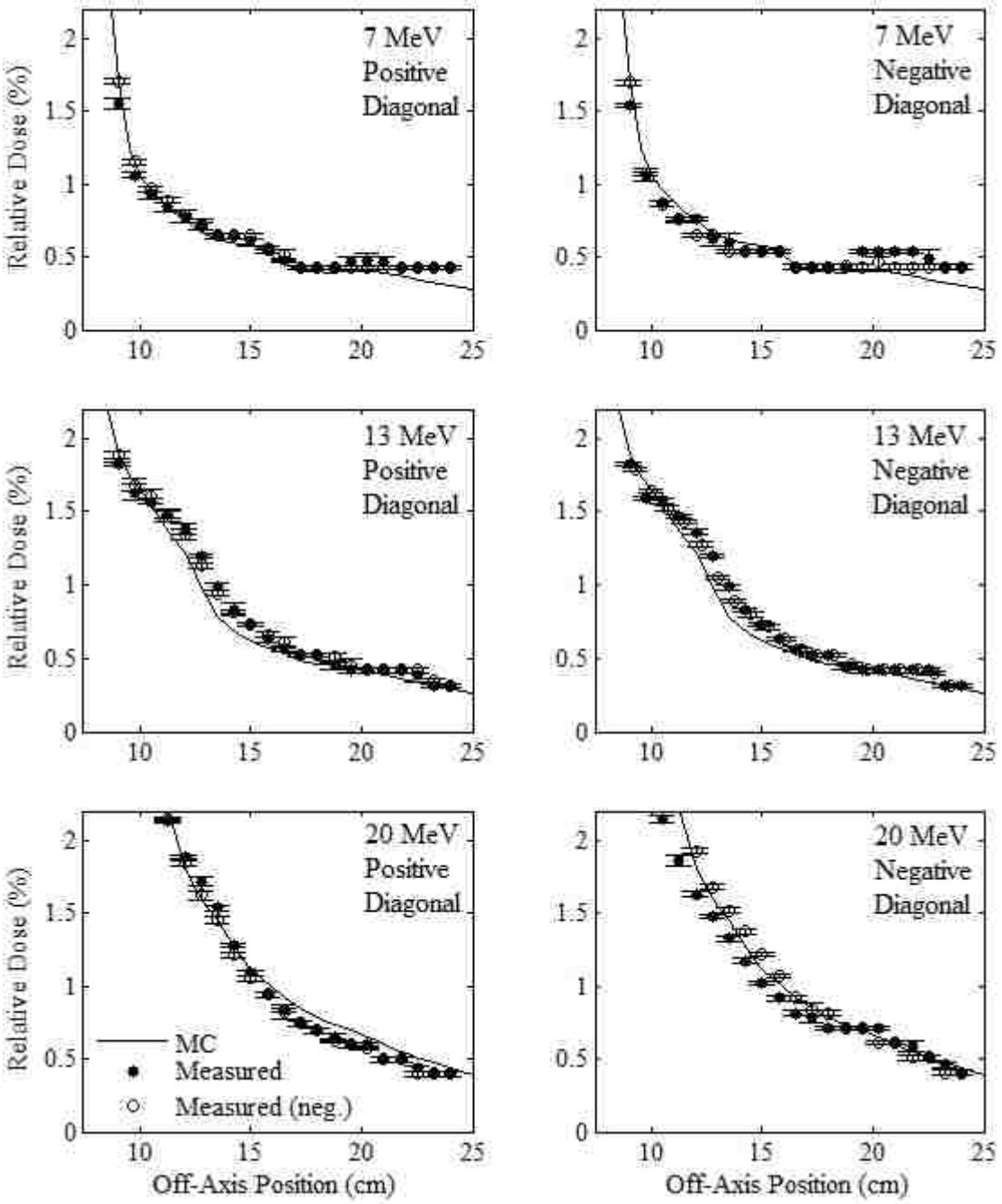

Figure 2-9. Comparison of measured and MC calculated major axes profiles of relative dose versus off-axis position in the out-of-field region for the 10x10 cm^2 applicator. Positive diagonal and negative diagonal profiles are compared at beam energies of 7 (upper row), 13 (middle row), and 20 MeV (lower row). The solid circular markers, ●, represent the measured profiles. The open circular markers, ○, represent the same profiles, mirrored about central axis, such that each point is plotted against its negative off-axis position. The error bars indicate the standard error of the mean for each measurement point.

measured data in all regions other than the in-plane profiles near the edge of the field. This discrepancy is attributed to the structural and electrical components along the in-plane side of the applicator being omitted from the model. The MC profiles in these figures have uncertainty values of roughly 0.01% of central-axis dose.

Table 2-5 shows the minimum and maximum differences of the MC-calculated minus measured relative dose (expressed as [minimum difference, maximum difference]) for each profile in the leakage region. The data confirm that the MC-calculations significantly over-predicted the measured data in the in-plane dimension, with a maximum difference of 0.56%, which is again attributed to the structural andelectrical components along the in-plane side of the applicator being omitted from the MC model. For all other profiles the MC-calculations agree with the measured data within 0.26%. This level of agreement is similar to a previous study by Shimozato *et al.* (2012) in which MC calculations using a BEAMnrc model was compared with cylindrical ionization chamber measurements in the same region for a Varian Clinac 2100CD accelerator, which had a maximum difference of 0.23% for a 10x10 cm^2 applicator in the leakage region.

Table 2-5. Minimum and maximum differences of the MC-calculated minus measured relative dose for each off-axis profile in the leakage region (expressed as [minimum difference, maximum difference]). Values are calculated as a percent of central-axis dose at 1 cm depth.

Profile Dimensions	10x10 cm^2 Applicator		
	7 MeV	13 MeV	20 MeV
In-Plane	[-0.07%, 0.50%]	[-0.24%, 0.13%]	[-0.15%, 0.20%]
Cross-Plane	[-0.19%, 0. 24%]	[-0.18%, 0.17%]	[-0.25%, 0.26%]
Diagonal (Pos)[a]	[-0.18%, 0.05%]	[-0.13%, 0.02%]	[-0.10%, 0.13%]
Diagonal (Neg)[b]	[-0.13%, 0.00%]	[-0.14%, 0.01%]	[-0.02%, 0.13%]
	20x20 cm^2 Applicator		
	7 MeV	13 MeV	20 MeV
In-Plane	[-0.05%, 0.56%]	[-0.01%, 0.41%]	[-0.04%, 0.33%]
Cross-Plane	[-0.07%, 0.20%]	[-0.14%, 0.16%]	[-0.10%, 0.22%]
Diagonal (Pos)[a]	[-0.07%, 0.01%]	[-0.08%, -0.01%]	[-0.07%, 0.12%]
Diagonal (Neg)[b]	[-0.07%, 0.02%]	[-0.07%, 0.03%]	[0.01%, 0.12%]

[a] Positive diagonal profile extends from negative in-plane and cross-plane quadrant to positive in-plane and cross-plane quadrant

[b] Negative diagonal profile runs perpendicular to positive diagonal profile

2.3.3.2. Evaluation of Collimation System Leakage Levels

Mean leakage levels at the patient plane were calculated for each beam according to the procedure specified by the IEC (c.f. Section 1.3.2). The analysis reveals that the accelerator met IEC specified limits for mean leakage for all beam energies and applicators studied. Table 2-6 shows these results for both the MC-calculated and measured data. The percentages shown in this table are normalized to D_{max}, the dose at R_{100} on central axis, as specified by the IEC, calculated by multiplying the mean leakage dose normalized to central axis dose at 1 cm depth by the PDD at 1 cm depth in water.

Table 2-6. Mean percent leakage doses calculated per IEC specifications for MC-calculated and measured off-axis profiles. Values displayed are calculated as percent of D_{max}. The far right column shows the maximum mean percent leakage dose value allowed by the IEC for nominal particular beam energy (calculated using $E_{p,0}$ for each beam).

Beam Energy (MeV)	Monte Carlo		Measured		Differences (MC - Measured)		IEC-Specified Maximum % Mean Leakage
	10x10 cm^2	20x20 cm^2	10x10 cm^2	20x20 cm^2	10x10 cm^2	20x20 cm^2	
7	0.70	0.67	0.66	0.56	0.04	0.11	1.00
13	0.65	0.69	0.67	0.65	-0.02	0.04	1.10
20	0.99	0.93	0.93	0.85	0.06	0.08	1.34

Additionally, the maximum leakages were determined by IEC guidelines for all energy-applicator combinations studied and are listed in Table 2-7. These percentages are normalized to D_{max}, as specified by the IEC. This investigation revealed that the maximum leakage for all beams was significantly below the IEC specified threshold of 10%. The maximum dose found for all beams was 4.38% for the MC-calculated data and 4.09% for the measured data. These maxima were found in the cross-plane profile of the 20 MeV beam with the 10x10 cm^2 applicator.

Table 2-7. Maximum percent leakage doses calculated per IEC specifications for MC-calculated and measured off-axis profiles. Values displayed are calculated as percent of D_{max}.

Beam Energy	Monte Carlo		Measured	
	10x10 cm^2	20x20 cm^2	10x10 cm^2	20x20 cm^2
7 MeV	2.11	1.65	2.14	1.74
13 MeV	2.75	1.95	2.78	2.03
20 MeV	4.38	2.83	4.09	2.73

Comparing our 7 and 13 MeV Elekta leakage dose profiles for the 10x10 cm^2 applicator to 6 and 12 MeV leakage dose profiles reported by Shimozato *et al.* (2012) for the Varian Clinac 2100CD showed Elekta leakage doses to be greater. Because Shimozato *et al.*'s profiles were measured at 0.5 cm depth, comparing to our profiles at 1.0 cm depth required their being scaled by the ratios of dose at a depth of 1.0 cm to that at 0.5 cm (≈0.7 and 0.8 at 15 cm off-axis for Varian 6 and 12 MeV beams, respectively, using preliminary measured data reported by Cardenas *et al.* (2015)). At 20 cm off-axis the Elekta in-plane and cross-plane leakage doses were approximately 2 and 4 times, respectively, those of Shimozato *et al.* comparing 7 and 6 MeV beams, and approximately equal and 2 times, respectively, those of Shimozato *et al.* comparing 13 and 12 MeV beams. Comparing our 7, 13, and 20 MeV Elekta leakage dose profiles at 15-25 cm off-axis for the 10x10 cm^2 and 20x20 cm^2 applicators to 6, 12, and 18 MeV leakage dose profiles reported by Yeboah *et al.* (2010) for the Siemens EA200 electron applicators showed Elekta leakage doses to be less for most cases. At 7 MeV Elekta leakage doses were comparable to Yeboah *et al.*'s leakage doses, except for being approximately 2.5 times greater 25 cm off-axis for the 10x10 cm^2 applicator and 15 cm off-axis for the 20x20 cm^2 applicator. At 20 MeV Elekta leakage doses were always less, being approximately 0.25-0.5 those of Yeboah *et al.* for the 10x10 cm^2 applicator and 0.2-0.6 those for the 20x20 cm^2 applicator; at 13 MeV Elekta leakage doses were 0.4-1.0 those of Yeboah *et al*. The differences in magnitude and shape of the leakage dose profiles for different manufacturers illustrate the impact that differences in collimation systems (x-ray jaws and applicators) can have.

2.3.4. Leakage Dose Component Analysis

A MC study was performed using the LATCH bit filtering feature of EGSnrc to quantify various components of the leakage dose for the 20x20 cm^2 applicator for the 7, 13 and 20 MeV beams. The study calculated the leakage dose distributions from ten different dose components. These components include: total leakage dose, total electron leakage, total photon leakage, and primary electron leakage, along with dose due to electrons scattered from the MLC, upper jaw, lower jaw, and the upper, middle, and lower trimmers of the applicator.

Figures 2-10 and 2-11 display the results of this study. For the 20x20 cm^2 applicator, the cross-plane leakage component profiles are plotted versus off-axis position in Figure 2-10 and the in-plane profiles are plotted versus off-axis position in Figure 2-11. The upper, middle, and lower rows of plots show the results for the 7, 13, and 20 MeV beams, respectively. In these figures, the left column of plots depicts the total leakage dose, along with its two components, the total electron component and total photon component, for each beam energy. The results indicate that electrons are the primary contributor to leakage dose, though less so for higher energy beams.

The right column of plots further magnifies the low dose region and breaks down the electron leakage dose into contributions from primary electrons and from electrons scattered from various collimation components. The calculated profiles reveal that the primary electron dose is small, particularly at 13 and 20 MeV, indicating that the large majority of the total electron dose comes from particles which interacted in the collimating system. However, further investigation would be required to determine what portion of this total electron dose is due to electrons scattered from the edges of the collimation system and from electrons produced within the collimation system by photons undergoing photoelectric, Compton, or pair production interactions.

The scatter off the lower and middle trimmers increases with energy. This was attributed to the increased range of the higher energy particles, allowing more electrons to escape the edges of the collimation component. However, this was not the case for the upper trimmer, as the scatter off this trimmer decreased with increasing beam energy. It is suspected that this effect is caused by the variation of jaw position with beam energy. For higher beam energies, the Elekta Infinity collimation system positions the photon jaws closer to central axis. For example, the in-plane jaw is positioned 7.4 cm from central axis for the 7 MeV beam with the 20x20 cm^2 applicator, but moved to 6.0 cm off-axis for the 20 MeV beam with the same applicator. This adjustment causes fewer electrons to interact with the upper trimmer for higher energy beams.

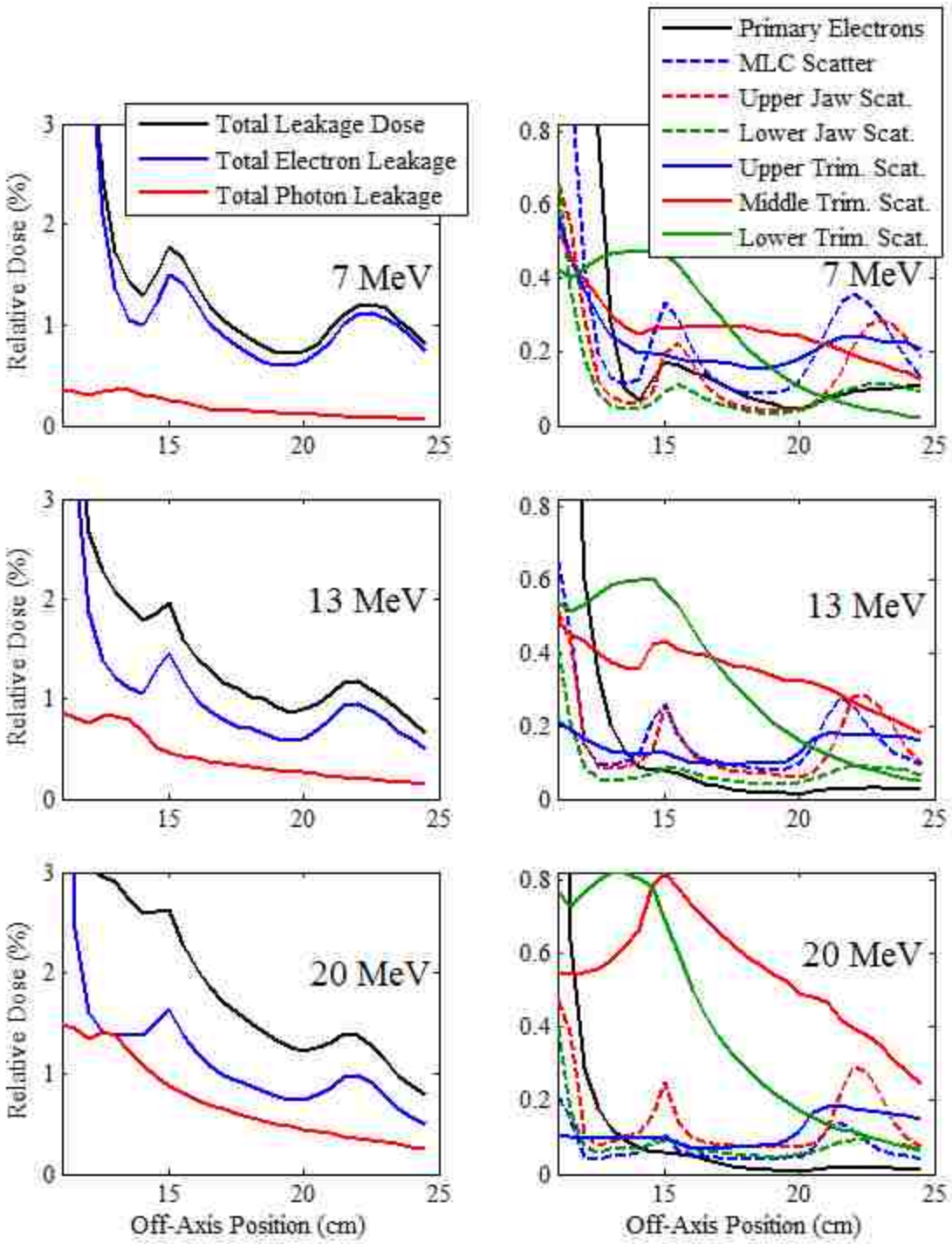

Figure 2-10. Cross-plane leakage dose component profiles for the 20x20 cm^2 applicator. 7 MeV beam profiles are shown on the top row, 13 MeV in the middle, and 20 MeV profiles on the bottom row. The left column of plots show a breakdown of the total leakage dose (black) along with the differentiated electron (blue) and photon components (red). The right column further breaks down the electron leakage dose into primary electrons and various scattered electron components.

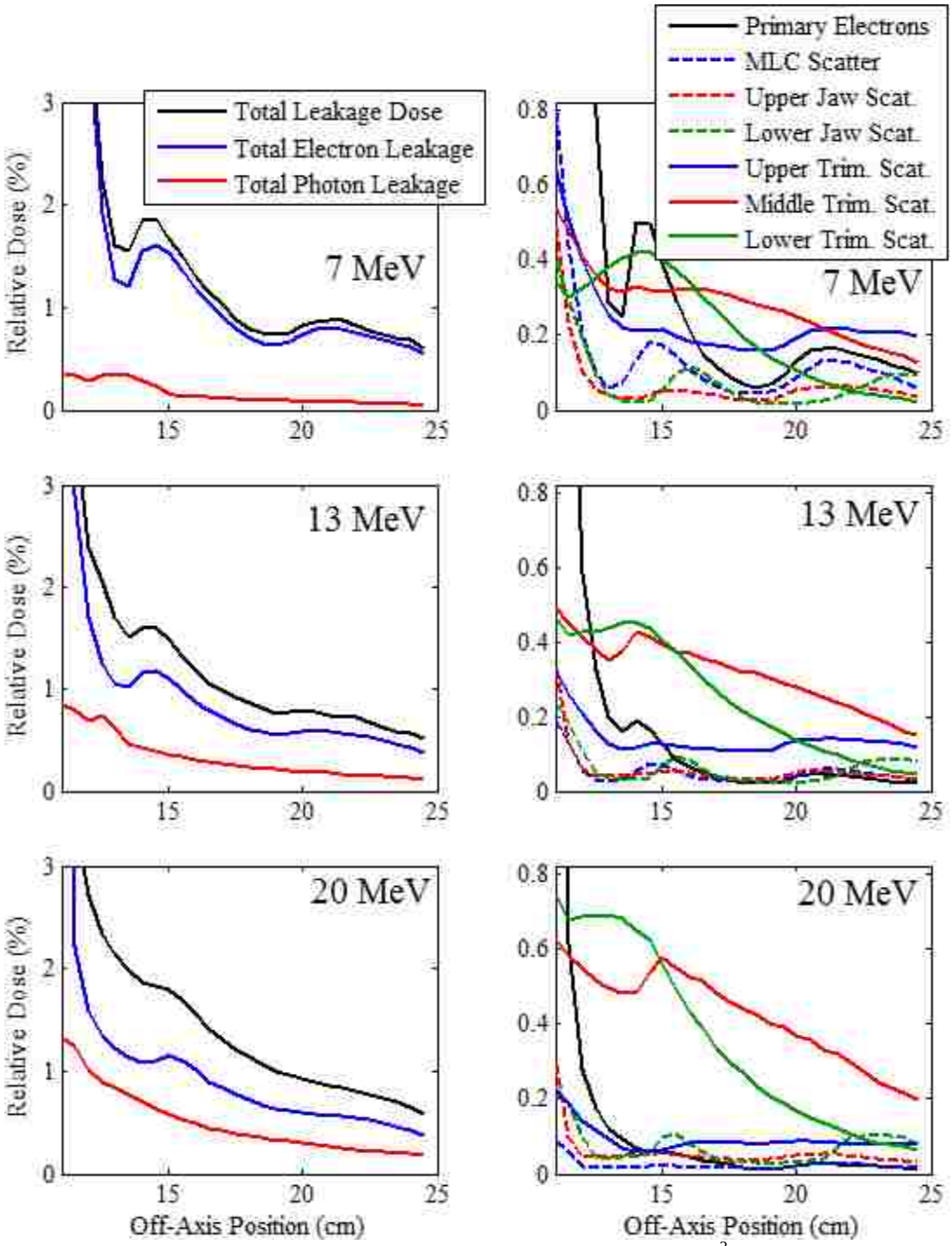

Figure 2-11. In-plane leakage dose component profiles for the 20x20 cm^2 applicator. 7 MeV beam profiles are shown on the top row, 13 MeV in the middle, and 20 MeV profiles on the bottom row. The left column of plots show a breakdown of the total leakage dose (black) along with the differentiated electron (blue) and photon components (red). The right column further breaks down the electron leakage dose into primary electrons and various scattered electron components.

Figure 2-12 illustrates this concept. In this figure, the gray upper jaw represents the jaw positioned for a high energy beam (20 MeV), while the black upper jaw represents the jaw positioned for a low energy beam (7 MeV). The possible trajectory of an upper trimmer scattered electron is labelled in the figure. From the image, it is evident that if the jaw is positioned for a low energy beam, it is possible for a particle of this trajectory (or similar) to reach and scatter off of the upper trimmer inner edge. However, if the jaw is re-positioned for a high energy beam, the particle will intersect the jaw and be absorbed, never reaching the upper trimmer. This absorption is represented in the figure by the transition of the trajectory line from solid to dashed at the jaw height. By this reasoning, moving the jaws in towards central axis decreases the electron fluence at the upper trimmer inner edge position, which in turn, decreases the amount of scatter from the upper trimmer.

Figures 2-10 and 2-11 also show that MLC scatter leakage dose decreases as beam energy increases. This is believed due to two effects. First, the relative electron fluence striking the photon jaws is greater for the lower energy beams. Analytical calculations using a dual scattering foil simulator (Carver *et al.*, 2014) revealed the electron fluence at the MLC inner edge to be 101%, 70%, and 34% of central axis fluence for the 7, 13, and 20 MeV beams, respectively. Second, electrons scattered from the MLC are less likely to be removed from the beam by the upper photon jaw at the lower beam energies, as it is opened wider. This later concept is illustrated in Figure 2-12, with the trajectory of a possible MLC scattered electron labelled. When treating in electron mode, the Elekta Infinity MLC leaves are parked in their farthest possible lateral extent off-axis for all energies and applicators. It can be seen that if the upper jaw is positioned for a low energy electron beam, a particle of this trajectory would scatter off the MLC, bypass the jaw, and continue to the patient plane. However, if the jaw is re-positioned for a high energy beam, a particle of this trajectory would scatter off the MLC and be absorbed by the jaw, never reaching the patient plane. This absorption is represented by the transition of the trajectory line from solid to dashed at the jaw height. Therefore, moving the jaws in towards central axis decreases the amount of scatter dose from the MLC.

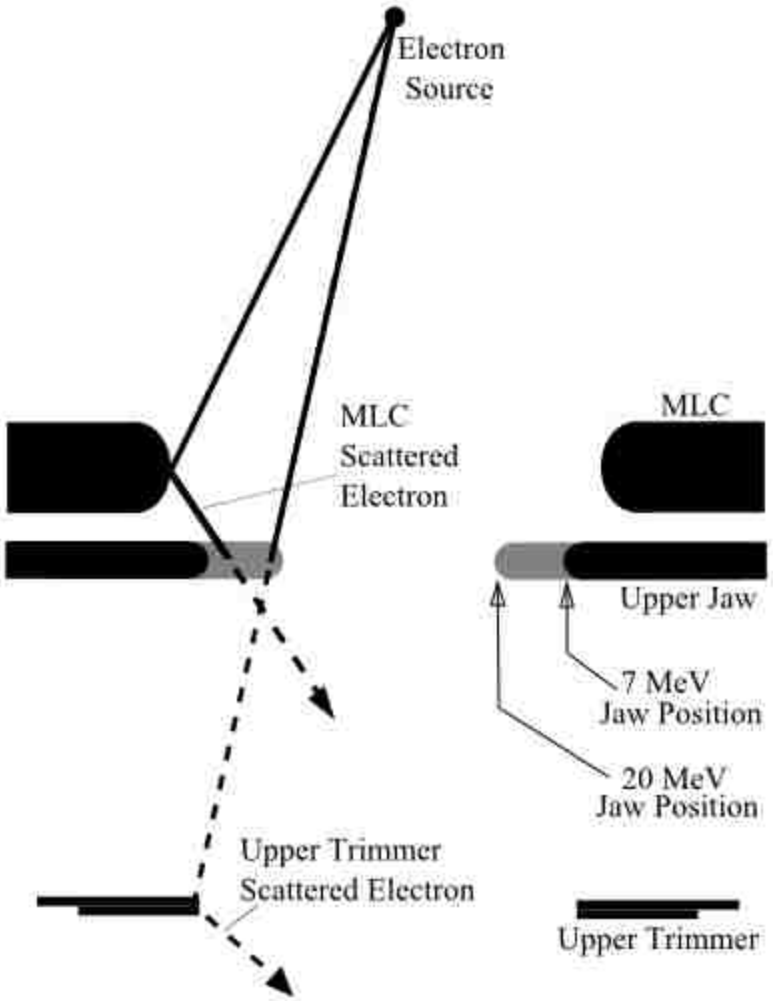

Figure 2-12. Effects of jaw position on collimator scatter. The figure shows a cross sectional view of the MLC, upper jaw, and upper trimmer in the cross-plane dimension. The gray jaw represents the jaw position for high energy beams and the black jaw represents the jaw position for low energy beams. The figure depicts how jaw position likely effects scatter off the MLC and upper trimmer. Possible trajectories for an MLC or upper trimmer scattered electron are labelled. The absorption of the electron in the upper jaw when positioned for a low energy beam is represented by the transition of the trajectory lines from solid to dashed.

Table 2-8 summarizes the results of this study. This table shows the contribution to mean leakage dose from each component normalized to D_{max} (left columns) and normalized to the total leakage dose (right columns), calculated per IEC specifications. The calculations show the increasing photon dose and middle and lower trimmer electron scatter dose with increasing energy. The results also show the decreasing primary electron dose with increasing energy. This is not surprising due to the decreased scattering power in air of the higher energy electrons. The table also confirms the decreased dose from

MLC and upper trimmer scattered electrons for higher energy beams due to the repositioning of the jaw closer to central axis. It should be noted that the values in this table do not necessary add up to the expected sum of their contributions, e.g. the sum of the electron components may not necessarily be equal to the total electron dose. This can be attributed to the bit filtering feature causing a particle to be attributed to more than one dose component. For instance, if an electron interacts in more than one collimation component, e.g. both the MLC and the upper trimmer, then the dose from that electron will be attributed to both leakage components.

Table 2-8. Contributions to mean leakage dose for the 20x20 cm^2 applicator. The columns on the left are normalized as percent of total dose at R_{100} (D_{max}), while the columns on the right are normalized as percent of total leakage dose. All values are determined based on IEC methodology for mean leakage calculation.

Leakage Dose Contributions	Normalized to D_{max}			Normalized to Total Leakage Dose		
	7 MeV	13 MeV	20 MeV	7 MeV	13 MeV	20 MeV
Total Leakage Dose	0.67	0.69	0.93	100.0	100.0	100.0
Total Electron	0.58	0.49	0.56	85.8	70.9	60.4
Total Photon	0.09	0.20	0.34	13.3	28.6	36.6
Primary Electrons	0.08	0.02	0.02	11.1	3.2	1.7
MLC Scatter	0.10	0.07	0.03	14.6	9.7	3.5
Upper Jaw Scatter	0.06	0.06	0.06	9.2	9.2	6.6
Lower Jaw Scatter	0.04	0.04	0.05	6.3	5.7	5.2
Upper Trimmer Scat.	0.13	0.09	0.07	19.9	13.4	7.8
Middle Trimmer Scat.	0.16	0.21	0.35	23.9	30.7	37.7
Lower Trimmer Scat.	0.11	0.13	0.17	16.2	19.5	17.9

2.4. Aim 1 - Conclusions

This study investigated both the in-field flatness and patient plane leakage levels of the 7, 13, and 20 MeV beams with the 10x10 and 20x20 cm^2 applicators for the Elekta Infinity accelerator. Based on the results of this investigation the following was concluded:

- Beam acceptance criteria: The current Elekta collimation system produced clinically acceptable dose distributions for the uniquely configured beams at MBPCC for each beam energy-applicator combination studied. Within the field the collimation system produced an acceptably flat beam for all energy-applicator combinations, meeting the acceptance criteria as specified by Hogstrom

(2004) for in-field beam flatness. Outside the field, the mean and maximum percent leakage dose met acceptance criteria as specified by the IEC (1998) for all applicators and beam energies studied at the patient plane. These leakage levels were shown to be greater than those from electron collimation systems of previously studied Varian accelerators (Chow and Grigorov, 2006; Shimozato *et al.*, 2012) and mostly less than those of Siemens accelerators (Yeboah *et al.*, 2010).

- Comparison of measured and MC-calculated data: MC-calculated doses were shown be sufficiently accurate to be used for the design of new electron collimation system. Although in-field dose calculations disagreed with measurements by as much as 2.59% at the uniformity region edge, these small differences can be accounted for in the collimation system design process. The out-of-field MC calculations were sufficiently accurate, with IEC specified mean leakage doses agreeing within 0.11%, and maximum leakage doses agreed within 0.19% of measured.
- Leakage dose components: Analysis of MC-calculated out-of-field leakage dose showed that electron dose dominated over photon dose, though photon dose became increasingly important as energy increased. The study revealed that most out-of-field electron dose came from electrons scattered from the collimation system, particularly the electron applicator at higher beam energies, indicating that applicator design features which reduce this scatter dose should be of interest in the design process. Additionally, it was discovered that moving the jaw positions inward for higher beam energies reduced MLC and upper trimmer electron scatter leakage dose.

Chapter 3 - Aim 2 - Develop and Validate an Analytical Radiation Transport Code for Optimizing Trimmer Designs

Aim 2: Develop an analytical electron transport model based on pencil-beam theory to use in collimation system design. The model will incorporate both a primary electron and photon component, and its accuracy will be assessed. The impetus for creating this analytical model is to evaluate new collimation designs created within the design process for both in-field flatness and out-of-field leakage dose.

3.1. Aim 2 - Introduction

Electron beams are typically broadened and flattened by a series of dual scattering foils and shaped by collimation trimmers. The dual scattering foils consist of a primary foil, used to broaden the beam, and a flattening foil used to make the beam uniform over the useful lateral extent of the field. These foils are the first accelerator components with which the electrons interact after exiting the vacuum window. The collimation system shapes the beam to conform to the projection of the PTV, while removing as much stray radiation as possible outside the field. This is typically performed using the photon jaws and an electron applicator attached externally to the treatment head. The electron applicators consist of a series of trimmer bars which, in addition to the photon jaws, absorb the electrons scattering out of the field into the leakage region. These components ensure that the PTV receives a uniform dose, while dose to normal tissue outside the PTV is kept to a minimum.

This process of broadening, flattening, and collimating the beam results in multiple dose components, through electron scatter and bremsstrahlung photon production. The largest component is the primary beam electrons, which exit the secondary flattening foil and reach the patient plane without interacting with any collimation components. The scattered electron dose comes from electrons which reach the patient plane after scattering off the edges of the collimation. The photon component comes from bremsstrahlung photons created in the dual scattering foils and collimation system. While the primary electrons constitute the large majority of the dose within the field, approximately 92% at the surface, the various dose components contribute much more equal portions to the leakage dose outside the

field. This study will focus on two of these components, the primary beam electrons and the bremsstrahlung photons created within the scattering foils.

In this investigation, analytical models have been developed to calculate the distributions of both the primary electrons and the bremsstrahlung photons produced in the scattering foil elements. Both of these models utilize multiple scattering theory to determine the dose distributions. Dose contributions both from collimation scattered electrons and from photons created within the collimation material are neglected.

The primary electrons are modeled as they scatter through air while traversing the collimation system. This component model is based on the work of Huizenga and Storchi (1985; 1987), who calculated the scattering moment profiles for a broad electron beam passing through a collimation level, such as a set of photon jaws. The model discussed here builds upon this work by propagating the divergent beam through a series of collimation levels, as well as propagating the electrons outside the trimmers (leakage) to the patient plane.

The photon dose component model focuses on the angular distribution of the electrons within the accelerator exit window and both scattering foils. This model integrates this angular distribution over the thickness of the exit window, the primary foil, and the secondary foil to produce a mean angular distribution of the electrons within each scattering element. Because the large majority of the photons are emitted in a highly forward peaked direction relative to the trajectory of the electron, the mean angular electron distributions can be considered equivalent to the angular distribution of the emitted photons. The distributions from each scattering foil element can then be weighted by the radiative energy lost within each element and summed to find the total angular photon distribution from all scattering elements.

The purpose of developing these models is to obtain a tool for quickly evaluating initial collimation designs. Analytical calculations are known to be significantly faster than other techniques, such as MC calculations. Therefore, with these models it could be possible to quickly, initially evaluate a collimation system design's in-field dose flatness and out-of-field leakage dose.

3.2. Aim 2 - Methods

3.2.1. Analytical Model

The components modeled in this investigation include the primary electrons and the bremsstrahlung photons. For the purposes of this study, the primary electrons include only those electrons which are scattered by the dual scattering foils but do not interact in any other beam shaping components. Their distribution is influenced only by their trajectory exiting the secondary foil and scatter off air in route to the patient plane. This means that the contributions to the dose at the patient plane from electrons which scatter from the collimation system are not included in the model.

The photon dose model includes only bremsstrahlung photons created in the vacuum exit window, the primary scattering foil, and the secondary flattening foil. While additional bremsstrahlung photons are created in the collimator jaws and trimmer bars, these particles are not included in the photon dose model. These two dose components are calculated independently using computer codes written in MATLAB 7.7.0 (The MathWorks, Inc., Natick, MA), then summed to produce a total dose distribution.

3.2.1.1. Primary Electron Dose Component

MCS theory has been used to describe the scatter of electrons within a material for a variety of purposes. This theory describes the angular distribution of a beam of particles which undergo a large number of nuclear elastic collisions as they traverse a material. In 1981, it was used by Hogstrom for the purposes of dose distribution calculation of a broad electron beam with the development of his "pencil-beam" model (Hogstrom *et al.*, 1981). Storchi and Huizenga built upon this model to numerically calculate the scattering moment profiles in air of a broad electron beam (1985). This derivation was then expanded using a series of transformations to the scattering moments to apply to the specific conditions of a divergent beam emanating from a point source passing through a collimator set (Huizenga and Storchi, 1987). The current work will be based upon this numerical approach to a divergent beam. Though the work of Huizenga and Storchi was originally performed for a scanned beam, the theory can be applied just as well to a beam broadened and flattened by a dual foil scattering system.

In this model the scattering moment profiles are first calculated at each trimmer height using equations outlined by Huizenga and Storchi (1987). These scattering moment profiles are then used to determine profiles of the mean projected angle and variance about the mean projected angle at each off-axis position at the trimmer height. These values are then used to transport pencil-beams of electron fluence to the subsequent calculation planes.

According to Huizenga and Storchi (1987), the scattering moment profiles, F_n, are calculated by integrating the electron distribution over all possible angles, i.e.

$$F_n(z,x) = \int_{-\infty}^{\infty} {\theta_x}^n \, F(z,x,\theta_x)\, d\theta_x \tag{3-1}$$

The first three moment profiles can then be used to determine the profiles of the mean projected angle ($\overline{\theta}_x(z,x)$) and variance about the mean projected angle ($\sigma_{\theta x}^2(z,x)$). These terms can then be used to further propagate the beam down to the next calculation plane. Equations 3-2 through 3-6 show the results of these integrations and the equations for determining $\overline{\theta}_x$ and $\sigma_{\theta x}^2$.

$$F_0(z,x,E) = \frac{z'/z}{2}\left[erf\left\{\frac{\frac{bz}{z'}-x}{\sqrt{2\hat{A}_2}}\right\} - erf\left\{\frac{\frac{az}{z'}-x}{\sqrt{2\hat{A}_2}}\right\}\right] \tag{3-2}$$

$$F_1(z,x,E) = \frac{x}{z}F_0(z,x,E) + \frac{\hat{A}_1 z'/z}{\sqrt{2\pi\hat{A}_2}}\left[exp\left\{-\frac{[bz/z'-x]^2}{2\hat{A}_2}\right\} - exp\left\{-\frac{[az/z'-x]^2}{2\hat{A}_2}\right\}\right] \tag{3-3}$$

$$\begin{aligned} F_2(z,x,E) = {} & \left[\hat{A}_0 + \frac{x^2}{z^2}\right]F_0(z,x,E) \\ & - \frac{\hat{A}_1^2 z'}{\hat{A}_2 z}\left[\frac{bz/z'-x}{\sqrt{2\pi\hat{A}_2}}exp\left\{-\frac{\{bz/z'-x\}^2}{2\hat{A}_2}\right\} - \frac{az/z'-x}{\sqrt{2\pi\hat{A}_2}}exp\left\{-\frac{\{az/z'-x\}^2}{2\hat{A}_2}\right\}\right] \\ & + \frac{2xz'\hat{A}_1}{z^2\sqrt{2\pi\hat{A}_2}}\left[exp\left\{-\frac{[bz/z'-x]^2}{2\hat{A}_2}\right\} - exp\left\{-\frac{[az/z'-x]^2}{2\hat{A}_2}\right\}\right] \end{aligned} \tag{3-4}$$

$$\bar{\theta}_x(z,x,E) = F_1(z,x,E)/F_0(z,x,E) \tag{3-5}$$

$$\sigma^2_{\theta_x}(z,x,E) = F_2(z,x,E)/F_0(z,x,E) \; - \; \bar{\theta}_x{}^2(z,x,E) \tag{3-6}$$

In these equations, the $\hat{A}_n$ values represent the scattering moments for the broad divergent beam. They are determined through a series of transformations performed to the scattering moments of a parallel beam, A_n, as:

$$\hat{A}_0(z,E) = A_0(z,E) - \frac{2A_1(z,E)}{z} + \frac{A_2(z,E)}{z^2} \tag{3-7}$$

$$\hat{A}_1(z,E) = A_1(z,E) - \frac{A_2(z,E)}{z} \tag{3-8}$$

$$\hat{A}_2(z,E) = A_2(z,E) \tag{3-9}$$

where, for a beam of energy E

$$A_n(z,E) \; = \tfrac{1}{6}[z - z']^n \, T_{air}(E) \, z' \; + \; \frac{1}{2}\int_{z'}^{z} T_{air}(E) \, [z - z"]^n \, dz" \tag{3-10}$$

$$T_{air}(E) = \; 0.00554 * E^{-1.78} \tag{3-11}$$

In these equations, x represents the distance off central axis and z represents the distance along central axis from the nominal source position, which is defined as 100 cm upstream from accelerator isocenter. The symbol z' indicates the distance from the nominal source position to the collimation plane immediately upstream of z. The a and b symbols represent the distances from central axis of the upstream collimator inner edges, a in the negative direction and b in the positive. T_{air} represents the scattering power in air of an electron of energy E. For more information on these terms and the derivations of these equations, refer to the appendix of "The In-Air Scattering of Clinical Electron Beams as Produced by Scanning Beams and Diaphragm Collimators" (Huizenga and Storchi, 1987). Equation 3-11 was

produced by applying the relation described by Werner *et al.* (1982), which states that the scattering power (in rad^2/cm) of electrons within of a material is approximately equal to $cE^{-1.78}$, where E is the beam energy in MeV and c is a constant which varies with material, to the case of a 10 MeV electron in air.

An additional feature of the model is the ability to adjust the virtual source height position and the virtual source width. The virtual source of an electron beam refers to the point in space from which the beam appears to emanate. Due to the effects of the scattering foils in an accelerator, the virtual source position of an electron beam is typically somewhat lower than the nominal source position, (i.e. $z > 0$, where $z = 0$ at a position 100 cm upstream from isocenter). To account for this in the model, the distances from the virtual source to all trimmer levels and calculation planes are adjusted for calculation purposes. This virtual source height can be modified as a model input parameter.

In addition to affecting the virtual source height position, the scattering foils can also cause the virtual source to have a non-zero width. This means that not all particles in the beam seem to emanate from central axis, but rather from a distribution of points about central axis at the virtual source height. To account for this, the virtual source is modeled as distribution of point sources with Gaussian shape centered at central axis. Several moment profiles are calculated with sources positioned at small distances off axis and then weighted by a Gaussian and summed to produce a total moment profile. The standard deviation of this Gaussian distribution can be modified as a model input parameter to adjust the width of the virtual source. This has the effect of increasing the width of the beam penumbra at the edge of the field.

Assuming the fluence is uniform across the full width of the field at the immediately upstream collimation level, the zeroth order moment profile calculated in Equation 3-2, F_0, represents the fluence distribution at the calculation plane. This is true for the upper trimmer; therefore F_0 is used as the fluence profile at this first calculation plane (the height of the upper trimmer). Any electrons which intersect a trimmer are assumed to be absorbed, and removed from the fluence distributions. For the electrons that do not intersect the trimmer, the mean angle and variance about the mean angle are used to propagate the fluence down to the next calculation plane. The next calculation plane varies depending on the region

from which the fluence is propogated. Figure 3-1 shows the next calculation plane for each region of the fluence profile at each trimmer height. For electrons which pass inside the trimmer, the next calculation plane is the immediately downstream trimmer level. This propagation of the fluence inside the trimmers is shown in Figure 3-1. In this figure, the upper trimmer fluence profile (red) within the field is

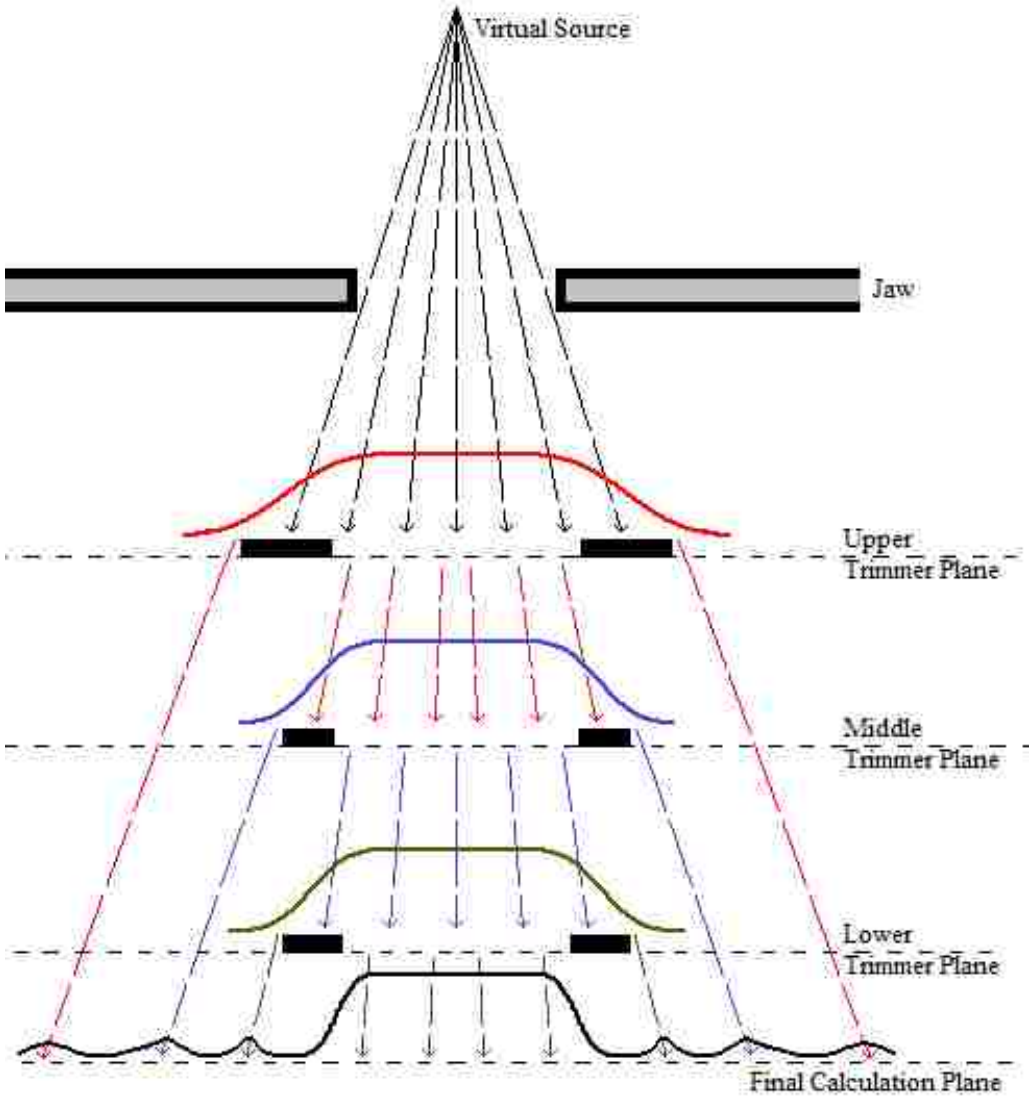

Figure 3-1. Propagation of the primary electron fluence to the subsequent calculation planes. The red, blue, and green curves represent the fluence profiles at the upper, middle, and lower trimmers, respectively. The red, blue and green arrows depict the calculation plane to which each portion of each profile is propogated. The leakage fluence outside the trimmer is propogated down to the final calculation plane, regardless of trimmer level. Within the field, the fluence is propogated to the next trimmer plane. For the lowest trimmer level, the fluence is propogated to the final calculation plane and recombined with each of the leakage components to produce a total primary electron fluence profile, shown in black.

propogated down to the middle trimmer plane, as shown by the red arrows within the field. The middle trimmer fluence profile (blue) is propogated down to the lower trimmer plane, as shown by the blue arrows within the field. For the lowest trimmer level fluence profile (green), the electrons are propagated to the final calculation plane, typically positioned at the patient plane (z = 101 cm), as shown by the green arrows. Electrons which scatter outside the trimmers are always propagated down to the final calculation plane, regardless of trimmer position. This is depicted in Figure 3-1 by the arrows outside the trimmers for the upper (red), middle (blue), and lower (green) trimmer plane profiles. Each of these leakage fluence profiles originating from the three trimmer levels are summed and recombined with the in-field fluence to produce a total primary electron fluence distribution (black) at the final calculation plane.

This fluence propagation is performed using Equations 3-12 through 3-15. Each of the terms in these equations is depicted in Figure 3-2, which illustrates the methodology of this propagation. In these equations and this figure, the electron fluence, Φ_e, at a plane at height z_{j-1} is being transported down to a plane at z_j. To do this, the fluence distribution at z_{j-1} is separated into "pencil-beams" of width Δx and centered about $x_{i,j-1}$. Equations 3-12 and 3-13 are used to determine the position of the projection of the edges of each pencil-beam at plane z, as indicated by $x^+_{i,j}$ and $x^-_{i,j}$. This projection occurs at angles of $\bar{\theta}_x(z_{j-1},x_{i,j-1}+\Delta x/2)$ and $\bar{\theta}_x(z_{j-1},x_{i,j-1}-\Delta x/2)$ for $x^+_{i,j}$ and $x^-_{i,j}$, respectively, as shown in Figure 3-2. These values for $\bar{\theta}_x$ are determined from Equation 3-5. Equation 3-14 is used to calculate the penumbral width (σ_x) of each pencil-beam. In this equation, the variance about the mean angle ($\sigma_{\theta x}^2$) is obtained from equation 3-6. The sum of these pencil-beams is then calculated using Equation 3-15 to produce a total fluence distribution for each component ($\Phi_{e,comp}$) at plane z_j propogated from z_{j-1}. For the in-field electron fluence components, this propagation is performed from each upstream trimmer plane to the immediately downstream calculation plane. For the out-of-field fluence components, this propagation is performed from each trimmer plane to the final calculation plane, regardless of trimer level. Once all fluence components have been propagated to the final calculation plane, the contributions from the in-field fluence component ($\Phi_{e,infield}$) and leakage components from each upstream trimmer level ($\Phi_{e,k,leakage}$), are recombined to produce a total primary electron fluence distribution (Φ_e), as shown in Equation 3-16.

$$x_{i,j}^{+} = \left[x_{i,j-1} + \frac{\Delta x}{2}\right] + \bar{\theta}_x\left(z_{j-1}, x_{i,j} + \Delta x/2\right)\left[z_j - z_{j-1}\right] \tag{3-12}$$

$$x_{i,j}^{-} = \left[x_{i,j-1} - \frac{\Delta x}{2}\right] + \bar{\theta}_x\left(z_{j-1}, x_{i,j} - \Delta x/2\right)\left[z_j - z_{j-1}\right] \tag{3-13}$$

$$\sigma_{x_{i,j}} = \left[\sigma_{\theta_x}^2\left(z_{j-1},\, x_{i,j-1}\right)\left[z_j - z_{j-1}\right]^2 + \frac{T_{air}(E)\left[z_j - z_{j-1}\right]^2}{6}\right]^{1/2} \tag{3-14}$$

$$\Phi_{e,comp}\left(z_j, x, E\right) = \sum_{i=-\infty}^{\infty} \frac{\Phi_{e,i}\left(z_{j-1}, x_{i,j-1}, E\right)\Delta x}{2\left[x_{i,j}^{+} - x_{i,j}^{-}\right]} \left[\operatorname{erf}\left\{\frac{x_{i,j}^{+} - x}{\sqrt{2}\sigma_{x_{i,j}}}\right\} - \operatorname{erf}\left\{\frac{x_{i,j}^{-} - x}{\sqrt{2}\sigma_{x_{i,j}}}\right\}\right] \tag{3-15}$$

$$\Phi_e(z, x, E) = \Phi_{e,infield}(z, x, E) + \sum_{k=1}^{3} \Phi_{e,k,leakage}(z, x, E) \tag{3-16}$$

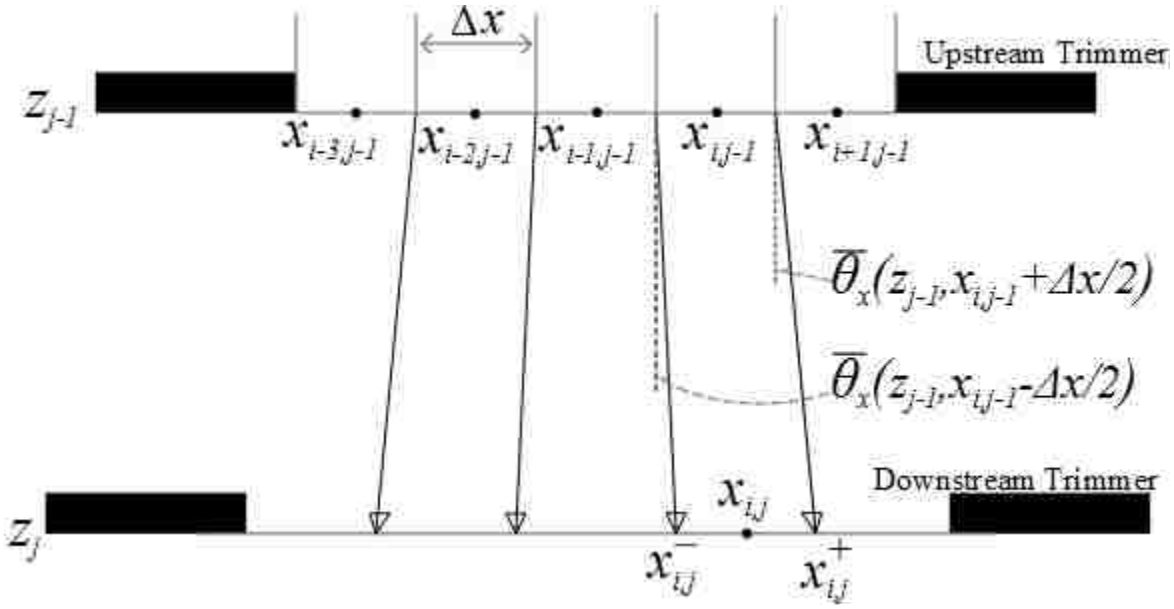

Figure 3-2. Electron pencil-beam fluence propagation and depiction of terms for the primary electron model. The figure illustrates the fluence propagation from an upstream trimmer level (located at height z_{j-1}) to a downstream trimmer level (located at height z_j) within the field. The edges of each pencil beam are projected down at angles of $\bar{\theta}_x(z_{j-1}, x_{i,j-1}+\Delta x/2)$ and $\bar{\theta}_x(z_{j-1}, x_{i,j-1}-\Delta x/2)$ to determine the locations of $x^{+}_{i,j}$ and $x^{-}_{i,j}$, respectively.

The primary electron model assumes the beam is monoenergetic and does not lose energy in air in route to the patient. This allows for the dose to be considered proportional to the fluence throughout the field, since the mass stopping power in water should be uniform over the full profile of the beam. Therefore, the primary electron dose (D_e) can be determined by multiplying the total primary electron fluence by a constant, K_e, as shown in Equation 3-17. Additionally, this allows for the use of a constant scattering power, since neither the material nor the electron energy change in route to the patient plane.

$$D_e(z, x, E) = K_e \, \Phi_e(z, x, E) \tag{3-17}$$

3.2.1.2. Photon Dose Component

The analytical photon component models the bremsstrahlung photons created in the accelerator scattering foil elements. Bremsstrahlung radiation is created in a material when an electron is deflected by a Coulombic interaction with a nucleus, resulting in the emission of a bremsstrahlung photon. The direction of photon emission is extremely forward peaked relative to the direction of electron travel, with the differential cross section per solid angle at the angle of emission (θ) being approximately proportional to $cos(\theta/2)^2 * sin(\theta/2)^{-4}$ (Hough, 1948). This radiative energy loss increases with both beam energy and the atomic number of the material (Whycoff *et al.*, 1984). Because the scattering foil elements are both composed of high atomic number material and situated entirely in the path of the electron beam, the bremsstrahlung photon distributions produced within them are of particular interest.

Because the emitted bremsstrahlung distribution is so forward peaked, i.e. approximately a delta function, the angular distribution of the photons closely follows the angular distribution of the electrons from which they are emitted. To obtain the photon distributions from each scattering element, the angular distribution of electrons within the foil must be integrated over the foil thickness (Schiff, 1946). The application of Schiff's solution to the exit window and dual scattering foils of an accelerator has been previously described by Carver *et al.* (2014). For a beam of energy E, the number of photons (ΔN_γ) per unit solid angle ($\Delta\Omega$) is given by:

$$\frac{\Delta N_\gamma}{\Delta\Omega}(\theta_r, E) = P_\gamma \sum_{i=1}^{3} \frac{S_{rad,i}(E)\, t_i}{\pi T_i(E) t_i} \left[\mathrm{E}_1 \left\{ \frac{{\theta_r}^2}{T_i(E)t_i + 2A_{0,i}(E)} \right\} - \mathrm{E}_1 \left\{ \frac{{\theta_r}^2}{2A_{0,i}(E)} \right\} \right] \tag{3-18}$$

where

$$A_{0,i} = A_{0,initial} + \frac{1}{2} \sum_{j=1}^{j-1} T_j(E) t_j \tag{3-19}$$

Equation 3-18 sums the angular photon emission distribution from the three scattering elements: the nickel vacuum exit window, the tantalum primary scattering foil, and the aluminum secondary flattening foil. These elements are designated with *i* values of 1, 2, and 3, respectively. In Equations 3-18 and 3-19, θ_r is the radial angle of emission from central axis and P_γ is a constant of proportionality. T_i, $S_{rad,i}$, and t_i indicate the scattering power, radiative stopping power, and thickness, respectively, of the *i*th scattering element. Equation 3-19 calculates the zeroth order scattering moment, $A_{0,i}$, of the electrons entering i^{th} scattering element, and $A_{0,initial}$ is the scattering moment of the beam exiting the accelerator prior to entering the exit window. To calculate the radiative stopping power, Equations 60 and 61 from Part II of *Experimental Nuclear Physics, Vol. I* were used (Bethe and Ashkin, 1953).

It should be noted that at $\theta_r = 0$, the function E_1 goes to infinity, which leads to difficulties in evaluating Equation 3-18. According to Carver *et al.* (2014), by evaluating the term in the brackets in Equation 3-18 using a series expansion, the distribution value at $\theta_r = 0$ for each scattering element can be determined by

$$\lim_{\theta_r \to 0} \left[\mathrm{E}_1 \left\{ \frac{{\theta_r}^2}{T_i(E)t_i + 2A_{0,i}(E)} \right\} - \mathrm{E}_1 \left\{ \frac{{\theta_r}^2}{2A_{0,i}(E)} \right\} \right] = \ln \left\{ 1 + \frac{T_i(E)t_i}{2A_{0,i}(E)} \right\} \tag{3-20}$$

Once the angular distribution of the beam within the head is determined, a ray tracing technique is used to geometrically project the distribution down to the patient plane. To perform this projection, $tan^{-1}(x/z)$ is substituted for θ_r, converting $\Delta N_\gamma/\Delta\Omega$ to a spatial photon fluence (Φ'_γ) at the patient plane. In this process it is approximated that all photons originate from central axis within the primary scattering

foil, which produces the largest portion of the radiative energy. By performing this substitution, Equation 3-18 becomes

$$\Phi'_{\gamma}(z,x,E) = P_{\gamma}\sum_{i=1}^{3}\frac{S_{rad,i}(E)\,t_i}{\pi T_i(E)t_i}\left[\mathrm{E}_1\left\{\frac{[tan^{-1}\{x/z\}]^2}{T_i(E)t_i + 2A_{0,i}(E)}\right\} - \mathrm{E}_1\left\{\frac{[tan^{-1}\{x/z\}]^2}{2A_{0,i}(E)}\right\}\right] \quad (3\text{-}21)$$

Photon attenuation within the collimation system is also accounted for in the model. To do this, the amount of collimation material present in each ray path is determined. The photon attenuation in this collimation material is accounted for by multiplying each ray in the original angular distribution by a transmission factor. This is performed using Equation 3-22, in which the original photon fluence profile (Φ'_{γ}) is converted to an attenuated photon fluence profile (Φ_{γ}). In this equation μ_j is the collimation material attenuation factor and t_j is the collimator thickness. N_{trim} is the number of trimmers through which a ray passes to arrive at position *(z,x)*.

$$\Phi_{\gamma}(z,x,E) = \Phi'_{\gamma}(z,x,E) * \prod_{j=1}^{N_{trim}} exp\{-\mu_j(E)t_j(x,z)\} \quad (3\text{-}22)$$

This process of accounting for collimation attenuation is illustrated in Figure 3-3, along with the ray tracing process to convert the angular photon distribution to a spatial photon distribution at plane height *z* (typically the patient plane). In the upper portion of this figure, the rays are traced at an angle θ_r to arrive at an off-axis position *x* at plane height *z*. Outside the field, the rays pass through the applicator trimmers. In doing so, some of the photons along those rays are attenuated. This is depicted in the figure by the rays transitioning from black (no attenuation) to blue (attenuation in one trimmer) and green (attenuation in two trimmers). The lower portion of the figure illustrates how the photon distribution is affected by the attenuation. This portion of the figure plots the relative photon fluence verses off-axis position (*x*) for both the original profile (i.e. the profile prior to accounting for attenuation) and the attenuated profile. The off-axis position of each data point in this plot corresponds to a ray depicted in the upper portion of the figure. The original profile is shown with the red star markers, and the attenuated profile is shown with the circular markers. The black circles correspond to rays which pass through no

trimmers, the blue circles correspond to rays which pass through one trimmer, and the green circles correspond to rays which pass through two trimmers. Within the field, where no collimation is present, the fluence profile is unaltered, causing the attenuated profile to perfectly match the original profile. Rays

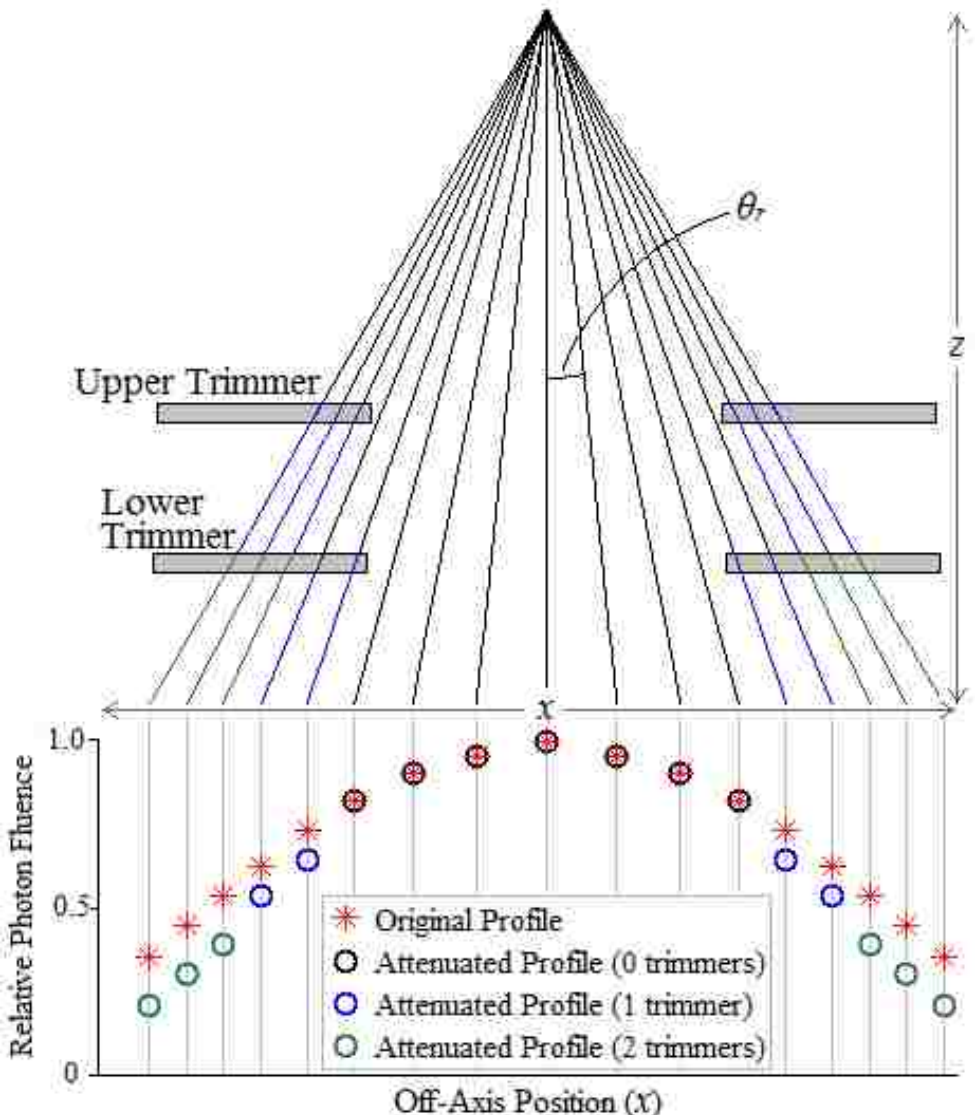

Figure 3-3. Photon ray tracing and attenuation within the collimation system. The upper portion of the image illustrates process of projecting the angular photon distribution from the source down to the patient plane to create spatial distribution. Each ray is projected at angle θ_r to an off-axis position x at plane height z. The lower portion of the image illustrates the effect of attenuation on the photon distribution. This portion of the figure plots the relative photon fluence verses off-axis position (x) for both the original (red star markers) and attenuated (circular markers) profiles. The off-axis position of each data point in this plot corresponds to a ray depicted in the upper portion of the image. The black, blue, and green circular markers represent photon fluence levels from rays which pass through 0, 1, and 2 trimmers, respectively.

which pass through greater thicknesses of trimmer material are more affected by attenuation, as seen by the blue circular markers (attenuation in 1 trimmer) being removed from the original profile markers, but less so than the green circular markers (attenuation in 2 trimmers). In this process, it is assumed that any rays which pass through the photon jaws are completely attenuated.

For the purpose of determining the attenuation factors, the photons are approximated as monoenergetic over the full extent of the profile with an energy of one third the electron beam energy. This approximation also allows the photon dose to be considered proportional to photon fluence throughout the field. Therefore, the photon dose (D_γ) can be determined by multiplying the total photon fluence by a constant, K_γ, as shown in Equation 3-23.

$$D_\gamma(z,x,E) \;=\; K_\gamma\, \Phi_\gamma(z,x,E) \tag{3-23}$$

3.2.1.3. Dose Recombination

To determine the contribution to the total dose from each dose component, a MC study was performed using EGSnrc. Calculations were performed for the 7, 13 and 20 MeV beams with the same setup as described in Aim 1. Simulations were performed with the BEAMnrc Elekta Infinity model with the 20x20 cm^2 applicator to produce a phase space file, which was used as input to DOSXYZnrc to calculate the total dose at 100 SSD. The total dose was calculated in a 0.5x0.5x0.5 cm^3 voxel in water centered at 1 cm depth (extending from 0.75 to 1.25 cm depth) on central axis. Additionally, the LATCH bit filtering feature was used to calculate the photon dose within the same voxel using the same phase space as input. This photon dose value was divided by the total dose at the same point to determine a dose component relation coefficient, C, for each beam energy. With this coefficient, Equation 3-24 was used to determine a total relative dose profile (D_{total}).

$$D_{total}(z,x,E) = [1 - C(E)]\, D_e(z,x,E) \;+\; C(E)\, D_\gamma(z,x,E) \tag{3-24}$$

3.2.2. MC Simulations for Model Evaluation

3.2.2.1. Primary Electron Dose Calculation

To evaluate the accuracy of the dose calculated by the primary electron component model, a set of MC calculations was performed. The MC-calculated profiles were then compared to the analytical results to evaluate the model's performance. The study was performed using only the 7 MeV beam for both the 10x10 and 20x20 cm^2 applicators. It was decided that the lowest energy electrons, having higher scattering power in air, were best suited for evaluating the analytical model. Initial calculations (MC and analytical) performed with higher beam energies were found to produce negligible primary electron leakage dose, and therefore were poorly suited for evaluating the analytical model.

The analytical primary electron model calculates only the primary electron distribution from an "ideal" electron beam. That is to say, the model predicts the distribution of a beam of electrons emanating from a well-defined source and that is collimated by "perfect collimators" that create no other dose components, e.g. bremsstrahlung photons or scattered electrons. To reflect this ideal setup in the MC calculations, a series of modifications to the model for the current Elekta Infinity system were made. First, the source was redefined as a monoenergetic point source positioned at $z = 0$ on central axis (100 cm upstream from isocenter). This produced an approximately uniform beam passing through the collimators and at isocenter without the dual scattering foils, ensuring that no bremsstrahlung would be produced. Second, the collimation system was specified to eliminate scatter contamination to the beam. The aluminum plates were removed from each trimmer bar, and the lead trimmer plates and tungsten jaws were specified to be as thin as allowable within the EGSnrc system. Then, the LATCH bit filtering feature was used to remove any contribution from those particles which enter these collimation components during the dose calculation. Third, all other accelerator components which could affect the fluence distribution (e.g. scattering foils, MLC, monitor chambers, etc.) were removed. All other aspects of the model, including jaw and trimmer positions and all transport parameters (boundary crossing algorithm, global cutoff energies, etc.), were maintained.

To evaluate the fluence model, calculations were performed with the collimation system arranged in four different configurations. First, all three applicator trimmers were removed from the model with only the photon jaws remaining to collimate the beam. With this configuration, profiles were calculated at seven different horizontal downstream planes, with *z*-positions of 65, 73.3, 80, 86.6, 90, 95, and 101 cm. The *z*-positions of 73.3, 86.2, and 95 cm were selected for corresponding to the position of the downstream surface of the three trimmers. The 101 cm value was selected for corresponding to the plane at 1 cm depth in a 100 cm SSD water phantom, which provides dose profiles specified by the IEC. All other heights were selected as being spaced approximately halfway between the collimation levels. Second, the uppermost trimmer was added, and the calculations were re-performed at the five lower plans, with *z*-positions of 80, 86.6, 90, 95, and 101 cm. Third, the middle trimmer was added, and the calculations were re-performed at the three lower planes, with *z*-positions of 90, 95, and 101 cm. Fourth, the collimation system was completed by adding the third trimmer, and the calculation was re-performed at 101 cm.

To calculate the dose, phase space files were scored at planes 2 cm upstream from each calculation plane. These phase spaces were then used as input to DOSXYZnrc to calculate the dose distribution. Particles were transported through 1 cm of air into a water phantom. As in Aim 1, the profiles were calculated in 0.5x0.5x0.5 cm^3 voxels centered at 1 cm depth (extending from 0.75 cm to 1.25 cm depth). Dose profiles were calculated at each plane height with each collimation configuration using 10^9 particles. To reduce statistical uncertainty, the dose distributions were symmetrized about central axis in both the in-plane and cross-plane dimensions. Each dose distribution was normalized to the mean dose calculated within a 3x3 set of voxels centered at central axis at 1 cm depth at the SSD of the profile.

3.2.2.2. Photon Dose Calculation

To evaluate the accuracy of the dose calculated by the analytical photon model, two sets of MC calculations were performed. The first set was performed using the current Elekta Infinity model with the LATCH bit filtering feature used to calculate only the photon dose. In the second set, the Elekta model

was modified by removing all collimation materials below the secondary scattering foils, with LATCH bit filtering again used to calculate only the photon dose. This isolated the dose from photons produced within the scattering elements, as is calculated by the analytical photon dose model.

As in Aim 1, a phase space file was created using the BEAMnrc model and was used as input to DOSXYZnrc to calculate the dose. Dose profiles were calculated at 100 cm SSD in water with 0.5x0.5x0.5 cm^3 voxels centered at 1 cm depth. Both sets of calculations were performed for the 7, 13, and 20 MeV beams using 10^9 particles, and the calculation set with collimation system present used the 20x20 cm^2 applicator. The MC results were compared with analytically calculated results for the evaluation of the analytical bremsstrahlung component model. The profiles were normalized to the total dose (electron and photon) calculated at 1 cm depth on central axis for the same model configurations.

3.3. Aim 2 - Results and Discussion

3.3.1. Comparison of Analytical Primary Electron Model with MC

Figures 3-4 through 3-6 show the results for the comparison of the primary electron analytical model with MC calculations. Figure 3-4 shows a cross sectional view of the 20x20 cm^2 applicator with the relative cross-plane dose profiles calculated at each calculation plane (*z*-positions of 65, 73.3, 80, 86.6, 90, 95, and 101 cm) superimposed. The black rectangles demarcate the cross section of each trimmer. The plotted solid curves in the figure reperesent the analytical model calculations and the dashed curves represent the MC calculations. The blue curves represent the calculations performed with all trimmers removed from the collimation system, such that the beam is defined only by the photon jaws. The red curves represents the calculation performed with only the upper trimmer added. The black curves represents the calculation with both the upper and middle trimmers added, and the green curves shows the calculations with all three trimmers added.

The left side of the figure (negative off-axis positions) shows plots of the full magnitude of the profiles. In this region of the plot, the cenral axis dose (off-axis position = 0) corresponds to 100% of the dose and the long-dashed base line corresponds to 0%. The right side of the figure (positive off-axis

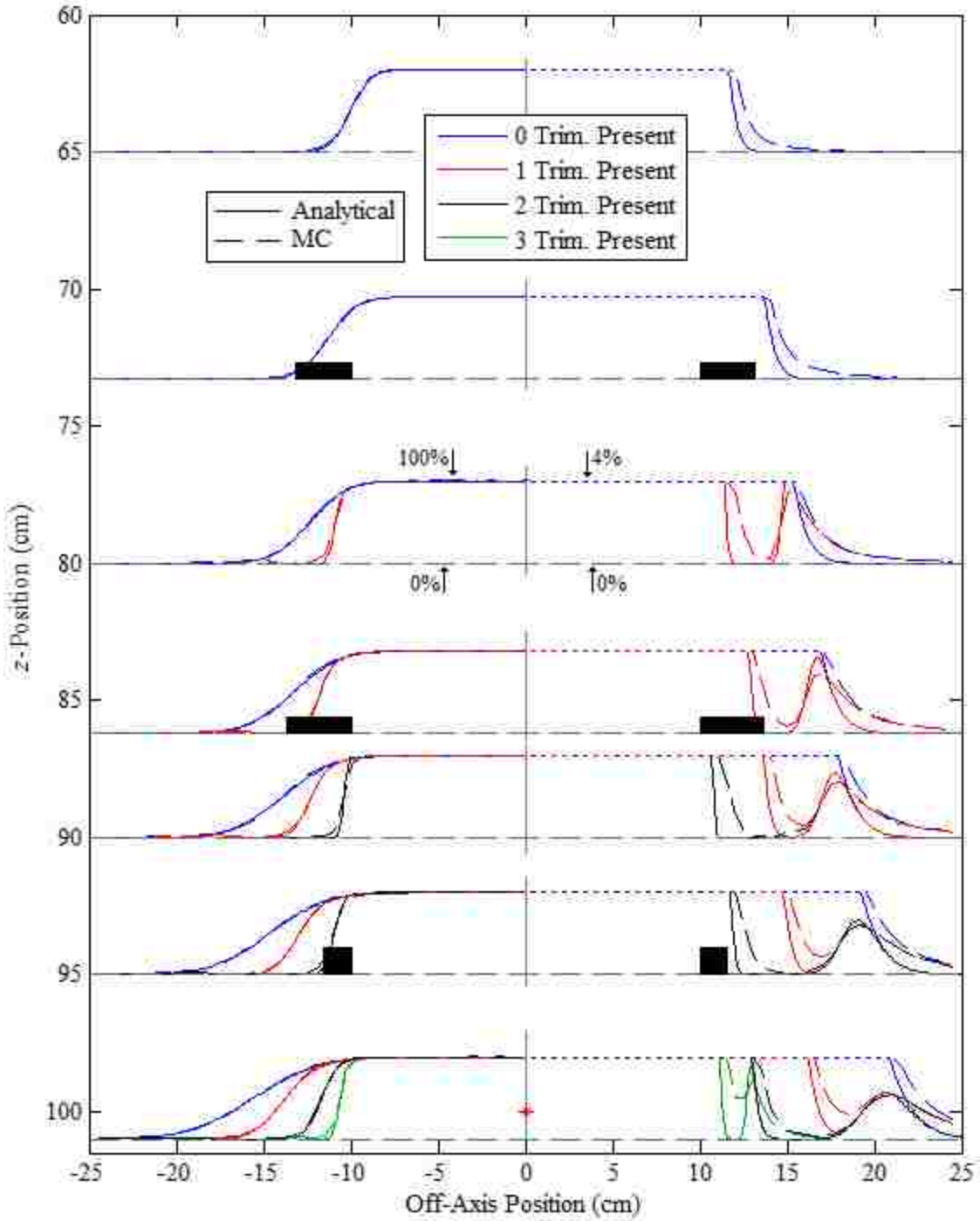

Figure 3-4. Full cross-plane primary electron dose profile comparisons of analytical and MC calculations for the 20x20 cm^2 applicator with a monoenergetic 7 MeV beam. The figure shows a cross-sectional view of the 20x20 cm^2 applitor with the relative dose profiles calculated at various heights. The left side of the figure (negative off-axis positions) shows plots of the full magnitude of the profiles, with the cenral axis dose (off-axis position = 0) corresponding to 100% of the dose and the dashed base line corresponding to 0%. The right side of the figure (positive off-axis positions) magnifies the same profiles showing the low dose region to more clearly see the behavior of the leakage dose. In this region, a the maximum dose plotted is 4% of central-axis dose. Refer to the text for further description.

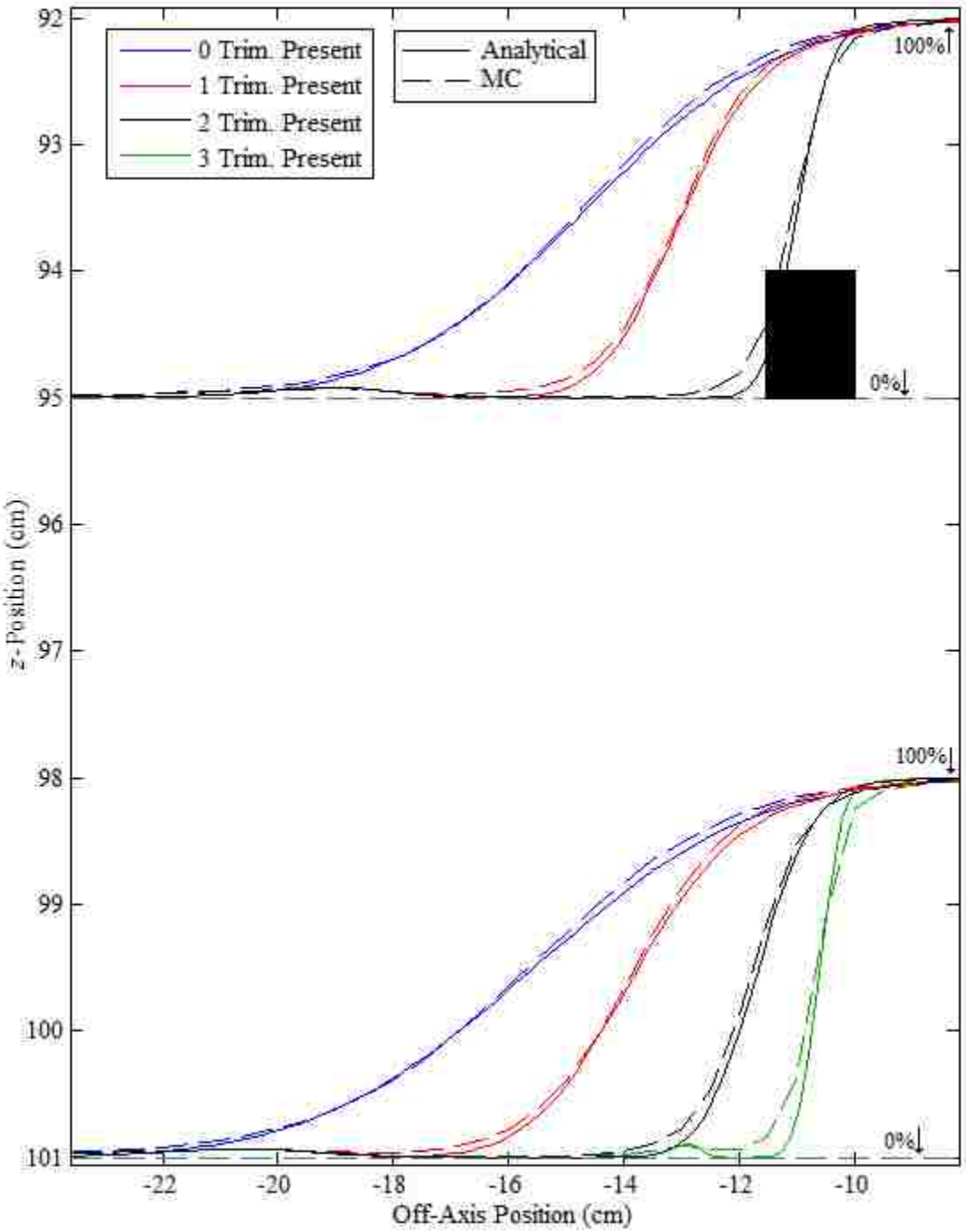

Figure 3-5. Cross-plane primary electron dose profile comparisons of analytical and MC calculations for the 20x20 cm^2 applicator with a monoenergetic 7 MeV beam in the penumbral fall-off region. The figure shows a cross-sectional view of the 20x20 cm^2 applitor with the relative dose profiles calculated at *z*-positions of 95 and 101 cm. The plot shows the full magnitude of the dose profiles with in-field region of the plots corresponding to 100% of the central-axis dose and the dashed base line corresponding to 0%. Refer to the text for further description.

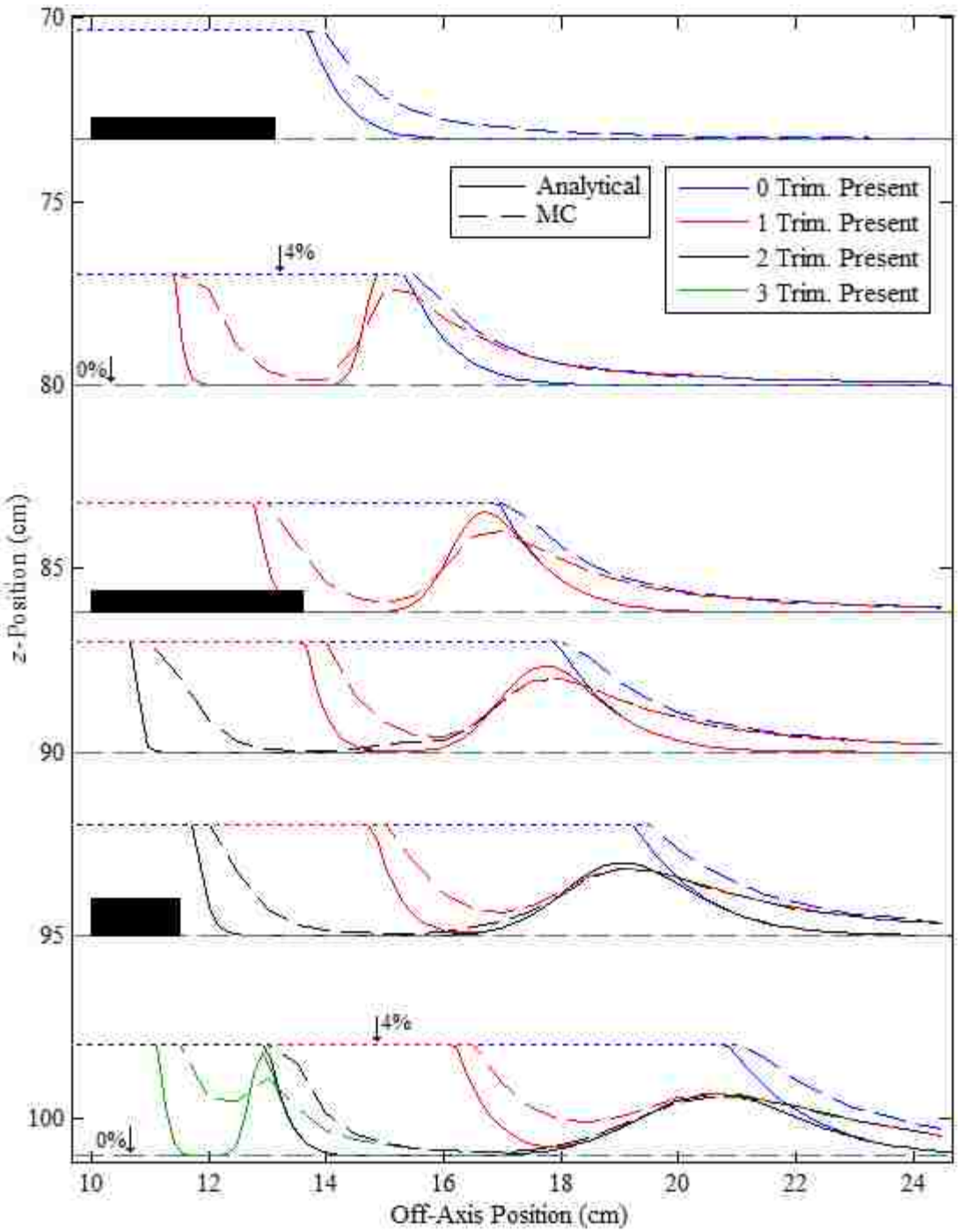

Figure 3-6. Cross-plane primary electron dose profile comparisons of analytical and MC calculations for the 20x20 cm^2 applicator with a monoenergetic 7 MeV beam in the low dose leakage region The figure shows a cross-sectional view of the 20x20 cm^2 applitor with the relative dose profiles calculated at various heights. The plot shows the profiles magnified to highlight the low dose region with the horizontal short-dashed line corresponding to 4% of the central-axis dose and the horizontal long-dashed base line corresponding to 0%. Refer to the text for further description.

positions) magnifies the same profiles showing the low dose region to more clearly see the behavior of the leakage dose. In this region, the maximum dose plotted is 4% of central-axis dose. Regions of the profile which have a greater than 4% magnitude are truncated and shown in the plot as a horizontal short-dashed line. This was done so that behavior of the full range of the penumbra could be easily seen on the left side of the figure, while the behavior of the leakage dose outside the trimmers could be seen on the right. These dose magnitude regions of 100% and 4% are labelled in the figures.

Figure 3-4 shows that the plots of the analytical model (solid curves) generally agree with the dashed lines of the MC calculations. This can be better seen by zooming in on the penumbral and out-of-field regions as in Figures 3-5 and 3-6, respectively. Figure 3-5 focuses on the penumbral region of the profile at *z*-positions of 95 and 101 cm. The black rectangle at z = 95 cm demarcates the cross section of the lower trimmer. Figure 3-3 shows how well the model is able to predict both the location and width of the penumbra. The analytical dose profile slightly over-predicts the MC dose profile in the high-dose, shoulder region of the curve and slightly under-predicts the MC dose in the low dose region (0-20%). These effects are most evident in the analytical full collimation curve (green) at z = 101 cm. This curve over-predicts the MC just inside the field edge and under-predicts the MC in the low dose region just outside the field edge. These differences are believed to most likely be due to an approximation made in the analytical model that assumes that the fluence is uniform across the full extent of the field at each collimation level when calculating the scattering moment profiles. While this is true for the middle of the field, the approximation can become slightly invalid near the field edge where charged particle equilibrium is not fully maintained. This causes the model to slightly under-predict $\overline{\theta}_x$ for the pencil-beams just inside the inner trimmer edge. Subsequently, this is believed to cause an over-prediction in fluence in the high-dose shoulder region and an under-prediction in the low dose region of the profile near the edge of the field at the downstream calculation planes.

Additionally, the analytical model's use of an error function did not perfectly match the penumbral fall-off of the beam as the penumbra grew large. This is displayed in the profiles for calculations with no trimmers present (blue). For this profile, the analytical model slightly under-predicts

the MC dose in both the shoulder and low dose region. This small discrepancy is presumed to be due to the scatter distribution being approximated as a Gaussian in pencil-beam theory.

Figure 3-6 magnifies the dose profiles in the leakage region with the three black rectangles demarcating the cross sections of the three trimmers. The plots illustrate the behavior of the primary electron leakage dose as it travels to the patient plane. At the most upstream calculation plane in the figure (z = 73.3 cm), both the analytical and MC plots show the tail of the penumbra passing outside the upper trimmer. This leakage radiation creates a leakage dose "bump" in the immediately downstream profile (z = 80 cm). This bump can be seen in the profile calculated for a single trimmer (red) positioned approximately 15 cm off axis. In the subsequent downstream calculation planes the figure shows the bump broadening as it propagates downstream, eventually reaching the patient plane at an off-axis position of approximately 21 cm. The bump broadens as σ_x (Equation 3-14) increases with increasing z and travels downward at an angle $\overline{\theta}_x$ (Equation 3-5). Likewise, a leakage bump can be seen in the full collimation profile (green) calculated at the 101 cm z-position calculation plane. This bump, located approximately 13 cm off axis, is formed by primary electrons scattering outside the lower trimmer (as seen in the black profiles at z = 95 cm). No significant bump was produced from leakage outside the middle trimmer because the outer trimmer edge was positioned to nearly fully intercept the profile. The analytical model was able to predict both the location and magnitude of these leakage bumps within 0.2% of central-axis dose. However, in the regions between and outside these bumps, the MC profiles showed a small amount of leakage dose that was not predicted by the analytical model. For instance, at the most downstream calculation plane (z = 101 cm), the configuration with one trimmer present (red) resulted in a MC calculated dose of 1.2% at an off-axis position of 18 cm, while the analytical model predicted a dose of only 0.3% at the same position. It was presumed that this dose difference was caused by the Gaussian approximation to the scattering angle and not accounting for large angle scattering in the analytical model. Results of the in-plane 20x20 cm^2 profiles, and the in-plane and cross-plane 10x10 cm^2 profiles, shown in Appendix A, showed similar trends.

3.3.2. Comparison of Analytical Photon Model with MC

The results of the bremmstrahlung model are shown in Figure 3-7. This figure plots the analytically and MC calculated cross-plane profiles at a depth of 1 cm for the 7, 13, and 20 MeV beams with the 20x20 cm^2 applicator. The MC calculations were performed with all accelerator components (○ marker and indicated as "full collimation") and with the collimation system absent (+ marker and indicated as "foils only"). The MC profiles were normalized to total dose (electron and photon) on central axis for both the "foils only" and "full collimation" configurations. For the "full collimation" profiles these normalization values are equal to the *C* coefficient described in Section 2.1.3. These values are 0.9%, 2.4%, and 4.4% for the 7, 13, and 20 MeV beams, respectively. The "foils only" analytical profile is normalized to best fit the MC profile within ±20 cm of central axis, while the "full collimation" analytical profile is normalized to best fit the MC profile within ±10.5 cm of central axis (extent of field width).

The initial angular spread ($A_{0,initial}$ in Equation 3-19) of the analytical calculation was adjusted to best match the MC data. The best fit was produced using $A_{0,initial}$ values of 0.003, 0.001 and 0.0001 rad^2 cm^{-1} for the 7, 13, and 20 MeV beam calculations, respectively. It should be noted that these values were similar, though not identical, to the values of 0.0022, 0.0008, and 0.0004 rad^2 cm^{-1}, respectively, found by Carver *et al.*(2014). Using these initial spread values the model was able to predict the "foils only" profile to within 0.15% of total dose on central axis. However, when the collimation system was added to the profiles, the accuracy of the analytical model declined. The plots show that as the analytical profiles (dashed lines) reach the edge of the field (10.5 cm off axis) the profile drops off rapidly due to attenuation in the applicator trimmers. Outside the projection of the photon jaws the dose goes to 0%. This same feature, however, is not present in the MC "full collimation" profile. This discrepancy is believed due to the analytical model neglecting the dose from bremsstrahlung photons created within the collimating system. This effect causes the analytical model to under-predict the dose outside the field by as much as 0.2%, 0.5%, and 1.2% for the 7, 13, and 20 MeV beams, respectively.

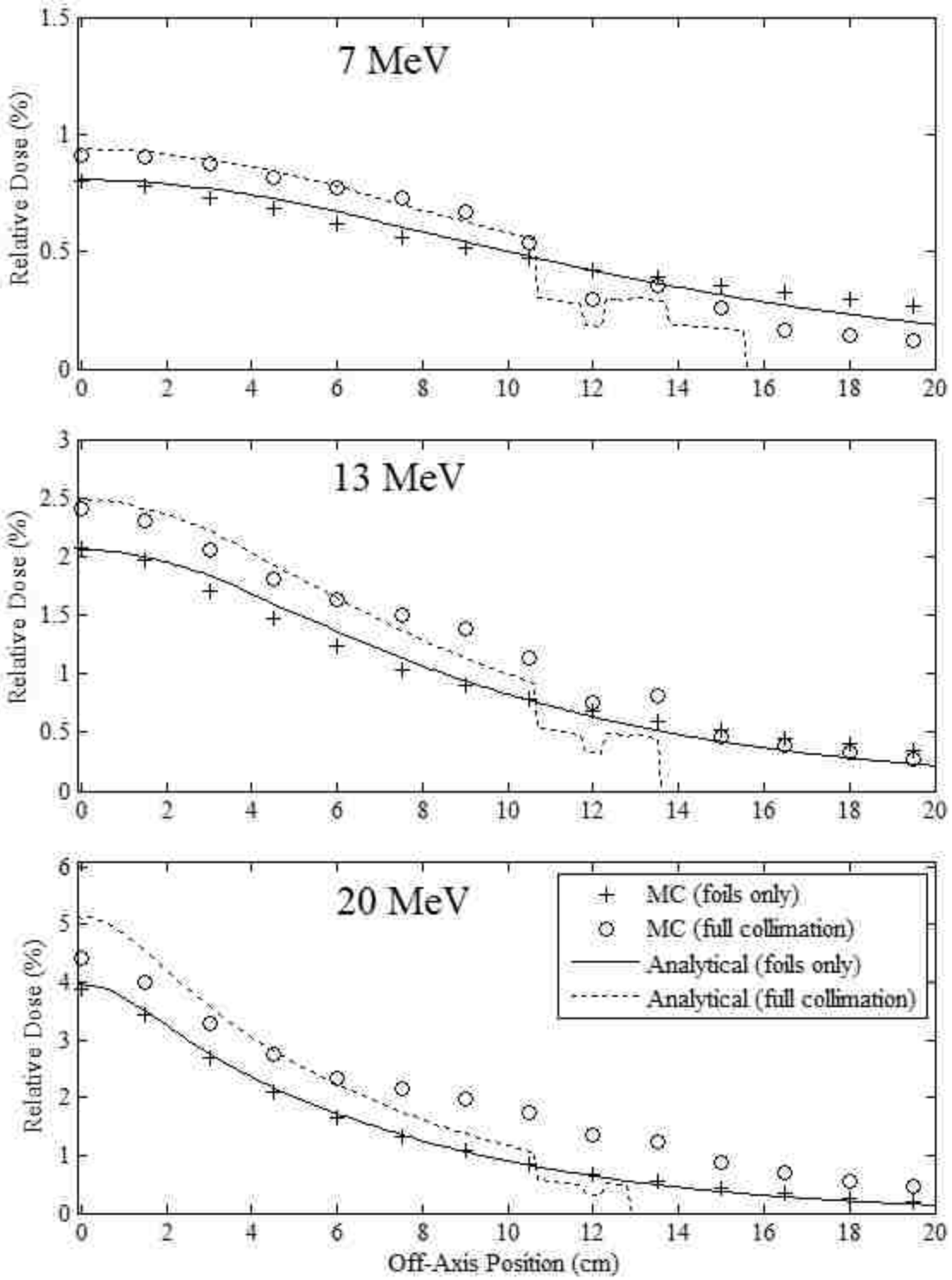

Figure 3-7. Comparison of MC and analytically calculated bremsstrahlung profiles. The figure shows the MC calculated profiles plotted against the analytical calculations for the 7, 13, and 20 MeV beams at 1 cm depth. Profiles labelled "foils only" represent calculations performed with no collimation (MLCs, jaws or trimmers), while the "full collimation" profiles were calculated with all accelerator components present.

It is also worth noting that the presence of the collimation system increases the photon dose within the field. This is evident by the magnitude of the "full collimation" MC profiles being greater than the "foils only" MC profiles. At central axis, the "full collimation" MC-calculated dose was 0.1%, 0.3%, and 0.5% greater than the "foils only" dose for the 7, 13, and 20 MeV beams, respectively.

3.4. Aim 2 - Conclusions

The purpose of Aim 2 was to create an analytical model for predicting the dose distribution of electron beams traversing new collimation system designs. This model would serve as a tool for quickly evaluating multiple unique designs created in the design process. This would provide a distinct advantage over relying solely on time-intensive MC calculations which limits the number of designs that can be evaluated.

- Primary electron dose model within the field: Within the field, the analytical primary electron model performed reasonably well. This model slightly over-predicted the MC-calculated dose at the edge of the field. This was attributed to the analytical model approximating the fluence as uniform at all collimation levels when calculating the scattering moment profiles, which was believed to cause an under-prediction in $\overline{\theta}\,x$ for the pencil-beams near the field edge. In the design process of the new applicator, the trimmer inner edges were brought in as far as possible toward central axis to minimize the applicator weight, while maintaining acceptable flatness within the field (this process is discussed in detail in Aim 5). This procedure of bringing in the trimmer edges magnifies the effect on $\overline{\theta}\,x$ when analytically modeling the distribution of the new design. For this reason, while the primary electron model was a useful tool in modeling the in-field distribution during the design process, in-field beam flatness evaluations were supplemented with MC calculations when determining the inner trimmer edge positions.
- Primary electron dose model outside the field: Outside the field, the primary electron model performed reasonably well. The location and magnitude of the leakage bumps were modeled accurately, typically within 0.2% at the leakage bump peak at the patient plane. However, due to the inaccuracy caused by the Gaussian approximation within the pencil-beam model, the

analytical code under-predicted the dose between these leakage bumps by approximately 1.2%. In addition to these inaccuracies, the model does not account for dose due to electrons scattered off the collimation system, which (as discussed in Aims 1 and 3) has been found to constitute a significant portion of the leakage dose. Due to these factors and the complexity of the components contributing to the dose distribution in this region, it was decided that the analytical primary electron model would not be a suitable tool for predicting the out-of-field dose when evaluating the leakage dose in the collimation system design process.

- Photon dose model inside the field: The analytical photon dose model performed reasonably well within the field, predicting the MC-calculated data throughout the profile to within 0.15% of total dose on central axis. However, the photon contribution to the in-field dose is small compared to other dose components. For instance, for the 7 MeV beam with the 20x20 cm^2 applicator, the photon component constitutes a maximum of 0.9% of the dose within the field. The total dose within the field was found to vary by roughly this same amount for the same beam energy and applicator (c.f. Figure 2-4). These variations are presumably due to collimation scatter dose and non-uniformity of the beam exiting the dual scattering foils, neither of which is accounted for in the analytical model. Therefore, any gains made by predicting the photon distribution in this region will be outweighed by these other inaccuracies. For this reason, the photon model was not considered useful for in-field dose calculation for evaluating the beam flatness within the field during the design process.
- Photon dose model outside the field: The analytical photon model greatly under-predicted the dose in the leakage region for the full collimation calculation. This under-prediction was believed to be caused by the model neglecting photons created within the collimation system. Due of these inaccuracies, the model was not considered useful for predicting the out-of-field dose when evaluating the leakage in the collimation system design process.

Chapter 4 -Aim 3 - Perform Material and Range Analysis to Determine the Best Trimmer Material and Thickness

Aim 3: Determine the optimal high-density material and thickness for the applicator trimmer bars, i.e. the material and range combination which produces the least amount of leakage dose while allowing the applicator to be designed with minimal weight.

4.1. Aim 3 - Introduction

The use of high density metals for the shielding of electron beams is a common practice in electron radiotherapy. These materials are used not only for applicator trimmer fabrication, but for field shaping inserts and skin collimation as well. It has been shown that material selection can have a significant impact on the dose distribution. Lax and Brahme (1980) noted that by using a high density material, the scatter out the side of the applicator could be reduced. These scattered electrons degrade the quality of the beam within the field (beam uniformity and depth of penetration) while tending to increase the dose near the surface. By reducing the number of electrons scattered from the collimating system, this effect can be minimized. An ideal material would have a very large density so that the collimation thickness would be very thin; osmium, has been suggested as "optimal" in ICRU Report 35 for applicator trimmer design due to its high density (ρ = 22.48 g cm^{-3}) (Whycoff *et al.*, 1984). Ebert and Hoban (1995a) went on to further investigate this dose component within the field by using the LATCH bit filtering feature of EGSnrc to calculate dose from electrons scattered from each applicator trimmer, noting that the effects these scattered particles have on the dose distribution vary with both energy and angle of incidence. Additionally, the choice of collimation material has been shown to impact the level of photon production, due to changes in atomic mass affecting the amount radiative energy lost within the material (Prasad *et al.*, 1998).

Many of these previously mentioned investigators, and several others (Choi *et al.*, 1979; Kassaee *et al.*, 1994), primarily focused on the influence of the scattered radiation within the field. However, of equal concern to this study is the effect of trimmer material design on the leakage dose outside the field, whether from scattered electrons or bremsstrahlung photons. Design features which reduce the leakage

dose will aid in the collimation system design, allowing as much shielding material weight as possible to be removed from the trimmers before increasing the leakage dose to unacceptable levels (as defined by the IEC). Therefore, the effect that material has on the leakage dose should be considered when selecting a material for trimmer design.

In addition to determining the proper material for trimmer design, it is also necessary to develop an equation for calculating the range of an electron within the material based on the particle's energy. This energy-range relation equation is used for both calculating the maximum thickness of the trimmer, as well as determining the bevel shape of the trimmer's outer edge (lower electron energies require thinner but wider trimmer material due to increased scatter). When developing this relation, care should be taken to strike a balance between trimmer weight and transmitted dose. If the trimmers are designed too thin, some electrons will penetrate and be transmitted to the patient. If they are designed too thick, the applicator will be needlessly heavy. Several studies have been published which investigate the necessary thickness of lead required to shield electron beams of various energies (Giarratano *et al.*, 1975; Khan *et al.*, 1981). In addition to lead, Prasad *et al.* (1998) expanded these studies to apply them to both copper and aluminum, as did Hogstrom *et al.* (1985) for brass. In each of these studies, electron beam measurements were taken immediately behind material slabs (zero thickness between material and water equivalent slabs) placed within the beam. Similar methods were used in this aim to determine the material thickness necessary to sufficiently reduce the radiation transmitted by the trimmers.

The goal of Aim 3 is to select both the best trimmer material and to determine a suitable equation for relating the beam energy to material thickness. To develop an energy-range relation equation, three methods have been used: (1) a linear fit to previously measured data, (2) the continuous slowing down approximation (CSDA) to calculate the electron range, and (3) a MC analysis in which the slab thickness required to reduce the transmitted electron dose to 1% of maximum was determined. These methods are compared in order to determine the preferred energy-range relation equation for use in the applicator design process.

To determine the preferred trimmer material, a MC analysis is performed which analyzes the leakage dose from applicators modeled of different materials. LATCH bit filtering is used to distinguish dose from particles scattered from various components. These dose components are compared for the different applicator designs to analyze how the trimmer material impacts the dose distribution in the leakage region. This information will be used for the selection of material for the design process.

4.2. Aim 3 - Methods

4.2.1. Determination of Energy-Range Relation

The present study was limited to three materials of considerably different densities, copper (ρ = 8.9 g cm^{-3}), lead (ρ = 11.1 g cm^{-3}), and tungsten (ρ = 18.0 g cm^{-3}). These materials were selected due to their availability, relatively low cost, and common use in accelerator component manufacturing. Osmium, as suggested by ICRU Report 35 (Whycoff *et al.*, 1984), was not considered because it did not fit these criteria.

A key aspect of the applicator design process is developing an equation to relate electron energy to material thickness. This equation is necessary for both calculating the outer trimmer edge bevel shape and for determining the maximum thickness of the applicator trimmers. To develop an energy-range relation equation, three different methods were investigated: (1) a linear fit to previously measured data, (2) the CSDA to calculate the electron range, and (3) a MC analysis for calculating the 1% threshold dose beyond a material thickness.

4.2.1.1. Linear Fit to Measured Data

The first method investigated was a linear fit to previously measured data. Many measurement studies have been performed to determine the thickness of material required to shield electron beams of various energies (Giarratano *et al.*, 1975; Khan *et al.*, 1976; Purdy *et al.*, 1980; Hogstrom *et al.*, 1985; Prasad *et al.*, 1998). In each of these studies, measurements were taken at the distal surface of a material slab placed within electron beams of varying energies. The material thicknesses were varied and compared with the relative ionization measured immediately behind the material to determine the

thickness required to stop the electrons. The measurement results obtained from these studies were used to develop an energy-range relation equation.

In the report of AAPM Task Group 25 (Khan *et al.,* 1991), the results of several of these studies were compiled for lead shielding. The thickness required to stop the electrons was plotted versus $E_{p,0}$ for each beam, and a linear fit was made to the data, as shown in Figure 4-1. This linear fit was used as the energy-range relation equation for lead for the current study.

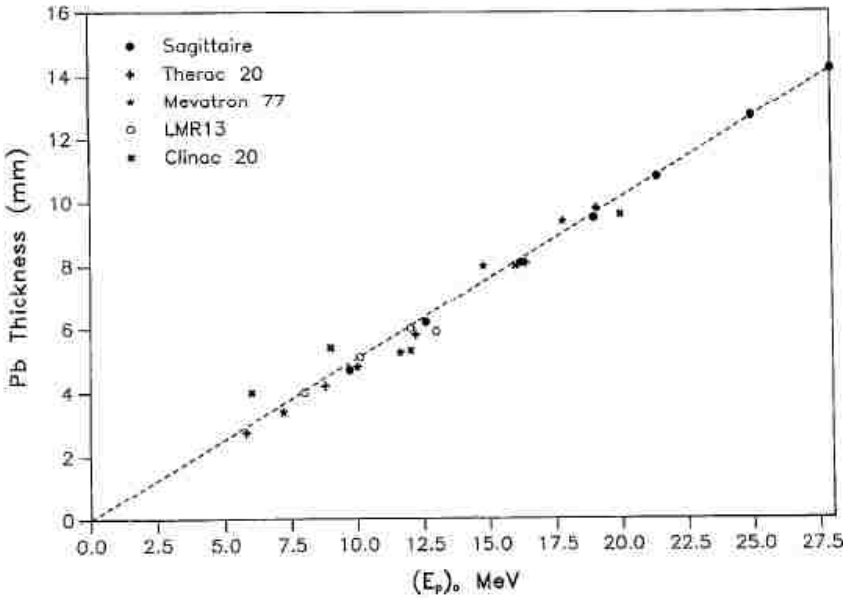

Figure 4-1. Linear fit of lead thickness required to stop electron beams as a function of beam energy. Data were compiled by AAPM Task Group 25 from previously published measured data using various accelerators (Khan *et al.,* 1991).

This process was additionally performed for copper and brass in the current study. For the purposes of this analysis, these two materials were assumed equivalent after accounting for differences in density. Data were obtained from Hogstrom (1985) for brass and Prasad (1998) for copper to create the relation. A linear fit was made to the data to obtain a relation for the copper thickness required to stop electrons for various beam energies. When not otherwise specified in the literature, the densities of lead and copper were assumed to be 11.34 g cm^{-3} and 8.93 g cm^{-3}, respectively, to develop these equations. Because no data could be obtained for tungsten shielding, this material was not investigated.

4.2.1.2. Continuous Slowing Down Approximation

The CSDA is a method for approximating the mean path length of an electron. In this approximation, it is assumed that the rate of energy loss of an electron is always equal to the mean rate of energy loss along the entire track of the particle. This mean rate of energy loss is specified as the reciprocal of the total (radiative and collisional) mass stopping power. The path length for a particle with initial energy E_0 is then found by integrating this mean energy loss over the full energy range, i.e.

$$r_0 = \int_0^{E_0} \left(\frac{S(E)}{\rho}\right)_{tot}^{-1} dE \tag{4-1}$$

In this equation, *S(E)* represents the total stopping power in the material, and the material density is represented by ρ. The total mass stopping power is then represented by $S(E)/\rho$. This equation was evaluated for copper, lead, and tungsten for several energies between 6 and 20 MeV. A second degree polynomial was fit to the data to determine a range versus energy function for each material. For further explanation of the CSDA and determination of *S(E)*, refer to ICRU Report 35 (Whycoff *et al.*, 1984).

4.2.1.3. MC study of 1 Percent Threshold

A third study was performed using EGSnrc to calculate the transmitted dose from electron beams of various energies incident on material slabs of various thicknesses. This study is conceptually similar to that of the first method discussed, the linear fit to measured data, except that MC techniques were used rather than measurement. Using MC methods has two advantages over the measurement study. First, the raw collected data would be available for analysis, rather than attempting to collect range data from published figures and data compiled by others. Second, the exact materials from the MC model used for the applicator design would be available for analysis, eliminating any small errors caused by the use of slightly different metal alloys.

In this analysis, a set of parallel monoenergetic electron beams with varying energies was simulated to traverse various thicknesses of metal material modeled in BEAMnrc. The beams were incident perpendicular to a metal slab such that the dose could be scored in water immediately beyond the

distal surface of the slab. A beam's-eye view image of this slab is shown in Figure 4-2. The slab was divided into 25 subsections of different thicknesses, indicated by the light gray squares in the figure, each with an area of 5x5 cm^2. Simulations were performed with six different monoenergetic electron energies, 6, 9, 12, 15, 18, and 21 MeV. The dose was scored in a phase space file at the distal surface of the metal slab, which was used as input to DOSXYZnrc to calculate the dose. Dose was calculated in water voxels with an area of 2x2 cm^2, and a depth of 0.5 cm. These voxels are shown as the dark gray squares in Figure 4-2. The voxels were situated with the proximal voxel surface flush against the distal surface of the slab, centered behind the center of each corresponding material thickness subsection. This allowed for a 1.5 cm gap between each dose calculation voxels and the other thickness subsections, eliminating any contamination dose from particles scattered from other subsections. The dose was normalized to the maximum dose of the beam in water with no slab, per the recommendations of AAPM Task Group 25 (Khan *et al.*, 1991).

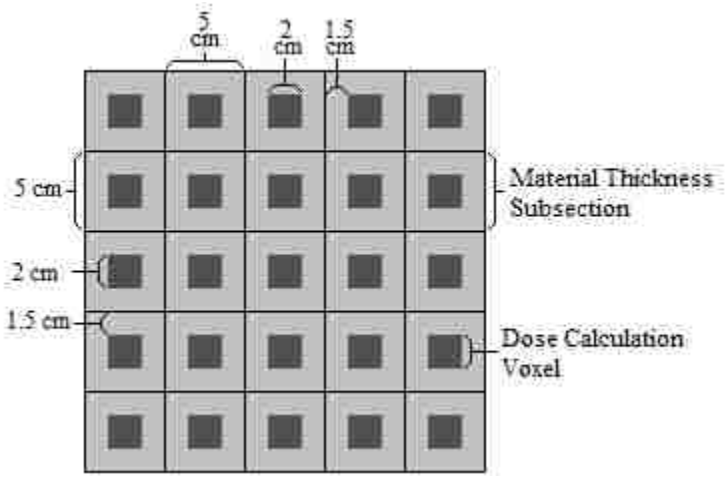

Figure 4-2. Beam's-eye view of metal slab divided into 25 subsections of different thicknesses for MC calculations. The light gray squares represent the 5x5 cm^2 material thickness subsections and the dark gray squares represent the 2x2 cm^2 dose calculation voxels, each centered behind the corresponding material thickness subsection.

These calculations were performed using material slabs composed of copper, lead and tungsten alloys. All transport parameters (e.g. boundary crossing algorithm, global cutoff energies, etc.) used in the Elekta Infinity BEAMnrc model, were also used in this study. When the calculated relative dose is

plotted against material thickness, the dose falls off with thickness beyond R_{100}, and below 10% it transitions into an approximately linear photon dose region. This transition occurs at the material thickness required to stop all electrons of a particular energy, leaving only bremmstrahlung photons created within the material to deposit dose distal to the slab. Figure 4-3 shows this transition, plotting the relative dose calculated immediately behind a slab versus the slab thickness for a low, medium, and high energy electron beam. In this figure the photon dose region is labelled, and the dotted lines depict linear extrapolations of the photon dose region. The 1% threshold markers designate the material thickness at which the relative dose diverges from the linear extrapolation of the photon dose region by 1% for each beam energy, indicating the approximate thickness of material required to reduce transmitted electron dose to 1% of maximum total dose with no material present. These 1% threshold thickness values were calculated for each beam energy used in the MC calculations (6, 9, 12, 15, 18, and 21 MeV) for the copper, lead, and tungsten slabs. The resulting plots and 1% threshold thicknesses for all materials and energies in this analysis are plotted in Figure B-1 in Appendix B To create an equation relating this material thickness to energy, a second degree polynomial was fit to the data for each material.

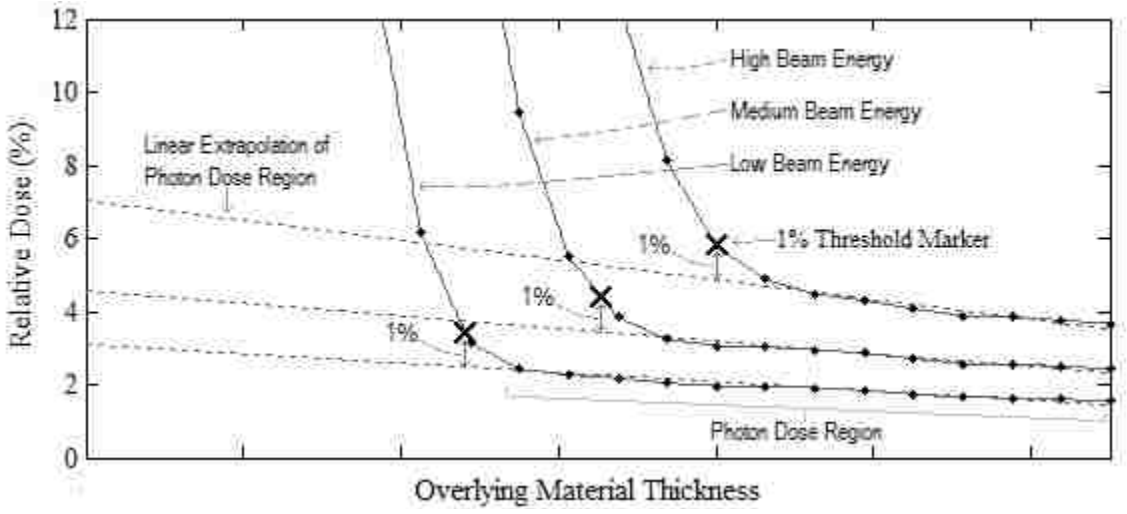

Figure 4-3. Comparison of relative dose calculated versus material thickness in the low dose region. This figure plots the relative dose calculated in water immediately behind various thicknesses of material for various energy beams. The black dots represent each dose calculation value and the dashed lines show a linear extrapolation of the photon region for each beam energy. The 1% threshold markers, designate the thickness at which the relative dose diverges from the linear extrapolation of the photon dose by 1%.

4.2.2. Effects of Trimmer Material on Leakage Dose

Collimation material has been shown to greatly influence the dose distribution at the patient plane due to electron scatter from the applicator edges. Lax and Brahme noted that by using a high density material, the contribution of collimator scattered electrons to the in-field dose can be reduced. This has the effect of lowering the surface dose within the field and increasing R_{100} (Lax and Brahme, 1980; Whycoff *et al.*, 1984). However, of equal concern in this investigation, is how the trimmer material may affect the scatter dose in the out-of-field region. It was determined from the results of Aim 1 that the scatter from the applicator can constitute a significant portion of the dose in the leakage region (approximately 60% of the mean percent leakage dose for the current clinical Elekta Infinity collimation system).

To study the effects of trimmer material on this scatter dose component, a MC study was performed. In this study, three different 20x20 cm^2 applicators were investigated, modeled in BEAMnrc using copper, lead, and tungsten trimmers. Geometric specifications used for these applicator models were obtained from a preliminary applicator design created within the collimation system design process. These specifications were obtained from an optimization performed using a non-finalized version of the analytical primary electron model, and are therefore not discussed in the collimation system design process. Each applicator was designed using a method of matching the trimmer inner and outer trimmer edges to the width of the beam penumbra. In the in-plane dimension, the inner edges were positioned to intercept the penumbra at off-axis ratio (OAR) percentages of 67.5%, 93%, and 93.5% for the upper, middle, and lower trimmers, respectively. For the cross-plane dimension these inner edge penumbral OAR intercepts were 86.5%, 93.5%, and 94% for the upper, middle, and lower trimmers, respectively. The outer trimmer edges were beveled with the outermost extent of the bevel positioned to intercept the penumbra of a 6 MeV beam at an OAR of 2%. Refer to Aim 5 for a detailed explanation of this design methodology. The distal trimmer surfaces were positioned at *z*-values of 64.5, 77.5, and 95 cm. The maximum thickness of the trimmers was calculated using the CSDA method for a 20 MeV electron beam, and the inner trimmer edges were designed vertical (non-divergent). All lateral dimension design

specifications (e.g. jaw positions and inner and outer trimmer edge positions) were held constant for applicators modeled of each material.

These applicator models were inserted into the BEAMnrc model for the Elekta Infinity accelerator, replacing the current clinical applicator models. Simulations were performed with these new applicators while maintaining all source parameters (peak energy, spectrum FWHM, number of generated particles, etc.), accelerator head specifications, and transport parameters from the original model. As in the previous studies, these simulations were used to produce phase space files which were used as input to DOSXYZnrc to calculate the dose. Dose was calculated in a water phantom positioned at 100 cm SSD with 0.5x0.5x0.5 cm^3 voxels centered at a depth of 1 cm. The calculations were performed for all three material applicator designs with the 7, 13, and 20 MeV beams.

In addition to the total dose calculations, the LATCH bit filtering feature in EGSnrc was used to independently calculate the dose from various dose components using DOSXYZnrc, similar to the methodology used in Aim 1. This feature was used to differentiate electrons scattered from the MLC, the photon jaws, and the upper, middle, and lower trimmers, and calculate their dose distributions independently. Additionally, the total photon dose, total electron dose, and primary electron dose distributions were independently calculated.

The total dose was calculated using 10^9 particles sampled from the phase space, while the LATCH bit dose component calculations were performed with $2.5x10^8$ particles. To reduce statistical uncertainty, the dose distributions were symmetrized about central axis in both the in-plane and cross-plane dimensions. All distributions were normalized to the mean total dose calculated within a 3x3 set of voxels centered at central axis at the calculation depth of the distributions. The mean percent leakage dose was calculated for each dose component per IEC specifications at each energy for each applicator material.

4.3. Aim 3 - Results and Discussion

4.3.1. Determination of Energy-Range Relation

The results from each of the three methods for determining the energy-range relation (linear fit to measured data, CSDA, and MC 1% threshold) are shown in Figure 4-4 and Table 4-1. Figure 4-4 plots the calculated material thickness versus beam energy for each energy-range relation method, showing results for copper in blue, lead in green, and tungsten in red. The vertical dashed magenta line indicates a beam energy of 20 MeV. Because 20 MeV is the upper limit of the energy range accounted for in the applicator design, the intersection of each curve with this line indicates the full range thickness of the

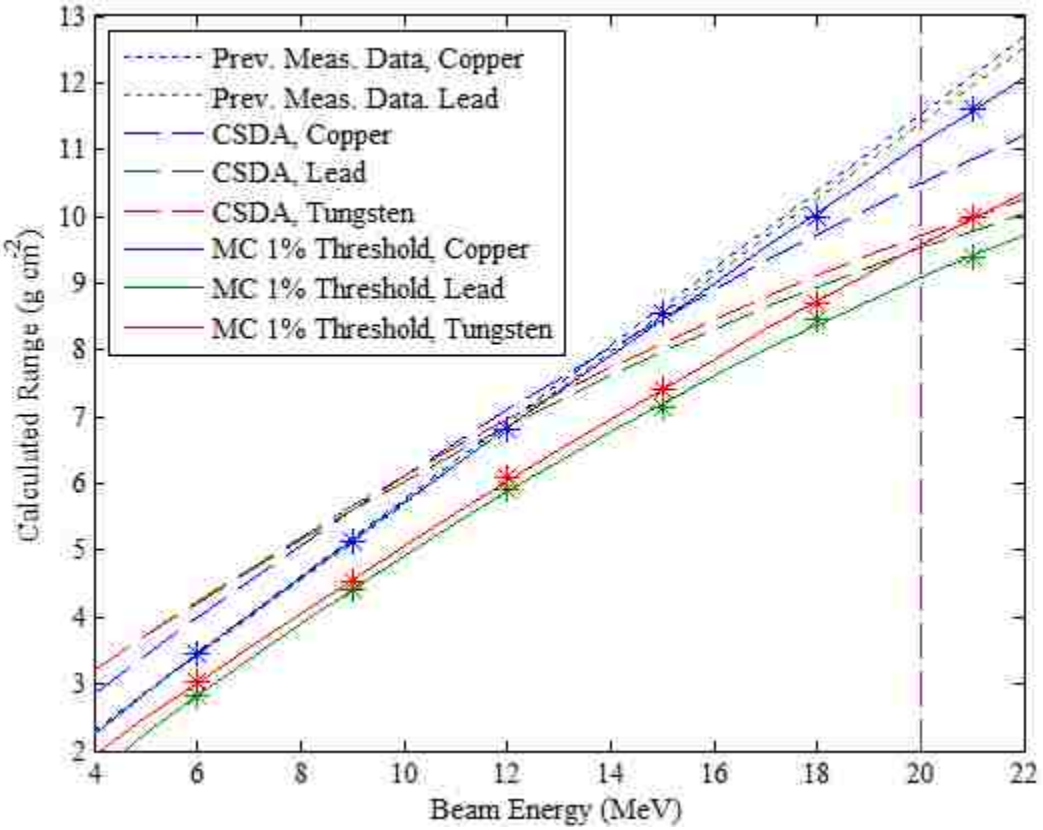

Figure 4-4. Comparison of methods for determining the energy-range relation for each material. The figure plots the calculated thickness of material required to shield electrons of various energies. The results for copper are shown in blue, lead in green and tungsten in red. The stars represent the thicknesses calculated for each of the six energies used in the MC 1% threshold method. The intersection of each curve with the vertical dashed magenta line illustrates the range calculated at 20 MeV, which designates the full thickness of the trimmer.

trimmer calculated using each method. It should be noted that the $E_{p,0}$ and width of the 20 MeV spectrum results in a significant portion of the 20 MeV beam electrons having an energy between 20 and 22 MeV; however, the few electrons that might penetrate are small in number, low in energy, and large in angular spread, and can be ignored. Table 4-1 shows these trimmer thickness values, expressed in both g cm^{-2} and cm, for each calculation method and material.

The results for the linear fit to previously measured data are shown with the short-dashed curves. There is little difference between the copper (blue) and lead (green) results, with the copper curve having a slope of 0.58 g cm^{-2} MeV^{-1} and lead having a slope of 0.57 g cm^{-2} MeV^{-1}. As Table 4-1 indicates, this method results in full trimmer thicknesses of 11.54 and 11.40 g cm^{-2} for the copper and lead calculations, respectively. This also corresponds with the "1 mm per 2 MeV" rule of thumb for lead shielding from AAPM Task Group 25 (Khan *et al.*, 1991).

Table 4-1. Full trimmer thicknesses as calculated by each range-energy relation method. The full thicknesses were determined by using each method to calculate the electron range for a 20 MeV beam. The ranges are expressed in both units of g cm^{-2} and cm for each calculation.

	Copper (ρ = 8.9 g cm^{-3})		Lead (ρ = 11.1 g cm^{-3})		Tungsten (ρ = 18.0 g cm^{-3})	
	g cm^{-2}	cm	g cm^{-2}	cm	g cm^{-2}	cm
Measured Data	11.54	1.30	11.40	1.03	NA	NA
CSDA	10.49	1.18	9.52	0.86	9.72	0.54
MC 1% Threshold	11.08	1.24	9.08	0.82	9.56	0.53

The long-dashed curves in the figure show the results for the CSDA calculations. When compared with the curves for the previously measured data, the CSDA calculations produce a greater necessary thickness for low beam energies, but a lesser necessary thickness for high energy beams. The figure shows that as the energy increases, the slopes of the CSDA curves decrease. This decrease can be attributed to the increased radiative energy loss for higher energy electrons, which is accounted for in the CSDA. This effect is due to the high atomic numbers of these elements increasing the radiative energy loss. It is most evident in tungsten and lead, which have atomic numbers of 74 and 82, respectively, as opposed to 29 for copper.

The results of the MC 1% threshold method are shown by star markers (✳) and the solid lines. The star markers show the calculated 1% threshold for each energy studied in this investigation; the solid curves show the second degree polynomial fit to this data. This method produced the smallest calculated ranges at 20 MeV for both tungsten and lead. As indicated in Table 4-1, the calculations produce full trimmer thicknesses of 9.08 and 9.56 g cm^{-2} for lead and tungsten, respectively. For lead, this is a 5% reduction in the full trimmer thickness compared with the CSDA method, and a 20% reduction when compared with the method using previously measured data. This implies that using the 1% threshold method to determine the trimmer thickness should reduce the trimmer weight by approximately these percentages. The effect of radiative energy loss causing the slope to decrease at higher energies is also observed in these curves, though the change is less significant than with the CSDA method.

4.3.2. Effects of Trimmer Material on Leakage Dose

Similar to the results shown in Aim 1 for the current clinical 20x20 cm^2 applicator, components of the leakage dose for 20x20 cm^2 copper, lead and tungsten applicators for the 7, 13, and 20 MeV beams are shown in Figure 4-5, as well as Figures B-2 through B-6 in Appendix B. These data are used to determine the contribution of each dose component to the mean percent leakage dose per IEC specifications, shown in Table 4-2.

The MC-calculated cross-plane dose profiles for this study are plotted versus off-axis position in Figure 4-5 for the 20 MeV beam. The results for the copper applicator are shown in the upper row of plots, lead in the middle row, and tungsten on the bottom row. In this figure, the left column of plots shows the total leakage dose, along with the total electron and total photon contributions for each applicator. From these plots, a decrease in both the total dose and electron dose can be seen as the applicator material changes from copper (upper plot) to lead (middle plot), and then again from lead to tungsten (lower plot). Additionally, an increase in photon dose can be seen as the material changes from copper to lead and tungsten.

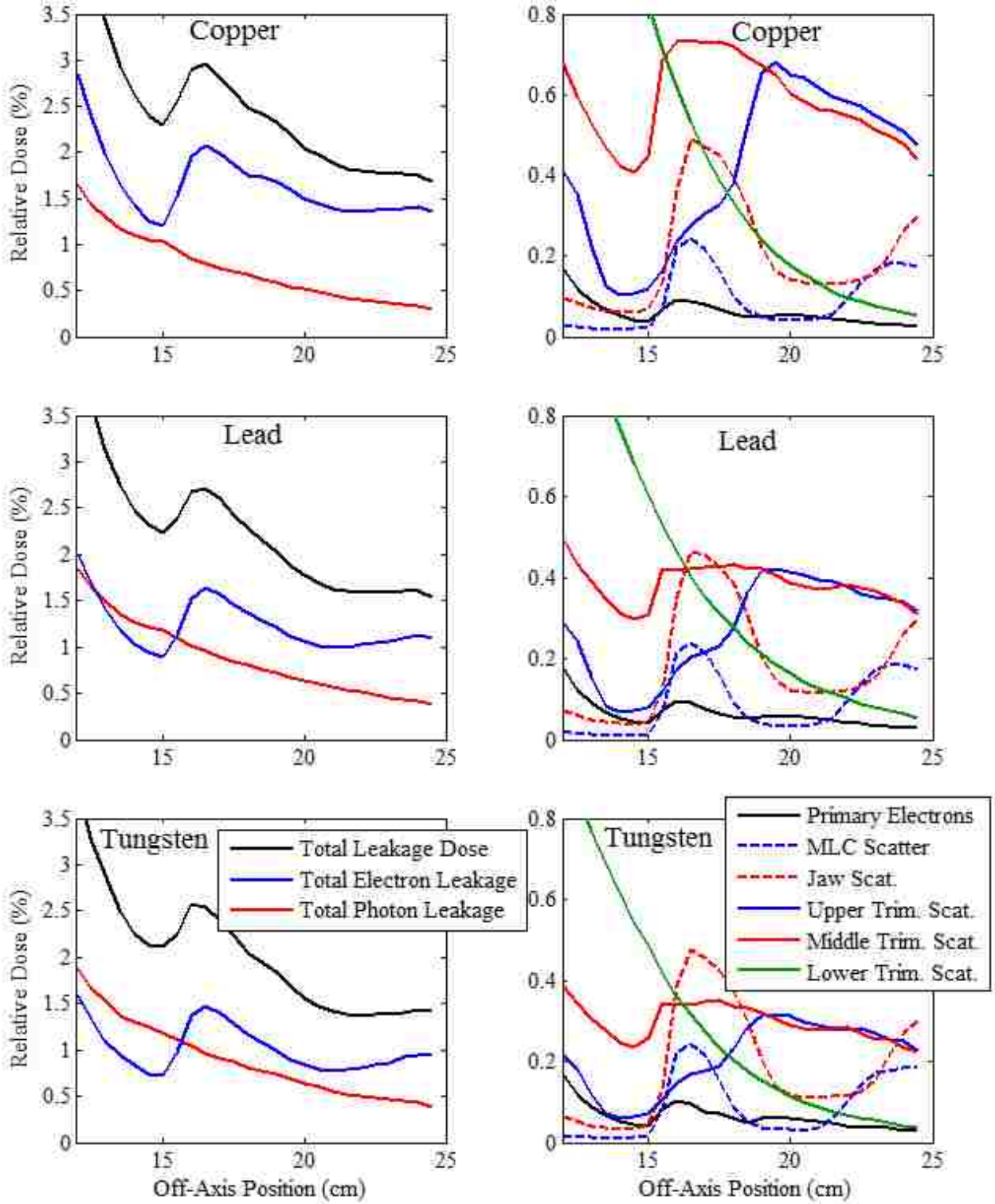

Figure 4-5. Cross-plane leakage dose component profiles for copper, lead and tungsten 20x20 cm^2 applicators for the 20 MeV beam.The copper profiles are shown on the top row, lead in the middle, and tungsten profiles on the bottom row. The left column of plots shows a breakdown of the total leakage dose (black) along with the differentiated electron (blue) and photon components (red). The right column further breaks down the electron leakage dose into primary electrons and various scattered electron components.

Table 4-2. Mean percent leakage for each dose component for each applicator material. The mean leakage from each component, calculated by IEC specifications, is shown for applicators constructed of copper, lead, and tungsten. Results are shown for the 7, 13 and 20 MeV beams and are normalized to both D_{max} (left columns) and the total mean leakage (right columns).

Leakage Dose Components	Copper Applicator					
	Normalized to D_{max}			Normalized to Total Leakage		
	7 MeV	13 MeV	20 MeV	7 MeV	13 MeV	20 MeV
Total Dose	0.87	0.94	1.51	100.0	100.0	100.0
Total Electron	0.78	0.71	1.02	89.0	74.9	67.5
Total Photon	0.09	0.23	0.45	10.8	24.2	30.0
Primary Electrons	0.19	0.06	0.03	21.8	6.3	2.2
MLC Scatter	0.16	0.08	0.04	18.2	9.0	2.8
Jaw Scatter	0.16	0.12	0.12	18.2	12.4	8.1
Upper Trimmer Scat.	0.14	0.18	0.30	15.6	19.4	20.0
Middle Trimmer Scat.	0.15	0.24	0.43	16.7	25.1	28.6
Lower Trimmer Scat.	0.03	0.10	0.23	4.0	10.3	15.0

Leakage Dose Components	Lead Applicator					
	Normalized to D_{max}			Normalized to Total Leakage		
	7 MeV	13 MeV	20 MeV	7 MeV	13 MeV	20 MeV
Total Dose	0.84	0.88	1.39	100.0	100.0	100.0
Total Electron	0.73	0.59	0.75	86.9	66.4	54.3
Total Photon	0.11	0.29	0.57	13.0	31.9	40.5
Primary Electrons	0.20	0.06	0.03	23.8	6.9	2.5
MLC Scatter	0.16	0.08	0.04	19.1	9.4	3.0
Jaw Scatter	0.16	0.11	0.11	19.2	12.8	8.1
Upper Trimmer Scat.	0.11	0.13	0.20	12.7	14.8	14.5
Middle Trimmer Scat.	0.11	0.17	0.28	13.3	18.9	19.9
Lower Trimmer Scat.	0.03	0.09	0.18	3.8	9.8	13.1

Leakage Dose Components	Tungsten Applicator					
	Normalized to D_{max}			Normalized to Total Leakage		
	7 MeV	13 MeV	20 MeV	7 MeV	13 MeV	20 MeV
Total Dose	0.79	0.79	1.27	100.0	100.0	100.0
Total Electron	0.69	0.50	0.62	86.7	63.7	48.8
Total Photon	0.11	0.29	0.57	13.8	36.6	45.1
Primary Electrons	0.22	0.06	0.04	27.3	8.2	3.0
MLC Scatter	0.17	0.08	0.04	21.3	10.6	3.3
Jaw Scatter	0.16	0.11	0.11	20.7	14.2	8.8
Upper Trimmer Scat.	0.07	0.10	0.16	9.5	12.7	12.4
Middle Trimmer Scat.	0.08	0.12	0.22	9.9	15.6	17.0
Lower Trimmer Scat.	0.02	0.06	0.14	2.7	7.5	10.9

The right column of plots further magnifies the low dose region and breaks down the electron leakage dose into contributions from primary electrons and electrons scattered from various collimation components. These plots show the decrease in dose from the scatter components from the upper trimmer (solid blue line), middle trimmer (solid red line), and lower trimmer (solid green line) as the trimmer material changes from copper to lead, and then again from lead to tungsten. The profiles of the other three components, primary electrons, MLC scattered electrons, and jaw scattered electrons, were unaffected by the different applicator materials. The cross-plane profiles for the 7 and 13 MeV beams are shown in Figures B-2 and B-3, respectively. Figures B-4, B-5, and B-6 show the in-plane results for the 7, 13, and 20 MeV beams, respectively.

The mean percent leakage dose was calculated for each dose distribution per IEC specifications, shown in Table 4-2. In this table the mean leakage is normalized both to maximum total dose on central axis (D_{max}) and to the total mean leakage dose. From the table, it is evident that for all energies, the tungsten applicator produced the least total mean leakage dose with the copper design producing the greatest mean leakage. This difference was most evident for the 20 MeV beam, where the mean leakage was reduced from 1.51% to 1.27% of D_{max} by designing the applicator out of tungsten rather than copper. The contributions of MLC and jaw scatter to the leakage dose were unaffected by applicator material. However, the leakage contribution from the each trimmer was largely affected. The upper, middle, and lower trimmer mean leakage contributions for the copper applicator with the 20 MeV beam were found to be 0.30%, 0.43%, and 0.23%, respectively. When calculations were performed with the tungsten applicator at the same energy, these trimmer scatter values were reduced to 0.16%, 0.22%, and 0.14%, respectively. This results in a combined trimmer scatter dose difference of 0.44% [(0.30 + 0.43 + 0.23) - (0.16 + 0.22 + 0.14) = 0.44] between the copper and tungsten applicators, which fully accounts for the differences in the total electron leakage contributions for these two materials [1.02% - 0.62% = 0.40%] at 20 MeV. The scatter values for the lead applicator fall in between those of copper and tungsten, with mean leakage dose contributions of 0.20%, 0.28%, and 0.18% for the upper, middle, and lower lead trimmers, respectively. This change in scatter contribution can be attributed to the density of each

material. The density of the tungsten alloy used in the MC model (18.0 g cm^{-3}) is significantly greater than either the copper (8.9 g cm^{-3}) or lead (11.1 g cm^{-3}) materials. As the density of the material increases, the range of the electrons within the material decreases. This causes the electrons entering the upper surface of a trimmer to travel farther laterally in a copper trimmer than a tungsten trimmer, which gives the electron a greater chance of escaping from edge of the copper trimmer.

Conversely, the photon dose increased with the higher density materials. For the 20 MeV beam, the photon contribution to the mean leakage was increased from 0.45% for the copper applicator to 0.57% for both the lead and tungsten applicators. This effect can be attributed to the differences in atomic numbers of the materials. The large atomic numbers of lead and tungsten (82 and 74, respectively) cause these materials to produce more radiative energy loss while stopping the electrons than copper (atomic number of 29). This radiative energy is lost in the form of bremsstrahlung photons, many of which ultimately reach the patient plane and deposit their dose in the leakage region. The influence of this effect on the mean leakage, however, is far less significant than that of the decreased trimmer scatter with increasing trimmer density.

4.4. Aim 3 - Conclusions

The purpose of Aim 3 was to both select a material for the trimmer fabrication and the method for calculating the thickness of material necessary to shield electrons of a specified energy. Three methods were investigated for developing this energy-range relation: a linear fit to previously measured data, the CSDA to calculate the mean electron range, and a MC analysis for calculating the 1% threshold dose at the distal surface of a material thickness. Additionally, a MC study was performed to gain insight into the best material for the applicator design, which calculated the leakage dose from applicators modeled of copper, lead, and tungsten.

4.4.1. Determination of Energy-Range Relation Equation

- Calculation method effect on trimmer thickness: The results of the energy-range relation study showed that the MC 1% threshold method produced the smallest calculated range at 20 MeV for both tungsten and lead. This implies that by using the equation derived from this method, rather

than the previously measured data or CSDA methods, the trimmers would be designed thinner, and therefore lighter. For this reason, the 1% threshold method equation was selected for use in the design process.

- Material effect on trimmer thickness: Additionally, the data show that by using a high atomic number material (e.g. lead or tungsten) the calculated range at 20 MeV was reduced. This can be attributed to the increased radiative energy lost by the electrons within these materials.

4.4.2. Effects of Trimmer Material on Leakage Dose

- Effect of trimmer material on out-of-field applicator scatter dose: To gain insight into the best material to use for the applicator design, a MC study was performed which calculated the leakage dose from applicators modeled of copper, lead, and tungsten. The results showed that designing the trimmers out of higher density materials decreases the mean leakage due to the decreased electron scatter from the trimmer edges. This effect was attributed to the high material density decreasing the extent of lateral scatter of the electrons, causing fewer particles to escape the edge of the trimmer.
- Effect of trimmer material on out-of-field photon dose: The study also showed that using a lower atomic number material decreased the photon dose in the out-of-field region, but this effect had much less of an impact on the mean leakage dose than the electrons scattered from the applicator.
- Selection of trimmer material: Due to this result of high density materials decreasing the leakage dose, along with the effect of high atomic number materials decreasing the trimmer thickness, tungsten (ρ of 18.0 g cm^{-3} and atomic number of 74) was selected for use in the design process.

Chapter 5 - Aim 4 - Determine Inner Edge Divergence Angles for Each Trimmer

Aim 4: Determine whether it is more suitable for the inner edge of each trimmer to be situated parallel to central axis or divergent such that it is emanating from the virtual source of the beam. The divergence angles that minimize out-of-field leakage dose are more suitable.

5.1. Aim 4 - Introduction

In Aim 1, it was shown that electron scatter from the applicator trimmer bars constitute a significant portion of the leakage dose (approximately 60% for the current clinical Elekta Infinity collimation system). Design features were sought to keep this scattered leakage dose to a minimum. This aided in the applicator design process, allowing the trimmers to be composed of as little material as possible without increasing the leakage dose to unacceptable levels. In Aim 3, a MC analysis showed that trimmer material can have a significant impact on scattered electron dose. It was shown that applicator trimmers composed of higher density metal reduce the dose from electrons scattered from the trimmers into the leakage region.

Another aspect of collimation design that affects the dose distribution from applicator scattered electrons is the divergence of the inner edges of the trimmers. Previous studies have shown that the angle of beam incidence relative to the trimmer edge can affect the scatter distribution from a collimator. A MC study performed by Ebert and Hoban (1995b) demonstrated that when the beam trajectory angle is small with respect to the trimmer edge, the fluence from scattered electrons is reduced. This angle of incidence was found to not only affect the number of particles scattered from the trimmer, but the directional and energy distributions of the scattered particles as well. Several studies have been performed analyzing the effects of these scattered particles on the in-field distribution (Choi *et al.*, 1979; Kassaee *et al.*, 1994; Ebert and Hoban, 1995a); however, of greater importance for evaluating the hypothesis of this project is how these applicator scattered electrons affect the leakage dose outside the field. To investigate this matter, a MC study using EGSnrc was performed analyzing the leakage dose from applicators designed with varying inner trimmer edge angles. The applicators were designed such

that the inner edges of the trimmers were situated at different angles with respect to central axis. MC calculations were performed with 20x20 cm^2 applicators modeled with three different inner edge divergences and the mean percent leakage from each inner edge design was determined. The purpose of Aim 4 was to select the optimal inner trimmer edge configuration that minimizes this leakage dose for the applicator design process.

5.2. Aim 4 - Methods

The applicator trimmers can be designed such that the inner edges are angled either vertically (i.e. parallel with central axis), divergent such that the edge surfaces are aligned with the divergence of the beam for each trimmer, or at any angle between the two. For the current clinical Elekta Infinity applicators the upper and middle trimmers are designed with vertical, or non-divergent, inner edges. The lower trimmers consist of an aluminum plate with a non-divergent inner edge situated atop a lead field insert with an inner edge divergence angle of 10˚ from vertical, which does not vary with applicator (field size).

The purpose of this study was to investigate whether adjusting this angle reduces the leakage dose from applicator scattered electrons. For this purpose, a MC study was performed in which three different 20x20 cm^2 applicator models were analyzed. The applicators were modeled in BEAMnrc with the inner trimmer edge angles situated in three different configurations: (1) non-divergent (i.e. parallel to central axis), (2) fully-divergent (i.e. as if emanating from the virtual electron source), and (3) semi-divergent (i.e. at an angle halfway between the two). Figure 5-1 illustrates each of these configurations. The figure also depicts the divergence angle, which is defined as the angle between the inner trimmer edge and beam central axis, i.e. a non-divergent edge would have a divergence angle of 0˚.

To model the trimmers in this manner required modifications to the applicator component module within the Elekta Infinity BEAMnrc model. Instead of modeling the applicator using the APPLLICAT module (Harris, 2012), three successive PYRAMIDS modules were used, one for each trimmer. This was

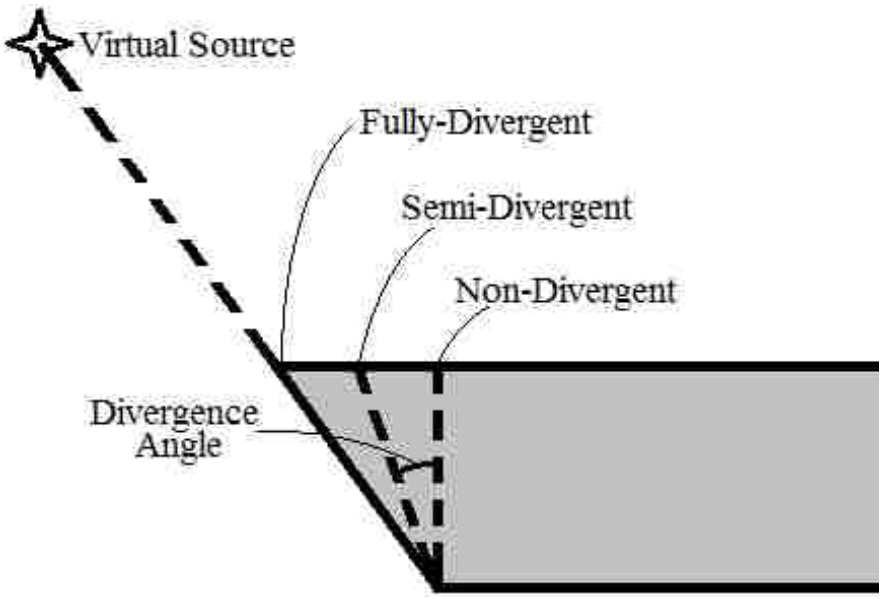

Figure 5-1. Depiction of trimmer inner edge angled to be fully-divergent, semi-divergent, or non-divergent.

done because the PYRAMIDS module in BEAMnrc allows for angled inner edges while the APPLLICAT module does not. The applicators were modeled using the same design parameters used in Aim 3 (e.g. collimation edge positions, trimmer thicknesses, etc.), which were obtained from an optimization performed using a non-finalized version of the analytical primary electron model, and are therefore not discussed in the collimation system design process. In the in-plane dimension, the inner edges of the upper, middle, and lower trimmers were positioned to intercept the penumbra at OAR percentage values of 67.5%, 93%, and 93.5%, respectively. For the cross-plane dimension these inner edge penumbral OAR intercepts were 86.5%, 93.5%, and 94% for the upper, middle, and lower trimmers. The outer trimmer edges were beveled with the outermost extent of the bevel positioned to intercept the penumbra of a 6 MeV beam at an OAR of 2%. Refer to Aim 5 for a detailed explanation of this design methodology. The distal trimmer surfaces were placed at *z*-positions of 64.5, 77.5, and 95 cm, and the trimmers were modeled of tungsten with thicknesses calculated using the CSDA method for a 20 MeV electron beam. Since all specifications other than inner edge angle were maintained from the previous aim, the non-divergent applicator in this study was identical to the tungsten model in Aim 3. All lateral

dimension design specifications (e.g. jaw positions, inner and outer trimmer edge positions, and bevel shape) were held constant for each of the three applicator inner edge divergence designs. This configuration and methodology resulted in the applicator designed with fully-divergent inner edges having divergence angles of 8.2˚, 7.2˚, and 6.1˚ for the upper, middle, and lower trimmers, respectively. These divergence angles were reduced to 4.1˚, 3.6˚, and 3.1˚, respectively, for the semi-divergent edge applicator design.

These applicators were inserted into the BEAMnrc model for the Elekta Infinity accelerator, replacing the current clinical applicator models. Calculations were performed with these new applicators while maintaining all source parameters, accelerator head specifications, and transport parameters from the original model to produce phase space files which were used as input to DOSXYZnrc to calculate the dose. As in Aim 3, total dose was calculated in a water phantom positioned at 100 cm SSD with 0.5x0.5x0.5 cm^3 voxels centered at 1 cm depth using 10^9 initial particles sampled from the phase space. The calculations were performed for all three applicator designs with the 7, 13, and 20 MeV beams. Additionally, like in the previous studies, the LATCH bit filtering feature in EGSnrc was used to distinguish various dose components. Electrons scattered from the upper, middle, and lower trimmers were latched, and the electron scatter dose from each of these three collimation components was independently calculated. These LATCH bit dose calculations were performed using $2.5x10^8$ initial particles sampled from the same phase spaces used in the total dose calculations for each beam energy and applicator inner edge design. To reduce statistical uncertainty, the dose distributions were symmetrized about central axis in both the in-plane and cross-plane dimensions for all calculations. Mean percent leakage doses were calculated for the total dose and for each trimmer scatter dose component based on IEC specifications for each beam energy-applicator trimmer inner edge design combination.

Based on the results of these calculations it was decided that an additional applicator design should be investigated. A fourth 20x20 cm^2 applicator model was created in which the upper and middle trimmers were designed with fully-divergent inner edges and the lower trimmer was designed with non-divergent inner edges, while maintaining all other design parameters. MC calculations were performed

with this applicator inserted into the BEAMnrc accelerator model with the 7, 13, and 20 MeV beams. Total dose was again calculated using DOSXYZnrc with 10^9 particles using the same parameters as the previous dose calculations. For this model only total dose was calculated, and calculations for individual scatter dose components were not preformed. The dose distributions were symmetrized about central axis in both the in-plane and cross-plane dimensions to reduce statistical uncertainty. All profiles were normalized to the mean total dose calculated within a 3x3 set of voxels centered at central axis at the calculation depth of the profiles. Mean percent leakage dose values were again calculated for the total dose based on IEC specifications for each beam energy.

5.3. Aim 4 - Results and Discussion

Results of the MC calculations performed to analyze leakage dose from applicators designed with varying inner trimmer edge divergence angles are shown in Figures 5-2, 5-3, and 5-4, plotting cross-plane relative dose profiles versus off-axis position in the leakage region for the 7, 13, and 20 MeV beams, respectively. The plot in the upper left of each figure shows results for the total dose calculation; the other three plots show the LATCH bit filter calculation dose profiles for the upper, middle, and lower trimmer scatter components. Each of these plots contains curves representing calculations performed with applicators designed with non-divergent, semi-divergent, and fully-divergent inner trimmer edges.

The total dose data show that for all energies the non-divergent applicator design resulted in the most total dose in the leakage region, while the fully-divergent design resulted in the least total leakage dose. The same was true for each of the plots for upper, middle, and lower trimmer scatter, with the fully-divergent design producing the least scattered electron leakage and the non-divergent design producing the most scattered electron leakage for all beam energies. The semi-divergent relative dose profile fell between the non-divergent and fully-divergent relative dose profiles for the total dose and each trimmer scatter dose component at all beam energies.

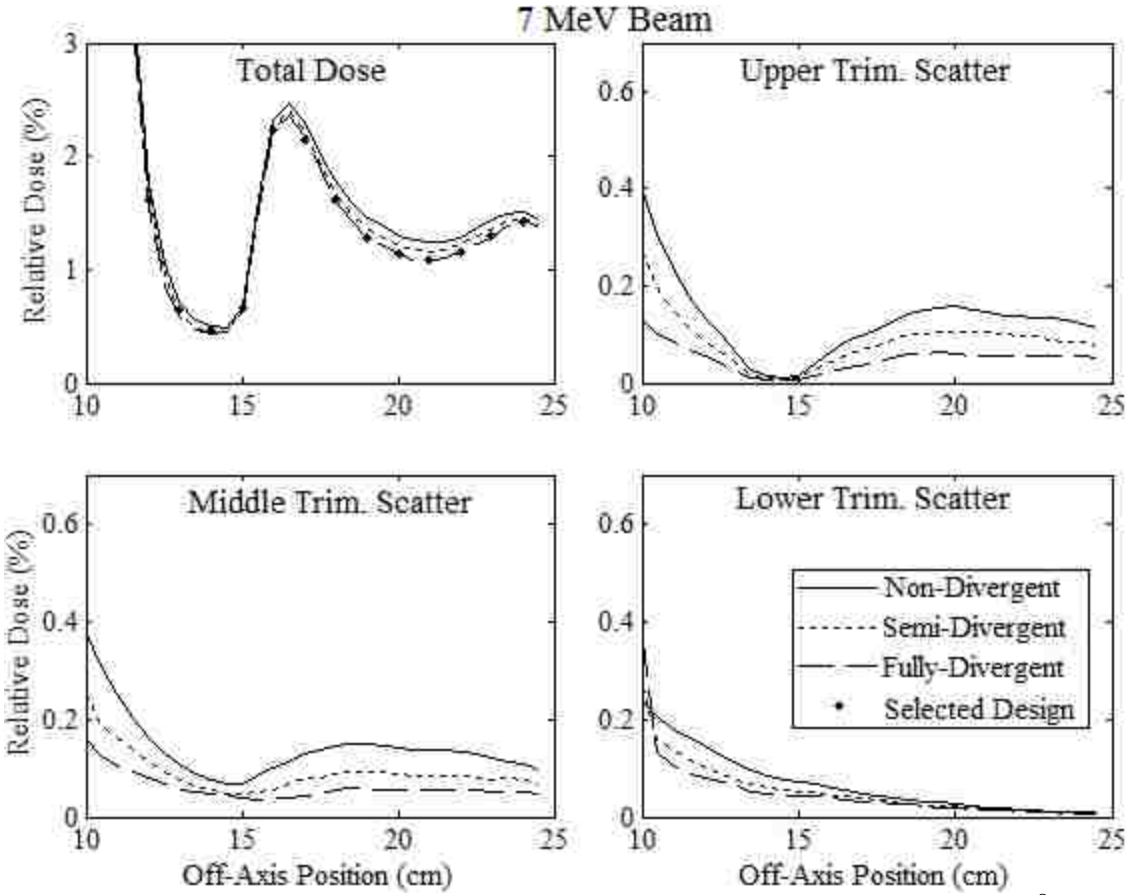

Figure 5-2. Leakage dose component profiles plotted versus off-axis position for 20x20 cm^2 applicators designed with non-divergent, semi-divergent, and fully-divergent inner edges for the 7 MeV beam. The plot in the upper left shows the cross-plane total dose leakage profiles. The cross-plane trimmer scattered electron dose profiles are plotted for the upper trimmer (upper right), middle trimmer (lower left), and lower trimmer (lower right). The Selected Design profile in the total dose plot indicates the leakage from an applicator designed with fully-divergent upper and middle trimmer inner edges and non-divergent lower trimmer inner edges.

The mean percent leakage dose was calculated with each applicator (inner edge divergence angle) design according to IEC specified criteria for each beam energy and dose component. These results are displayed in Table 5-1. The data revealed that, similar to the results of Aim 3, the mean percent leakage dose from electrons scattered from each of the trimmers increased with increasing beam energy. The table also confirms that designing the applicator with divergent inner edges reduced the total leakage dose. For example, for the 20 MeV beam, designing the inner edges to be fully-divergent rather than non-divergent, reduced the total mean percent leakage from 1.25% to 1.11%. Designing the trimmers with

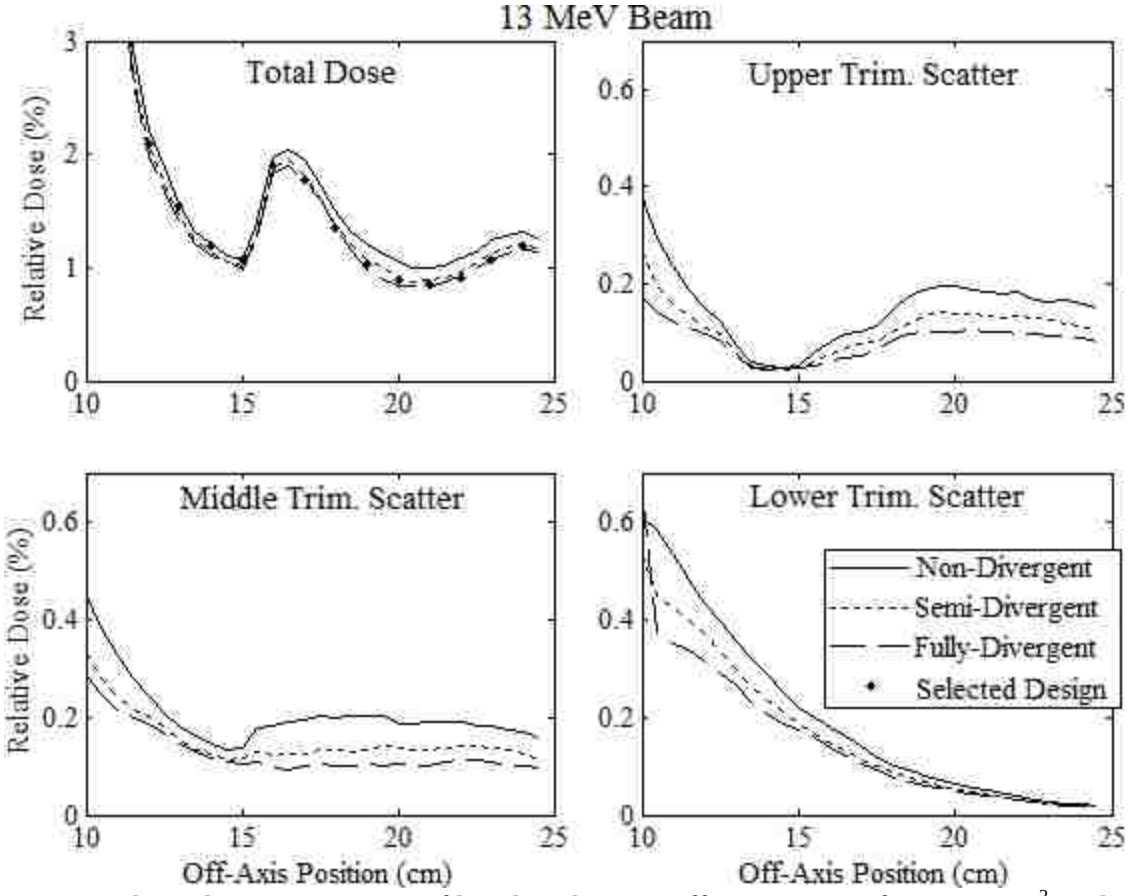

Figure 5-3. Leakage dose component profiles plotted versus off-axis position for 20x20 cm^2 applicators designed with non-divergent, semi-divergent, and fully-divergent inner edges for the 13 MeV beam. The plot in the upper left shows the cross-plane total dose leakage profiles. The cross-plane trimmer scattered electron dose profiles are plotted for the upper trimmer (upper right), middle trimmer (lower left), and lower trimmer (lower right). The Selected Design profile in the total dose plot indicates the leakage from an applicator designed with fully-divergent upper and middle trimmer inner edges and non-divergent lower trimmer inner edges.

divergent inner edges also reduced the scattered electron leakage dose from each trimmer, though the effect was most significant for the upper and middle trimmers. For both the 7 and 13 MeV beams, designing the inner edges of the upper and middle trimmers to be fully-divergent rather than non-divergent reduced the mean percent leakage dose contribution from scatter off these trimmers by 0.04% and 0.05%, respectively. For the 20 MeV beam, the trimmer scatter reductions were 0.05% and 0.06% for the upper and middle trimmers, respectively. In contrast, making the lower trimmer inner edge fully-divergent rather than non-divergent only reduced the leakage component by 0.01% for the 7 and 13 MeV beams and 0.02% for the 20 MeV beam.

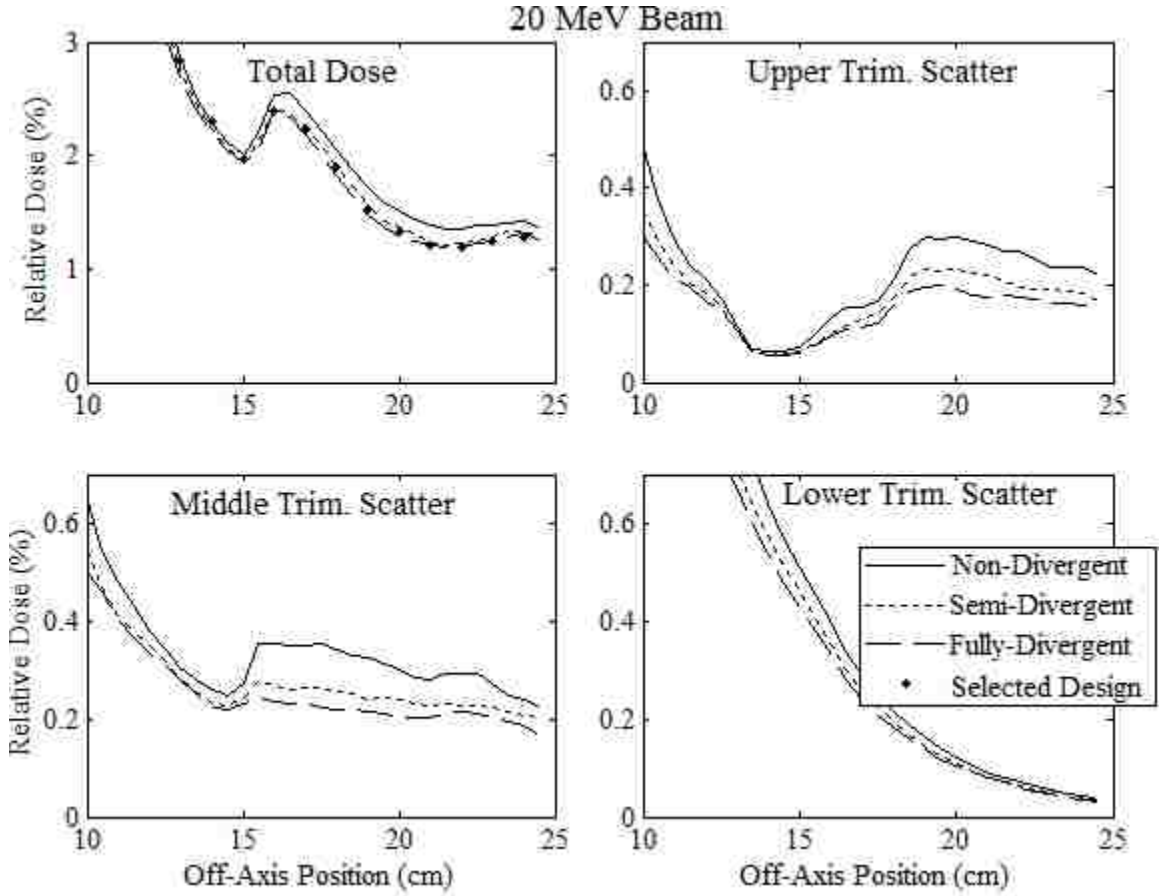

Figure 5-4. Leakage dose component profiles plotted versus off-axis position for 20x20 cm^2 applicators designed with non-divergent, semi-divergent, and fully-divergent inner edges for the 20 MeV beam. The plot in the upper left shows the cross-plane total dose leakage profiles. The cross-plane trimmer scattered electron dose profiles are plotted for the upper trimmer (upper right), middle trimmer (lower left), and lower trimmer (lower right). The Selected Design profile in the total dose plot indicates the leakage from an applicator designed with fully-divergent upper and middle trimmer inner edges and non-divergent lower trimmer inner edges.

The results of this study indicate that the inner edges of the upper and middle trimmers should be made fully-divergent to decrease the leakage dose. However, because the lower trimmer inner edge divergence had little impact on the leakage, additional factors were considered when making the decision for the lower trimmer inner edge divergence angle. When treating a patient with electrons, the field is typically defined by a patient specific insert composed of Cerrobend. These inserts are usually made in house with vertical inner edges. To maintain as much constancy as possible in the impact of scattered electrons on the in-field dose distribution for treatment planning purposes, it is best to keep the inner edge angles consistent when switching from the standard "open field" insert to a custom patient insert. For this

reason and that the lower trimmer edge divergence was shown to have little effect on the leakage dose, it was considered that the inner edge of the lower trimmer should be non-divergent for the applicator design.

Table 5-1. Mean percent leakage dose calculated per IEC specifications for 20x20 cm^2 applicators designed with varying inner trimmer edge divergence angles at 7, 13, and 20 MeV. The total mean percent leakage dose and the contributions from electrons scattered from each trimmer are shown for applicators designed with non-divergent, semi-divergent, and fully-divergent inner trimmer edges. Total mean percent leakage dose is also shown for the Selected Design, modeled with fully-divergent upper and middle trimmer inner edges and non-divergent lower trimmer inner edges.

		Total Leakage	Upper Trimmer Scatter	Middle Trimmer Scatter	Lower Trimmer Scatter
7 MeV	Non-Divergent	0.80%	0.07%	0.08%	0.02%
	Semi-Divergent	0.76%	0.05%	0.05%	0.02%
	Fully-Divergent	0.71%	0.03%	0.03%	0.01%
	Selected Design	0.72%	-	-	-
13 MeV	Non-Divergent	0.78%	0.09%	0.12%	0.06%
	Semi-Divergent	0.71%	0.07%	0.09%	0.05%
	Fully-Divergent	0.68%	0.05%	0.07%	0.05%
	Selected Design	0.69%	-	-	-
20 MeV	Non-Divergent	1.25%	0.15%	0.22%	0.14%
	Semi-Divergent	1.15%	0.12%	0.18%	0.13%
	Fully-Divergent	1.11%	0.10%	0.16%	0.12%
	Selected Design	1.12%	-	-	-

To investigate this thought, a separate set of MC calculations was performed for the 20x20 cm^2 applicator with this design, modeled with fully-divergent upper and middle trimmers and a non-divergent lower trimmer. These results are included in the total dose plots of Figures 5-2, 5-3, and 5-4, for the 7, 13, and 20 MeV beams, respectively. As expected, the profiles for this "Selected Design" vary only slightly from the applicator designed with fully-divergent inner edges for all three trimmers, supporting total mean percent leakage dose values shown in Table 51, which differs from the fully-divergent design by only 0.01% for all energies.

5.4. Aim 4 - Conclusions

The purpose of Aim 4 was to determine the inner edge divergence angle for each trimmer based on results of a MC study that investigated the effect of this design feature on leakage dose. The out-of-field total leakage dose and those dose components from electrons scattered from each of the trimmers in the out-of-field region were calculated. From these results, the following was concluded:

- Optimal trimmer inner edge divergence: Making the trimmer inner edges fully divergent reduces the out-of-field total dose. This conclusion was based on MC calculations, which revealed that out-of-field mean percent leakage dose was less with fully divergent than semi-divergent or non-divergent inner edges for all three trimmers of the 20x20 cm^2 applicator at 7, 13, and 20 MeV. For instance, the 20 MeV mean percent leakage was reduced from 1.25% to 1.11% by designing the trimmer inner edges fully-divergent rather than non-divergent. Additionally, the electron scatter dose outside the field from each trimmer was reduced for all beam energies studied by making the trimmers fully-divergent.
- Recommendation for non-divergent inner edge of lower trimmer: To maintain as much constancy as possible in the impact of scattered electrons on the dose distribution inside the field for treatment planning purposes, it is best to keep the inner edge angle consistent for both the standard "open field" insert and custom patient Cerrobend inserts; hence, the inner edge of the lower trimmer should be non-divergent. This is possible because the lower trimmer edge was shown to have little effect on the mean percent leakage dose as compared to the effects of the upper and middle trimmers. For example, by making the lower trimmer edge fully-divergent rather than non-divergent, the scatter from this trimmer was only reduced by 0.02% for the 20 MeV beam, rather than 0.05% and 0.06% for the upper and middle trimmers, respectively. For the upper and middle trimmers, however, their inner edges should be fully-divergent to decrease the leakage dose.

Chapter 6 - Aim 5 - Determine Optimal Applicator Geometry

Aim 5: Determine the optimal thickness, shape, and position of each trimmer bar, along with the photon jaw positions for each beam energy. These specifications will be selected such that the applicator weight is minimized while meeting leakage dose and beam flatness criteria.

6.1. Aim 5 - Introduction

The electron applicators of modern collimation systems are typically comprised of a series of trimmer bars positioned at different distances from isocenter which continually collimate and sharpen the beam penumbra at the height of each trimmer as the beam travels toward isocenter (patient). The final collimation level defines the shape of the field (typically using a custom Cerrobend insert) and is positioned close to the patient surface to ensure a sharp penumbra as the beam enters the patient. These trimmers should be designed sufficiently thick to shield the high energy electrons outside the radiation field and broad enough to sufficiently intercept the penumbras of the low energy beams in order to adequately reduce the out-of-field leakage dose. Additionally, the trimmers should be positioned to meet flatness specifications over the full extent of the field.

The current clinical electron applicators for the Elekta Infinity accelerator employ this design of using a series of three trimmers to collimate the beam. As shown in Aim 1, the current collimation system sufficiently reduces the leakage dose while maintaining acceptable beam flatness within the field for both the 10x10 and 20x20 cm^2 applicators. However, these applicators were shown to be excessively heavy, with the 10x10 and 20x20 cm^2 applicators weighing 7.7 and 10.9 kg, respectively, of which the trimmers comprised 5.52 and 8.36 kg. These weights are significantly greater than applicator designs of other competing manufacturers within the industry. For instance, the 10x10 cm^2 and 20x20 cm^2 Varian applicators weigh 6.5 and 8.6 kg, respectively, of which the trimmers comprise approximately 5.00 and 7.10 kg. This excessive weight, along with the cumbersome design of the latching mechanism, makes attaching the applicator to the accelerator a burdensome task.

The purpose of Aim 5 was to design a lighter set of trimmers for the electron applicators of the Elekta Infinity accelerator. The goal of this aim, as outlined in the hypothesis, was to redesign the

trimmer bars of the 10x10 and 20x20 cm^2 applicators such that the total trimmer weights were reduced to less than 5.00 and 7.10 kg, respectively, corresponding to the approximate weights of the Varian trimmers for the same applicator sizes.

This aim was completed by executing a series of seven collimation system design steps. The first step (Design Step 1) was to develop initial applicator designs for the 10x10 and 20x20 cm^2 applicators using a method of matching the lateral trimmer edge positions to the width of the penumbra at each trimmer level. A series of six adjustments (Design Steps 2 through 7) were then applied to the geometry of these initial designs to reduce the trimmer weight, including: (Design Step 2) specifying the field size at isocenter as opposed to 95 cm SSD, (Design Step 3) beveling the outer trimmer edges, (Design Step 4) optimizing the trimmer *z*-positions, (Design Step 5) determining the inner edge fluence matching OARs, (Design Step 6) determining the photon jaw positions for each beam energy, and (Design Step 7) modifying the trimmer thickness and outer edge bevel shape.

In this aim, the methodology of each design step will be outlined, immediately followed by the results and discussion tracking the weight reduction in each step. These adjustments focused only on the trimmer dimensions, rather than any structural, electrical, collision protection, or other non-collimating components. For this reason, all applicator weights listed in this aim refer to the total weight of the three trimmers, neglecting any additional weight due to structural or electrical components. Throughout this process, care was taken to ensure that the designs met criteria for out-of-field leakage dose, as specified by the IEC (1998), and in-field beam flatness, as specified by Hogstrom (2004).

6.2. Aim 5 - Design Step 1 - Initial Collimation System Design

6.2.1. Methods

A process outlined by Hogstrom (1985; 1990) was used to develop initial 10x10 and 20x20 cm^2 collimation system designs. In this process, the lateral trimmer edge positions were matched to specified electron fluence OARs, expressed as a percentage of central axis fluence, along the beam penumbra cast by the upstream collimator. To develop the initial applicator designs, the inner trimmer edges were positioned to intercept this penumbra near the upper limit of the error function (95% OAR), and the outer

trimmer edges were positioned to intercept this penumbra near the lower limit of the error function (2% OAR), calculated at the height of each trimmer. This has the effect of redefining the beam edge to a sharp penumbra beyond the trimmer.

6.2.1.1. Calculation of Penumbral Width

As electrons traverse a collimation system, they undergo MCS in the air, causing a lateral spread in the beam penumbra at the edge of the field. According to multiple scattering theory, this penumbra can be described as an error function centered at the geometric projection of the immediately upstream collimator from the virtual source, calculated as

$$OAR(x) = \frac{1}{2} erf\left\{\frac{x - w}{\sqrt{2}\sigma_x}\right\} + \frac{1}{2} \tag{6-1}$$

where w is the off-axis geometric projection from the virtual source of an upstream trimmer at a downstream trimmer plane, and σ_x is the RMS spread at the downstream trimmer z-position of a pencil beam originating at the upstream trimmer.

To determine these collimation edge positions, σ_x was calculated for the penumbra cast by each upstream collimator at each downstream trimmer plane. This value was determined by summing in quadrature the two components that contribute to the penumbral spread, electron scatter in air ($\sigma_{x,air}$) and the source width ($\sigma_{x,SW}$), as

$$\sigma_x = \sqrt{\sigma_{x,air}^2 + \sigma_{x,SW}^2} \tag{6-2}$$

The contribution to the spread of the beam penumbra due to air scatter ($\sigma_{x,air}$) was calculated using Equations 6-3, in which z' and z represent the central axis distance from the virtual source to the position of the upstream and downstream trimmers, respectively. T_{air} represents the scattering power in air of an electron of energy E and is equal to $0.0054E^{-1.78}$ (identical to Equation 3-11). These calculations were performed for the lowest beam energy accounted for in the collimation system design process (6 MeV) because it produces the largest penumbral width.

$$\sigma_{x,air} = [T_{air}(E)\ [z - z']^2\ {}^{z}/_{6}]^{1/2} \quad (6\text{-}3)$$

As explained in Aim 2, the source created by the dual scattering foils in the treatment head typically has a small non-zero width, which can be described as a Gaussian distribution centered on central axis at the height of the virtual source, causing an additional broadening of the beam penumbra beyond a collimation level, independent of the broadening caused by air scatter. By geometrically projecting this width down to the penumbral calculation plane, the contribution of the source width to the penumbral spread of the beam ($\sigma_{x,SW}$) was calculated as

$$\sigma_{x,SW} = \sigma_{SW}\ \frac{z - z'}{z} \quad (6\text{-}4)$$

The virtual source position used in the applicator design process was determined by measuring off-axis dose profiles using a MapCHECK (Sun Nuclear, Melbourne FL) diode array at various *z*-positions with no applicator present and geometrically projecting the 50% OAR of these measurements back to central axis. This resulted in a virtual source position 94 cm above isocenter (z= 6 cm). The source width was calculated by determing the σ_x of the measured profiles and subtracting in quadrature the calculated broadening due to air scatter (i.e. $\sigma_{x,SW} = \sqrt{(\sigma_x^2 - \sigma_{x,air}^2)}$), resulting in a source width of 2 cm. These virtual source and source width parameters were maintained throughout the collimation system design process.

6.2.1.2. Determination of Trimmer Edge Positions

In the initial applicator design the inner and outer trimmer edges were positioned $1.64\sigma_x$ inside and $2.05\sigma_x$ outside, respectively, the geometric projection of the upstream collimator from the virtual source (w). These off-axis positions correspond to the 95% and 2% fluence OARs, respectively, as illustrated in Figure 6-1, which depicts the penumbra of an electron beam at a downstream trimmer collimated by an upstream trimmer inner edge. In the figure, the 50% OAR coincides with w at the lower trimmer plane. The inner trimmer edge is positioned $1.64\sigma_x$ inside (towards central axis) w to match the 95% fluence OAR off-axis position, and the outer trimmer edge is positioned $2.05\sigma_x$ outside (away from

central axis) *w* to match 2% fluence OAR off-axis position. For illustration purposes, Figure 6-1 ignores the divergence of the beam, depicting it as a parallel vertical downward beam. The 95% and 2% values were selected because they were used in previous collimation system designs (Hogstrom *et al.*, 1985; Hogstrom *et al.*, 1990).

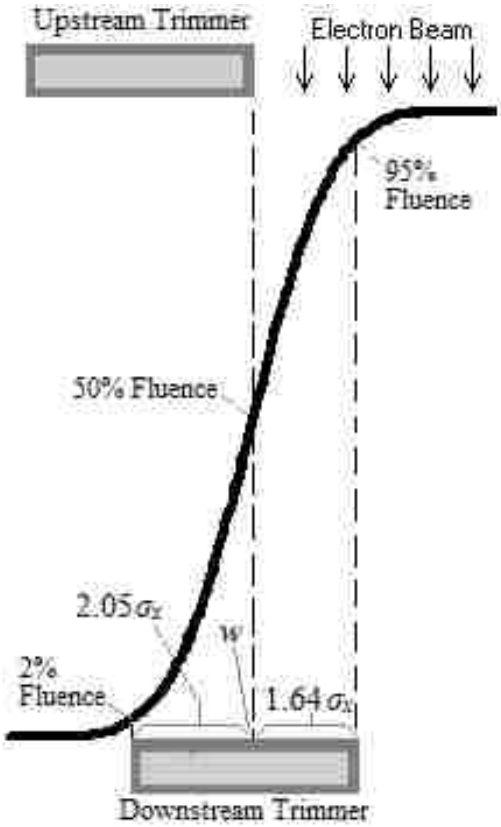

Figure 6-1. Schematic illustrating the basis for designing location of inner and outer edges of downstream trimmer. The solid curve plots the electron fluence relative to central axis (OAR) versus off-axis position of the penumbra cast by an upstream trimmer for a parallel vertical downward beam. The inner and outer downstream trimmer edges are matched to the 95% and 2% fluence OARs, respectively, with the 50% fluence OAR corresponding to the geometric projection (*w*) of the upstream trimmer inner edge (redrawn from Hogstrom *et al*., 1985).

Figure 6-2 illustrates how this methodology was used to determine the inner and outer edge positions for all three trimmers and the photon jaw, showing a cross sectional view of the right side of the collimation system (right jaw and right side of the applicator only). In this figure, the inner edge of the lower trimmer was positioned to define the size of the field specified for each applicator. Next, the inner edge of the middle trimmer was positioned to project to a point $1.64\sigma_x$ outside the lower trimmer inner

edge (where σ_x is calculated at the lower trimmer height). This process was then repeated to determine the upper trimmer and jaw inner edge positions. The outer edges of each trimmer were then positioned $(1.64+2.05)\sigma_x$ outside the inner edge.

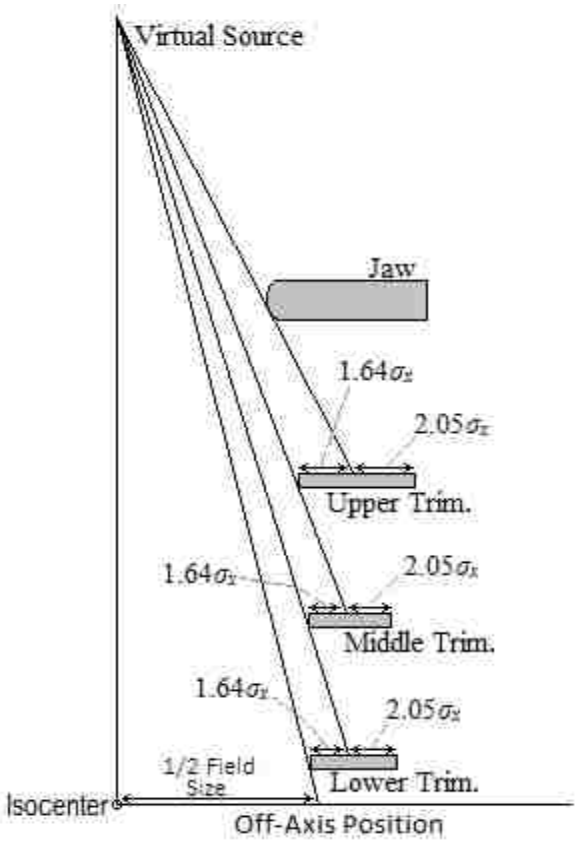

Figure 6-2. Schematic cross sectional view of the right half of the collimation system, in which the trimmer edges are positioned relative to the geometric projection of the immediately upstream collimator. The inner and outer edges are positioned $1.64\sigma_x$ inside and $2.05\sigma_x$ outside, respectively, the geometric projection of the immediately upstream collimator from the virtual source. The inner edge of the lower trimmer is always positioned to define the size of the field specified for each applicator.

6.2.1.3. Initial Collimation System Design Parameters

This process of matching the inner and outer trimmer edges to the calculated 95% and 2% OARs, respectively, was used to determine all trimmer edge positions and the photon jaw positions for initial 10x10 and 20x20 cm^2 applicator designs. In these initial designs the downstream surfaces of the upper, middle, and lower trimmers were positioned at *z*-values of 70, 80, and 95 cm. These *z*-positions were

selected for being between the positions of the current clinical Elekta (z = 73, 86, and 95 cm) and Varian (z = 65, 77, and 95 cm) applicator trimmers.

The collimation systems were designed for a beam energy range of 6 to 20 MeV. Therefore, trimmer edge positions were calculated for a 6 MeV electron beam, and the thickness of the trimmers was calculated for a 20 MeV beam (using the MC 1% threshold range calculation equation for tungsten). This beam energy range was a reduction from the 4 to 22 MeV range allowed with the current clinical Elekta Infinity applicators. The increase of the lower energy limit from 4 MeV to 6 MeV can be justified by the fact that any treatment requiring a beam energy less than 6 MeV can be treated with a 6 MeV beam and bolus (Hogstrom, 1991b). The decrease of the upper energy limit from 22 MeV to 20 MeV can be justified by the fact that for electron beams with dual scattering foils, the increase in R_{90} with increasing $E_{p,0}$ is small for energies greater than 20 MeV (Hogstrom, 1991a).

6.2.2. Results and Discussion

The decreased energy range from 4-22 MeV to 6-20 MeV allowed the trimmers to be designed with both narrower width and thinner thickness, decreasing the applicator weight. Initial calculations found this weight reduction to be approximately 35% for the 10x10 cm^2 applicator and 33% for the 20x20 cm^2 applicator. The in-plane trimmer cross sections of the initial 10x10 and 20x20 cm^2 applicator designs for the beam energy range 6 to 20 MeV are shown in red in Figures 6-3 and 6-4, respectively. The initial 10x10 and 20x20 cm^2 applicator designs were found to weigh 7.06 and 10.87 kg, respectively, greatly exceeding the hypothesized goals of 5.00 and 7.10 kg. Hence, the simplistic method formerly used by Hogstrom (1985; 1990) was found to be insufficient for reducing the applicator weight.

6.3. Aim 5 - Design Step 2 - Specify Applicator Field Size at Isocenter

The initial applicator designs were found to be excessively heavy, far surpassing the weight goals specified in the hypothesis for the 10x10 and 20x20 cm^2 applicators. To remedy this, in Design Steps 2 through 7 a series of modifications was made to the initial designs to sequentially reduce the applicator weight.

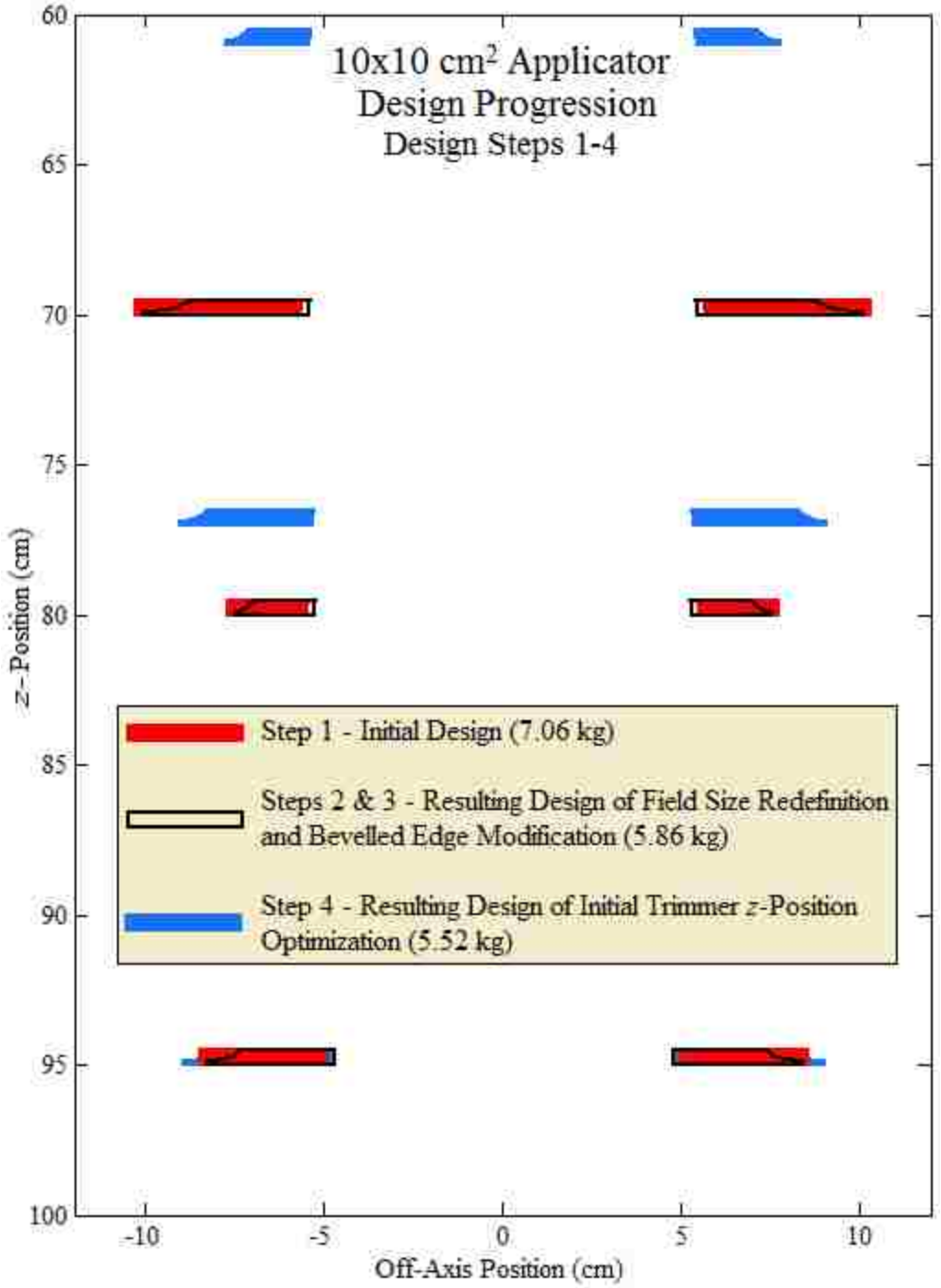

Figure 6-3. In-plane cross sectional view of the design progression of the 10x10 cm^2 applicator trimmers in Design Steps 1 through 4. The initial applicator model (Design Step 1) is shown in red, the design updated to include both the field size specification (Design Steps 2) and beveled edge modification (Design Step 3) is shown outlined in black, and the design resulting from the upper and middle trimmer positional height optimization (Design Step 4) is shown in blue. The applicator trimmer weight is listed in the legend for each design.

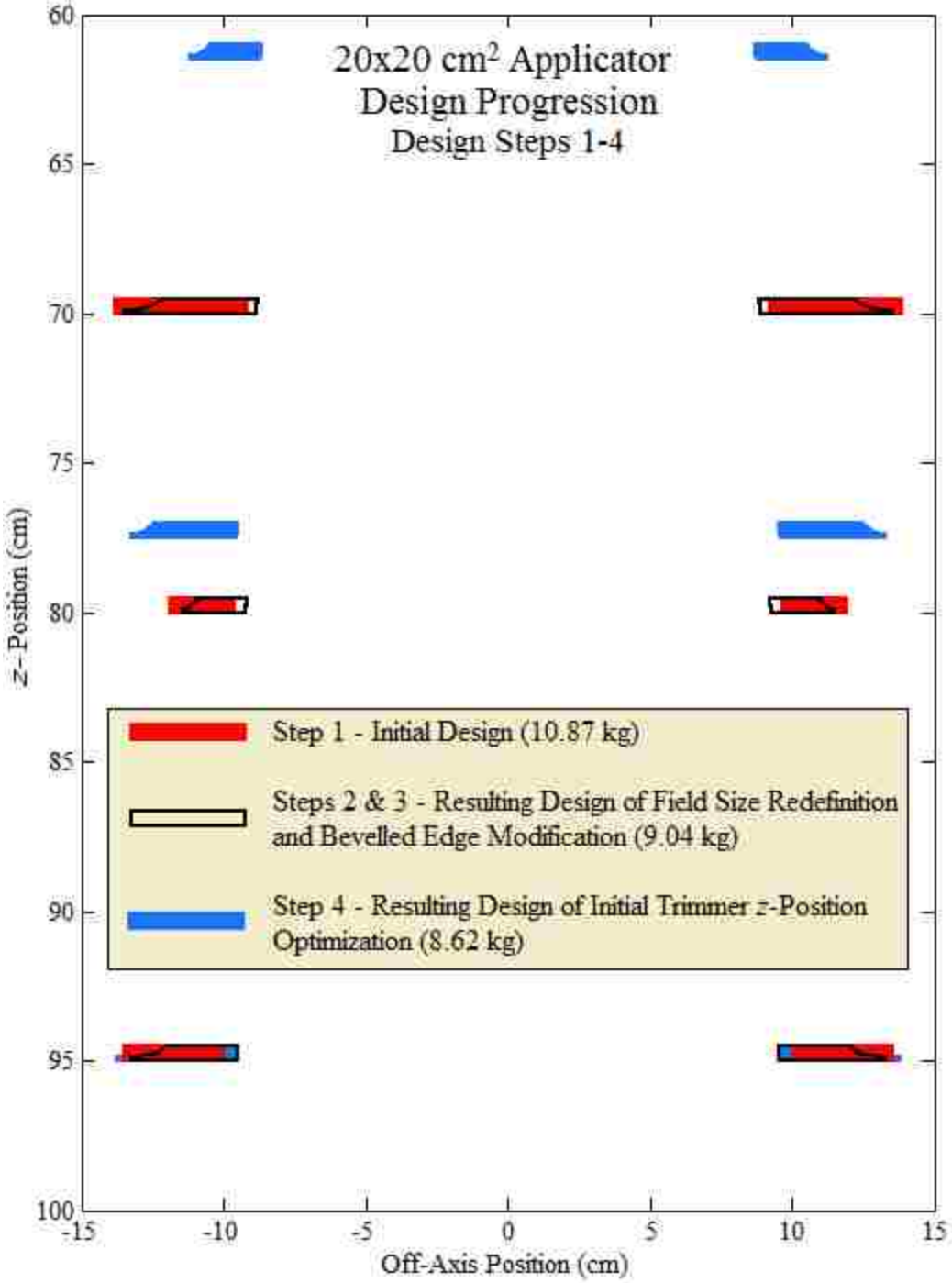

Figure 6-4. In-plane cross sectional view of the design progression of the 20x20 cm^2 applicator trimmers in Design Steps 1 through 4. The initial applicator model (Design Step 1) is shown in red, the design updated to include both the field size specification (Design Steps 2) and beveled edge modification (Design Step 3) is shown outlined in black, and the design resulting from the upper and middle trimmer positional height optimization (Design Step 4) is shown in blue. The applicator trimmer weight is listed in the legend for each design.

6.3.1. Methods

The first modification (Design Step 2) aimed at reducing the applicator weight was to specify applicator field size at isocenter (z = 100 cm). The field sizes of both the current clinical Elekta Infinity applicators and the initial applicator designs were specified at 95 cm SSD, meaning that the field insert for the 10x10 cm^2 applicator, positioned at a z-position of 95 cm, had sides of 10 cm in length. When projected down to isocenter these field side lengths increased to 10.53 cm [10*100/95]. However, for other manufacturers, e.g. Varian, it is standard practice to define the field sizes at isocenter, meaning that a 10x10 cm^2 applicator has a field size of 10x10 cm^2 at 100 cm SSD, not 95 cm. Therefore, the field insert for the 10x10 cm^2 Varian applicator (situated at 95 cm SSD) has sides of length 9.5 cm [10*(95/100) = 9.5]. This modification was implemented into the initial collimation system designs and the applicator weights were recalculated.

6.3.2. Results and Discussion

In-plane cross sectional views of the designs produced by specifying the field size at isocenter are shown outlined in black in Figures 6-3 and 6-4 for the 10x10 cm^2 and 20x20 cm^2 models, respectively. The images illustrate that redefining of the field size at 100 cm SSD rather than 95 cm SSD shifted the trimmer inner edges inward toward central axis. For the 10x10 cm^2 applicator, the inner edge of the lower trimmer moved inward from 5.0 cm to 4.75 cm off central axis. For the 20x20 cm^2 applicator, the inner edge of the lower trimmer moved inward from 10.0 cm to 9.5 cm off central axis. It should be noted that the designs shown in the figures also include the beveled outer edge feature, as described in the following section.

Implementing this field size redefinition modification into the initial designs reduced the 10x10 cm^2 applicator weight from 7.06 to 6.87 kg, a reduction of 2.7%, and the 20x20 cm^2 applicator weight from 10.87 to 10.49 kg, a 3.5% reduction. Not only did this change decrease the trimmer weight, but it also this allowed the new Elekta applicators to comply with the conventional practice of defining field sizes at isocenter, which is standard within the industry.

6.4. Aim 5 - Design Step 3 - Beveling Outer Trimmer Edges

In the Design Steps 1 and 2, the trimmer thickness calculated for the highest beam energy extended across the full width of the trimmer, from the inner edge to the outer edge, making the trimmer cross sections rectangular. Due to variations in scattering power, only the low energy particles scatter enough to reach the outer trimmer edge, meaning that the outer portion of the trimmer could be made thinner, since it does not have to shield the higher energy electrons. To take advantage of this fact and further reduce the trimmer weight, the trimmers were redesigned to incorporate an outer edge bevel. Though not explicitly described in the literature, this methodology of beveling the outer collimator edge was used by Hogstrom *et al.* (2004) in the design of a retractable electron MLC. Varian applicators also have tapered outer trimmer thicknesses, apparently the result of a similar design concept.

6.4.1. Methods

For every electron beam energy within the range accounted for in the collimation design, there exists both a calculable electron range and off-axis position matching the 2% fluence OAR. The outer trimmer edge was designed such that the off-axis position of the 2% OAR for each beam energy was matched to the thickness required to stop the electrons, so that the outer edge became tapered to form a bevel shape. Figure 6-5 illustrates this effect, showing the penumbras cast by an upstream trimmer for a high, medium, and low energy electron beam at a downstream trimmer plane. For illustration purposes, this figure again ignores beam divergence, depicting it as a parallel vertical downward beam. Similar to Figure 6-1, the 50% fluence level is positioned at the geometric projection of the upstream trimmer for each beam energy. The off-axis positions of the 2% fluence OARs of each penumbra match the off-axis positions $2.05\sigma_x$ outside the geometric projection of the upstream trimmer for each energy. The trimmer thickness at the off-axis position of the 2% OAR for the low, medium, and high energy penumbras corresponds to the low, medium, and high energy electron ranges, respectively. The $2.05\sigma_x$ off-axis positions were determined by recalculating σ_x for each beam energy using Equations 1 through 4.

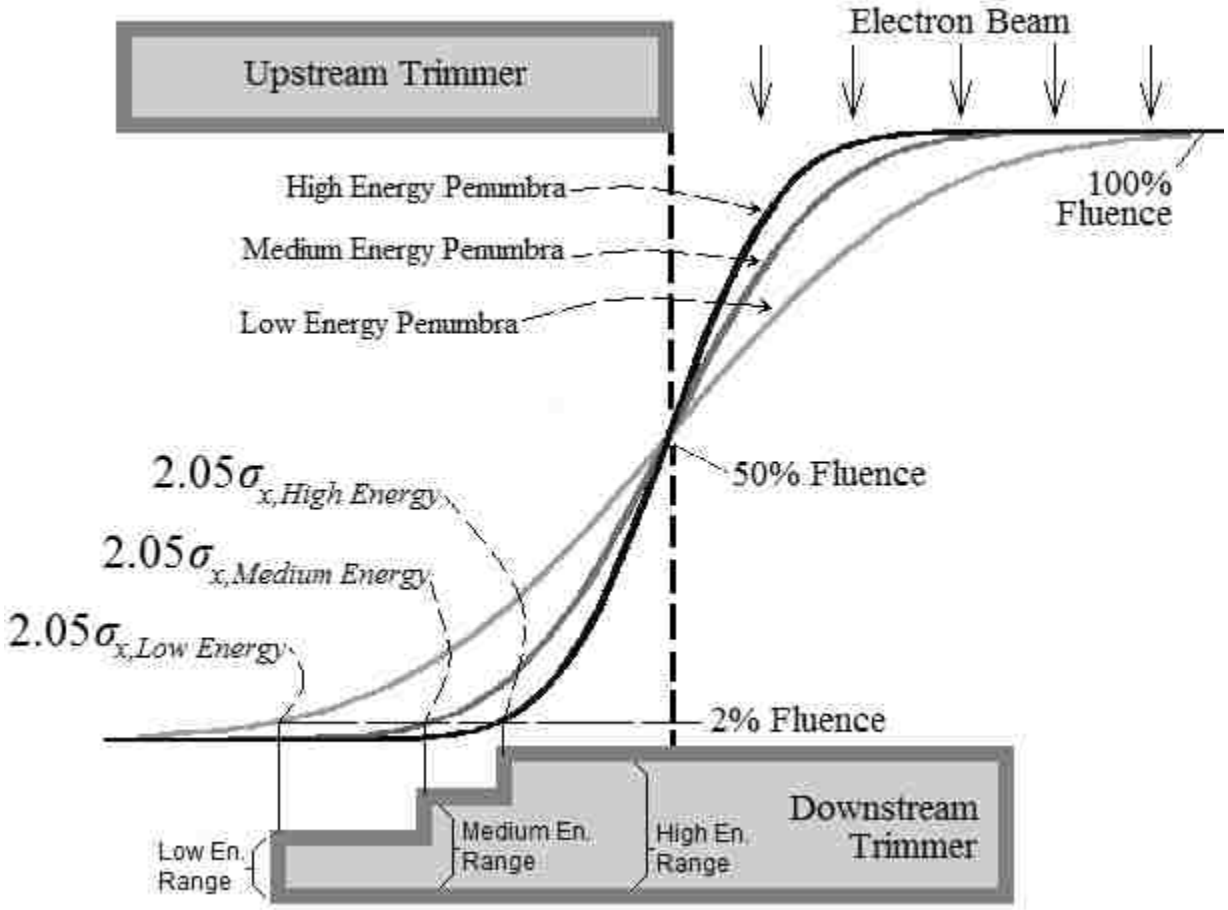

Figure 6-5. Bevel shape calculation method for outer trimmer edge. The penumbras cast by an upstream trimmer are shown for three beam energies. The off-axis position of the 2% fluence OAR is shown for each penumbra. The material thickness required to stop electrons of each beam energy is indicated and extends out to the calculated off-axis position of the 2% fluence OAR for each energy. This creates a tapered bevel shape in which the trimmer thickness is reduced towards the outer edge of the trimmer.

This process was performed for all energies within the applicable range, 6 to 20 MeV with 1 MeV spacing, forming the outer trimmer edges into a stepped bevel shape. This stepped bevel shape is shown in the black region in Figure 6-6, which depicts a cross sectional view of the trimmer designed with an outer edge bevel. The beveled edge steps were then "filled in" by linearly connecting the corners of each step to create a smooth bevel, as shown in gray in the figure. The region of material removed from the trimmer in the edge beveling process reducing the trimmer weight is labelled in the figure.

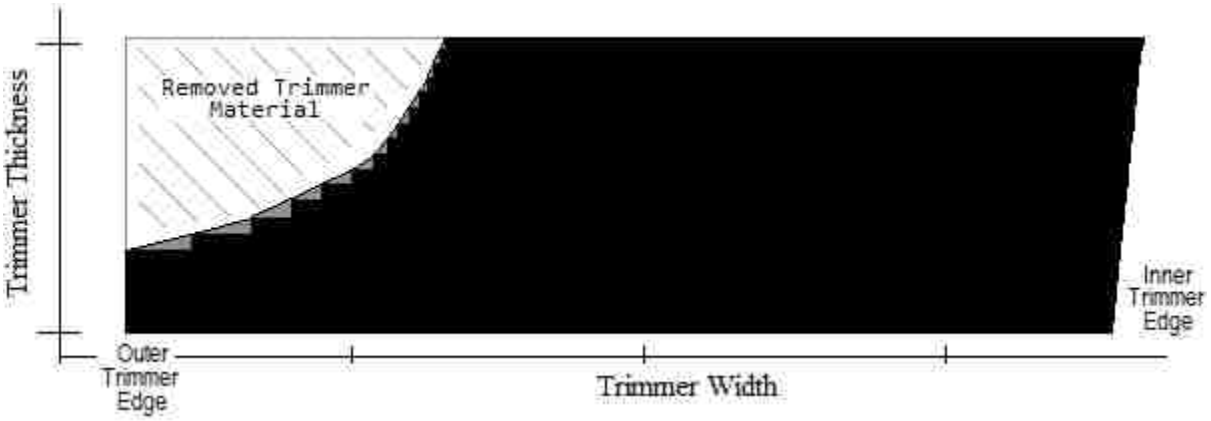

Figure 6-6. Cross sectional view of trimmer with outer edge bevel. The black region shows the outer trimmer edge formed into a stepped bevel shape by calculating the material thickness and 2% fluence matching OAR for each energy between 6 and 20 MeV at 1 MeV spacing. The gray regions between the steps indicate the material added to "fill in" the steps by linearly connecting the corners of each step, creating a smooth bevel shape. The material removed from the trimmer in the bevel shaping process is also indicated.

This modification of beveling the outer trimmer edges was implemented into the 10x10 and 20x20 cm^2 models produced from the previous design step (redefining the field sizes at isocenter) to reduce the applicator weights. The MC 1% threshold range calculation equation, as described in Aim 3, was used to calculate the thicknesses along the bevel for each energy. The weights of the trimmers after adding the outer edge bevel were calculated for both applicator sizes.

6.4.2. Results and Discussion

The effect of beveling the outer edge of each trimmer is illustrated by the outlined black applicator cross sections in Figures 6-3 and 6-4, showing the bevel shape incorporated into the outer edge of the trimmers. The bevel removed material from the trimmers, reducing the 10x10 cm^2 applicator weight from 6.87 to 5.86 kg, a reduction of 14.8%, and the 20x20 cm^2 applicator weight from 10.49 to 9.04 kg, a reduction of 13.8%.

6.5. Aim 5 - Design Step 4 - Optimization of Upper and Middle Trimmer *z*-Positions

In the Design Steps 1 through 3, the distal trimmer surfaces were positioned at *z*-values of 70, 80, and 95 cm. For the lower trimmer, this 95 cm *z*-position is constrained for purposes of convention and so that the beam penumbra is sharp when entering the patient. The other trimmers, however, can be

positioned at any *z*-value between the bottom of the treatment head (approximately 55 cm for the Elekta Infinity) and 95 cm. A study was performed to determine the optimal *z*-positions of the upper and middle trimmers in order to minimize the applicator weight.

6.5.1. Methods

An optimization was performed coded in MATLAB 7.7.0 in which the *z*-positions of the upper and middle trimmers was varied for the 10x10 and 20x20 cm^2 applicators to determine the *z*-positions which minimize the applicator weight. Within this optimization, the upper and middle trimmer *z*-positions were constrained between 55 cm and 93 cm with minimum of 2 cm spacing required between trimmers, and a *z*-position step size of 0.5 cm was used for varying each trimmer position. All other design parameters, such as 2% OAR bevel shape matching and 95% OAR inner edge matching, were maintained for all applicator designs. The upper and middle trimmer *z*-positions producing the minimum applicator weight were selected for proceeding with the design process.

6.5.2. Results and Discussion

The results of optimizing the upper and middle trimmer *z*-positions are plotted in Figure 6-7. This figure shows isomass plots for 10x10 (left) and 20x20 cm^2 (right) applicators designed with the upper and middle trimmers located at various *z*-positions. The results show that for both applicator sizes, as the upper and middle trimmers became approximately equally spaced between the jaws and lower trimmer, the weight (mass) was reduced. The optimal calculated configurations are indicated by the white stars in each plot. As the figure indicates, in the optimized design of the 10x10 cm^2 applicator, the downstream surfaces of the upper and middle trimmers were positioned at *z*-values of 61.0 and 77.0 cm, respectively, resulting in an applicator weight of 5.52 kg. For the optimized design of the 20x20 cm^2 applicator, the downstream surfaces of the upper and middle trimmers were positioned at *z*-values of 61.5 and 77.5 cm, respectively, resulting in an applicator weight of 8.62 kg. These modifications resulted in weight reductions of 5.9% and 4.6% from the previous design weights of 5.86 and 9.04 kg for the 10x10 and 20x20 cm^2 applicators, respectively.

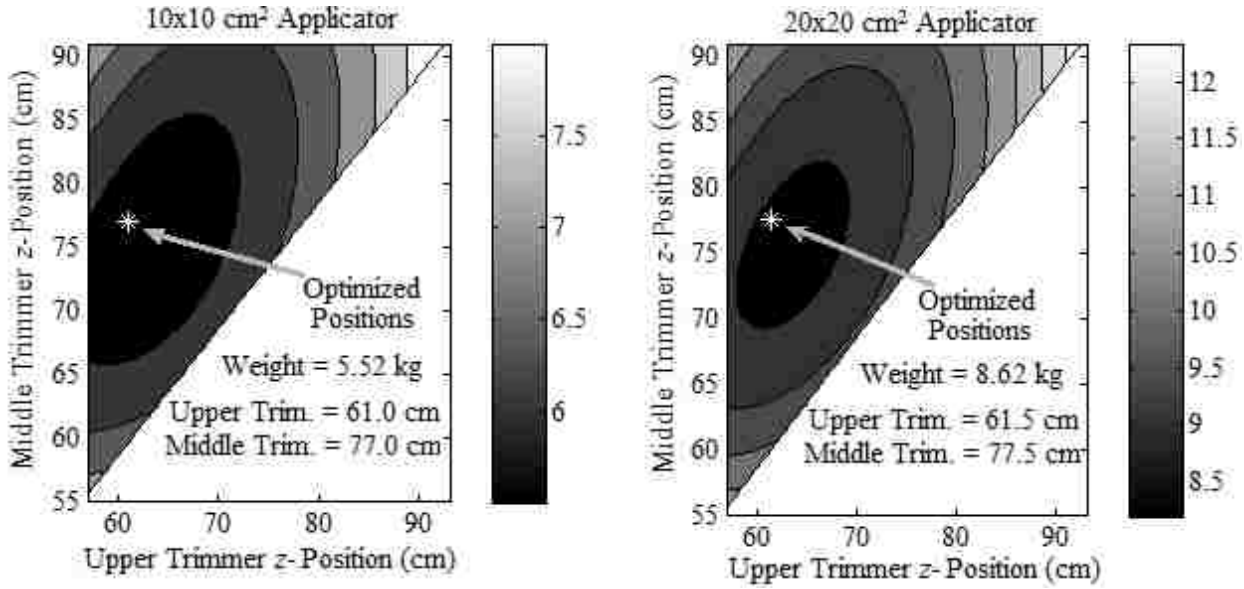

Figure 6-7. Calculated isomass plots applicators as a function of middle and upper trimmer *z*-positions optimization results. The vertical axis of the plots indicate the *z*-position of the downstream surface of the middle trimmer, and the horizontal axis indicates the *z*-position of the downstream surface of the upper trimmer. The contour plot indicates the calculated weight (in kg, corresponding to the color legend to the right of each plot) of the 10x10 (left) and 20x20 cm^2 (right) applicators. The positions for the upper and middle trimmers which produced the optimal (minimum) applicator weight are indicated in the plots by the white star.

In-plane cross sectional views of these optimized designs are shown in blue in Figures 6-3 and 6-4 for the 10x10 and 20x20 cm^2 models, respectively, illustrating that the upper and middle trimmers were moved upwards away from the patient plane in the optimization, while the downstream surface of the lower trimmer was maintained at 95 cm SSD. This had the effect of slightly increasing the width of both the middle and lower trimmers from the previous design, but significantly decreasing the width of the upper trimmer, causing the reduction in applicator weight. These trimmer *z*-positions served as a starting point for the next design step.

6.6. Aim 5 - Design Step 5 - Inner Trimmer Edge Fluence Matching OAR Determination

In the Design Steps 1 through 4, an inner edge fluence matching OAR of 95% was used for all trimmers and applicator sizes. If this OAR is reduced, the inner trimmer edges move inward toward central axis, reducing the weight of the applicator. However, doing so can negatively impact beam flatness near the field edge if lateral sidescatter equilibrium is not sufficiently maintained across the

extent of the field. For this reason, the collimation design process should strike a balance in which the trimmers are brought in as far as possible while also ensuring that acceptable in-field beam flatness at isocenter is maintained.

6.6.1. Methods

To determine the optimal inner edge fluence matching OARs, a study was performed comprised of two steps. First, an optimization using the analytical primary electron model was performed to determine an initial set of trimmer inner edge fluence matching OARs for both the 10x10 and 20x20 cm^2 applicators. Second, those optimized matching OARs were slightly adjusted using a series of MC calculations to ensure the in-field dose distributions were acceptably flat.

6.6.1.1. Optimization Using the Analytical Primary Electron Model

A search grid optimization was performed for both the 10x10 and 20x20 cm^2 applicators by creating a search grid of applicator trimmer weights calculated from applicator designs in which the inner edge fluence matching OARs for each trimmer were reduced from those used in the previous design steps (95%), shifting the trimmers inward and decreasing the applicator weight. Additionally, the upper and middle trimmer *z*-positions were varied from those determined in Design Step 4, as they had been optimized for 95% inner edge fluence matching OAR criteria. This resulted in a five dimensional search grid.

This grid of applicator trimmer weights was searched to determine the applicator design parameters that minimized applicator weight while maintaining acceptable in-field beam flatness per criteria specified by Hogstrom (2004). This search grid optimization was performed in three iterations, with grid step sizes of each parameter decreasing with each iteration. Approximate upper and lower boundaries and step sizes (i.e. parameter spacings within the grid) for each of the five parameters, specifying the search grid for each iteration, are exemplified in Table 6-1. The lightest applicator design in each iteration to produce acceptable in-field beam flatness was selected for proceeding with the next iteration in the search grid optimization. All other design parameters, including bevel shape calculation

parameters, were maintained and used for recalculation of the bevel shape for all applicator designs in the search grid.

The in-field beam flatness was evaluated for each applicator design in the search grid using the analytical primary electron model (c.f. Section 3.2.1) with the lowest beam energy, 6 MeV, the beam energy most likely to fail flatness criteria due to it having the greatest scattering power. Primary electron dose profiles were calculated in both the in-plane and cross-plane dimensions for each design and were considered acceptably flat if the dose varied (decreased) from central axis dose by no more than 2% at the edge of the uniformity region for the major axes, i.e. 2 cm inside the field edge. According to pencil-beam theory, using a 2% threshold at this off-axis position along the major axes should ensure that the dose does not vary from central axis by more than 4% (the maximum flatness variation allowed for diagonal profiles as specified by Hogstrom (2004)) at the corner uniformity region [1-0.98*0.98 = 0.0396]. If either the in-plane or cross-plane dose values were found to vary from central-axis dose by more than 2%, i.e. <98%, the design was rejected.

Table 6-1. Example of potential upper and lower boundaries and grid step sizes of each of the five parameters for each of the three iterations of the search grid optimization (written as [‘lower boundary’-‘upper boundary’ (‘step size’)]). These values are approximate and differed slightly for the 10x10 and 20x20 cm^2 applicators.

Design Parameters	Trimmer	First Iteration	Second Iteration	Third Iteration
Inner Trimmer Edge Matching OAR (%)	Upper	87.5-95.0% (1.5%)	84.0-89.0% (1.0%)	83.5-86.0% (0.5%)
	Middle	86.0-95.0% (1.5%)	87.0-92.0% (1.0%)	88.5-91.0% (0.5%)
	Lower	86.0-95.0% (1.5%)	88.5-93.5% (1.0%)	90.0-92.5% (0.5%)
Trimmer *z*-Position (cm)	Upper	58.5-64.5 (1.5)	62.5-66.5 (1.0)	64.5-66.5 (0.5)
	Middle	74.5-80.5 (1.5)	77.0-81.0 (1.0)	78.0-80.0 (0.5)

6.6.1.2. Adjustments Based on MC Calculations

When the analytical optimizations were complete, the optimal 10x10 and 20x20 cm^2 applicator (trimmer) designs were modeled in BEAMnrc and inserted into the Elekta Infinity BEAMnrc model. Simulations using the nominal 7 MeV beam ($E_{p,0}$ = 7.14 MeV, R_{90} = 2.1 cm), the lowest available energy in the MC model, were performed to evaluate the in-field beam flatness of both the 10x10 and 20x20 cm^2

applicator designs. For both applicators, the MC calculations resulted in doses near the field edge slightly lower than the analytically calculated dose, which narrowly failed beam flatness criteria. This failure was believed due to the analytical primary electron model assuming that the fluence was uniform across the extent of the field at each collimation level when calculating the scattering moment profiles. As explained in Aim 2, this caused the model to slightly under-predict $\bar{\theta}_x$ near the edge of the field, which was believed to subsequently cause an over-prediction in the dose profile just inside the penumbra at the edge of the field at the patient plane.

To remedy this narrow failure, a series of four modified applicator designs were created for both the 10x10 and 20x20 cm^2 applicators by incrementally increasing the inner edge fluence matching OARs produced from the optimizations based on the analytical primary electron model, while maintaining the trimmer *z*-positions. Correspondingly, this incrementally stepped the trimmers and jaws outward from central axis, which both improved the in-field beam flatness and increased the applicator weights with each step. The increased OARs for the modified applicators, listed in Table 6-2, were selected such that the applicator weight increases were fairly uniform with each adjustment (approximately 0.4 and 0.15 kg increases for the 10x10 and 20x20 cm^2 applicators, respectively). For simplicity, these designs are labelled 1.A through 1.E in the table, with Design 1.A representing the design produced from the analytical optimization and Designs 1.B-1.E representing the modified designs created by incrementally increasing the inner edge fluence matching OARs.

Each of these four modified applicator designs was modeled and inserted into the BEAMnrc model for the Elekta Infinity accelerator, along with the original analytically optimized model. MC simulations with the 7 MeV beam, the lowest beam energy available in the Elekta Infinity BEAMnrc model, were performed with each applicator. The 7 MeV beam was selected as the beam energy least likely to pass dose flatness criteria due to the increased scatter of the lower energy electrons.

These MC simulations produced phase space files 1 cm upstream of isocenter that were used as input into DOSXYZnrc to calculate dose distributions in a water phantom. As in the previous MC studies, dose was calculated in water at 100 cm SSD in 0.5x0.5x0.5 cm^3 voxels centered at 1 cm depth

(0.75 to 1.25 cm depth). Dose calculations were performed using 10^9 particles and the distributions were symmetrized about central axis in both the in-plane and cross-plane dimensions to reduce statistical uncertainty. All source and transport parameters used in the MC calculations from previous aims were maintained for these calculations. Dose distributions were normalized to the mean dose calculated within a 3x3 set of voxels centered on central axis at the calculation depth.

Table 6-2. Fluence matching OARs for the inner edges of each trimmer of each 10x10 and 20x20 cm^2 applicator modeled for the MC inner edge adjustment analysis. Design 1.A represents the design produced from the analytical optimization (based on the analytical primary electron model of Aim 2), and Designs 1.B through 1.E represent the modified designs created by incrementally increasing the inner edge fluence matching OARs.

	10x10 cm^2 Applicator			20x20 cm^2 Applicator		
	Upper Trimmer	Middle Trimmer	Lower Trimmer	Upper Trimmer	Middle Trimmer	Lower Trimmer
Design 1.A	85.0%	90.0%	92.0%	85.0%	89.0%	92.0%
Design 1.B	90.0%	92.0%	94.0%	86.0%	89.5%	92.5%
Design 1.C	93.0%	94.0%	95.0%	87.0%	90.0%	93.0%
Design 1.D	95.0%	96.0%	96.5%	89.0%	91.0%	93.0%
Design 1.E	96.5%	97.5%	98.0%	90.0%	92.0%	93.5%

The in-field beam flatness was evaluated for each applicator model based on the criteria outlined by Hogstrom (2004). Specifically, the dose uniformity was evaluated at an off-axis position $2\sqrt{2}$ cm inside the corner of the field along the diagonal axis. This off-axis position corresponds to the edge of the diagonal profile uniformity region, i.e. the region in which the dose must be maintained within ±4% of the central-axis dose. This position was selected as the position most likely to cause the beam to fail dose flatness criteria. The dose distributions were deemed acceptably flat if the dose calculated at these off-axis positions was at least 97.77% of the central-axis dose for the 10x10 cm^2 applicator and 99.59% for the 20x20 cm^2 applicator. These values correspond to the minimal acceptable OAR at this position (96%), plus the differences between the MC-calculated and measured diagonal dose profiles at the edge of the uniformity region previously determined in Aim 1 for the 7 MeV beam, plus a 1% cushion. The MC-calculated less measured dose differences at this position for the 7 MeV beam were 0.77% for the 10x10 cm^2 applicator and 2.59% for the 20x20 cm^2 applicator, as shown in Table 2-4. The 1% cushion

accounted for any error in the calculation process, as well as the fact that the collimation system should ensure beam flatness for a 6 MeV beam, but can only be evaluated using the lowest beam energy available in the BEAMnrc Elekta Infinity model, the nominal 7 MeV beam ($E_{p,0}$ = 7.14 MeV).

The weight was calculated for each of these models. For both the 10x10 and 20x20 cm^2 sizes, the applicator designs that produced the least trimmer weight and maintained acceptable in-field beam flatness were selected for proceeding with the collimation system design process.

6.6.2. Results and Discussion

6.6.2.1. Optimization Using the Analytical Primary Electron Model

To find the optimal inner collimator edge positions, an optimization was performed by varying the inner trimmer edge fluence matching OARs and evaluating the in-field beam flatness of each design using the analytical primary electron model. The optimization produced upper, middle, and lower trimmers inner edge fluence matching OARs of 85%, 90%, and 92%, respectively, for the 10x10 cm^2 applicator and 85%, 89%, and 92%, respectively, for the 20x20 cm^2 applicator. Additionally, the *z*-positions of the downstream surfaces of the upper and middle trimmers were re-optimized and adjusted to 66 and 79 cm, respectively, for both applicator sizes. The optimization reduced the 10x10 and 20x20 cm^2 applicator weights from 5.52 and 8.62 kg to 4.61 and 7.32 kg, respectively.

In-plane cross sectional views of these designs are shown outlined in black in Figures 6-8 and 6-9 for the 10x10 and 20x20 cm^2 applicators, respectively. These figures also show the models produced from Design Step 4 and from the subsequent MC inner trimmer edge position adjustments. As the figures illustrate, the optimization resulted in the upper and middle trimmers moving inward toward central axis from Design Step 4, reducing the applicator weight. These trimmers were also lowered closer to the patient plane, reducing the lower trimmer width.

6.6.2.2. Adjustments Based on MC Calculations

MC simulations were performed to evaluate the applicator designs produced from the analytical optimization, revealing that the designs narrowly failed criteria for acceptable in-field beam flatness for

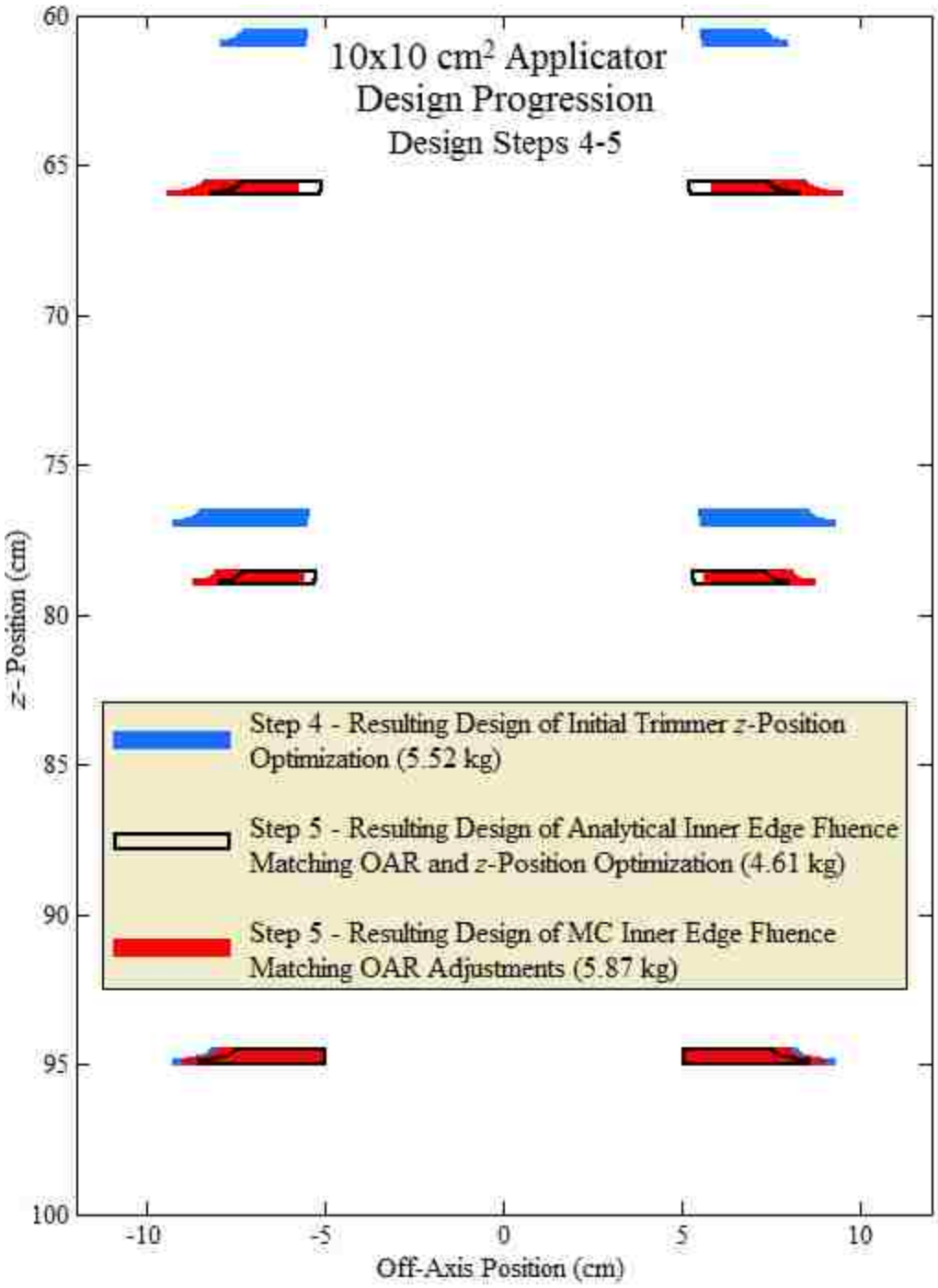

Figure 6-8. In-plane cross sectional view of the design progression of the 10x10 cm^2 applicator trimmers in Design Steps 4 and 5. The trimmer cross sections of the applicator designs resulting from Design Step 4, initial trimmer *z*-position optimization, are shown in blue. The trimmer cross sections of the designs resulting from the first part of Design Step 5, the analytical inner edge fluence matching OAR and *z*-position optimization, are shown outlined in black. The trimmer cross sections of the designs resulting from the second part of Design Step 5, the inner edge fluence matching OAR adjustments based on MC calculations, are shown in red. The applicator trimmer weight is listed in the legend for each design.

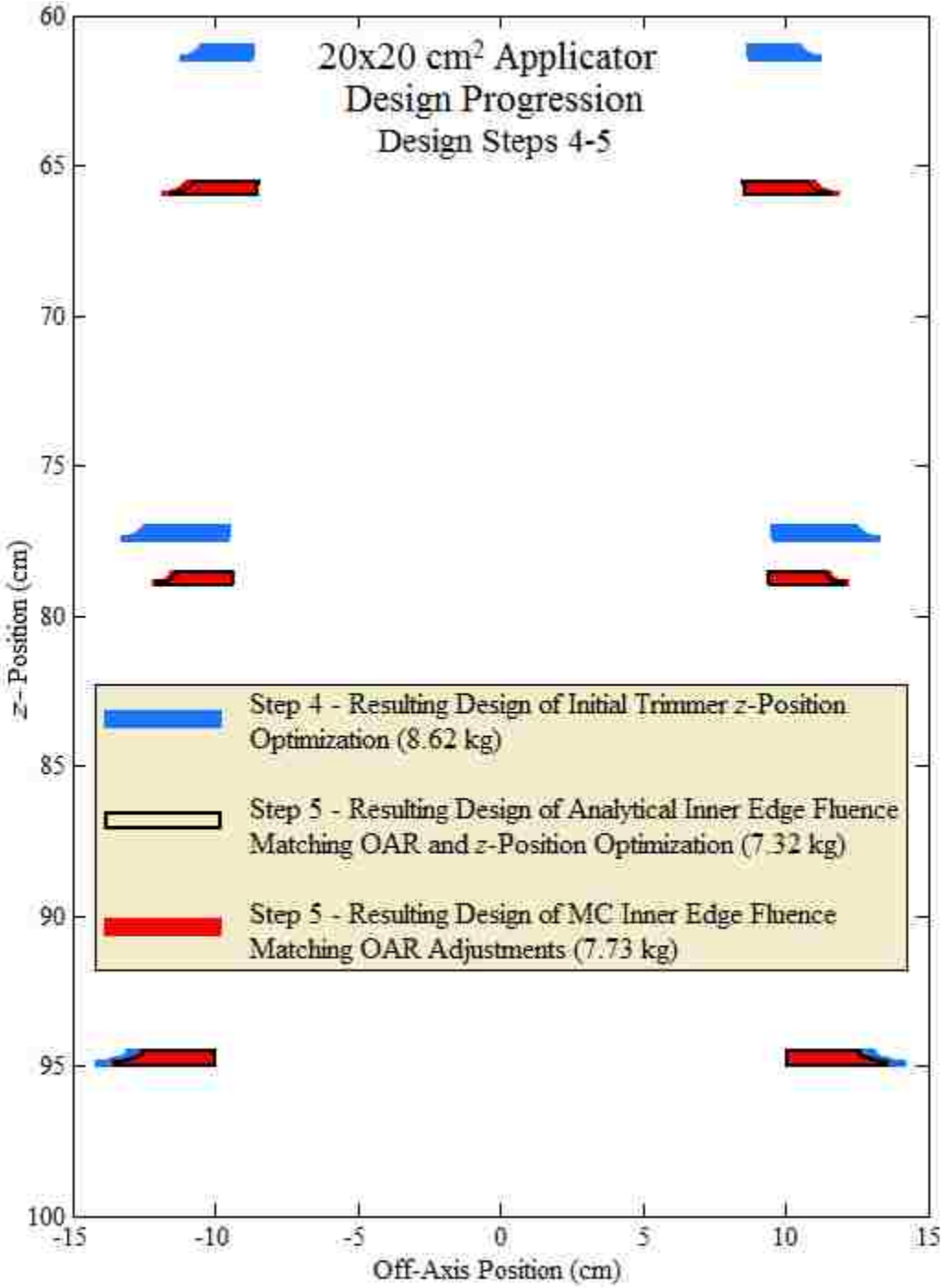

Figure 6-9. In-plane cross sectional view of the design progression of the 20x20 cm^2 applicator trimmers in Design Steps 4 and 5. The trimmer cross sections of the applicator designs resulting from Design Step 4, initial trimmer *z*-position optimization, are shown in blue. The trimmer cross sections of the designs resulting from the first part of Design Step 5, the analytical inner edge fluence matching OAR and *z*-position optimization, are shown outlined in black. The trimmer cross sections of the designs resulting from the second part of Design Step 5, the inner edge fluence matching OAR adjustments based on MC calculations, are shown in red. The applicator trimmer weight is listed in the legend for each design.

both the 10x10 or 20x20 cm^2 sizes. To remedy this, the inner trimmer edge positions of the applicators were adjusted to create a set of four modified collimation system designs for each applicator size by incrementally increasing the fluence matching OARs of each trimmer inner edge, which had the adverse effect of incrementally increasing the applicator weight. The purpose of this study was to select the applicator design which met in-field beam flatness criteria and increased the applicator weight by as little as possible.

The in-field diagonal dose profiles MC-calculated with each of the four modified applicator designs, along with the designs produced from the analytical optimization, are plotted versus off-axis position in Figure 6-10 for the 10x10 cm^2 (upper plot) and 20x20 cm^2 (lower plot) applicators. These MC calculations were performed at 1 cm depth in water with the 7 MeV beam. These designs are labelled 1.A through 1.E in the legend, with Design 1.A representing the design produced from the analytical optimization, and Designs 1.B through 1.E representing the designs created by incrementally increasing the inner edge fluence matching OARs. The weight of each applicator is shown in the legend next to each design. The plots reveal that as the fluence matching OARs increase, so too does both the applicator weight and the relative dose at the edge of the uniformity region, improving the in-field beam flatness.

A dose uniformity limit marker is labelled in each plot, denoting the minimum dose at the uniformity region edge necessary to achieve acceptable in-field beam flatness (similar to Figures 2-1 and 2-2). The markers are located 4.24 cm off axis for the 10x10 cm^2 field and 11.31 cm off axis for the 20x20 cm^2 field, corresponding to the off-axis positions $2\sqrt{2}$ cm inside the corner of the field edge for each applicator size, i.e. the edge of the uniformity region along the diagonals as specified by Hogstrom (2004) and AAPM Task Group 25 (Khan *et al.*, 1991). The markers are situated at relative doses of 97.77% and 99.59% for the 10x10 cm^2 and 20x20 cm^2 applicators, respectively. These dose values correspond to the minimally acceptable OAR at this position (96%, represented in the plots by the circular marker), plus the differences in the MC-calculated and measured diagonal dose profiles of the current clinical collimation system at the edge of the uniformity region as determined in Aim 1, plus a 1%

cushion. The MC-calculated and measured relative dose differences at 7 MeV were 0.77% and 2.59% for the 10x10 cm^2 and 20x20 cm^2 applicators, respectively, (c.f. Table 2-4).

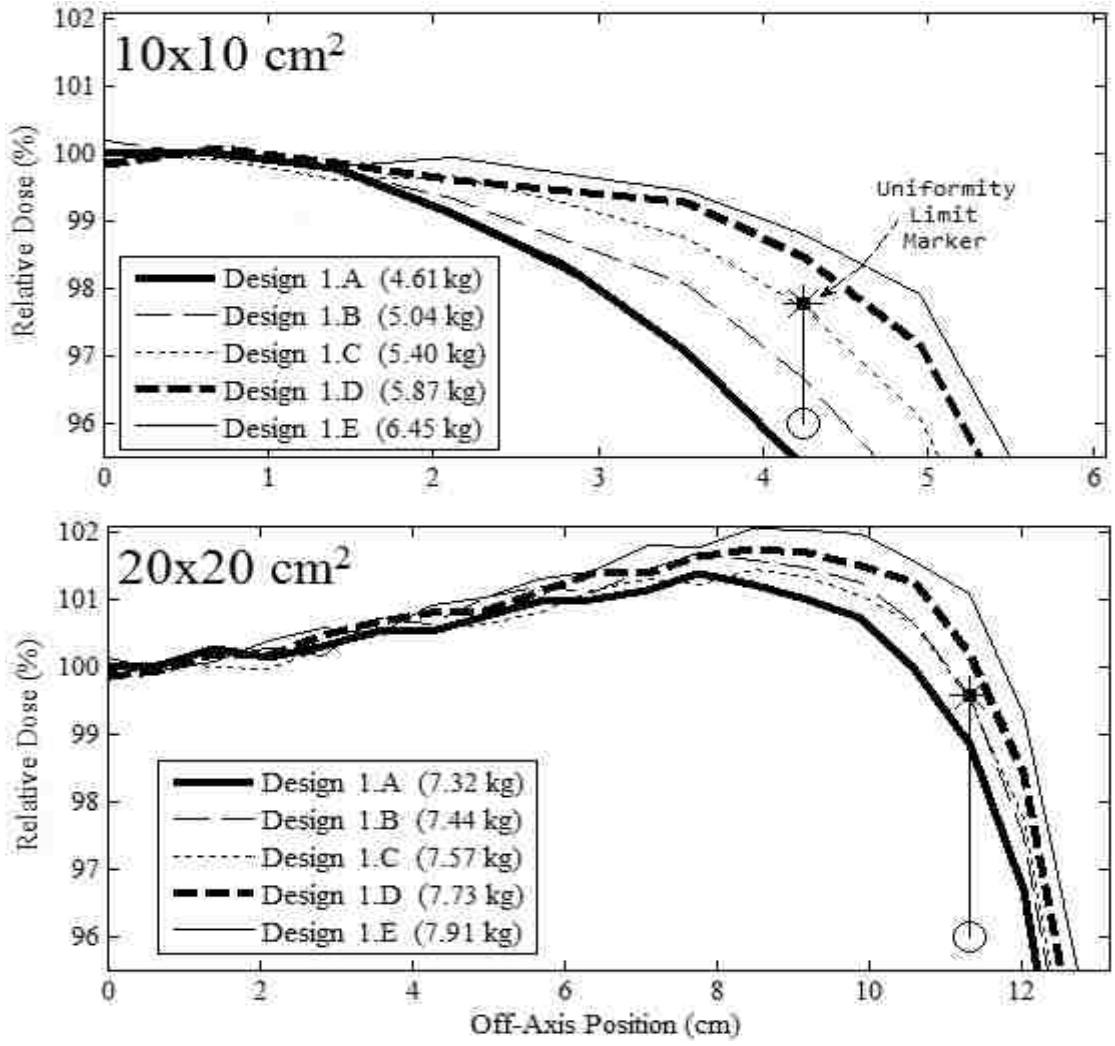

Figure 6-10. In-field off-axis dose profiles for the analysis to determine the inner trimmer edge positions. The figure shows the diagonal relative dose profiles plotted versus off-axis position for applicators modeled for the MC inner edge adjustment analysis calculated at 1 cm depth in water for a 7 MeV beam. The profiles for 10x10 cm^2 applicator are shown in the upper plot and the 20x20 cm^2 applicator profiles are shown in the lower plot. The uniformity limit marker in each plot indicates the point at which a profile must pass above and outside in order to be considered acceptably flat. These markers are positioned at the minimally acceptable OAR at this position (96%, represented by the circular markers), plus the differences found in the MC-calculated and measured diagonal dose profiles of the current clinical collimation system at the edge of the uniformity region, plus a 1% cushion.

Only dose profiles which exceeded the dose indicated by the uniformity limit marker at the edge of the uniformity region were deemed acceptably flat. For both the 10x10 and 20x20 cm^2 applicators, the

lightest models shown to meet this criterion were Designs 1.D, indicated in the plots by the thick dashed curves. For this reason, Designs 1.D were selected for moving forward in the collimation system design process. For the 10x10 cm^2 applicator, these trimmer position adjustments increased the inner edge fluence matching OARs for the upper, middle and lower trimmers from 85%, 90%, and 92% to 95%, 96%, and 96.5%, respectively, increasing the applicator weight from 4.61 to 5.87 kg. For the 20x20 cm^2 applicator, these trimmer position adjustments increased the inner edge fluence matching OARs for the upper, middle and lower trimmers from 85%, 89%, and 92% to 89%, 91%, and 93%, respectively, increasing the applicator weight by 7.32 kg to 7.73 kg.

The 10x10 and 20x20 cm^2 applicator designs produced from the inner edge position adjustments based on MC data can be seen in red in Figures 6-8 and 6-9, respectively. The figures show that the trimmers of this design are shifted outward away from central axis, compared with the design produced from the analytical optimization. This effect is more significant for the 10x10 cm^2 model than the 20x20 cm^2 model, causing the more significant weight increase for the 10x10 cm^2 model. With the determination of these inner edge fluence matching OARs, the trimmer inner edge positions were established for the collimation systems, and all subsequent modifications would only affect the shape and thickness of the trimmers to further reduce the applicator weight, as well as the photon jaw position for all but the lowest beam energy.

For the 20x20 cm^2 applicator, determining the optimal inner trimmer edge locations resulted in a weight reduction of 10.3% from the model produced in Design Step 4, from 8.62 to 7.73 kg. For the 10x10 cm^2 applicator, determining these optimal inner edge positions increased the applicator weight by 6.3%, from 5.52 to 5.87 kg, which was necessary to ensure acceptable beam flatness within the field for the low energy beams.

6.7. Aim 5 - Design Step 6 - Jaw Position Variation with Beam Energy

In Design Step 5, the inner edge positions for all collimators were determined for the lowest beam energy accounted for in the collimation system design process, 6 MeV. The optimum upper trimmer inner edge matching OARs along the penumbra cast by the jaw were found to be 95% for the 10x10 cm^2

applicator design and 89% for the 20x20 cm^2 applicator design. Because the trimmers are stationary, these inner trimmer edge positions are used for all beam energies. This is not the case for the photon jaws, however, which can be moved in toward central axis for higher beam energies.

6.7.1. Methods

A study was performed to investigate the effects on applicator weight and leakage dose of decreasing the upper trimmer inner edge matching OARs for higher energy beams. Three collimation system designs were developed for both the 10x10 and 20x20 cm^2 applicators. The first design was identical to that produced from Design Step 5, in which the upper trimmer fluence matching OARs were held constant for all beam energies. These designs had upper trimmer inner edge matching OARs of 95% for the 10x10 cm^2 model and 89% for the 20x20 cm^2 model for all beam energies. For the other two collimation designs, these fluence matching OARs were decreased for higher energy beams, causing the jaws to be repositioned closer to central axis.

For the 10x10 cm^2 applicator, these alternate designs had 20 MeV fluence matching OARs of 75% and 55%. For all intermediate beam energies, the matching OARs were scaled linearly between the 6 MeV matching OAR (95%) and the 20MeV matching OAR (e.g. for the design with a 75% fluence matching OAR for the 20 MeV beam and an 89% fluence matching OAR for the 6 MeV beam, the 13 MeV beam had a fluence matching OAR of 82% [0.75 + (0.89-0.75)*(13-6)/(20-6) = 0.82]). By adjusting the 20 MeV upper trimmer fluence matching OAR from 95% to 75%, the upper (cross-plane) and lower (in-plane) jaws were repositioned from 4.75 and 5.09 cm off-axis to 3.94 and 4.57 cm off-axis, respectively. By adjusting the upper trimmer fluence matching OAR from 95% to 55%, the upper and lower jaws were repositioned to 3.48 and 4.27 cm off-axis, respectively, for the 20 MeV beam for the 10x10 cm^2 applicator.

For the 20x20 cm^2 applicator, the alternate designs had 20 MeV fluence matching OARs of 72% and 55%, with all intermediate energy matching OARs scaled linearly with energy. By adjusting the 20 MeV upper trimmer fluence matching OAR from 89% to 72%, the upper and lower jaws were repositioned from 6.02 and 6.89 cm off-axis to 5.48 and 6.54 cm off-axis, respectively. By adjusting the

upper trimmer fluence matching OAR from 89% to 55%, the upper and lower jaws were repositioned to 5.10 and 6.29 cm off-axis, respectively, for a 20 MeV beam for the 20x20 cm^2 applicator.

This jaw position adjustment can be performed for higher electron energies without adversely impacting in-field beam flatness, because of the lower scattering power of the higher energy particles. Redesigning the collimation system in this way has two benefits: (1) the upper trimmer weight is reduced because the outer edge bevel shape is adjusted, and (2) the leakage dose produced from the collimation system is reduced.

6.7.1.1. Upper Trimmer Weight Reduction

The first benefit of decreasing the upper trimmer inner edge fluence matching OAR to adjust the jaw position is that doing so reduces the upper trimmer weight. Figure 6-11 illustrates this effect, showing a cross sectional view of the upper trimmer and photon jaw positioned using two different upper trimmer inner edge fluence matching OARs, as well as the 20 MeV beam penumbras cast by the jaw at each position. When the jaw is in the "original" position, the off-axis position of the upper trimmer inner edge is matched to the 95% fluence OAR of the 20 MeV beam penumbra, shown in gray. When the jaw is moved inward toward central axis to the "adjusted" jaw position, the penumbra (shown in black) is shifted inward such that the inner trimmer edge intercepts the penumbra at the 75% fluence OAR. The geometric projections of the divergent beam from each jaw position are shown as the dashed lines, in gray for the original jaw position and black for the adjusted jaw position, each of which matches the 50% OAR position of the corresponding penumbras at the upper trimmer plane. The cross sections of the upper trimmer designed with each jaw configuration are shown at the bottom of the figure. The black cross section indicates the trimmer shape designed with the jaw situated in the adjusted position (75% OAR inner edge fluence matching). The gray region indicates the change in the trimmer cross sectional shape when the trimmer is designed with the jaw situated in the original position (95% OAR inner edge fluence matching). For both trimmer designs, the full trimmer thickness, which corresponds to the calculated range of a 20 MeV electron, extends out to the off-axis position of the 2% fluence OAR. The gray region

indicates the material removed from the trimmer by adjusting the 20 MeV inner edge fluence matching OAR from 95% to 75%, resulting in a trimmer weight reduction.

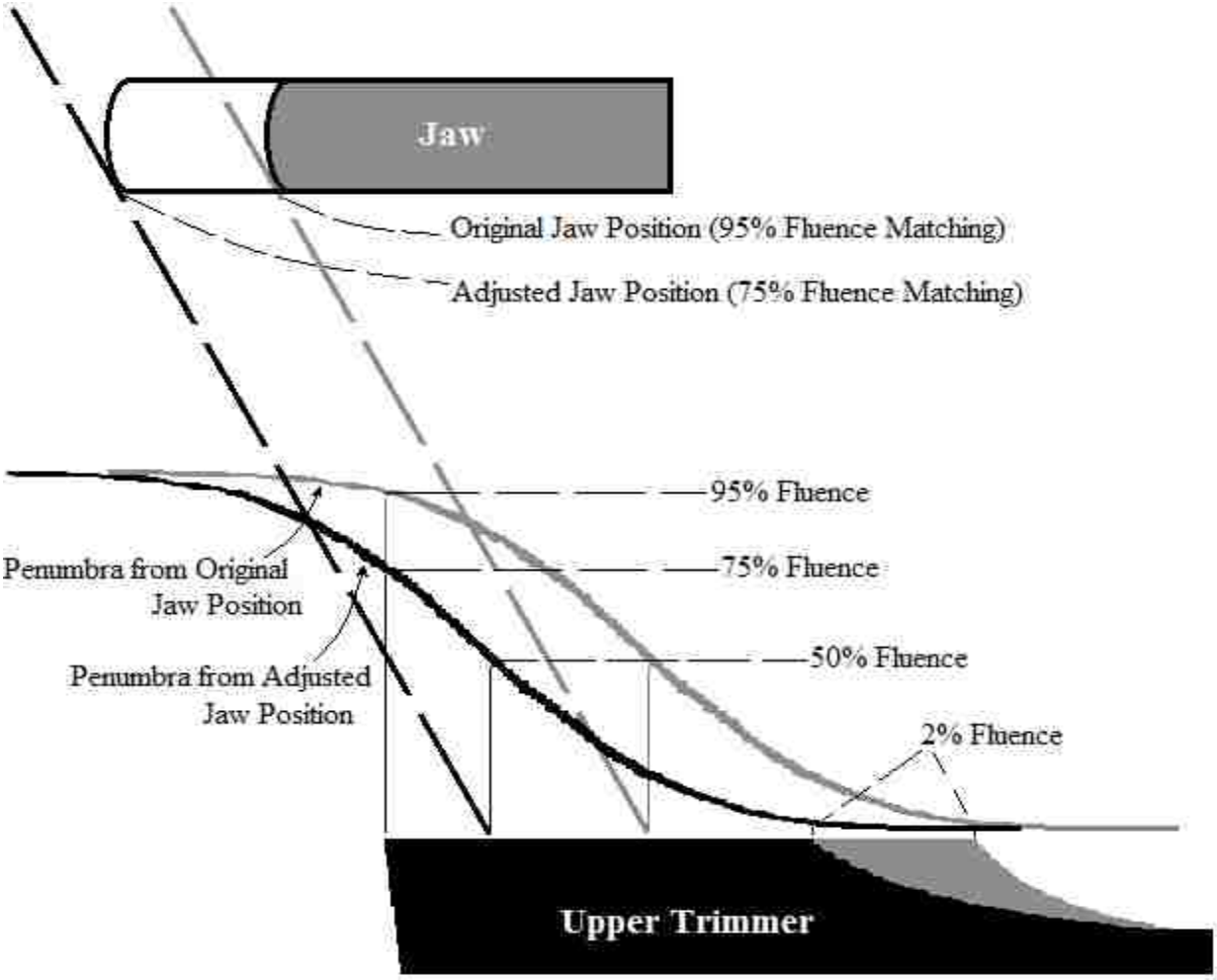

Figure 6-11. Effect of jaw position adjustments for high energy beams on the upper trimmer shape. This figure shows the effect of adjusting the jaw position on the shape of the outer edge bevel. In tis process, trimmer material is removed, reducing the upper trimmer weight. Penumbra cast by a 20 MeV beam are shown with jaws positioned such that the penumbra intercepts the inner edge at fluence levels at 95% (original) and 75% (adjusted). The black region depicts the cross section of the upper trimmer designed with 75% OAR inner edge matching for the 20 MeV beam. The gray region represents the additional material present if the trimmer is designed with 95% OAR inner edge matching for the 20 MeV beam. For both configurations, the off-axis limit of the full trimmer thickness matches the 2% fluence OAR position for a 20 MeV beam.

The weight was calculated for each 10x10 and 20x20 cm^2 applicator designed with the original and adjusted 20 MeV fluence matching OARs to evaluate the effect of these jaw position modifications on applicator weight.

6.7.1.2. Leakage Reduction and Beam Flatness Evaluation

A second benefit of repositioning the jaws closer to central axis for high energy beams is the reduction in leakage dose. In Aim 1, the effects of jaw position on leakage dose distributions were observed for the current clinical Elekta Infinity collimation system. To study this effect on the current applicator model within the design process, a set of MC calculations was performed.

The three collimation systems designs with varying jaw positions for the 10x10 and 20x20 cm^2 applicators were modeled and inserted into the Elekta Infinity BEAMnrc model. As previously described, for the 10x10 cm^2 applicator with the 20 MeV beam, the jaws were positioned with upper trimmer inner edge fluence matching OARs of 55%, 75%, and 95% for the three designs. For the 20x20 cm^2 applicator with the 20 MeV beam the jaws were positioned with upper trimmer inner edge fluence matching OARs of 55%, 72%, and 89%. Simulations were performed with each applicator model at beam energies of 7, 13 and 20 MeV. All source and transport parameters were maintained from the original BEAMnrc model.

These simulations were used to produce phase space files 1 cm upstream of isocenter used as input to DOSXYZnrc to calculate the dose distributions in a water phantom at 100 cm SSD. Dose was calculated using 10^9 initial particles in 0.5x0.5x0.5 cm^3 voxels centered at 1 and 2 cm depth. The dose distributions were symmetrized about central axis in both the in-plane and cross-plane dimensions to reduce statistical uncertainty. All distributions were normalized to the mean dose calculated within a 3x3 set of voxels centered at central axis at the calculation depth.

Within the field, the profiles were evaluated at 1 cm depth for the 7 MeV beam and 2 cm depth for the 13 and 20 MeV beams to ensure that acceptable flatness was maintained for all jaw positions at each beam energy using the same criteria specified in Section 6.2.5.2.

The leakage dose distributions were also evaluated. The mean percent leakage dose was calculated for each design at each beam energy based on IEC specifications to analyze the effect of jaw position on leakage dose and to ensure designs were not exceeding IEC specified limits. Additionally, the LATCH bit filtering feature in EGSnrc was used to separately calculate the leakage from various leakage

dose components. Dose components thought to be most affected by the jaw repositioning were selected for bit filtering calculations, including photons and electrons scattered from the MLC, upper jaw, lower jaw, and upper trimmer. These LATCH bit calculations were performed only for the 20x20 cm^2 applicator with the 20 MeV beams. The bit filtered dose component calculations were performed using $2.5x10^8$ particles sampled from the same phase spaces used for total dose calculations. The dose calculations were performed in 0.5x0.5x0.5 cm^3 voxels centered at 1 depth within water phantoms at 100 cm SSD. All distributions were normalized to the mean total dose calculated within a 3x3 set of voxels centered at central axis at the calculation depth. To reduce statistical uncertainty, the dose distributions were symmetrized about central axis in both the in-plane and cross-plane dimensions. Mean percent leakage doses were calculated for each dose component based on IEC specifications for beam energy.

6.7.2. Results and Discussion

6.7.2.1. Trimmer Weight and In-Field Dose Profile Evaluation

By decreasing the 20 MeV upper trimmer inner edge fluence matching OAR of the 10x10 cm^2 applicator from 95% (as specified in Design Step 5) to 75% and 55%, the applicator weight was reduced from 5.87 to 5.59 and 5.43 kg, respectively. For the 20x20 cm^2 applicator, by decreasing the 20 MeV upper trimmer inner edge fluence matching OAR from 89% (as specified in Design Step 5) to 72% and 55%, the 10x10 cm^2 applicator weight was reduced from 7.73 to 7.51 and 7.35 kg, respectively.

The in-field results of MC calculations performed on each of these applicator designs are shown in Figure 6-12, plotting the diagonal relative dose profiles versus off-axis position for each model at 7, 13, and 20 MeV. The 7 MeV beam profiles were calculated at 1 cm depth in water, and the 13 and 20 MeV beam profiles were calculated at 2 cm depth. Similar to Figure 6-10, the applicator models are labelled Designs 2.A through 2.C in the legend for simplicity. Designs 2.A were modeled using constant upper trimmer inner edge matching OARs of 95% and 89% for all beam energies for the 10x10 and 20x20 cm^2 applicators, respectively. The modified 10x10 cm^2 applicator models using 20 MeV matching OARs of 75% and 55% are labelled as 2.B and 2.C, respectively. The modified 20x20 cm^2 applicator models using 20 MeV matching OARs of 72% and 55% are labelled as 2.B and 2.C, respectively.

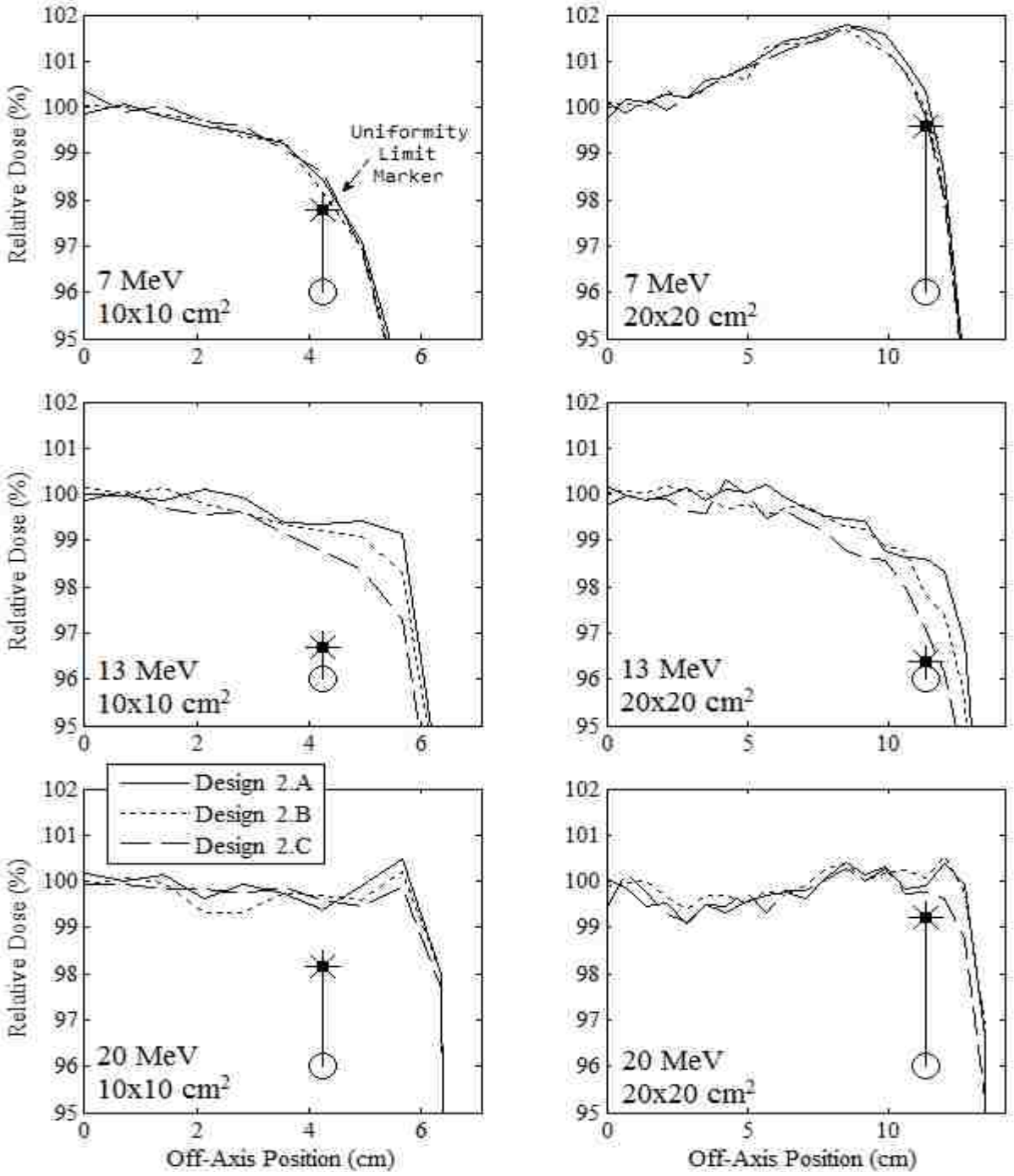

Figure 6-12. In-field diagonal dose profiles for the analysis of jaw position dependence on energy. The figure shows the MC calculated diagonal dose profiles plotted verses off-axis position for the 10x10 cm^2 (left column) and 20x20 cm^2 (right column) applicators. The 7 MeV beam profiles (upper row) were calculated at 1 cm depth in water, and the 13 (middle row) and 20 MeV (lower row) profiles were calculated at 2 cm depth. The uniformity limit marker indicates the point at which a profile must pass above and outside in order to be considered acceptably flat. These markers are positioned at the minimally acceptable OAR at this position (96%, represented by the circular markers), plus the differences found in the MC-calculated and measured diagonal dose profiles of the current clinical collimation system at the edge of the uniformity region, plus a 1% cushion.

Each plot also shows the dose uniformity limit marker for each beam. Like in Figure 6-10, these markers indicate the minimum relative dose at the edge of the uniformity region necessary to achieve acceptable in-field beam flatness. These markers are placed at the minimally acceptable OAR at this off-axis position (96%, represented in the plots by the circular marker), plus the differences found in the MC-calculated and measured diagonal dose profiles at the uniformity region edge for each beam energy as previously determined in Aim 1 (c.f. Table 2-4), plus a 1% cushion. Because all profiles are shown to pass above and outside this uniformity limit marker for all beam energies, all collimation systems are deemed to produce acceptable in-field beam flatness at all beam energies studied.

6.7.2.2. Leakage Dose Reduction Evaluation

The out-of-field dose profiles were also evaluated for each model to analyze the effect of jaw position adjustments on the leakage dose. These results are shown in Figure 6-13, as well as Figure C-1 in Appendix C. Figure 6-13 plots the cross-plane total dose profiles versus off-axis position in the leakage region calculated at 1 cm depth normalized to central axis dose. The results reveal that by moving the jaws inward for high beam energies, the leakage dose is decreased. The effect is insignificant for the 7 MeV beam, because the jaw movement is slight. However, for the 13 MeV and, more substantially, the 20 MeV beam the dose reduction is great. The in-plane dose profiles are plotted versus off-axis position in Figure C-1 and the similar effects are observed.

The mean percent leakage doses were calculated per IEC specifications for each profile and are shown Table 6-3. This table also displays the upper trimmer inner edge fluence matching OARs and calculated applicator weight for each design. The total mean percent leakage dose results in this table confirm that moving the jaw in toward central axis reduces the leakage dose. For the 7 MeV beam, modifying the collimation system from Design 2.A to 2.C reduced the mean leakage dose by only 0.02% for the 20x20 cm^2 applicator. For the higher beam energies the effect was much more significant. Modifying the 20x20 cm^2 collimation system from Design 2.A to 2.C reduced the mean leakage dose by 0.10% for the 13 MeV beam and 0.32% for the 20 MeV beam.

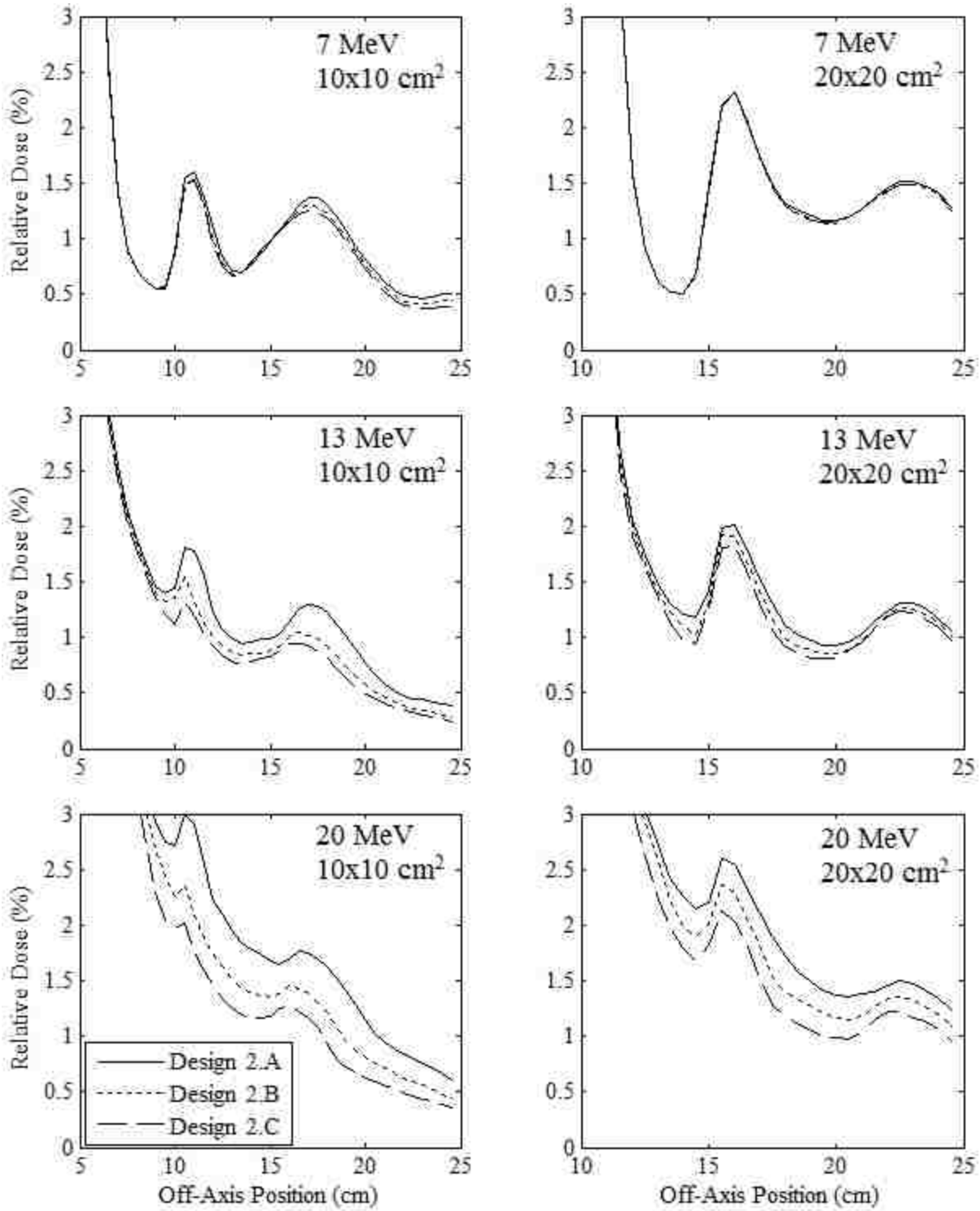

Figure 6-13. Cross-plane total dose profiles plotted versus off-axis position in the leakage region for the analysis of jaw position variation with beam energy. The 10x10 cm^2 applicator results are shown in the left column of plots and the 20x20 cm^2 results are shown on the right for the 7 (upper row), 13 (middle row), and 20 MeV (lower row) beams. All profiles were normalized to central axis dose at the calculation depth, 1 cm in water. Refer to the text for a description of Designs 2.A, 2.B and 2.C.

Table 6-3. Results of jaw position variation with beam energy analysis. The table shows the 6 and 20 MeV upper trimmer inner edge fluence matching OARs for each design along with their calculated applicator weight. The total mean percent leakage doses normalized to D_{max} per IEC specifications are also shown, along with mean leakage dose contributions of various dose components for the 20x20 cm^2 models with the 20 MeV beam .

		10x10 cm^2 Applicator			20x20 cm^2 Applicator		
		2.A	2.B	2.C	2.A	2.B	2.C
Upper Trimmer Matching OAR	6 MeV Beam	95%	95%	95%	89%	89%	89%
	20 MeV Beam	95%	75%	55%	89%	72%	55%
Applicator Weight (kg)		5.87	5.59	5.43	7.73	7.51	7.35
Total Mean % Leakage Dose	7 MeV Beam	0.56	0.53	0.52	0.78	0.76	0.76
	13 MeV Beam	0.69	0.58	0.52	0.75	0.69	0.65
	20 MeV Beam	1.26	0.98	0.82	1.21	1.04	0.89
Dose Component Mean % Leakage Contributions (20 MeV Beam)	Photon Dose	-	-	-	0.54	0.46	0.38
	MLC Scatter	-	-	-	0.05	0.04	0.03
	Upper Jaw Scat.	-	-	-	0.08	0.08	0.08
	Lower Jaw Scat.	-	-	-	0.05	0.05	0.05
	Upper Trim. Scat.	-	-	-	0.14	0.09	0.06

To further investigate the effect of jaw position adjustments on the leakage dose, a MC study was performed at 20 MeV for the 20x20 cm^2 applicator using the LATCH bit filtering feature in EGSnrc to separately calculate the leakage dose contributions from various dose components, including the total dose, total photon dose, and dose from electrons scattered from the MLC, upper and lower photon jaws, and the upper trimmer. The cross-plane leakage dose profiles for each dose component were plotted versus off-axis position in Figure 6-14. The results reveal that the dose components most affected by the jaw position modifications were the photon dose and upper trimmer electron scatter dose. The cross-plane MLC scatter dose profile was also moderately affected, most notably in the leakage bump closest to central axis. The effects on both the upper and lower jaw scatter dose component profiles were slight. The in-plane dose profiles for these calculations are plotted versus off-axis position in Figure C-2, and similar effects are observed.

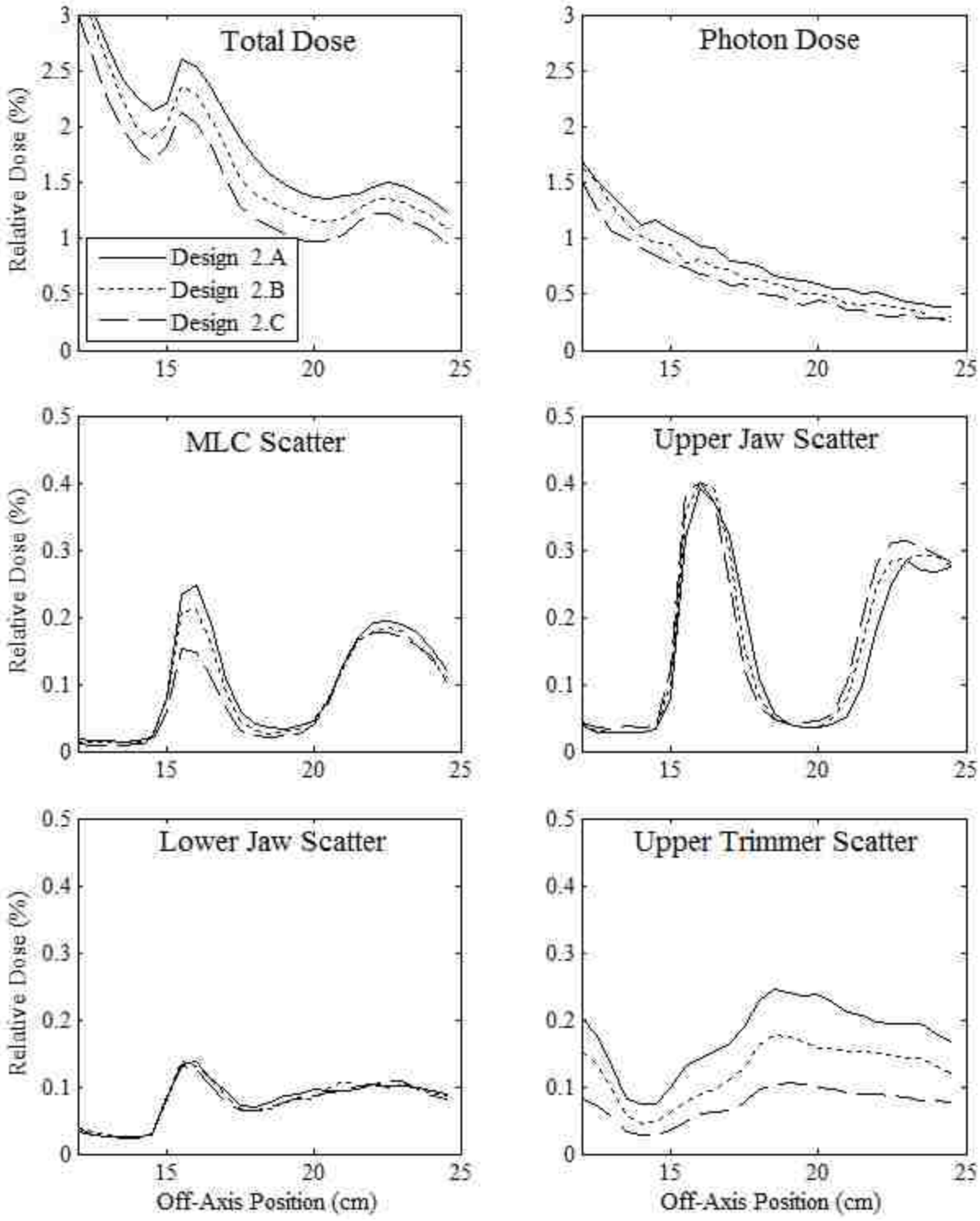

Figure 6-14. Cross-plane leakage component profiles for analysis of jaw position variation with beam energy. All profiles were calculated at 1 cm depth in water for a 20 MeV beam with the 20x20 cm^2 applicator designs and normalized to total central axis dose at the calculation depth. The range of the relative dose axis for the electron scatter dose component plots was reduced to magnify these lower dose profiles. Refer to the text for a description of Designs 2.A, 2.B, and 2.C.

The IEC specified mean percent leakage doses for each dose component are reported in Table 6-3. These data confirm that by adjusting the jaw position inward towards central axis, the photon and upper trimmer scatter dose components were reduced. By modifying the 20x20 cm^2 collimation system from Design 2.A to Design 2.C, the photon dose mean leakage dose contribution was reduced by0.16%, from 0.54% to 0.38%, and the upper trimmer electron scatter dose component mean leakage dose was reduced by 0.08%, from 0.14% to 0.06%. The MLC scatter dose component mean leakage dose was also moderately reduced from 0.05% to 0.03%.

Because of the decreased leakage dose and reduced applicator weight, Designs 2.C were selected for both applicator sizes for proceeding with the collimation system design process. In doing so, the 10x10 cm^2 applicator weight was reduced by 7.5% from the model produced by the inner edge position analysis, from 5.87 to 5.43 kg. The 20x20 cm^2 applicator weight was reduced by 4.9%, from 7.73 to 7.35 kg. These design modifications finalized all inner and outer trimmer edge positions for the collimation system, as well as all jaw positions for all beam energies.

6.8. Aim 5 - Design Step 7 - Trimmer Thickness and Outer Bevel Shape Adjustments

With the completion of Design Step 6, all jaw and inner trimmer edge positions were determined for all beam energies. To further reduce the applicator weight, methods were needed for decreasing the amount of trimmer material used in the design, which would necessarily increase the leakage dose transmitted by the applicator. The jaw positioning study revealed that the applicator models at this point in the design process produced mean percent leakage doses well below the IEC specified limits. Therefore, adjustments could be made to decrease the trimmer weight, so long as care was taken to ensure the leakage dose did not increase beyond acceptable limits. Furthermore, the jaw positioning study revealed that for the high energy beams, the mean percent leakage dose passed criteria by a larger margin than for the low energy beams. For example, for the 20x20 cm^2 applicator the 20 MeV beam produced a mean leakage dose of 0.89% (c.f. Table 6-3), 0.45% less than the IEC specified threshold of 1.34%. For the 7 MeV beam the mean leakage dose was calculated to be 0.76%, only 0.24% less than the IEC specified limit of 1.00%. Additionally, the energy range accounted for in the collimation system design

has a lower limit of 6 MeV. Since the MC model can only evaluate the collimation system for a minimum nominal beam energy of 7 MeV ($E_{p,0}$ = 7.14), a more significant cushion should be maintained for the lower energy mean percent leakage dose limit to ensure that criteria are met for the full energy range. For these reasons, only methods for reducing trimmer weight primarily affecting the high energy beam leakage dose were considered. This meant that adjustments which altered the position of the thin outer edge of the trimmer bars were excluded.

6.8.1. Methods

Two methods to reduce the trimmer weight, both primarily affecting the leakage dose at higher beam energies, were analyzed: 1) reducing the trimmer thickness and 2) adjusting the outer trimmer edge bevel shape. MC investigations were performed in parallel in which the thickness and bevel shape of each trimmer was varied. These simulations were performed only with the 20x20 cm^2 applicator and 20 MeV beam to determine the effect of these modifications on the mean percent leakage dose. Once both the trimmer thickness and bevel shape investigations were complete, the results were used to determine the best method for modifying each trimmer to reduce the applicator weight, considering the extent of trimmer weight reduction relative to the mean leakage dose increase.

6.8.1.1. Trimmer Thickness Reduction Analysis

A MC study was performed to analyze the effect of decreasing the trimmer thickness on both applicator weight and 20 MeV percent mean leakage dose. In this study, the 20x20 cm^2 applicator design produced from the jaw positioning study was modified to reduce the trimmer thickness. Modifications were performed to only one trimmer at a time, with the other two trimmers maintaining full thickness by various percentages. To perform this thickness reduction, the range calculation equation (derived from the MC 1% threshold method) was multiplied by a coefficient (< 1.0) to reduce the trimmer thickness along the full width of the trimmer, including the beveled outer edge. The effect of this reduction is depicted in Figure 6-15, which shows a cross sectional view of a trimmer designed with full thickness (gray) and reduced thickness (black). The gray area represents the material removed from the trimmer by the thickness reduction.

For the lower and middle trimmers, applicator designs were created in which the trimmer thicknesses were reduced by 7%, 14%, 21%, and 35%. For the upper trimmer, designs were created in which the thickness was reduced by 7%, 14%, 21%, 35%, and 49%, producing 13 separate modified applicator models in total.

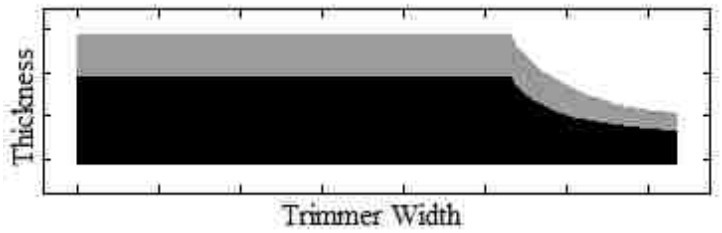

Figure 6-15. Effect of thickness reduction on trimmer cross sectional shape. The image illustrates the effect on trimmer shape when the trimmer is designed with full thickness (gray) and reduced thickness (black). The gray region represents the material removed by the modification.

Each of these designs was modeled and inserted into the Elekta Infinity BEAMnrc model. Simulations were performed with the 20 MeV beam to produce phase space files 1 cm upstream of isocenter which were used as input to DOSXYZnrc to calculate the dose in a water phantom. Dose was again calculated at 100 cm SSD in 0.5x0.5x0.5 cm^3 water voxels centered at a depth of 1 cm. All source and transport parameters used in the previous MC studies were maintained for these calculations. To reduce statistical uncertainty, the dose distributions were symmetrized about central axis in both the in-plane and cross-plane dimensions. Dose distributions were normalized to the mean dose calculated within a 3x3 set of voxels centered at central axis at the calculation depth. Mean percent leakage doses were calculated based on IEC specifications for each applicator model.

6.8.1.2. Bevel Shape Adjustment Analysis

For all previous designs, an outer trimmer edge fluence matching OAR of 2% was used for all energies to form the outer edge bevel, meaning the trimmer thickness at each off-axis position along the outer edge bevel is calculated using the beam energy producing a 2% fluence OAR at that position. This 2% value was selected because it had been used in previous applicator design studies (Hogstrom *et al.*, 1985; Hogstrom *et al.*, 1990), but could be adjusted to modify the shape of the outer edge bevel.

A study was performed to investigate the effect of adjusting the bevel shape on applicator weight and leakage dose. In this study, a pair of modified 20x20 cm^2 applicators was created by adjusting the bevel of the applicators produced from Design Step 6, which was designed with a 2% outer edge fluence matching OAR for all beam energies. These two modified applicator designs by increasing the outer edge matching OAR to 25% and 48% at 20 MeV. Because it was decided that only applicator design modifications which primarily affect high energy leakage dose would be investigated, the outer edge fluence matching OAR for the 6 MeV beam was maintained at 2% for all designs. For all intermediate energies, the fluence matching OARs were scaled linearly between the matching OARs for the 6 and 20 MeV beams. Modifications were performed on only one trimmer at a time, with the other two trimmers maintaining their original bevel shape, creating six modified applicators in total. The weight of each modified applicator was calculated to evaluate the effects of these adjustments.

Increasing the 20 MeV fluence matching OAR had the effect of pulling the outer edge bevel in toward central axis, while maintaining the full width of the trimmer. This effect is depicted in Figure 6-16, which shows the penumbra of a 20 MeV beam cast on a trimmer designed with two different outer edge bevel shapes. The trimmer cross section shown in black depicts the trimmer shape calculated with a 48% outer edge fluence matching OAR for the 20 MeV beam. The gray region depicts the bevel shape for a trimmer designed with a 2% fluence matching OAR for the 20 MeV beam. Both trimmer designs in the figure maintain a 2% fluence matching OAR for the 6 MeV beam. For all intermediate energies, the matching OARs were scaled linearly between the matching OARs for the 6 and 20 MeV beams. As the figure shows, increasing the matching OAR for the 20 MeV beam pulls the bevel inward toward central axis. The gray region in the figure represents the material removed by this edge bevel modification, decreasing the applicator weight.

To determine the effect of these modifications on leakage dose, a MC study was performed in which the six new designs were modeled and inserted into the Elekta Infinity BEAMnrc model. Simulations were performed with the new applicators with the 20 MeV beam to produce phase space files 1 cm upstream of isocenter which were used as input to DOSXYZnrc to calculate dose in a water

phantom. Dose was calculated at 100 cm SSD in 0.5x0.5x0.5 cm^3 water voxels centered at 1 cm depth. To reduce statistical uncertainty, the dose distributions were symmetrized about central axis in both the in-plane and cross-plane dimensions. All source and transport parameters were maintained from the previous MC studies. Dose distributions were normalized to the mean dose calculated within a 3x3 set of voxels centered at central axis at the calculation depth. Mean percent leakage doses were calculated for the dose distributions of each design based on IEC specifications.

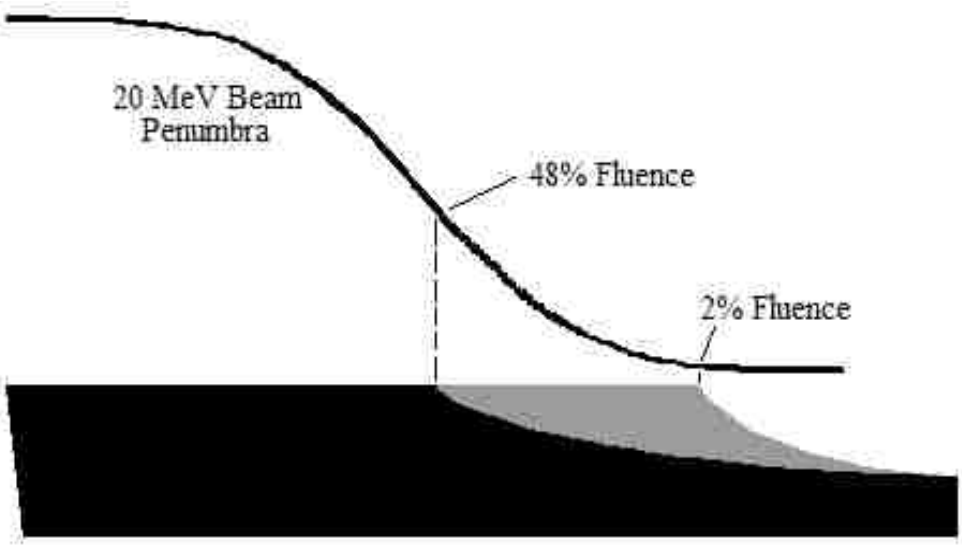

Figure 6-16. Effect of bevel shape adjustment on trimmer cross sectional shape. The image shows the penumbra of a 20 MeV beam cast on a trimmer designed with two different outer edge bevel shapes. The trimmer cross section shown in black depicts the trimmer shape calculated with a 48% outer edge fluence matching OAR for the 20 MeV beam. The gray region represents the bevel shape for a trimmer designed with a 2% fluence matching OAR for the 20 MeV beam. Both trimmer designs maintained a 2% fluence matching OAR for the 6 MeV beam. The gray region represents the material removed by this edge bevel modification.

These mean percent leakage doses, along with the mean leakage doses from the trimmer thickness reduction analysis, were compared against the applicator weight reduction for each modification to decide the best method for modifying each trimmer to reduce the applicator weight, while maintaining acceptable 20 MeV leakage dose levels.

6.8.2. Results and Discussion

The results of the trimmer thickness reduction and bevel shape adjustment studies are displayed in Figure 6-17, Table 6-4, and Figure 6-18. The upper plot in Figure 6-17 shows the MC-calculated 20 MeV cross-plane leakage dose profiles plotted versus off-axis position for each 20x20 cm^2 applicator modeled in the trimmer thickness reduction analysis. The thick solid black curve represents the profile of the unmodified design produced from the analysis of the jaw position variation with energy. This profile was shown to have the lowest dose outside the field, with all modifications only increasing the leakage dose. The dose profiles of the four designs modifying the lower trimmer (thickness reductions of 7%, 14%, 21%, and 35%) are shown with the long-dashed curves, the dose profiles of the four designs modifying the middle trimmer (thickness reductions of 7%, 14%, 21%, and 35%) are shown with the short-dashed curves, and the dose profiles of the five designs modifying the upper trimmer (thickness reductions of 7%, 14%, 21%, 35% and 49%) are shown with the solid curves, each calculated at 1 cm depth in water and normalized to central axis dose. In each of these designs, the original bevel shape was maintained, designed using a 2% outer edge fluence matching OAR for all beam energies.

The profiles reveal that by reducing the lower and middle trimmer thickness, the leakage dose was increased substantially. The lower trimmer increase was more significant near the edge of the field, and the middle trimmer increase was more uniform throughout the leakage region. The upper trimmer thickness reduction caused an increase in leakage dose, though the effect was much less substantial than the middle and lower trimmers.

The 20 MeV cross-plane leakage dose profiles are plotted versus off-axis position in the lower plot of Figure 6-17 for each 20x20 cm^2 applicator modeled in the bevel shape adjustment analysis. The thick solid black curve represents the profile of the unmodified design and was again shown to have the lowest dose outside the field. This plot shows the dose profiles of designs with modified lower (long-dashed curves), middle (short-dashed curves), and upper trimmers (solid curves). For each trimmer, modifications were performed in which the 20 MeV outer edge fluence matching OAR was increased

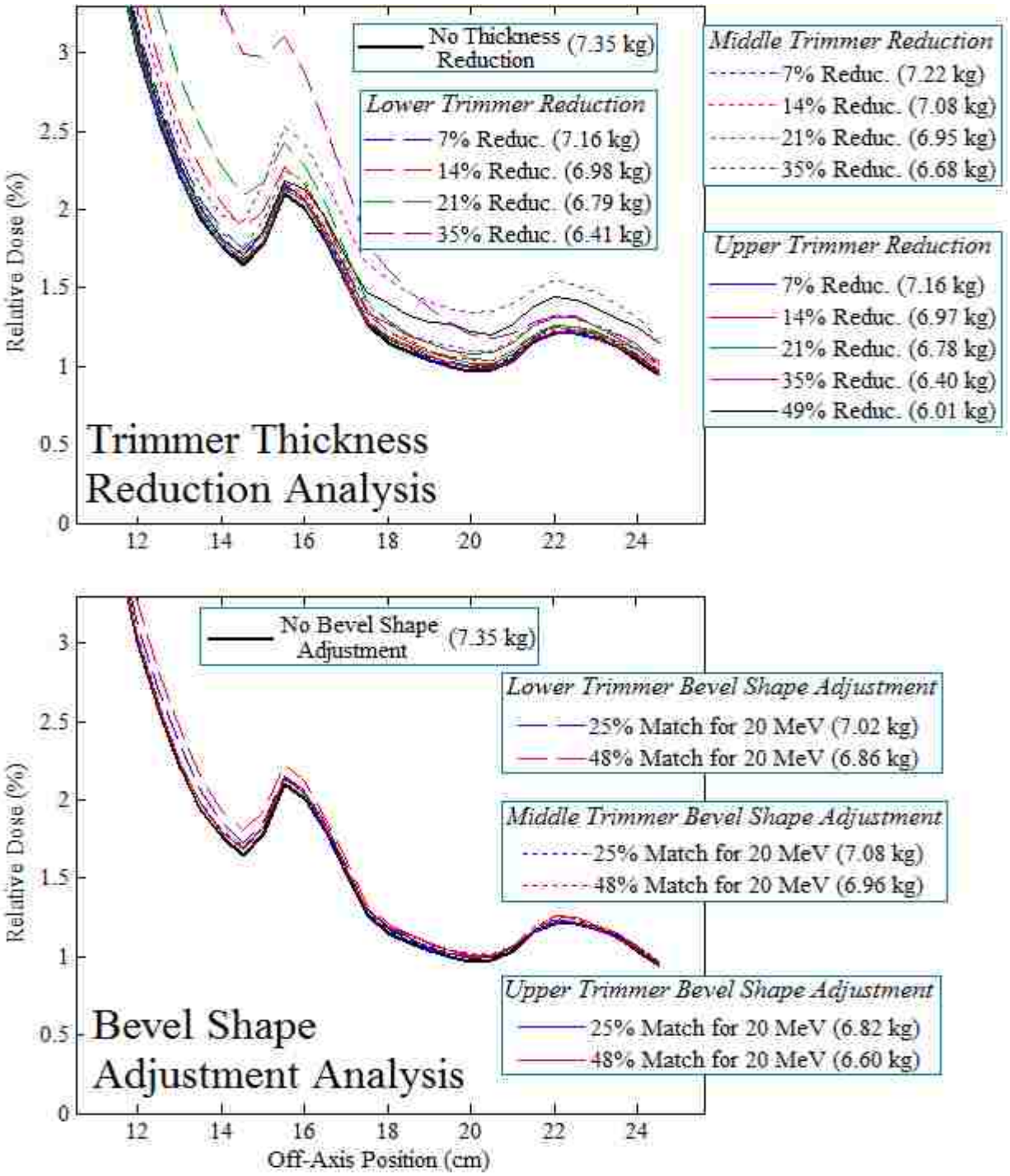

Figure 6-17. 20 MeV cross-plane leakage dose profiles plotted versus off-axis position for the trimmer thickness reduction and bevel shape analyses. The trimmer thickness reduction analysis profiles are shown in the upper plot, and the bevel shape adjustment analysis profiles are shown in the lower plot, calculated at 1 cm depth in water and normalized to central axis dose. For both plots the lower trimmer adjustments are shown with the long-dashed curves, the middle trimmer adjustments are shown with the short-dashed curves and the upper trimmer adjustments are shown with the solid curves. The weight of each 20x20 cm^2 applicator design is indicated in the legends.

Table 6-4. Results of the trimmer thickness reduction and bevel shape analyses. The trimmer thickness reduction results are shown on the left, and the bevel shape adjustment results are shown on the right. For each design, the calculated applicator weight and mean percent leakage dose are shown normalized to D_{max} per IEC specifications. For all trimmer thickness reduction designs, a 2% outer bevel fluence matching OAR at 20 MeV was maintained for all trimmers. For all adjusted outer edge bevel designs, a 0% thickness reduction was maintained for all trimmers.

Trimmer Thickness Reduction				Bevel Shape Variation			
	Trimmer Thickness Reduction	Applicator Weight (kg)	Mean % Leakage		20 MeV Fluence Matching OAR	Applicator Weight (kg)	Mean % Leakage
Upper Trimmer Variation	0%	7.35	0.89	Upper Trimmer Variation	2%	7.35	0.89
	7%	7.16	0.90		25%	6.82	0.90
	14%	6.97	0.89		48%	6.60	0.91
	21%	6.78	0.91				
	35%	6.40	0.95				
	49%	6.01	1.02				
Middle Trimmer Variation	0%	7.35	0.89	Middle Trimmer Variation	2%	7.35	0.89
	7%	7.22	0.91		25%	7.08	0.91
	14%	7.08	0.94		48%	6.96	0.92
	21%	6.95	0.98				
	35%	6.68	1.20				
Lower Trimmer Variation	0%	7.35	0.89	Lower Trimmer Variation	2%	7.35	0.89
	7%	7.16	0.91		25%	7.02	0.91
	14%	6.98	0.95		48%	6.86	0.91
	21%	6.79	1.00				
	35%	6.41	1.24%				

from 2% to 25% (blue curves) and 48% (red curves). Like in the upper plot, the calculated applicator weight for each design is displayed in the legends. These plots reveal that by adjusting the bevel shape rather than reducing the trimmer thickness, the increase in the leakage dose was much less substantial. Near the edge of field, moderate dose increases were seen due to lower trimmer adjustments, but all other effects were slight.

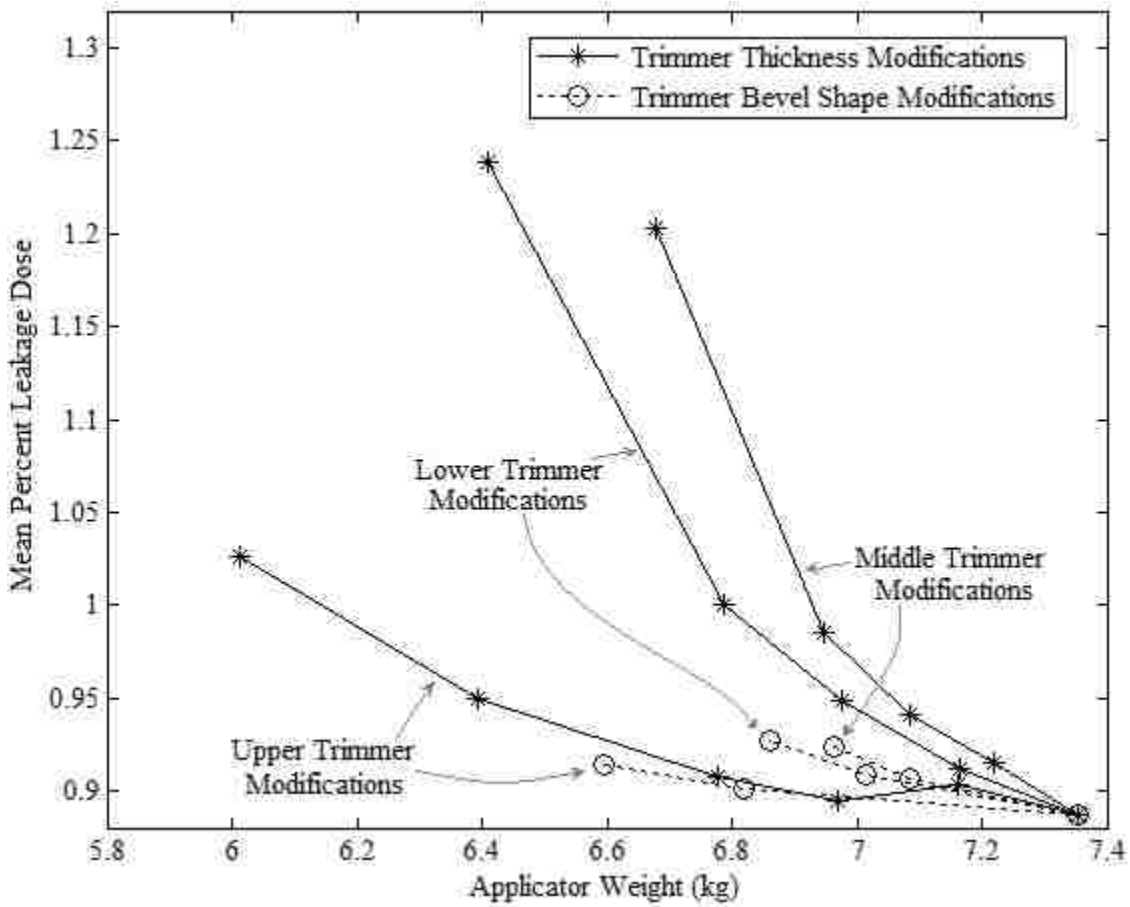

Figure 6-18. Mean percent leakage dose plotted versus applicator weight for the applicator designs produced in the trimmer thickness reduction and bevel shape analyses. Each marker on the figure represents a the 20 MeV mean percent leakage dose of each 20x20 cm^2 applicator design plotted versus the applicator weight. Designs which modified the trimmer thickness are shown with solid curves and star markers, and designs which modified the bevel shape are shown with dashed curves and circular markers. Curves representing modifications made to the upper, middle, and lower trimmers are labelled. The marker in the lower right corner of the plot represents the unmodified 20x20 cm^2 design produced from Design Step 6. The mean percent leakage doses were calculated per IEC specifications and normalized to D_{max}.

The IEC specified mean percent leakage doses were calculated for each of these dose distributions and are displayed is Table 6-4 normalized to D_{max}, along with the calculated weight of each applicator. These data show that for the middle and lower trimmers, reducing the trimmer thickness increased the mean leakage dose far more than adjusting the outer edge bevel. To better visualize this, the same data were plotted in Figure 6-18. This figure plots the 20 MeV mean percent leakage dose for each applicator design against the applicator weight. Each marker in the plot represents a different applicator

design. The marker in the lower right corner of the plot (7.35 kg) represents the unmodified design produced from Design Step 6. The data revealed that all adjustments made to this unmodified design only decrease the applicator weight and increase the 20 MeV beam mean percent leakage dose.

The purpose of plotting the data in this manner was to more clearly depict which modification methods for each trimmer reduced the applicator weight as much as possible while increasing the leakage dose as little as possible. In this plot the more gradually sloped curves (i.e. less dose increase per unit weight decrease) represent the more beneficial techniques. For the lower and middle trimmers, the bevel shape modifications were significantly more beneficial than the trimmer thickness reductions, as indicated by the more gradual slope of these curves. For the upper trimmer, the slopes of the curves for both modification techniques were similar. However, the applicator weight was able to be further decreased by reducing the upper trimmer thickness than by reshaping the outer edge bevel.

Using the data from Table 6-4 and Figure 6-18, it was decided that adjusting the bevel shape would be the best method for reducing the middle and lower trimmer weights. A 20 MeV fluence matching OAR for the outer bevel of 50% was selected for the design of the lower two trimmers (only a slight deviation from the 48% fluence matching OAR value used in the study). For the upper trimmer, both techniques for weight reduction performed nearly equally well. Because the trimmer weight was able to be further reduced using the thickness reduction method rather than the bevel shape modifications, the former method was selected for modifying the upper trimmer. A 50% thickness reduction was selected for this trimmer (only a slight deviation from the 49% reduction value used in the study). According to the MC calculations, these modifications to the upper, middle, and lower trimmer caused mean leakage dose increases of roughly 0.13%, 0.02%, and 0.03%, respectively. Assuming the mean percent leakage dose increases due to modifications made to each trimmer are independent of one another, these upper, middle, and lower trimmer modifications should result in the new design producing a 20 MeV mean percent leakage dose of roughly 1.07% [0.89 + 0.13 + 0.02 + 0.03 = 1.07], well short of the IEC specified mean leakage dose limit of 1.34%.

Though only investigated for the 20x20 cm^2 applicator, these modifications were implemented for both applicator sizes. With these adjustments, the 10x10 cm^2 applicator weight was reduced by 31.3%, from 5.43 to 3.73 kg, and the 20x20 cm^2 applicator weight was reduced by 30.8%, from 7.35 to 5.09 kg.

6.9. Aim 5 - Evaluation of Final Design

6.9.1. Methods

Once a final set of design modifications was selected for each trimmer in Design Step 7, 10x10 and 20x20 cm^2 applicators incorporating these modifications were modeled in BEAMnrc and inserted into the BEAMnrc Elekta Infinity model. To evaluate in-field beam flatness and patient plane leakage dose of the new collimation designs, simulations were performed with the 7, 13, and 20 MeV beams to produce phase space files 1 cm upstream of isocenter which were used as input to DOSXYZ to calculated dose in a water phantom at 100 SSD. Dose was again calculated in 0.5x0.5x0.5 cm^3 water voxels centered at depths of 1 and 2 cm. All source and transport parameters were maintained from the previous MC studies. To reduce statistical uncertainty, the dose distributions were again symmetrized about central axis in both the in-plane and cross-plane dimensions and normalized to a 3x3 set of voxels centered about central axis at the calculation depth.

6.9.2. Results and Discussion

To evaluate the collimation system designs produced from Design Step 7, MC simulations were performed on the 10x10 and 20x20 cm^2 applicators. The in-field results of these calculations are shown in Figure 6-19, as well as Figures C-3 and C-4 in Appendix C. The diagonal relative dose profiles are plotted versus off-axis position in Figure 6-19. The diagonal profiles were selected for plotting as the profiles most likely to fail dose flatness criteria. The 7 MeV dose profiles were calculated at 1 cm depth in water, and the 13 and 20 MeV dose profiles were calculated at 2 cm depth. The plots also show the uniformity limit markers for each beam. Like in Figures 6-10 and 6-12, these markers indicate the

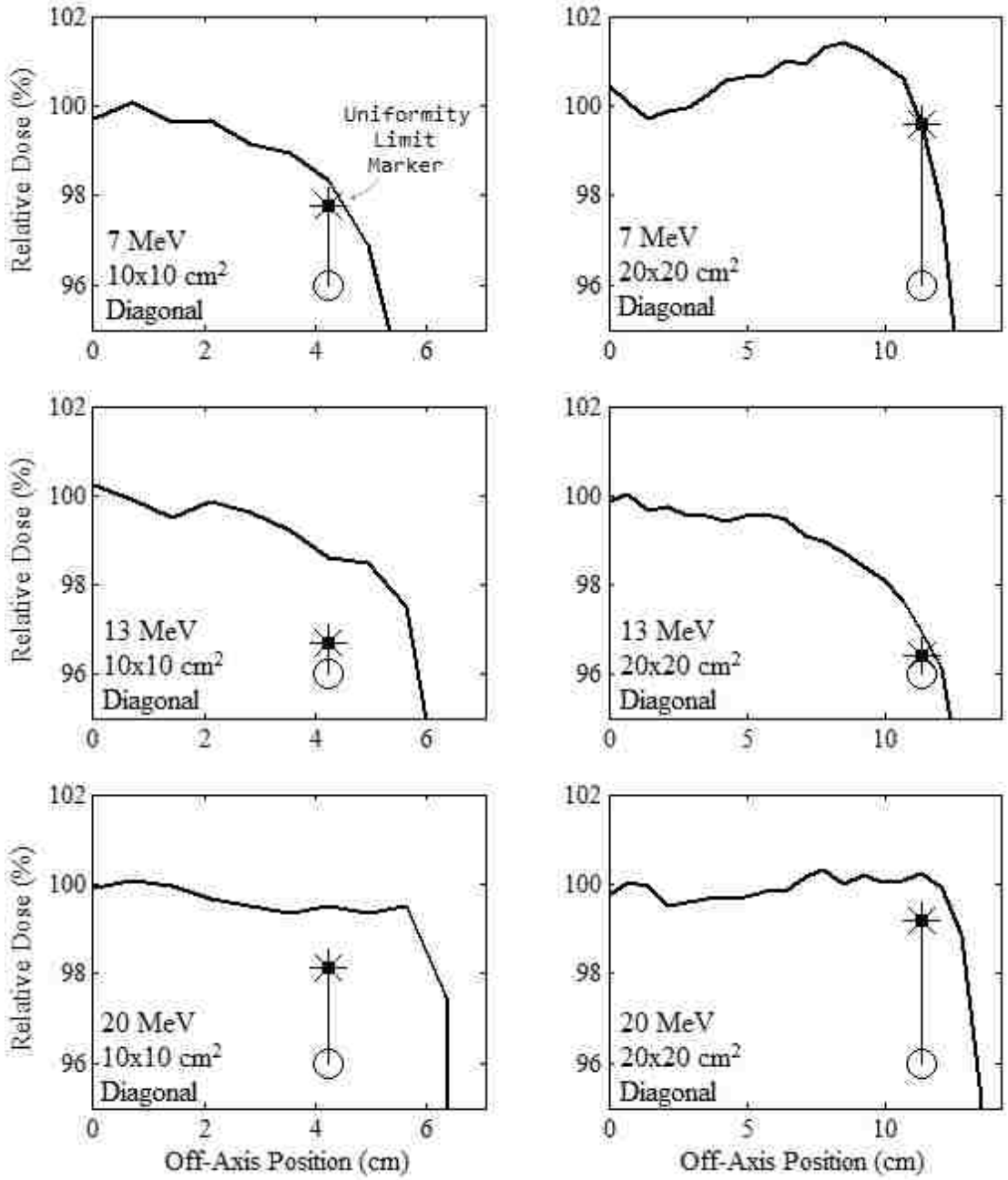

Figure 6-19. In-field diagonal dose profiles plotted versus off-axis position for the selected 10x10 and 20x20 cm^2 collimation designs. The 10x10 cm^2 applicator profiles are shown in the left column of plots and the 20x20 cm^2 profiles are shown on the right for the 7 (upper row), 13 (middle row), and 20 MeV (lower row) beams. The 7 MeV dose profiles were calculated at 1 cm depth in water, and the 13 and 20 MeV dose profiles were calculated at 2 cm depth. The uniformity limit marker indicates the point at which a profile must pass above and outside in order to be considered acceptably flat. These markers are positioned at the minimally acceptable OAR at this position (96%, represented by the circular markers), plus the differences found in the MC-calculated and measured diagonal dose profiles of the current clinical collimation system at the edge of the uniformity region, plus a 1% cushion.

minimum relative dose at the edge of the uniformity region necessary to achieve acceptable in-field beam flatness. As in the previous studies, these markers are placed at the minimally acceptable OAR at this position (96%), plus the differences found between the MC-calculated and measured data at the edge of the uniformity region for each beam energy as determined in Aim 1 (c.f. Table 2-4), plus a 1% cushion. Because all dose profiles in the figure are shown to pass above and outside this marker for all beam energies, both collimation systems were deemed to produce acceptably flat in-field dose distributions for all energies in the diagonal dimension. The in-plane and cross-plane dose profiles are plotted versus off-axis position in Figures C-3 and C-4 for the 10x10 and 20x20 cm^2 applicators, respectively. In these figures the markers are placed at the minimally acceptable OAR for the major axes (97%), plus the differences found between the MC-calculated and measured data at the edge of the uniformity region, plus a 1% cushion. Again, all profiles in these figures pass above and outside the uniformity limit markers indicating that all fields met beam flatness criteria for the major axes.

The out-of-field dose profiles calculated at 1 cm depth are plotted versus off-axis position in Figure 6-20. In this figure, the 7, 13, and 20 MeV profiles are plotted with the solid, short-dashed, and long-dashed curves, respectively, normalized to central axis dose. The results reveal that for all profiles and field sizes, the 20 MeV beam produced the most leakage dose. This was confirmed by the mean percent leakage doses calculated for each beam per IEC specifications. For the 10x10 cm^2 model, the mean percent leakage doses were calculated to be 0.58%, 0.63%, and 1.03% of D_{max} at beam energies of 7, 13, and 20 MeV, respectively. These values were well below the IEC specified limits of 1.00%, 1.10%, and 1.34%, respectively, indicating that the design passed mean leakage criteria at the patient plane for all beam energies. The 20x20 cm^2 model also passed mean leakage dose criteria for all energies, with mean percent leakage dose values of 0.79%, 0.75%, and 1.11% of D_{max} at beam energies of 7, 13, and 20 MeV, respectively.

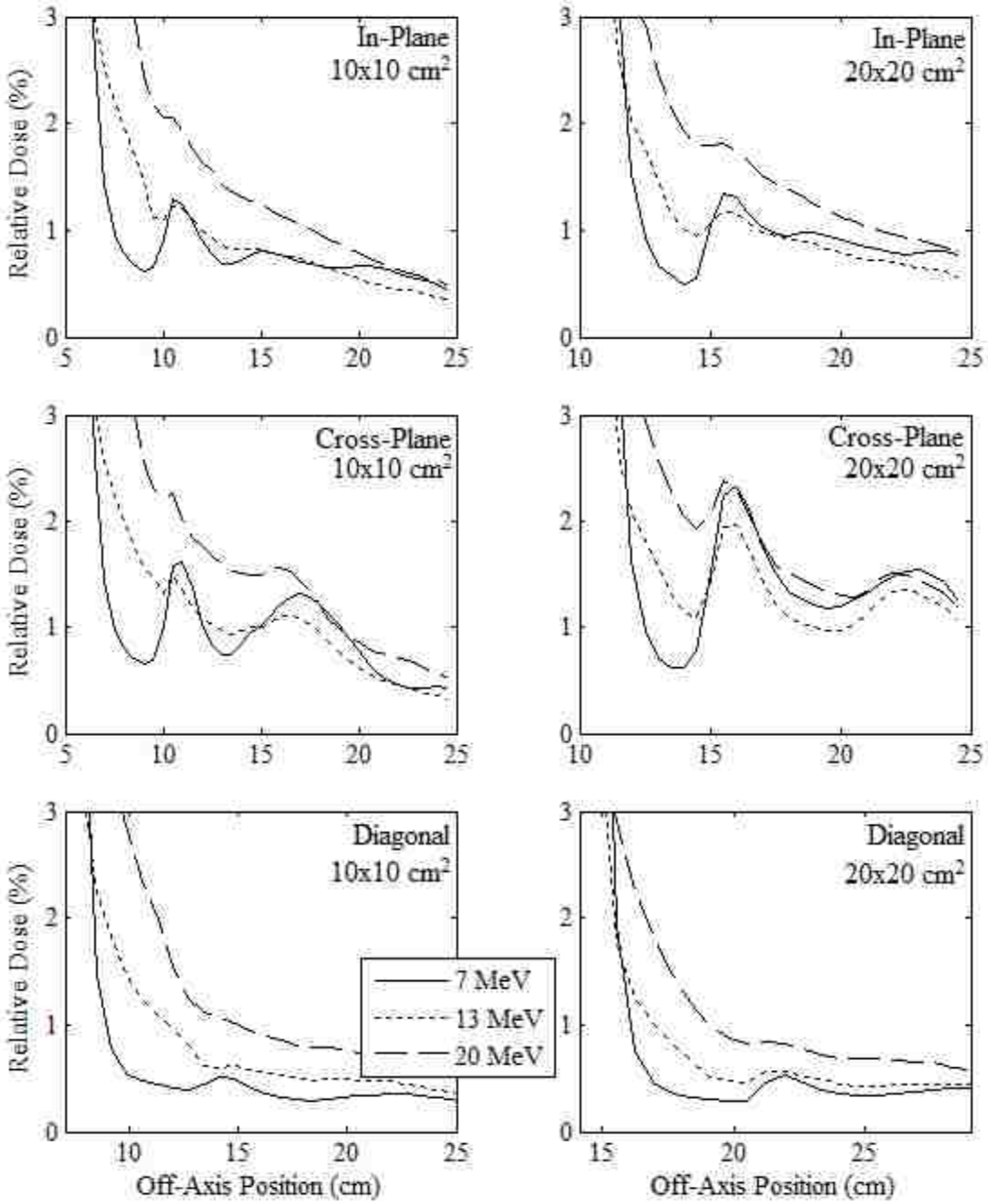

Figure 6-20. Leakage dose profiles plotted versus off-axis position for the selected 10x10 and 20x20 cm^2 collimation designs. The in-plane (upper row), cross-plane (middle row), and diagonal (lower row) profiles are plotted on the left for the 10x10 cm^2 applicator and the right for the 20x20 cm^2 applicator for the 7 (solid curve), 13 (short dashed curve), and 20 MeV (long dashed curve) beams. All profiles are normalized to central axis dose at the calculation depth, 1 cm in water.

6.10. Aim 5 - Summary and Conclusions

6.10.1. Summary of Weight Reduction in Design Process

In this aim, a series of seven design steps was performed to create a new collimation system with minimal applicator weight for the Elekta Infinity accelerator. In these steps an initial collimation design was first developed by matching the inner and outer trimmer edges to the calculated 95% and 2% OARs along the beam penumbra. This initial design was then adjusted through a series of modifications to reduce the amount of trimmer material. Table 6-5 lists the amount of weight reduction achieved in each step of the design process for the 10x10 and 20x20 cm^2 applicators. The only step which failed to reduce the applicator weight was the inner trimmer edge position determination analysis (Design Step 4) for the 10x10 cm^2 applicator, in which the weight was marginally increased in order to ensure acceptable

Table 6-5. Summary of design progression and weight reduction results. For the 10x10 and 20x20 cm^2 sizes, the applicator trimmer weight and corresponding weight reductions are shown for each step in the collimations system design process.

	10x10 cm^2 Applicator		20x20 cm^2 Applicator	
	Weight (kg)	Percent Reduction	Weight (kg)	Percent Reduction
Design Step 1 - Initial Design	7.06	-	10.87	-
Design Step 2 - Specify Field Size at 100 SSD	6.87	2.7%	10.49	3.5%
Design Step 3 - Bevel Outer Edges	5.86	14.8%	9.04	13.8%
Design Step 4 - Trimmer Height Optimization	5.52	5.9%	8.62	4.6%
Design Step 5 - Inner Trimmer Edge Position Analysis	5.87	-6.3%	7.73	10.3%
Design Step 6 - Beam Energy Dependence of Jaw Position Analysis	5.43	7.5%	7.35	4.9%
Design Step 7 - Trimmer Thickness & Outer Bevel Shape Adjustment	3.73	31.3%	5.09	30.8%

in-field beam flatness. The table shows that the most effective modifications for reducing the weight were the outer bevel shape and trimmer thickness adjustments (Design Step 7) and, to a lesser extent, the implementation of the outer edge bevel (Design Step 3). Design Step 7 reduced the weights of the 10x10 and 20x20 cm^2 applicators by 31.3% and 30.8%, respectively. Design Step 3 reduced the 10x10 and 20x20 cm^2 applicator weights by 14.8% and 13.8%, respectively.

6.10.2. Conclusions

The purpose of Aim 5 was to design new 10x10 and 20x20 cm^2 electron collimation systems for Elekta Infinity accelerators with minimal applicator weight. From this design process, the following was concluded:

- Weight reduction: A pair of 10x10 and 20x20 cm^2 applicators was designed with trimmer weights of 3.73 and 5.09 kg, respectively, surpassing the hypothesized trimmer weight goals of 5.00 and 7.10 kg. This was accomplished by first developing a pair of initial designs by matching the inner and outer trimmer edges to the 95% and 2% fluence OARs along the penumbra. A series of adjustments was then made to these designs to reduce the trimmer weights, modifying the thickness, shape, off-axis inner and outer edge positions, and *z*-positions of the trimmers.
- Evaluation of in-field beam flatness: These 10x10 and 20x20 cm^2 models were shown to produce acceptably flat dose distributions within the field according to criteria outlined by Hogstrom (2004) based on MC calculations performed with the 7, 13, and 20 MeV beams.
- Evaluation of out-of-field leakage dose: These 10x10 and 20x20 cm^2 models also produced acceptably low mean percent leakage doses in the patient plane for the 7, 13, and 20 MeV beams based on IEC criteria. MC calculations revealed that the 10x10 cm^2 applicator produced mean percent leakage doses of 0.58%, 0.63%, and 1.03% of D_{max}, and the 20x20 cm^2 applicator produced mean percent leakage doses of 0.79%, 0.75%, and 1.11% for the 7, 13, and 20 MeV beams, respectively. For both applicators these mean percent leakage doses were well below the IEC specified limits of 1.00%, 1.10% and 1.34% for the same beam energies.

Chapter 7 - Aim 6 - Construct Prototype Applicator and Evaluate Prototype Collimating System

Aim 6: Fabricate prototypes of the newly designed 10x10 and 20x20 cm^2 applicators in order to evaluate the prototype collimation system. Off-axis profiles will be measured in a water phantom to evaluate the in-field beam flatness and leakage dose of the prototype collimation system, and the prototype applicators will be weighed to determine the reduction in weight from the current clinical applicator designs. Additionally, MC calculations will be performed to evaluate the leakage dose along the side of the applicator and to investigate the effects of altering the designated photon jaw positions on the patient plane dose distribution.

7.1. Aim 6 - Introduction

A pair of collimation systems with open applicator field sizes of 10x10 and 20x20 cm^2 have been designed in Aim 5 for the Elekta Infinity linear accelerator. A design methodology in which the trimmer edges were matched to the calculated width of the beam penumbra was used to develop an initial design. This initial design was then adjusted based on results of both analytical and MC calculations to reduce the applicator weight. The resulting weights of the applicator trimmer bars were reduced well below those of both the current clinical Elekta and Varian applicator trimmer weights for both the 10x10 and 20x20 cm^2 applicators. MC calculations were performed to evaluate the final models produced in the design process, revealing that the final designs met criteria for both in-field beam flatness and mean percent leakage dose.

To assess the accuracy of these MC results and to ensure the collimation systems met standards, it was necessary to verify these calculations with measurement. This necessitated the fabrication of a set of prototype applicators based on the models produced from the collimation system design process. Constructing the applicators required accounting for engineering factors not previously considered in the design process. The model had to be adjusted to allow the trimmers to be fabricated with the available machining equipment. This required collaboration with the machinists to develop suitable modifications to allow the components to be machined without sacrificing the reduced applicator weight, the in-field beam flatness, or the low leakage dose. Additionally, the prototype models had to be constructed in such

a way that they could be integrated into the current electron beam delivery system of the Elekta Infinity accelerator. This included both ensuring compatibility with the mechanism of attaching the applicator to the treatment head and overriding applicator interlocks designed within the delivery system to prevent treatment errors.

In this aim, modifications were made to the applicator models produced from the collimation system design process to make possible the manufacturing of prototype applicators. These models were built and tested using measurements to ensure they met criteria for in-field beam flatness and leakage dose levels. These measurements were also compared with MC calculations to evaluate the performance of the BEAMnrc Elekta Infinity MC model modified to incorporate the prototype collimation system. Additionally, MC calculations were used to study both the leakage dose along the sides of the applicator and the effects on the off-axis dose distribution in the patient plane caused by adjusting the jaw positions (≈1 cm at isocenter) from those determined in the design process.

7.2. Aim 6 - Methods

7.2.1. Trimmer Modifications for Fabrication

The applicator designs produced from the collimation system design process in Aim 5 had trimmer weights of 3.73 and 5.09 kg for the 10x10 and 20x20 cm^2 applicator sizes, respectively, exceeding the hypothesized goals of 5.00 and 7.10 kg. MC calculations revealed that these applicators met criteria for both in-field beam flatness and out-of-field leakage dose in the patient plane.

To confirm these results, prototype applicators were fabricated for evaluation by off-axis dose measurement. The Louisiana State University (LSU) Physics machine shop was consulted for their construction. After discussions with the machinists, it was determined that the designs developed in Aim 5 would need to be adjusted in order to fabricate the models at this shop. Specifically, two modifications would need to be made. First, the prototype trimmers could not be milled out of tungsten at this shop; a softer metal had to be selected in order not to damage the available milling equipment. Second, the smooth outer bevel shape would have to be modified, due to the shop not possessing the equipment required to mill the shape of this curve with the necessary precision.

To determine a suitable replacement for tungsten, the other two materials studied in Aim 3, copper and lead, were reassessed. In Aim 3, it was shown that lead outperformed copper in producing a minimal amount of electron trimmer scatter dose outside the field due to its greater density (11.1 g cm^{-3} for lead versus 8.9 g cm^{-3} for copper). As shown in Table 4-2, the lead 20x20 cm^2 applicator produced a mean leakage dose of 1.39% while the copper applicator produced a mean leakage dose of 1.51% for the MC study performed in Aim 3. Additionally, lead required the least calculated trimmer thickness (in g cm^{-2}) of the three materials studied to shield a 20 MeV electron beam calculated using the equation derived from the MC 1% threshold method (c.f. Table 4-1), allowing the trimmers to be made thinner and lighter than using copper. For these reasons, lead was selected as the material to be used in the applicator fabrication.

However, due to the soft composition of lead, it was decided that the trimmers should be backed with a thin aluminum plate for structural support (similar to the current clinical Elekta applicator designs). Figure 7-1 illustrates this configuration, showing a cross sectional view of the prototype trimmer design with the black region demarcating the lead material and the gray region demarcating the aluminum plate. The plate was placed against the downstream surface of the lead trimmer, spanning the full trimmer width. Each aluminum plate had a thickness of 0.32 cm (1/8 inch) and a density of 2.7 g cm^{-3}. For the upper two trimmers, the aluminum plate inner edges were designed divergent to align with the divergent lead inner edge.

To compensate for the added weight of the aluminum plane, the lead plate's thickness was reduced by 9% for the middle and lower trimmers, such that the total g cm^{-2} thickness of the trimmers remained the same. This same reduction could not be performed to the upper trimmer, due to the fact that the thickness of this trimmer had already been reduced. The machinist was concerned that any further reduction in its thickness would cause difficulties in machining the lead. Additionally, as the density of the lead alloy available for use in the machine shop (11.3 g cm^{-3}) was slightly greater than that used by the BEAMnrc model used throughout the collimation system design process (11.1 g cm^{-3}), the lead thickness

was reduced by the ratio of the densities of the two lead alloys (≈2% reduction), maintaining the same g cm^{-2} thickness of the lead.

To modify the outer edge trimmer bevel shape to be millable by the available machining equipment, the bevel was approximated by a series of steps, rather than a smooth curve. To perform this modification, four discrete energies were selected to match the width and thickness of each step: 6, 9, 13, and 20 MeV. The outer edge of each step matched the off-axis position of the specified fluence OAR for the associated beam energy. The thickness of the step was calculated with the same electron energy using the equation developed from the MC 1% threshold analysis. The effect of this modification to the outer edge bevel can be seen in Figure 7-1.

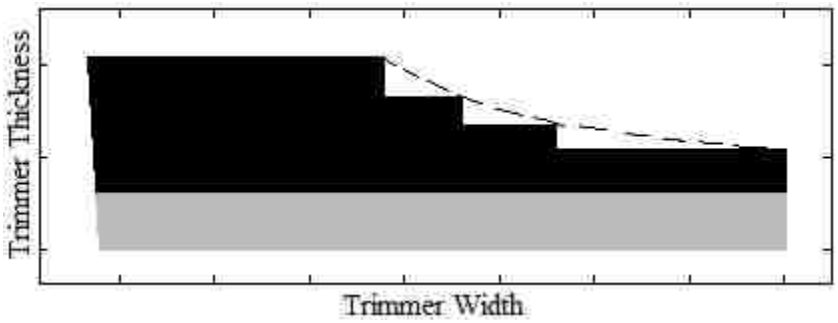

Figure 7-1. Cross sectional view of a trimmer designed with modifications for fabrication. The black region represents the lead material and the gray region represents aluminum. The stepped approximation to the smooth bevel (dashed line) can be seen along the outer edge of the lead trimmer component.

A pair of prototype applicators, sizes 10x10 and 20x20 cm^2, were machined and constructed with these modifications at the LSU Physics machine shop. For these prototypes, all design features not mentioned in this section (e.g. jaw positions, trimmer *z*-positions, and fluence matching OARs to determine the inner and outer edge trimmer positions) were maintained from the model produced in Aim 5. Figures 7-2 and 7-3 show pictures of these prototype 10x10 and 20x20 cm^2 applicators, respectively. The trimmers and attachment plate were separated at appropriate distances from one another using a set of aluminum spacer tubes, which can be seen in Figures 7-2 and 7-3 at the corners of each trimmer. Threaded rods were inserted though these spacing tubes and nuts were tightened on each of the ends of these rods to rigidly hold the entire assembly of trimmers and spacing tubes together. Appendices G and

H show fabrication drawings of these prototype 10x10 and 20x20 cm^2 prototype applicator models, respectively. These drawings give the dimensions of each of the trimmer component (both lead and aluminum plates) and the spacing tubes.

Figure 7-2. Fabricated 10x10 cm^2 applicator prototype.

Figure 7-3. Fabricated 20x20 cm^2 applicator prototype.

7.2.2. Evaluation of Prototype Collimation System

7.2.2.1. MC Calculations

The 10x10 and 20x20 cm^2 applicator designs updated with the modifications made for fabrication purposes were modeled in BEAMnrc. Additionally, applicators were designed and modeled in BEAMnrc for the 6x6, 14x14, and 25x25 cm^2 sizes. These prototype models retained all design parameters from the 10x10 and 20x20 cm^2 applicators, including the *z*-positions, materials, and thicknesses of the trimmers.

The upper and middle trimmer inner edges were again designed fully-divergent while the lower trimmer inner edges were designed non-divergent. The outer edge fluence matching OARs used to form the bevel were unchanged for all energies and trimmers. The 6x6 cm^2 applicator was designed with the same inner edge fluence matching OARs as the 10x10 cm^2 model, and the 25x25 cm^2 applicator was designed with the same inner edge fluence matching OARs as the 20x20 cm^2 model for a 6 MeV beam. For the 14x14 cm^2 model, the inner edge fluence matching OARs were linearly interpolated (rounded to the nearest 0.5%) between those found for the 10x10 and 20x20 cm^2 models for a 6 MeV beam. For the upper trimmer inner edge the fluence matching OAR was decreased linearly with energy from the 6 MeV matching OAR to 55% for a 20 MeV beam for all applicator sizes to determine the jaw positions for each energy. These inner edge fluence matching OARs are listed in Table 7-1 for each prototype applicator. The trimmer weight of each of these prototype applicator models was calculated.

Table 7-1. Trimmer inner edge fluence matching OARs for the design of each prototype applicator.

	6x6 cm^2	10x10 cm^2	14x14 cm^2	20x20 cm^2	25x25 cm^2
Lower Trimmer Inner Edge Matching OAR at 6 MeV	95.0%	95.0%	92.5%	89.0%	89.0%
Middle Trimmer Inner Edge Matching OAR at 6 MeV	96.0%	96.0%	94.0%	91.0%	91.0%
Upper Trimmer Inner Edge Matching OAR at 6 MeV	96.5%	96.5%	95.0%	93.0%	93.0%
Upper Trimmer Inner Edge Matching OAR at 20 MeV	55.0%	55.0%	55.0%	55.0%	55.0%

Each of these five prototype applicator models was inserted into the BEAMnrc model for the Elekta Infinity accelerator. Simulations were performed with these prototype collimation systems with the 7, 13 and 20 MeV beams while maintaining all source and transport parameters from the previous MC studies. Phase space files were created from these simulations and used as input to DOSXYZnrc to calculate the dose in a water phantom. Dose was calculated at 100 cm SSD in 0.5x0.5x0.5 cm^3 voxels centered at 1 and 2 cm depth. The dose was calculated using 10^9 particles and the distributions were

symmetrized in both the in-plane and cross-plane dimensions by reflecting the distributions about central axis to reduce statistical uncertainty. All profiles were normalized to the mean total dose calculated within a 3x3 set of voxels centered at central axis at the calculation depth.

7.2.2.2. Measurements

A set of off-axis dose measurements was performed to evaluate the prototype collimation system for both the in-field beam flatness and out-of-field leakage dose at the patient plane with the prototype 10x10 and 20x20 cm^2 applicators. The beam flatness was evaluated using criteria specified by Hogstrom (2004), and the leakage dose was evaluated according to the regulations outlined by the IEC (1998) for the 7, 13, and 20 MeV beams. Additionally, these measurements were used to compare the leakage dose of the prototype collimation system with those of the current clinical Elekta applicators.

The prototype applicators were attached to the Elekta Infinity accelerator with the gantry positioned such that the beam was aimed vertically downward. The jaws were positioned in their designated locations within the prototype collimation system design for each beam energy. Beam scanning measurements with the same setup used in Aim 1. Off-axis profiles were measured in the in-plane, cross-plane, and both diagonal directions using an OmniPro two-dimensional scanning tank with OmniPro (v. 6.2) scanning software package (Scanditronix Wellhofer AB RFA 20-SERVO, Uppsala, Sweden) at depths of 1 and 2 cm in water. Two N31011 cylindrical ionization chambers (PTW, Freiburg, Germany) were used for measurement, one for scanning and one for reference. The scanning chamber was oriented such that the stem was situated perpendicular to central axis of the beam and to the direction of the scan. The reference chamber was attached to the applicator in the corner of the field. For the diagonal scans the reference chamber was moved to a field corner not coinciding the with the scanned profile. The beam scanning system was rotated 0˚, 90˚, and ±45˚ by rotating the treatment couch to measure the in-plane, cross-plane, and diagonal profiles, respectively.

Each profile was normalized to the central axis ionization value at the depth of the scan. The profiles were then centered by shifting them such that the 50% ionization levels were equal distances from the central axis. For the evaluating the in-field results the profiles were symmetrized about central

axis by averaging the measurement values at each negative and positive off-axis position, i.e. averaging each profile with the corresponding "mirrored" profile reflected about central axis. No symmetrization was performed for evaluating the out-of-field results. Relative dose was assumed equal to relative ionization, i.e. conversion factors from ionization to dose were assumed identical for central axis and off-axis positions.

7.2.3. Lateral Leakage Analysis

In addition to the specifications for maximum and mean leakage dose at the patient plane, the IEC (1998) specifies that the leakage along the vertical sides of the applicator at a position 2 cm outside the volume contained by the applicator not exceed 10% of D_{max} (maximum dose on central axis at 100 cm SSD).

To investigate these leakage levels along the sides of the applicator, a MC investigation was performed with the prototype 10x10 and 20x20 cm^2 applicator models in the Elekta Infinity BEAMnrc model. In this study, simulations were performed with the 7, 13, and 20 MeV beams and phase space data were scored at three different horizontal planes, positioned at *z*-values of 79, 88, and 95 cm. These simulations maintained all source and transport parameters from the previous studies using the BEAMnrc model.

Using these phase space files as source input, DOSXYZnrc was used to calculate the horizontal leakage dose profiles along the side of the applicator. Particles were transported through 1 cm of air and dose profiles were calculated in 0.5x0.5x0.5 cm^3 voxels centered at 1 cm depth in water, such that the *z*-positions of the three dose calculation planes were 81, 90, and 97 cm. The DOSXYZnrc water phantoms used for these calculations were identical to those used in the other MC studies in this project, except that they were situated at different *z*-positions. 10^9 histories were used for these calculations. To reduce statistical uncertainty, the dose distributions were symmetrized in both the in-plane and cross-plane dimensions by reflecting them about central axis. Each of these profiles was normalized to D_{max} in a water phantom at 100 cm SSD for each beam energy. The calculated dose profiles outside the volume contained by the applicator were analyzed to evaluate the leakage dose along the side of the applicator.

7.2.4. Jaw Position Error Analysis

In the beam tuning process during the initial beam setup, it is not uncommon to make slight jaw position adjustments from those pre-specified for each electron beam, although not recommended because of the impact on other dose quantities such as dose output. This is done to obtain specific beam characteristics or to match the dose distribution to that of another accelerator. Also, the IEC (1998) allows for the jaw positions to vary from the specified jaw positions by up to 1 cm. In this project, the jaw positions determined for each beam energy and applicator size were selected based on the results of in-depth investigations which produced specific dose distribution characteristics. The beams were only verified to meet in-field beam flatness and leakage dose criteria with the jaws positioned at the locations specified in the collimation system design process. A MC study was performed to study the effect of modifying these designated positions on the in-field and out-of-field dose distributions.

In this study, the Elekta Infinity BEAMnrc model with the prototype 20x20 cm^2 applicator was modified by adjusting the jaw positions of for the 7, 13, and 20 MeV beams. The in-plane jaw was moved both inward (towards central axis) and outward (away from central axis) by 0.5 cm, as was the cross-plane jaw, to create four modified models for each beam energy. This 0.5 cm change in jaw position equated to a 1.0 cm change in position for the in-plane jaw and a 1.2 cm change for the cross-plane jaw when projected to isocenter from the nominal source position.

Simulations were performed with each of these modified BEAMnrc models to create phase space files which were used as input to DOSXYZnrc to calculate the dose. Dose was calculated at 100 cm SSD in 0.5x0.5x0.5 cm^3 voxels centered at 1 and 2 cm depth within a water phantom. The dose was calculated using 10^9 particles and the distributions were symmetrized about central axis in both the in-plane and cross-plane dimensions to reduce statistical uncertainty. All source and transport parameters were maintained from the original BEAMnrc model. All dose profiles were normalized to the mean total dose calculated within a 3x3 set of voxels centered at central axis at the calculation depth. These dose distributions were compared with the calculated results of the model with the original (unaltered) jaw

settings with the 20x20 cm^2 prototype applicator to analyze the effects on both the in-field beam flatness and patient plane leakage dose.

7.3. Aim 6 - Results and Discussion

7.3.1. Fabricated Applicator

Modifications were performed to the applicator models produced from the collimation system design process in order to make the trimmer designs machinable using the equipment available at the LSU machine shop. These modifications included using a combination of lead and aluminum, rather than tungsten, to fabricate the trimmers and approximating the smooth outer bevel shape as a set of four steps. In making these modifications, the trimmer weights of the 10x10 and 20x20 cm^2 applicators were decreased from the models produced from the collimation design process. The weight of the 10x10 cm^2 applicator's trimmers was reduced from 3.73 to 3.66 kg, and the 20x20 cm^2 weight was reduced from 5.09 to 4.95 kg. These slight weight reductions can be attributed to two factors. First, the g cm^{-2} range of a 20 MeV electron beam calculated using the MC 1% threshold method equation is slightly less for lead than tungsten (c.f. Table 4-1), causing the trimmers to be made slightly thinner. Second, in the process of approximating the outer edge bevel shape as a series of steps, a small amount of material was removed from the bevel to form the shape of the steps (c.f. Figure 7-1). In addition to the 10x10 and 20x20 cm^2 applicators, the trimmer weights were calculated for the prototype 6x6, 14x14, and 25x25 cm^2 models. These applicator designs were found to have trimmer weights of 2.79, 3.66, and 5.91 kg, respectively.

Once fabricated, the prototype 10x10 and 20x20 cm^2 applicators were weighed to determine the full applicator weight including all structural materials, such as the attachment plate, aluminum spacer tubes and threaded rods used to connect the trimmers. These constructed 10x10 and 20x20 cm^2 prototype applicators were found to weigh 5.5 and 6.8 kg, respectively, as opposed to 7.7 and 10.9 kg for the current clinical Elekta models.

These weight results, listed in Table 7-2, include the total trimmer weights of each applicator size for the prototype applicators and the current clinical Elekta and Varian applicators. Additionally, the fully constructed applicator weights are listed for each applicator other than the 6x6, 14x14, and 25x25

cm^2 prototypes. The weight results show that the prototype models surpassed both the current clinical Elekta and Varian designs for all sizes for both trimmer weight and full applicator weight. The full applicator weights of the 10x10 and 20x20 cm^2 models were reduced by 29% and 38%, respectively, from the current clinical Elekta applicators of the same sizes. It should be noted that the current clinical Elekta and Varian applicators have electrical components which are not present on the prototype applicator. These components would add an estimated weight of less than 0.5 kg.

Table 7-2. Weight comparison of prototype applicators with current clinical Elekta and Varian applicators. For each applicator size, the full applicator weights with all structural and electrical components are shown in kg along with the weights of the trimmers only.

Applicator Size (cm x cm)	Current Elekta		Current Varian		Prototype Elekta	
	Full Applicator	Trimmers Only	Full Applicator	Trimmers Only	Full Applicator	Trimmers Only
6 x 6	7	4.75	5.7	4.20[b]	-	2.79
10 x 10	7.7	5.52	6.5	5.00[b]	5.5	3.66
14 x 14	9.1	6.71	7.6[a]	6.10[ab]	-	4.15
20 x 20	10.9	8.36	8.6	7.10[b]	6.8	4.95
25 x 25	13.4	10.00	9.5	8.00[b]	-	5.91

[a]Weights are for 15x15 cm^2 applicator

[b]Varian trimmer weights were approximated as the full applicator weight minus 1.5 kg

Figures 7-4 and 7-5 show cross sectional views of the 10x10 and 20x20 cm^2 applicators, respectively, comparing the prototype models with the current clinical Elekta designs. The left side of the figures (negative off-axis positions) depict cross sectional views of the applicators in the in-plane dimension and the right side of the figures (positive off-axis positions) depict cross sectional views in the cross-plane dimension. Additionally in Appendix D, cross sectional views of the prototype and current clinical 6x6, 14x14, and 25x25 cm^2 applicator designs are compared in Figures D-1, D-2 and D-3, respectively. The differences in the in-plane and cross-plane designs are most apparent in the width of the

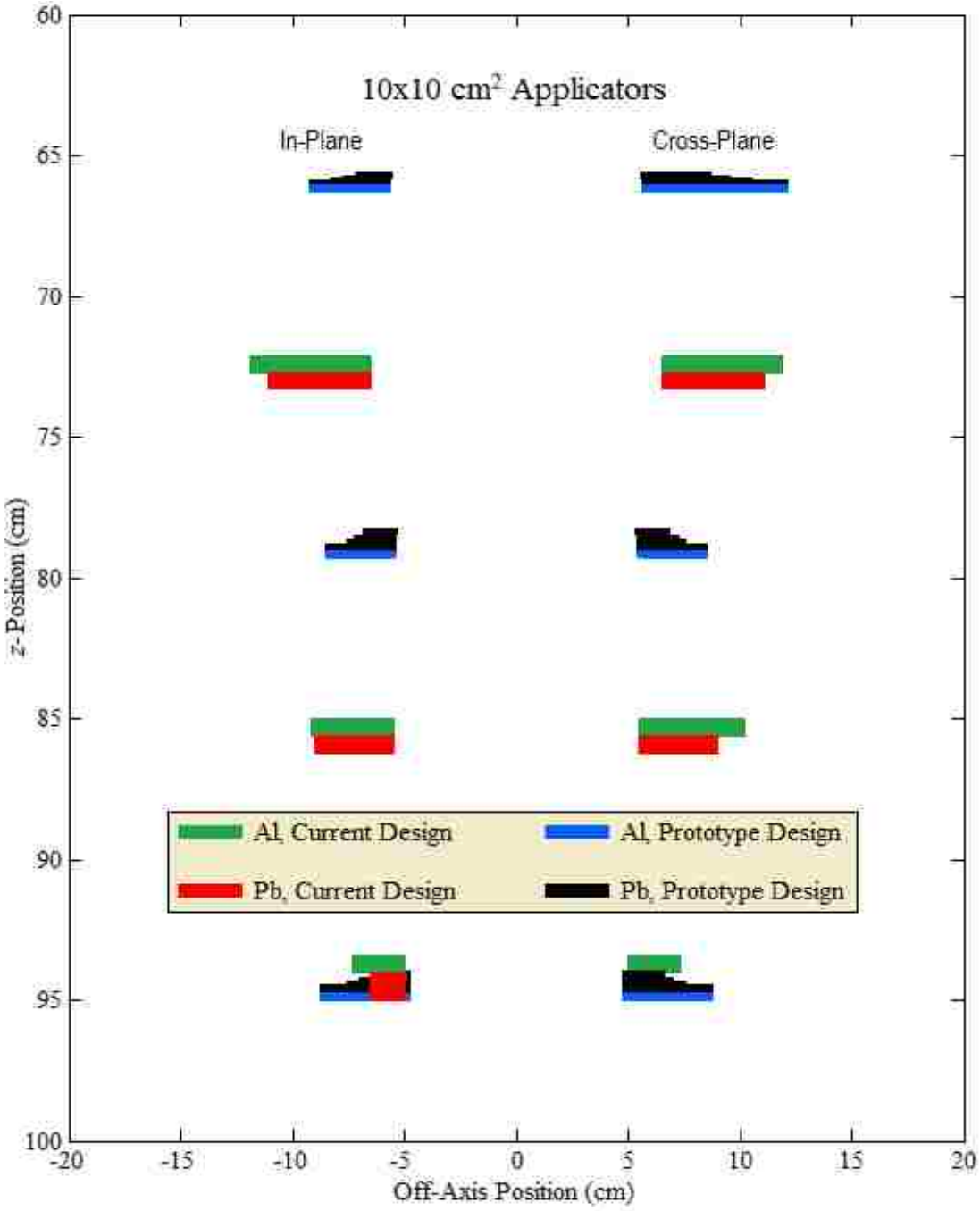

Figure 7-4. Cross sectional views of the prototype and current clinical Elekta 10x10 cm^2 applicator models. The left side of the figure depicts a cross sectional view of the applicators in the in-plane dimension, and the right side of the figure depicts a cross sectional view in the cross-plane dimension. The black and blue regions demarcate the lead and aluminum plates, respectively, of the prototype design, and the red and green regions demarcate the lead and aluminum plates, respectively, of the current Elekta design. The current applicator is shown in the foreground on the left side of the image and the prototype model is shown in the foreground on the right.

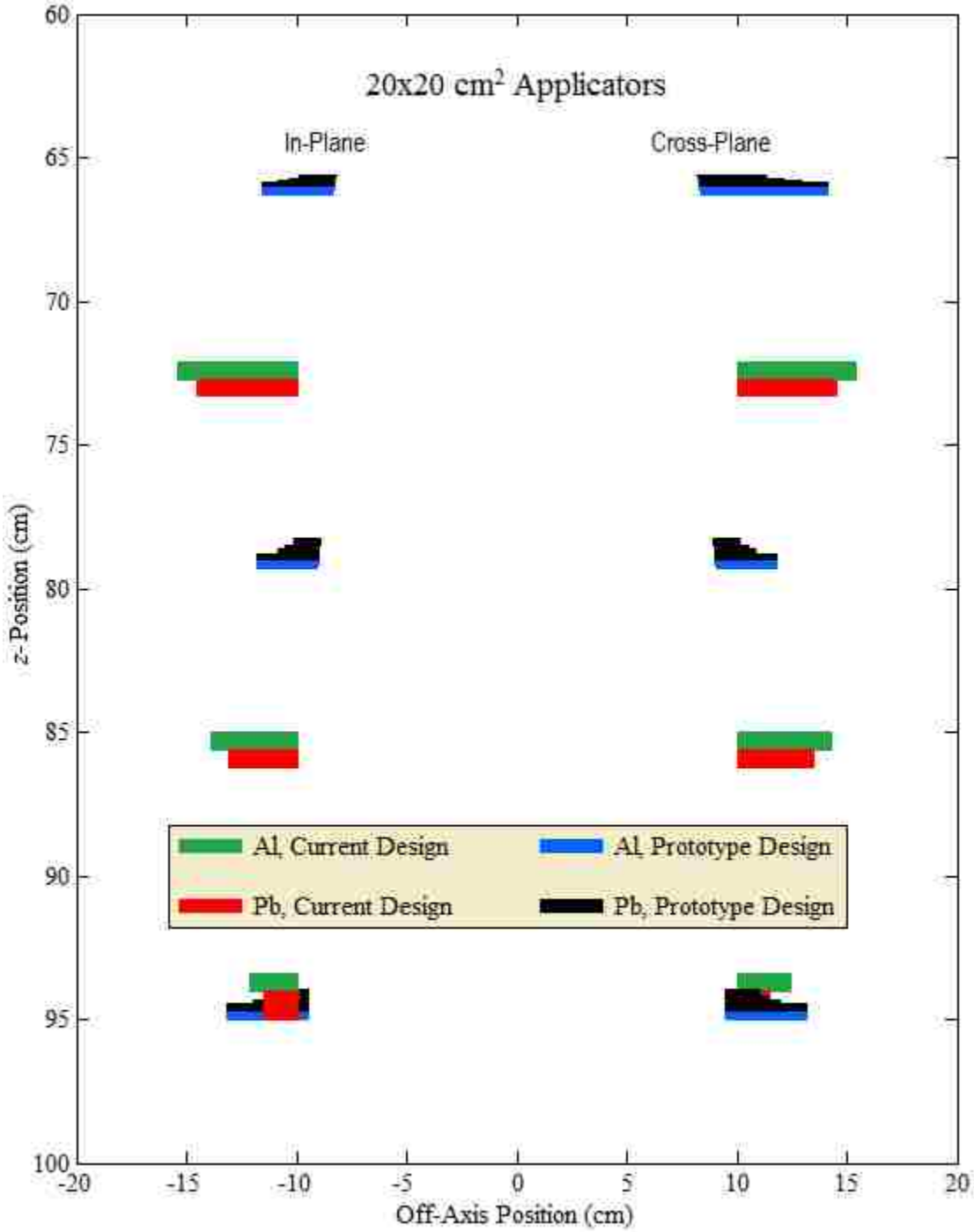

Figure 7-5. Cross sectional views of the prototype and current clinical Elekta 20x20 cm^2 applicator models. The left side of the figure depicts a cross sectional view of the applicators in the in-plane dimension, and the right side of the figure depicts a cross sectional view in the cross-plane dimension. The black and blue regions demarcate the lead and aluminum plates, respectively, of the prototype design, and the red and green regions demarcate the lead and aluminum plates, respectively, of the current Elekta design. The current applicator is shown in the foreground on the left side of the image and the prototype model is shown in the foreground on the right.

upper trimmers. The current applicator is shown in the foreground on the left side of the image and the prototype model is shown in the foreground on the right. The figures show that for all applicator sizes, the upper two trimmers of the prototype designs are positioned further from the patient plane, allowing them to be made narrower. The trimmers are also positioned closer to central axis on the prototype design, decreasing the applicator weight. In the prototype design, the lead plates are situated against the upstream surface of the aluminum plates, rather than the downstream surface. Positioning the plates in this way has two benefits. First, the scatter dose is decreased, because the electrons which hit the upper trimmer surface interact with the higher density lead rather than the lower density aluminum. This reduces the range of the electrons within the material, allowing fewer of them to escape the lateral edge of the trimmer as shown in Aim 3. Second, the high atomic number of lead causes increased radiative energy loss, decreasing the particle range and allowing the trimmers to be made thinner than with the current clinical design. The upper, middle and lower trimmers of the prototype applicators are designed with full trimmer thicknesses (lead plus aluminum) of 5.4, 9.2, and 9.2 g cm^{-2}, respectively. The upper, middle, and lower trimmers of the current clinical applicators have full trimmer thicknesses (lead plus aluminum) of 8.4, 8.4, and 12.9 g cm^{-2}, respectively. While the prototype applicator is designed with a somewhat thicker middle trimmer, the upper and lower trimmer thicknesses are significantly reduced.

In addition to adjusting the trimmer designs, the jaws were repositioned for all beam energies. The jaw positions for the prototype and current clinical collimation systems are compared in Figure 7-6, plotting the jaw positions versus $E_{p,0}$ for the 10x10 cm^2 (upper plot) and 20x20 cm^2 (lower plot) applicators for each of the seven beams available on the Elekta Infinity used in this study. These off-axis positions are plotted as the jaw locations projected from the nominal source position down to isocenter. The figure illustrates that for both systems, as the beam energy increases the jaws are moved inward towards central axis. This is done to minimize the leakage dose for the higher energy beams, where beam flatness near the field edge is more easily maintained. However, in the prototype system this decrease in off-axis position is smooth and well correlated with the beam energy, while in the current system the decrease is slightly erratic and poorly correlated with beam energy. Additionally, the plots show that in-

plane jaws are positioned closer to central axis than the cross-plane jaws for the current collimation system at all beam energies. This is also true for the prototype collimation system at low beam energies, but becomes untrue at approximately 18 MeV for the 10x10 cm^2 applicator and 16 MeV for the 20x20 cm^2 applicator. This is caused by a decrease in the upper trimmer inner edge fluence matching OAR for high energy beams.

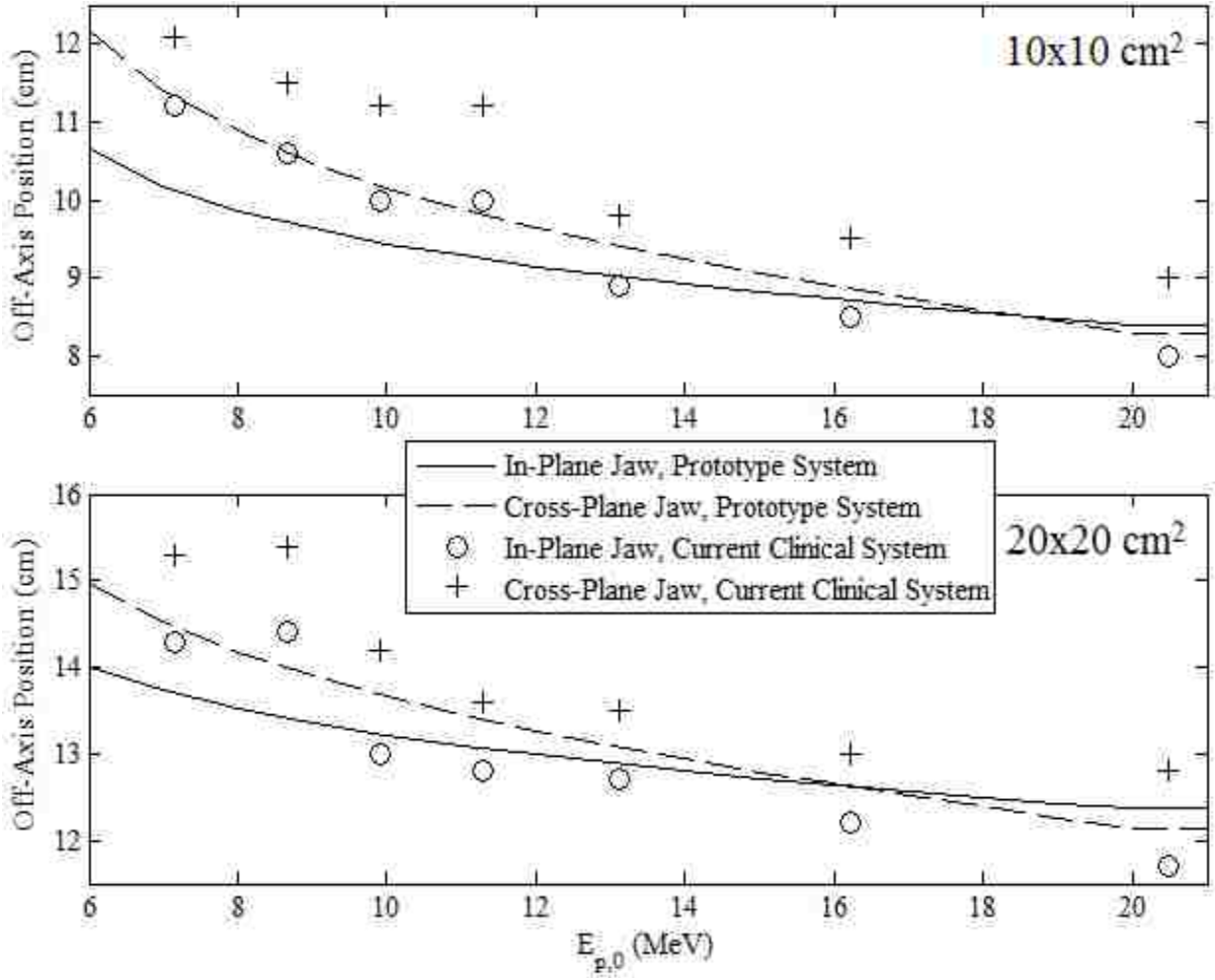

Figure 7-6. Jaw position comparison for the prototype and current Elekta collimation systems for all beam energies. The positions are shown as distance of the jaw from central axis projected to isocenter from the nominal source position. These positions are plotted versus the most probable electron energy of each beam for the 10x10 (top) and 20x20 cm^2 (bottom) applicators. Curves for prototype system were constructed by linearly connecting data points at 1 MeV intervals.

7.3.2. Evaluation of Prototype Collimation System

7.3.2.1. In-Field Dose Distributions

Figures 7-7 through 7-9 compare the MC calculations and beam measurements of off-axis dose on the prototype collimation system for the 7, 13, and 20 MeV beams within the field. These figures plot the calculated and measured relative dose profiles versus off-axis position for the 10x10 cm^2 (left column of plots) and 20x20 cm^2 (right column of plots) collimation systems. The 7 MeV beam profiles (top row) were measured at 1 cm depth in water, and the 13 MeV (middle row) and 20 MeV (bottom row) beam profiles were measured at 2 cm depth. The in-plane profiles are plotted in Figure 7-7, the cross-plane profiles are plotted in Figure 7-8, and the diagonal profiles are plotted in Figure 7-9. In Figure 7-9, measurement scans taken in the positive diagonal direction are shown with the long-dashed curve, and measurements scans taken in the negative diagonal direction are shown with the short-dashed curve. The positive diagonal profiles refer to measurement scans taken in the diagonal direction which extends from the negative in-plane (towards gantry) and negative cross-plane (to the left when facing the gantry) quadrant to the positive in-plane (away from gantry) and positive cross-plane (to the right when facing the gantry) quadrant. The negative diagonal profiles refer to measurements scans which run perpendicular to the positive diagonal profiles, extending from the positive in-plane and negative cross-plane quadrant, to the negative in-plane and positive cross-plane quadrant. Additionally in Appendix D, MC-calculated in-field dose profiles are plotted in the left column of plots in Figures D-4, D-5, and D-6 for the 6x6, 14x14, and 25x25 cm^2 applicators, respectively.

Relative dose profiles are deemed to be acceptably flat if they fall within 100 ± 3% (major axes) or 100 ± 4% (diagonal axes) between central axis and the uniformity limit marker located 2 cm inside the edge of the field for the major axes and $2\sqrt{2}$ cm for the diagonals. Figures 7-7 through 7-9 show that for all dose profiles, both measured and calculated, meet beam flatness criteria specified by Hogstrom (2004). Therefore, both the 10x10 and 20x20 cm^2 collimation systems were deemed to produce acceptable beam flatness.

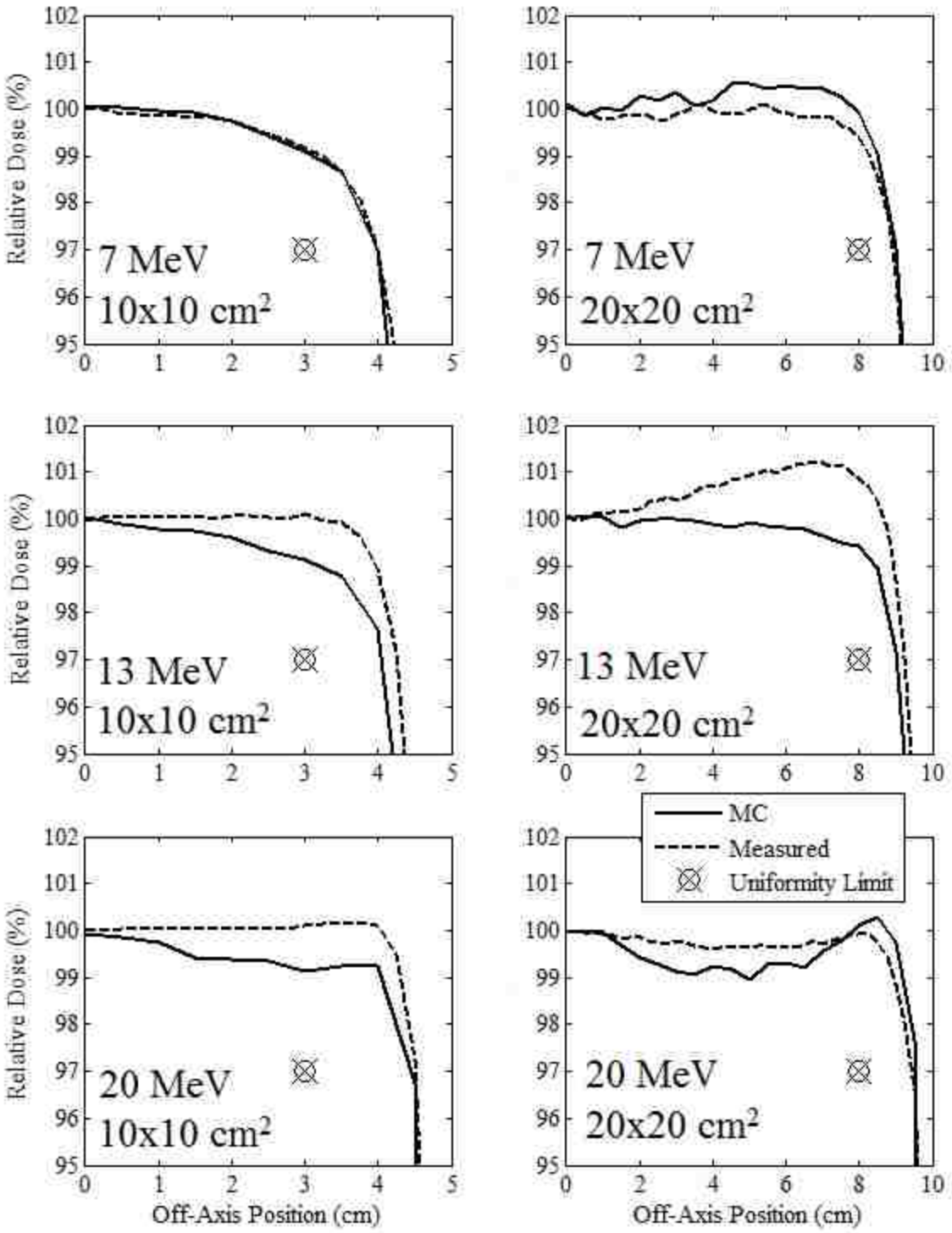

Figure 7-7. Comparison of measured and MC calculated in-plane profiles of relative dose versus off-axis position in the field. Dose profiles are compared at beam energies of 7 (upper row), 13 (middle row), and 20 MeV (lower row). The 10x10 and 20x20 cm^2 applicator results are shown in the left and right column, respectively. The uniformity limit marker (⊠) represents the minimum value that the profile can have at the edge of the uniformity region in order to pass flatness criteria. The 7 MeV profiles were calculated at 1 cm depth in water, and the 13 and 20 MeV profiles were calculated at 2 cm depth.

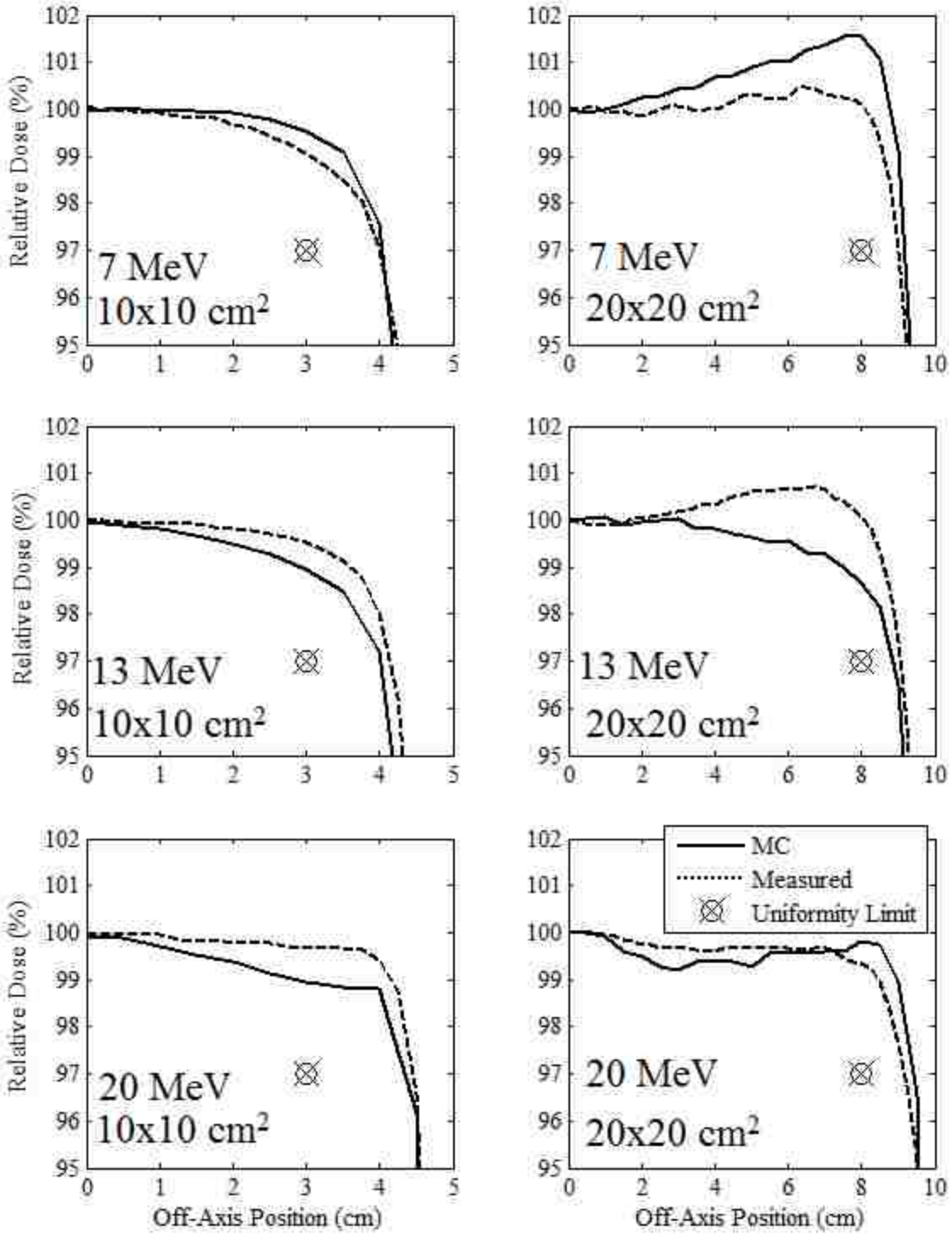

Figure 7-8. Comparison of measured and MC calculated cross-plane profiles of relative dose versus off-axis position in the field. Dose profiles are compared at beam energies of 7 (upper row), 13 (middle row), and 20 MeV (lower row). The 10x10 and 20x20 cm^2 applicator results are shown in the left and right column, respectively. The uniformity limit marker (⊠) represents the minimum value that the profile can have at the edge of the uniformity region in order to pass flatness criteria. The 7 MeV profiles were calculated at 1 cm depth in water, and the 13 and 20 MeV profiles were calculated at 2 cm depth.

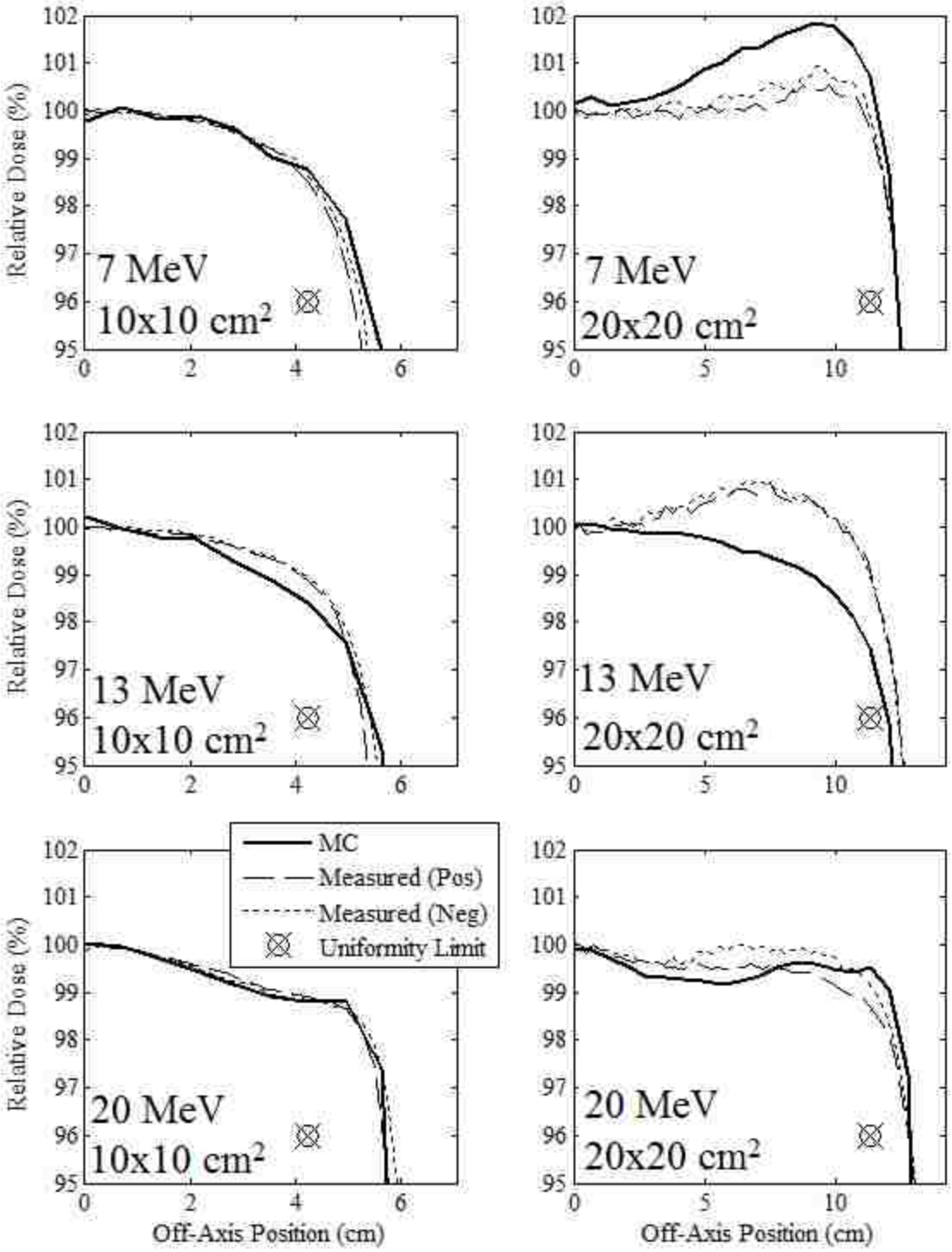

Figure 7-9. Comparison of measured and MC calculated diagonal profiles of relative dose versus off-axis position in the field. Dose profiles are compared at beam energies of 7 (upper row), 13 (middle row), and 20 MeV (lower row). The 10x10 and 20x20 cm^2 applicator results are shown in the left and right column, respectively. The uniformity limit marker (⊠) represents the minimum value that the profile can have at the edge of the uniformity region in order to pass flatness criteria. The 7 MeV profiles were calculated at 1 cm depth in water, and the 13 and 20 MeV profiles were calculated at 2 cm depth.

When comparing the MC-calculated and measured dose profiles, the plots show that the MC calculations over-predicted the measured dose near the edge of the field by as much as 1.5% for the 7 MeV profiles, and under-predicted the measured dose near the edge of the field by as much as 1.6% for the 13 MeV profiles. These differences are similar to those found in the MC-calculated and measured dose profiles of the current clinical system as shown in Aim 1 and by Harris (2012). For the 20 MeV profiles, the MC calculations in general slightly under-predicted the measured dose within roughly 7 cm of central axis, but slightly over-predicted the measured dose outside of 7 cm, consistent with the results of Aim 1 and Harris (2012).

7.3.2.2. Out-of-Field Dose Distributions

Figures 7-10 through 7-13 compare the MC calculations and beam measurements on the prototype collimation system for the 7, 13, and 20 MeV beams outside the field. Figures 7-10 and 7-11 compare off-axis profiles of relative dose versus off-axis position along the major axes for the 10x10cm^2 and 20x20 cm^2 collimation systems, respectively, and Figures 7-12 and 7-13 show the diagonal off-axis dose profiles for the 10x10 and 20x20 cm^2 applicators, respectively, normalized to central-axis dose at 1 cm depth. Additionally in Appendix D, the MC-calculated out-of-field dose profiles are plotted in the right column of plots in Figures D-4, D-5, and D-6 for the 6x6, 14x14, and 25x25 cm^2 applicators, respectively.

Figures 7-10 through 7-13 show that for all energies and applicators the cross-plane profiles produced the greatest leakage dose and the diagonal profiles produced the least leakage dose. In general, the MC calculations matched the measured data to within 0.2% of central axis dose. For the major axes profiles of the 7 and 13 MeV beams, the MC-calculated data generally over-predicted the measured data for both applicators, with a maximum difference of 0.39%. For the major axes profiles of the 20 MeV beam, the MC-calculated data generally slightly under-predicted the measured data for both applicators, with a maximum difference of 0.21%. For the diagonal profiles, the MC-calculated data generally over-

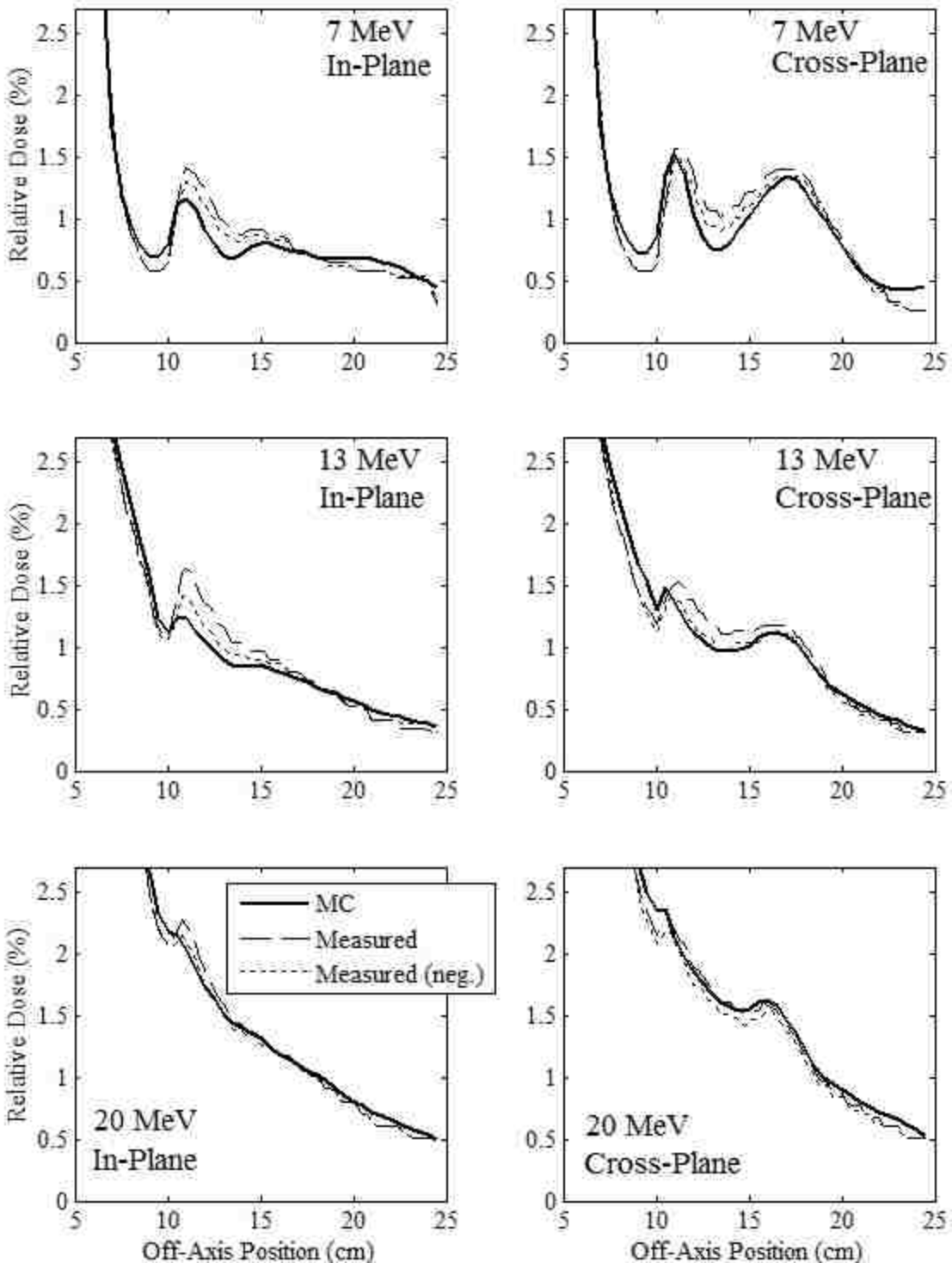

Figure 7-10. Comparison of measured and MC-calculated major axes relative dose profiles versus off-axis position outside the field for the prototype 10x10 cm^2 applicator. In-plane (left) and cross-plane (right) dose profiles are compared at beam energies of 7 (upper row), 13 (middle row), and 20 MeV (lower row) normalized to central axis dose at the measurement depth, 1 cm in water. The long-dashed curves represent the measured profiles. The short-dashed curves represent the same measured profiles in the negative half plane, mirrored about central axis. The solid curve represents the MC-calculated profile.

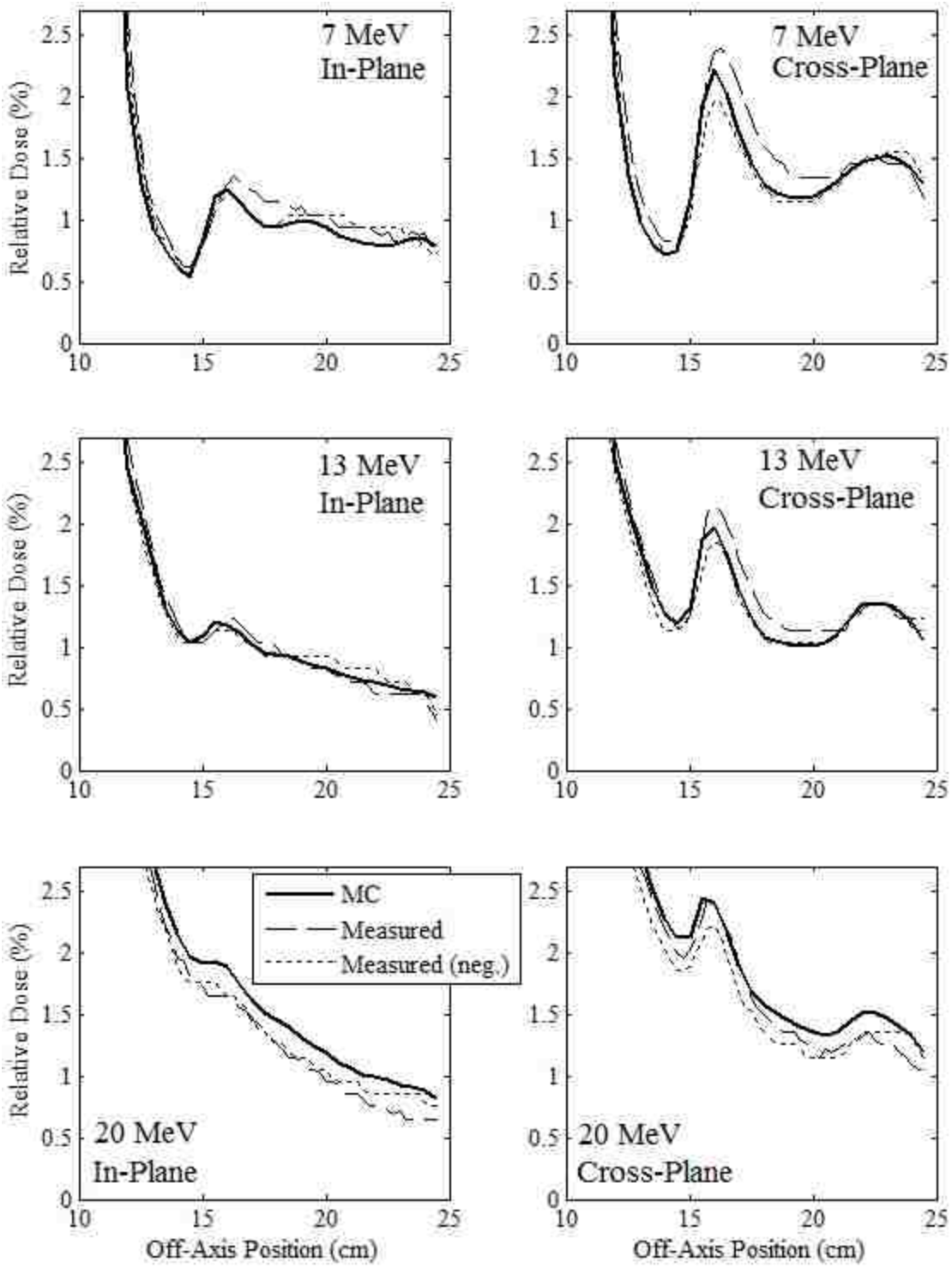

Figure 7-11. Comparison of measured and MC-calculated major axes relative dose profiles versus off-axis position outside the field for the prototype 20x20 cm^2 applicator. In-plane (left) and cross-plane (right) dose profiles are compared at beam energies of 7 (upper row), 13 (middle row), and 20 MeV (lower row) normalized to central axis dose at the measurement depth, 1 cm in water. The long-dashed curves represent the measured profiles. The short-dashed curves represent the same measured profiles in the negative half plane, mirrored about central axis. The solid curve represents the MC-calculated profile.

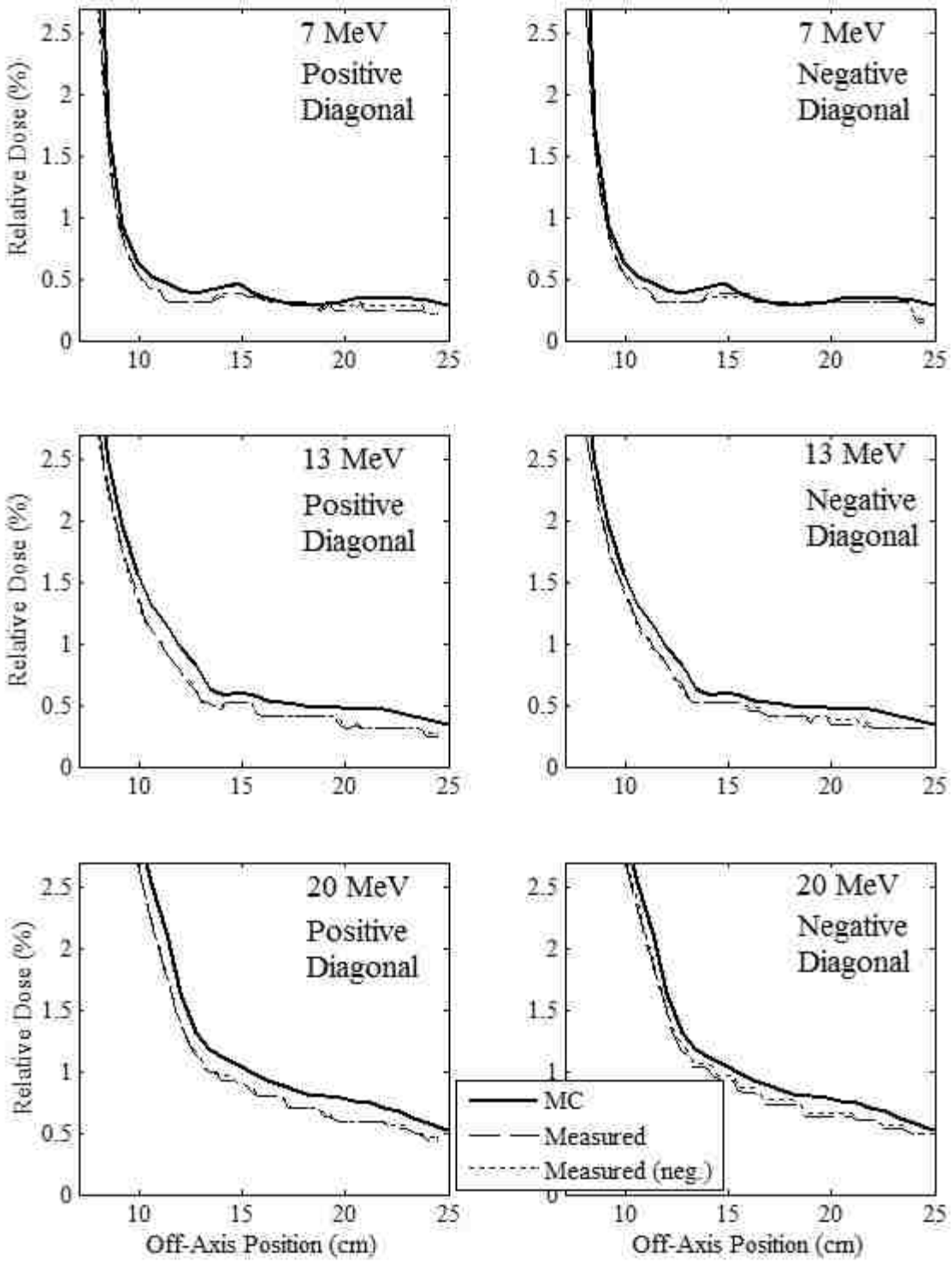

Figure 7-12. Comparison of measured and MC-calculated diagonal relative dose profiles versus off-axis position outside the field for the prototype 10x10 cm^2 applicator. In-plane (left) and cross-plane (right) dose profiles are compared at beam energies of 7 (upper row), 13 (middle row), and 20 MeV (lower row) normalized to central axis dose at the measurement depth, 1 cm in water. The long-dashed curves represent the measured profiles. The short-dashed curves represent the same measured profiles in the negative half plane, mirrored about central axis. The solid curve represents the MC-calculated profile.

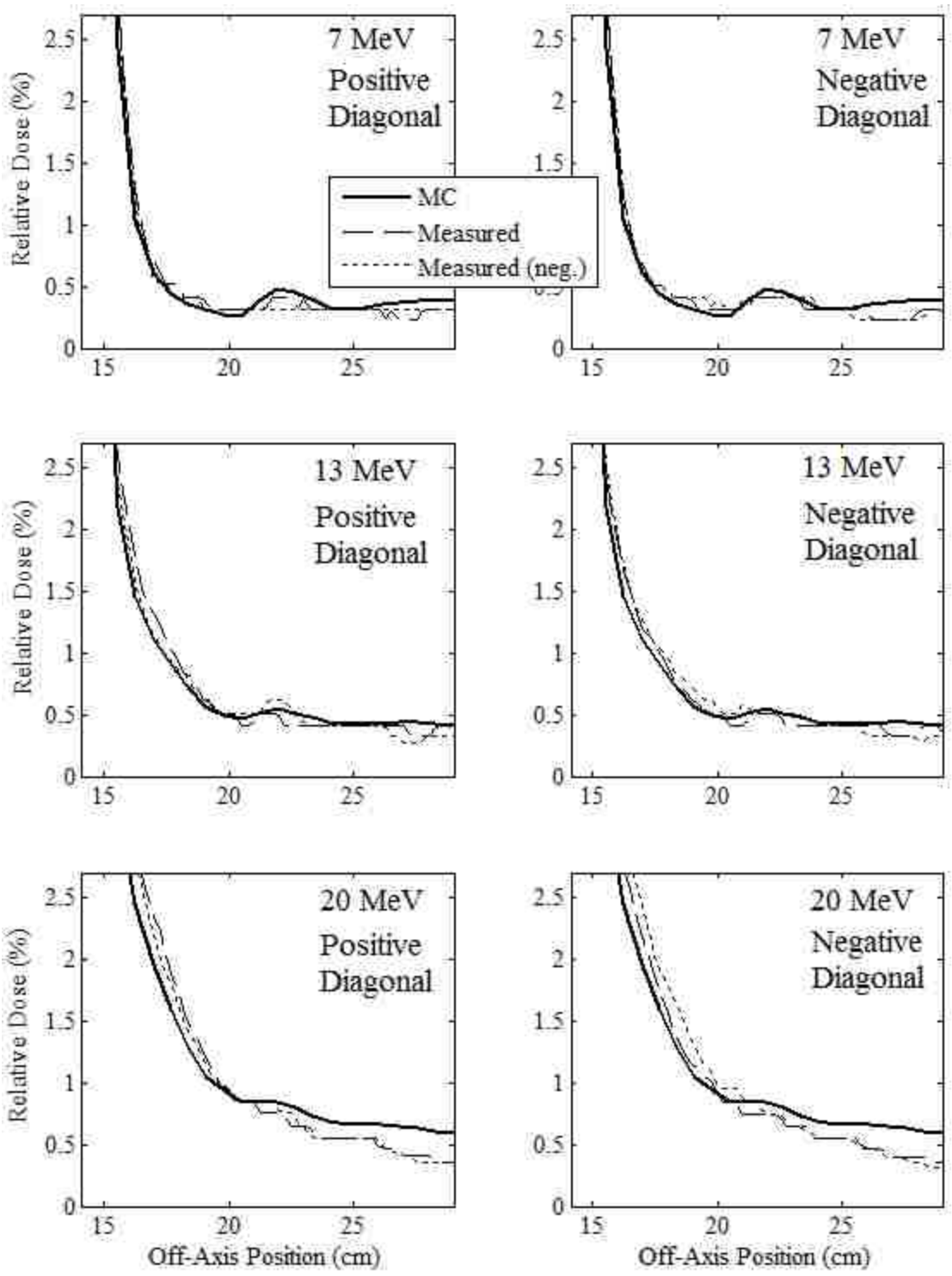

Figure 7-13. Comparison of measured and MC-calculated diagonal relative dose profiles versus off-axis position outside the field for the prototype 20x20 cm^2 applicator. In-plane (left) and cross-plane (right) dose profiles are compared at beam energies of 7 (upper row), 13 (middle row), and 20 MeV (lower row) normalized to central axis dose at the measurement depth, 1 cm in water. The long-dashed curves represent the measured profiles. The short-dashed curves represent the same measured profiles in the negative half plane, mirrored about central axis. The solid curve represents the MC-calculated profile.

predicted the measured data for all energies and applicators, with a maximum difference of 0.24%. The negative and positive measured profiles were shown to typically agree within 0.2% for all scans other than the cross-plane profiles with the 20x20 cm^2 applicator, which had a maximum difference of 0.48% with the 7 MeV beam.

The mean and maximum percent leakage doses, normalized to D_{max} per IEC specifications, are listed in Table 7-3 for both the MC-calculated and measured data for each beam energy and applicator investigated. Because no 6x6, 14x14, or 25x25 cm^2 prototypes were fabricated, no measurement values were available for these applicator sizes. For purposes of evaluation, the maximum values allowed by the IEC for mean and maximum percent leakage dose are listed in the bottom row of the table for the nominal 7, 13, and 20 MeV beams.

Table 7-3. Mean and maximum percent leakage dose for the MC-calculated and measured dose distributions for the nominal 7, 13, and 20 MeV beams with the prototype collimation system. The mean leakage dose is shown in the left columns and the maximum leakage dose is shown in the right columns normalized to D_{max}. Only measured mean and maximum dose values are shown for the prototype 10x10 and 20x20 cm^2 applicators. The bottom two rows show $E_{p,0}$ and the maximum values allowed by the IEC for mean percent leakage and maximum percent leakage for each nominal beam energy.

		Mean Percent Leakage Dose per IEC Specifications			Maximum Percent Leakage Dose per IEC Specifications		
		7 MeV	13 MeV	20 MeV	7 MeV	13 MeV	20 MeV
6x6 cm^2 Applicator	MC	0.45%	0.54%	0.91%	1.26%	2.17%	3.96%
	Measured	-	-	-	-	-	-
10x10 cm^2 Applicator	MC	0.56%	0.63%	1.06%	1.53%	2.19%	3.93%
	Measured	0.57%	0.60%	0.99%	1.57%	2.04%	3.58%
14x14 cm^2 Applicator	MC	0.68%	0.71%	1.16%	1.74%	2.00%	3.38%
	Measured	-	-	-	-	-	-
20x20 cm^2 Applicator	MC	0.75%	0.76%	1.14%	2.22%	1.97%	2.86%
	Measured	0.76%	0.75%	1.01%	2.39%	2.16%	2.73%
25x25 cm^2 Applicator	MC	0.74%	0.73%	1.06%	2.18%	1.95%	2.67%
	Measured	-	-	-	-	-	-
$E_{p,0}$ (MeV)		7.14	13.12	20.47	7.14	13.12	20.47
IEC Specified Maximum		1.00%	1.10%	1.34%	10.00%	10.00%	10.00%

Both the measured and MC-calculated data in Table 7-3 show that the prototype applicators produce low mean percent leakage doses that are within IEC specifications at each beam energy for all applicator sizes. For the measured data, the 7 MeV beam with the 20x20 cm^2 applicator came closest to exceeding the IEC specified maximum mean leakage dose, with a mean leakage dose within 0.24% of the 1.00% limit. For the MC-calculated data, the 20 MeV beam with the 14x14 cm^2 applicator came closest to exceeding the IEC specified maximum mean leakage dose, with a mean leakage dose within 0.18% of the 1.34% limit.

The IEC specifies that the maximum percent leakage dose be less than 10.00% of D_{max} for all beam energies at the patient plane. The data in Table 7-3 revealed that the maximum percent leakage dose was well below this limit for all applicators and beam energies. For the measured data, the 10x10 cm^2 applicator with the 20 MeV beam produced the largest maximum percent leakage dose at 3.58%. For the MC-calculated data, the 6x6 cm^2 applicator with the 20 MeV beam produced the largest maximum percent leakage dose at 3.96%.

Table 7-4 compares the mean and maximum percent leakage doses of the prototype applicators with those of the current clinical applicators calculated per IEC specifications. The table shows the increase in the measured mean leakage dose for the 20x20 cm^2 applicator for all three beam energies studied and for the 20 MeV beam with the 10x10 cm^2 applicator. The most significant increase occurred with the 20 MeV beam with the 20x20 cm^2 applicator, in which the measured mean percent leakage dose was increased by 0.16% [1.01% - 0.85%]. When the measured maximum percent leakage doses of the prototype applicators are compared with the current system, the maximum leakage dose was decreased for the 10x10 cm^2 applicator for all beam energies and increased for the 20x20 cm^2 applicator for the 7 and 13 MeV beams. The maximum percent leakage dose was maintained at 2.73% for the 20x20 cm^2 applicator with the 20 MeV beam.

Table 7-4. Comparison of mean and maximum percent leakage doses of the prototype applicators with the current clinical Elekta applicators for both the MC-calculated and measured dose distributions. The mean percent leakage values are shown in the upper portion of the table and the maximum percent leakage values are shown in the lower portion of the table for the 7, 13, and 20 MeV beams calculated per IEC criteria and normalized to D_{max}.

		Mean Percent Leakage Dose			
		Current Clinical Applicators		Prototype Applicators	
		MC	Measured	MC	Measured
10x10 cm^2 Applicator	7 MeV	0.70%	0.66%	0.56%	0.57%
	13 MeV	0.65%	0.67%	0.63%	0.60%
	20 MeV	0.99%	0.93%	1.06%	0.99%
20x20 cm^2 Applicator	7 MeV	0.67%	0.56%	0.75%	0.76%
	13 MeV	0.69%	0.65%	0.76%	0.75%
	20 MeV	0.93%	0.85%	1.14%	1.01%

		Maximum Percent Leakage Dose			
		Current Clinical Applicators		Prototype Applicators	
		MC	Measured	MC	Measured
10x10 cm^2 Applicator	7 MeV	2.11%	2.14%	1.53%	1.57%
	13 MeV	2.75%	2.78%	2.19%	2.04%
	20 MeV	4.38%	4.09%	3.93%	3.58%
20x20 cm^2 Applicator	7 MeV	1.65%	1.74%	2.22%	2.39%
	13 MeV	1.95%	2.03%	1.97%	2.16%
	20 MeV	2.83%	2.73%	2.86%	2.73%

7.3.3. Lateral Leakage Analysis

Along with the criteria for mean and maximum leakage at the patient plane, the IEC specifies that the maximum dose along the side of the applicator should not exceed 10% of D_{max}, measured 2 cm outside the volume contained by the applicator. To investigate this leakage along the side of the applicator a MC study was performed. The results of this study are shown in Figures 7-14 and 7-15 for the prototype 10x10 and 20x20 cm^2 applicators, respectively. These figures plot the in-plane and cross-plane dose profiles versus off-axis position calculated at *z*-positions of 81 (blue), 90 (green), and 97 cm (red), and at the patient plane (black, *z* = 101 cm) cm for the 7, 13, and 20 MeV beams. All profiles are

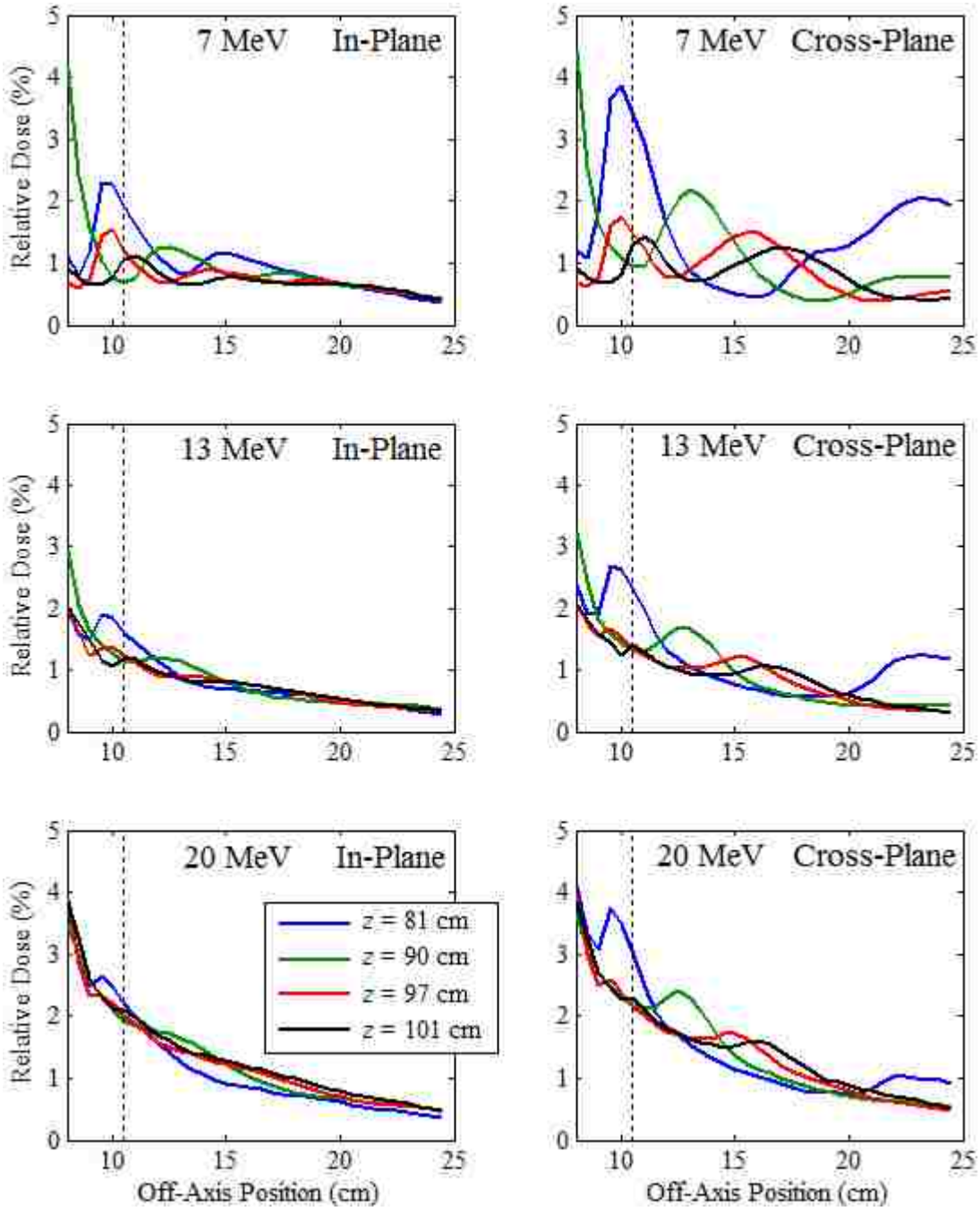

Figure 7-14. Leakage dose profiles MC-calculated at various *z*-positions along the side of the 10x10 cm^2 prototype applicators. The figure plots the in-plane (left) and cross-plane (right) dose profiles calculated at *z*-positions of 81 (blue), 90 (green), 97 (red), and 101 (black) cm the 7, 13, and 20 MeV beams. All profiles are calculated at 1 cm depth in water and normalized to D_{max}. The vertical dashed line represents the off-axis position 2 cm outside the outer edge of the middle trimmer.

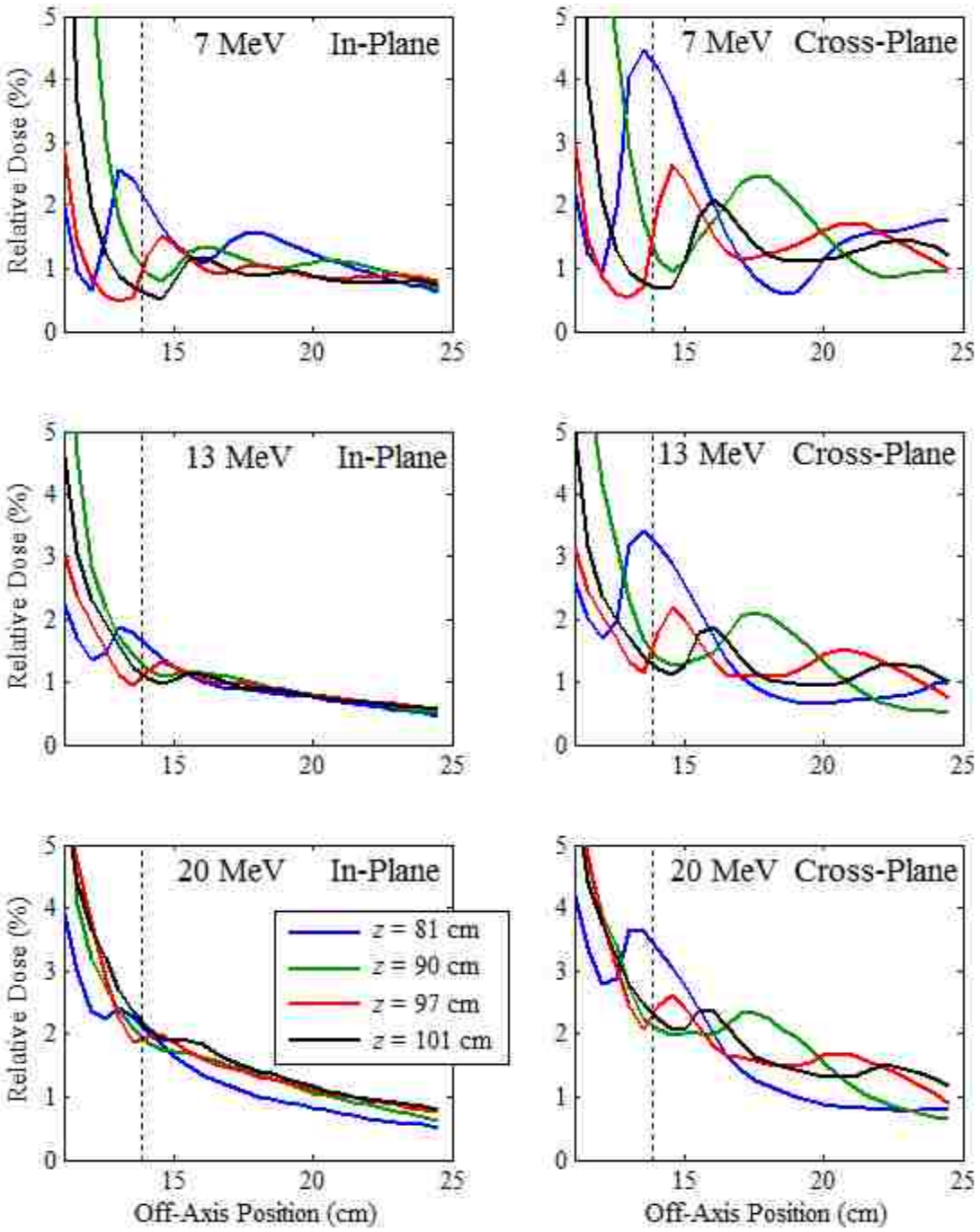

Figure 7-15. Leakage dose profiles MC-calculated at various *z*-positions along the side of the 20x20 cm^2 prototype applicators. The figure plots the in-plane (left) and cross-plane (right) dose profiles calculated at *z*-positions of 81 (blue), 90 (green), 97 (red), and 101 (black) cm the 7, 13, and 20 MeV beams. All profiles are calculated at 1 cm depth in water and normalized to D_{max}. The vertical dashed line represents the off-axis position 2 cm outside the outer edge of the middle trimmer.

calculated at 1 cm depth in water and normalized to D_{max} at 100 cm SSD. The vertical dashed line in the plots represents the off-axis position 2 cm outside the outer edge of the middle trimmer (at off-axis positions of 10.5 and 13.8 cm for the 10x10 and 20x20 cm^2 applicators, respectively). This off-axis position 2 cm outside this trimer was selected for evaluating the leakage dose along the side of the applicator both because all calculation planes were downstream of the middle trimmer, and because the middle trimmer outer edge was closer to central axis than the lower trimmer outer edge (and therefore is the more conservative value for defining the volume contained by the applicator). Therefore, the collimation system was deemed to pass leakage dose criteria along the side of the applicator if all calculated dose values at this off-axis position were below 10% of D_{max}. As the figures show, this was the case for both the 10x10 and 20x20 cm^2 applicators for all beam energies for both the in-plane and cross-plane profiles. Therefore, both collimation systems were deemed to pass leakage dose criteria along the side of the applicator. The maximum relative dose for all beams at this off-axis position was 4.29%, which occurred in the 7 MeV cross-plane profile with the 20x20 cm^2 applicator calculated at a *z*-position of 81 cm.

7.3.4. Jaw Position Error Analysis

The results of the jaw position error analysis are shown in Figures 7-16, 7-17, and 7-18 for the 7, 13, and 20 MeV beam calculations, respectively. These figures plot the MC-calculated in-plane, cross-plane and diagonal profiles of relative dose versus off-axis position for the original collimation system model with the 20x20 cm^2 prototype applicator (indicated as "No Jaw Adjustment" in the figures), and each of the four modified models with adjusted jaw positions. In the figures, the curves denoted with "0.5 cm Adj." indicate an outward (away from central axis) jaw adjustment, and the curves denoted as "-0.5 cm Adj." indicate an inward (towards from central axis) jaw adjustment for both the in-plane and cross-plane jaws. The ±0.5 cm adjustments correspond to 1.0 cm adjustments at isocenter for the in-plane jaw and 1.2 cm adjustments for the cross-plane jaw.

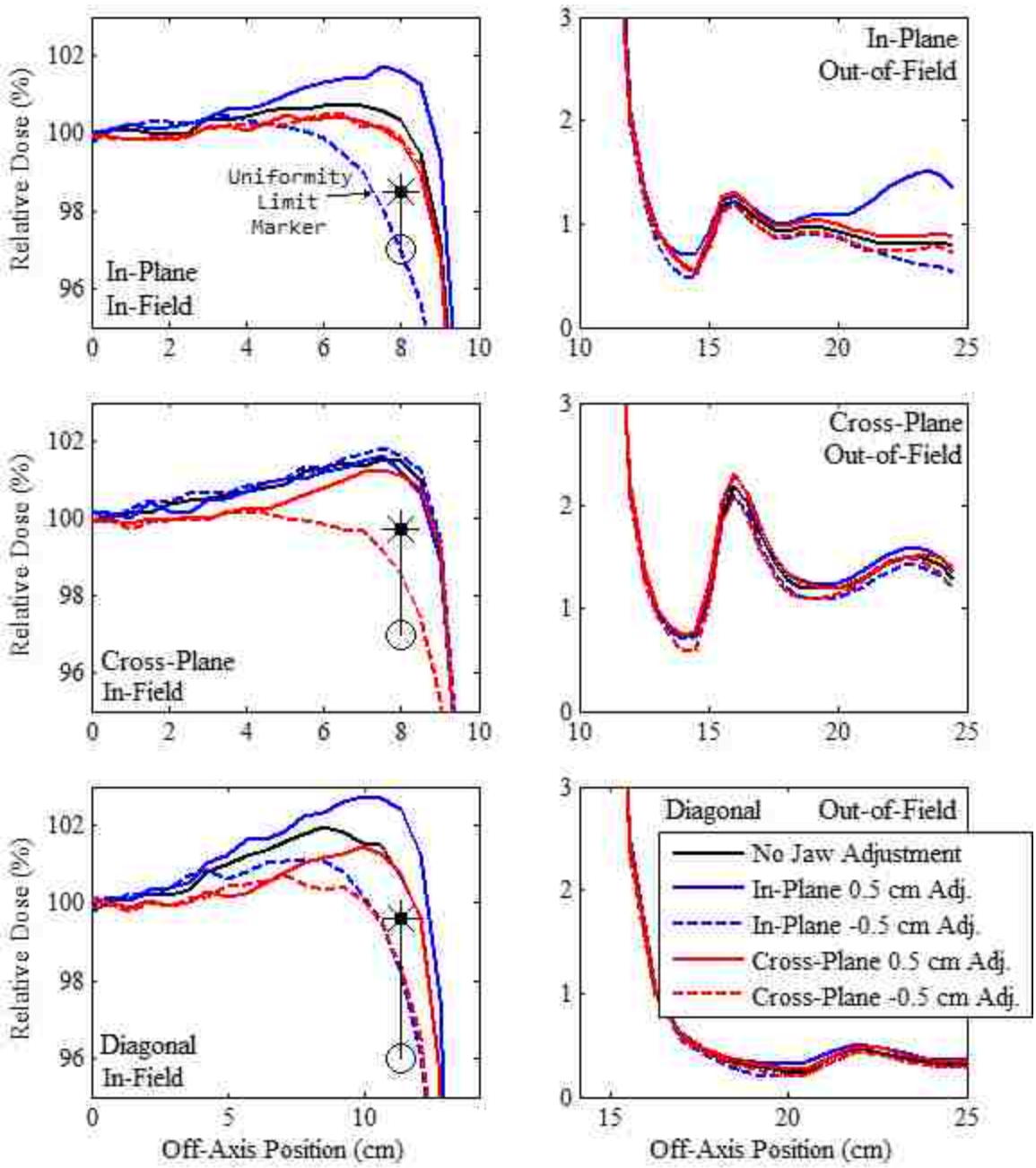

Figure 7-16. Profiles of MC-calculated relative dose versus off-axis position for the 7 MeV beam, 20x20 cm^2 prototype applicator. All profiles were calculated at 1 cm depth in water. In-field results are plotted in the left column, and out-of-field results are plotted in the right column for the in-plane (top row), cross-plane (middle row), and diagonal (bottom row) profiles. The black line ("No Jaw Adjustment") indicates the optimized prototype model. Curves labelled "0.5 cm Adj." indicate an outward jaw adjustment of 0.5 cm, and curves labelled as "-0.5 cm Adj." indicate an inward jaw adjustment of 0.5 cm for either the in-plane or cross-plane jaws. The uniformity limit marker indicates the minimum dose at the edge of the uniformity region necessary to achieve acceptable in-field beam flatness. The line segment shows the shift from the acceptance limit (96% or 97%) due to the error in the MC prediction of the measured dose (see text).

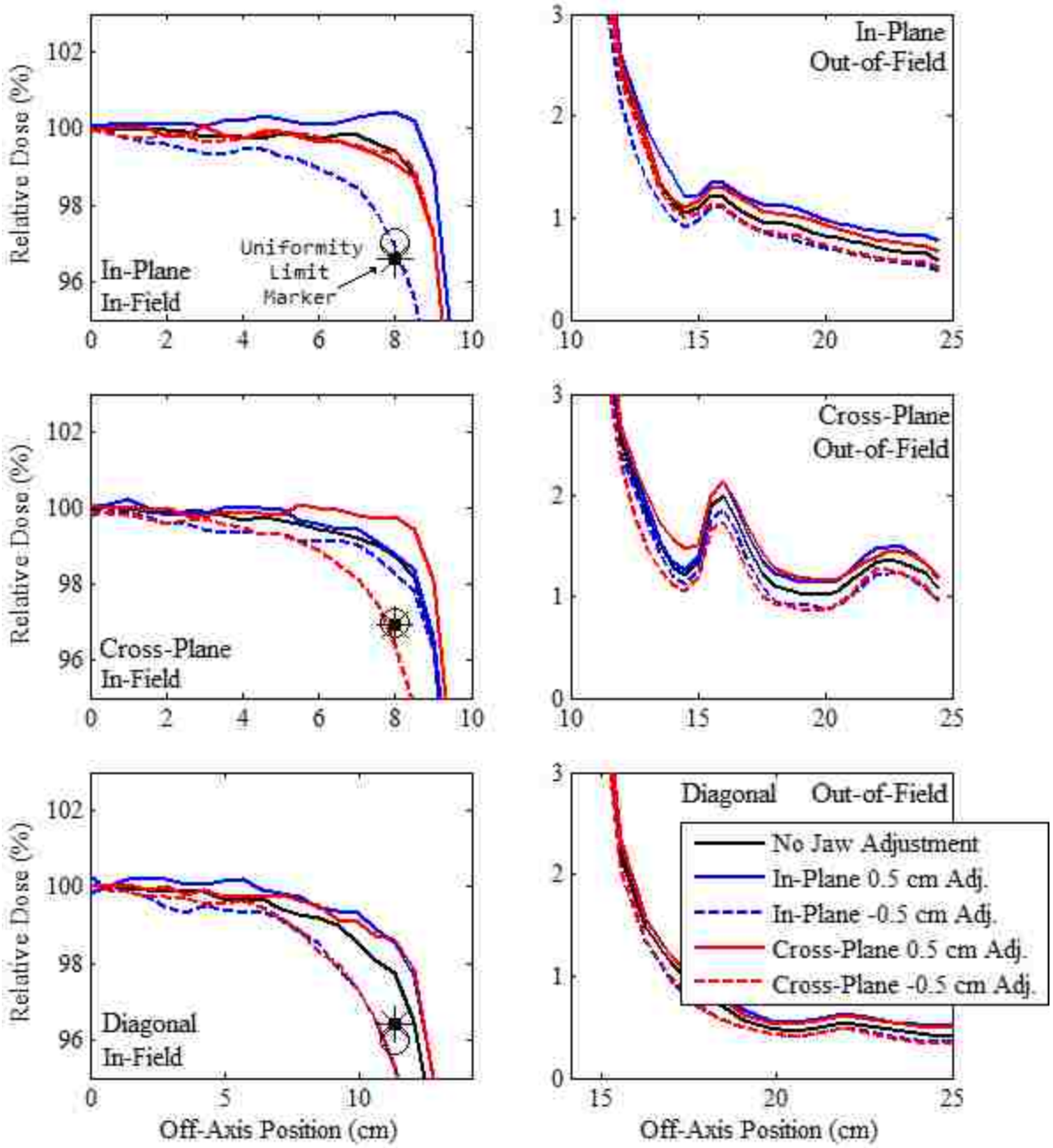

Figure 7-17. Profiles of MC-calculated relative dose versus off-axis position for the 13 MeV beam, 20x20 cm^2 prototype applicator. The in-field profiles were calculated at 2 cm depth and the out-of-field profiles were calculated at 1 cm depth in water. In-field results are plotted in the left column, and out-of-field results are plotted in the right column for the in-plane (top row), cross-plane (middle row), and diagonal (bottom row) profiles. The black line ("No Jaw Adjustment") indicates the optimized prototype model. Curves labelled "0.5 cm Adj." indicate an outward jaw adjustment of 0.5 cm, and curves labelled as "-0.5 cm Adj." indicate an inward jaw adjustment of 0.5 cm for either the in-plane or cross-plane jaws. The uniformity limit marker indicates the minimum dose at the edge of the uniformity region necessary to achieve acceptable in-field beam flatness. The line segment shows the shift from the acceptance limit (96% or 97%) due to the error in the MC prediction of the measured dose (see text).

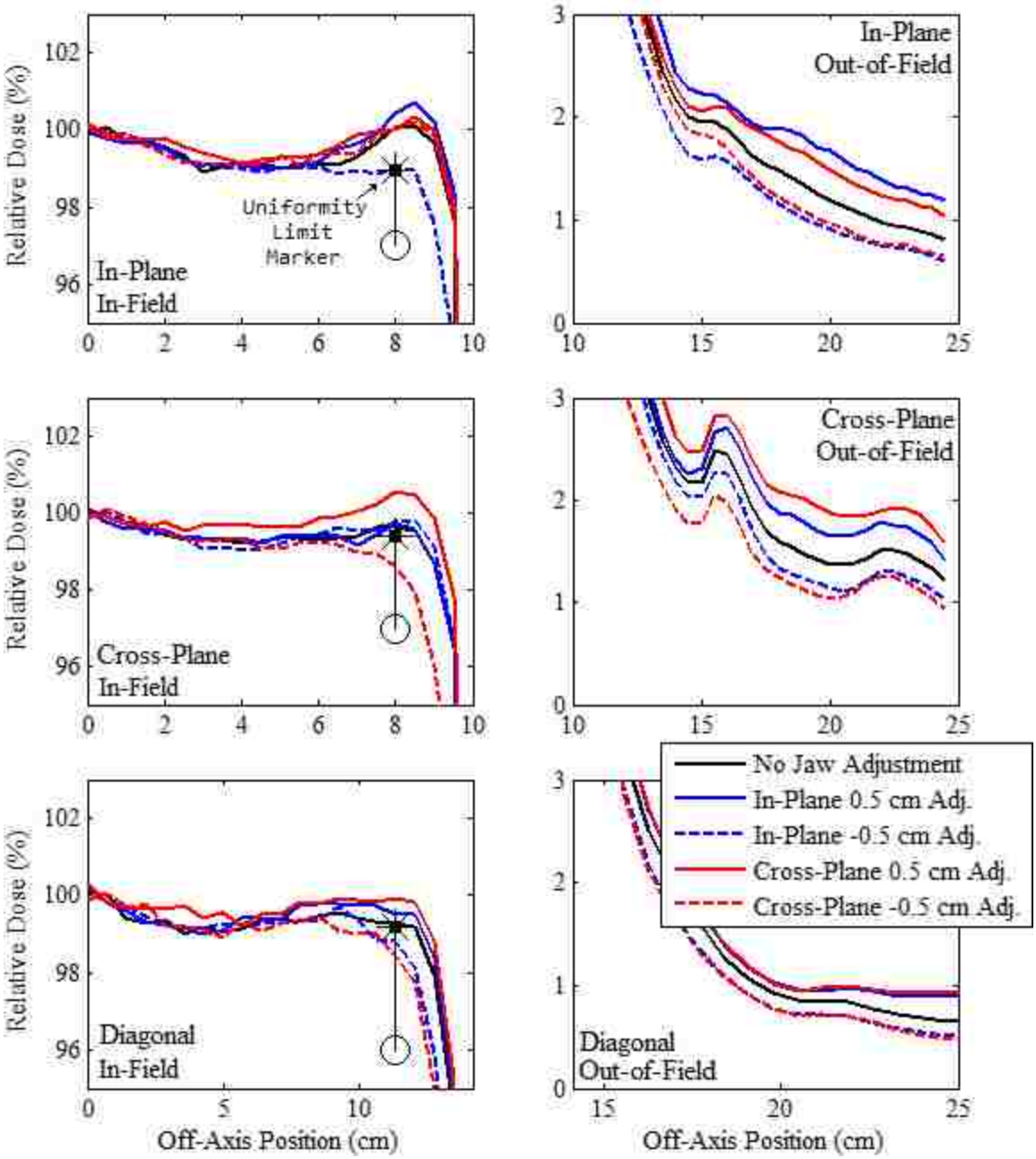

Figure 7-18. Profiles of MC-calculated relative dose versus off-axis position for the 20 MeV beam, 20x20 cm^2 prototype applicator. The in-field profiles were calculated at 2 cm depth and the out-of-field profiles were calculated at 1 cm depth in water. In-field results are plotted in the left column, and out-of-field results are plotted in the right column for the in-plane (top row), cross-plane (middle row), and diagonal (bottom row) profiles. The black line ("No Jaw Adjustment") indicates the optimized prototype model. Curves labelled "0.5 cm Adj." indicate an outward jaw adjustment of 0.5 cm, and curves labelled as "-0.5 cm Adj." indicate an inward jaw adjustment of 0.5 cm for either the in-plane or cross-plane jaws. The uniformity limit marker indicates the minimum dose at the edge of the uniformity region necessary to achieve acceptable in-field beam flatness. The line segment shows the shift from the acceptance limit (96% or 97%) due to the error in the MC prediction of the measured dose (see text).

The in-field dose profiles are shown in the left column of plots in the figures. In these plots, the 7 MeV dose profiles were calculated at a depth of 1 cm in water, and the 13 and 20 MeV profiles were calculated at 2 cm depth. Similar to Figures 6-13 and 6-14, these plots also show the uniformity limit marker for each beam profile, which indicates minimally acceptable OAR at the edge of the uniformity region (97% for the major axes profiles and 96% for the diagonal profiles), plus the differences between the MC-calculated and measured data at the field edge for each beam energy (as previously determined in Aim 1, see Table 2-4), plus a 1% cushion. Profiles were deemed to be acceptably flat if they passed above and outside this marker. Based on this criterion, the plots show that all unadjusted models produced acceptably flat beams for each beam energy. The figures also show that adjusting the in-plane and cross-plane jaws inward 0.5 cm resulted in the in-plane and cross-plane profiles, respectively, failing beam flatness criteria in most cases. Only the 13 MeV and 20 MeV in-plane profiles passed beam flatness criteria with a 0.5 cm inward in-plane jaw adjustment. For all three beam energies, adjusting the cross-plane jaw inward resulted in the cross-plane profile failing flatness criteria, and adjusting either the in-plane or cross-plane jaws inward resulted in the diagonal profiles failing beam flatness criteria.

The dose profiles are plotted versus off-axis position in the leakage region in the right column of plots in Figures 7-16 through 7-18. These plots show that adjusting the jaws inward decreases the leakage dose and adjusting the jaws outward increases the leakage dose for all profiles and beam energies. The effects are more significant in the profiles calculated in the same dimension as the jaw adjustment, e.g. the in-plane dose profiles are more impacted by the in-plane jaw adjustments, and the cross-plane profiles are more impacted by the cross-plane jaw adjustments. In general, the impact of the jaw adjustment on the leakage dose increased with energy. The one noteworthy exception to this is the in-plane profile for the 7 MeV beam with an outward 0.5 cm jaw adjustment. This profile showed a dose increase from the unadjusted model profile of approximately 0.7% at an off-axis position of approximately 23 cm. This increase was presumed to be due to primary electrons scattering outside the upper trimmer.

The mean percent leakage doses were calculated for each of these dose distributions per IEC specifications for each beam energy and are displayed in Table 7-5. These data showed that for all beam energies, adjusting the jaws inward decreased the mean percent leakage dose and adjusting the jaws outward increased the mean percent leakage dose for both the in-plane and cross-plane jaws. The effect of the jaw adjustments on mean percent leakage dose increased with increasing beam energy, with the most significant increase occurring for the outward cross-plane jaw adjustment with the 20 MeV beam, in which the mean percent leakage dose was increased by 0.29% [1.44% - 1.15%] from the unadjusted jaw position model. The outward adjustments of both the in-plane and cross-plane jaws also resulted in the 20 MeV beams failing mean percent leakage dose criteria as specified by the IEC, which states that the mean leakage dose should be below 1.34% for this nominal beam energy.

Table 7-5. Mean percent leakage dose values for each 20x20 cm^2 collimation system modeled in the jaw position error analysis for the 7, 13, and 20 MeV beams. The mean leakages are calculated per IEC specifications for the models with unadjusted jaw positions, and the models with the in-plane and cross-plane jaws adjusted inward and outward by 0.5 cm.

	7 MeV	13 MeV	20 MeV
Unadjusted Jaw Positions	0.75%	0.76%	1.15%
Outward In-Plane Jaw Adjustment	0.86%	0.87%	1.40%
Inward In-Plane Jaw Adjustment	0.69%	0.68%	0.96%
Outward Cross-Plane Jaw Adjustment	0.78%	0.85%	1.44%
Inward Cross-Plane Jaw Adjustment	0.70%	0.67%	0.93%

It might be beneficial for the new electron collimation system to allow photon jaw settings (at isocenter) to be varied by more than 1 cm to assist in achieving beam flatness. Such 'robustness' could be provided by increasing only the width of the constant-thickness portion of the upper trimmer bars, which increases the weight. For the 20x20 cm^2 applicator, the cost is estimated to be 0.4 kg cm^{-1}. Hence, increasing the allowed variation in the photon jaw setting from 1 to 3 cm would increase the weight of the new prototype 20x20 cm^2 applicator from 6.8 to 7.6 kg, still 1 kg below the targeted weight of 8.6 kg.

7.4. Aim 6 - Conclusions

The purpose of Aim 6 was to fabricate and evaluate the in-field and out-of-field dose for prototype 10x10 and 20x20 cm^2 applicators based on the collimation system designs developed in Aim 5. To allow for applicator fabrication at the LSU Physics machine shop, it was necessary to modify both the trimmer material and shape of the outer edge bevel from the design developed in Aim 5. The trimmer material was changed from tungsten to a combination of lead and aluminum, and the outer edge bevel shape was approximated as a series of four steps. Additionally, the leakage dose outside the outer edges of the applicators was investigated by MC calculations. Lastly, the effects of altering the designated jaw positions on the patient plane dose distribution were investigated based on MC calculations. In this process, the following was concluded:

- Weight reduction: It was possible to significantly reduce the Elekta electron applicator weight as compared to both current clinical Elekta and Varian electron applicators. The 10x10 cm^2 prototype applicator weighed 5.5 kg, as opposed to 7.7 kg for the current clinical Elekta applicator and 6.5 kg for the Varian applicator, corresponding to a 29% and 15% weight reduction, respectively. The 20x20 cm^2 prototype applicator weighed 6.8 kg, as opposed to 10.9 kg for the current clinical Elekta applicator and 8.6 kg for the Varian applicator, corresponding to a 38% and 21% weight reduction, respectively.
- In-field beam flatness: It was possible to design significantly lighter electron applicators that met criteria as specified by Hogstrom (2004). This was demonstrated for both the 10x10 and 20x20 cm^2 prototype applicators.
- Out-of-field leakage dose at the patient plane: It was possible to design significantly lighter electron applicators that met criteria for patient plane mean and maximum leakage dose as specified by the IEC. The 7, 13, and 20 MeV beams were found to produce mean percent leakage doses of 0.57%, 0.60%, and 0.99%, respectively, with the 10x10 cm^2 applicator, and 0.76%, 0.75%, and 1.01%, respectively, for the 20x20 cm^2 applicator, calculated per IEC specifications. Each of these values was below the IEC specified maxima of 1.00%, 1.10%, and 1.34% for the 7,

13, and 20 MeV beams, respectively. Additionally, each of the measured mean percent leakage doses were within 0.1% of the current collimation system mean percent leakage doses for the 10x10 cm^2 prototype applicator, but were 0.1% to 0.2% greater than the current collimation system mean percent leakage doses for the 20x20 cm^2 prototype applicator.

- Out-of-field leakage dose outside the lateral applicator edge: The prototype 10x10 and 20x20 cm^2 applicators met criteria for leakage dose outside the lateral applicator edges as specified by the IEC according to MC calculations. Off-axis dose profiles MC-calculated at *z*-positions of 81, 90, and 97 cm revealed that the maximum dose along the side of the applicator was 4.29% for all beam energies and applicator sizes, well below the IEC specified threshold of 10.00% of D_{max}.
- Sensitivity of in-field beam flatness and leakage dose to photon jaw position: Moving the photon jaws (±0.5 cm at the jaw height) from their designated positions caused failure to meet in-field beam flatness and out-of-field dose specifications for the 20x20 cm^2 collimation system. A MC study revealed that moving either the in-plane or cross-plane jaw inward 0.5 cm caused the collimation system to fail in-field beam flatness criteria for the 7, 13, and 20 MeV beams. The study also revealed that moving either the in-plane or cross-plane jaw outward 0.5 cm caused the collimation system to fail mean leakage dose criteria for the 20 MeV beam.

Chapter 8 - Summary of Results and Conclusions

8.1. Introduction

8.1.1. Purpose

The purpose of this investigation was to redesign the Elekta Infinity electron collimation system to allow for new prototype applicators at reduced weights. Because Varian 21EX applicators have been shown to perform adequately, new applicator designs that meet field flatness and leakage dose criteria with weights no greater than the Varian applicators should be attainable. Specifically, the goal of this study was to design new 10x10 and 20x20 cm^2 applicators for the Elekta Infinity accelerator with trimmer weights less than or equal to the trimmer weights of the Varian 10x10 and 20x20 cm^2 applicators. Additionally, the design should be based on a process that should allow similar improvements to Elekta's 6x6, 14x14, and 25x25 cm^2 applicators.

8.1.2. Hypothesis

Using a sound understanding of how radiation transport impacts the design of the Elekta electron collimating system, it is possible to design prototype 10x10 and 20x20 cm^2 applicators whose collimating components (trimmers) will (1) total less than 5.00 and 7.10 kg, respectively, (2) meet IEC radiation leakage dose specifications outside the field, and (3) achieve beam flatness inside the field as specified by Hogstrom (2004).

8.1.3. Approach

To test this hypothesis, a series of specific aims was completed. In these aims, tools were developed and evaluated for use in the design process, including a MC (Aim 1) and an analytical (Aim 2) electron beam transport model for calculating the dose distribution in the patient plane. These tools were used to determine the best material (Aim 3) and optimal geometric design features (Aims 4 and 5) that minimize the applicator weight while reducing the leakage dose to acceptable levels and maintaining acceptable in-field beam flatness. In the final specific aim (Aim 6), prototype 10x10 and 20x20 cm^2 applicators were fabricated based on parameters developed in the collimation system design process and

were tested via measurement and MC calculation to ensure the prototypes met criteria for beam flatness and leakage dose.

8.2. Aim 1 - Evaluation of the Current Collimation Design and MC Model Using Measurement

Aim 1: Measure off-axis dose profiles in a water phantom (100 cm SSD) at prescribed depths to document the beam flatness and leakage dose for the current clinical applicator design. Also, use that measured data to assess the accuracy of the electron MC model developed by Harris (2012) for the Elekta Infinity accelerator both in the field and in the leakage region.

8.2.1. Summary of Results

- In-Field Beam Flatness: The measured in-field dose profiles met beam flatness acceptance criteria as specified by Hogstrom (2004) for the current 10x10 and 20x20 cm^2 clinical Elekta applicators at beam energies of 7, 13, and 20 MeV.
- Accuracy of MC for In-Field Dose Calculation: The MC calculations over-predicted the measured relative dose at the edge of the uniformity region for the 7 and 20 MeV beams by as much as 2.59% and 2.20% of central axis dose. The MC calculations under-predicted the measured relative dose for the 13 MeV beam by as much as 1.40% at the edge of the uniformity region.
- Out-of-Field Leakage Dose in Patient Plane: The mean and maximum percent leakage doses met acceptance criteria as specified by the IEC (1998) in the patient plane for all applicators (10x10 and 20x20 cm^2) and beam energies (7, 13, and 20 MeV) studied. The maximum measured mean leakages were 0.66%, 0.67%, and 0.93% of D_{max} for the 10x10 cm^2 applicator and 0.56%, 0.65%, and 0.85% for the 20x20 cm^2 applicator at beam energies of 7, 13, and 20 MeV, respectively, well below the IEC specified limits of 1.00%, 1.10%, and 1.34%, respectively. The largest measured maximum leakage dose was found to be 4.09% of D_{max} for the 10x10 cm^2 applicator at a beam energy of 20 MeV, well below the IEC specified limit of 10.00%. Elekta leakage levels were generally greater than previously studied Varian electron collimation systems (Chow and

Grigorov, 2006; Shimozato *et al.*, 2012) and less than previously studied Siemens electron collimating systems (Yeboah *et al.*, 2010).

- Accuracy of MC for Out-of-Field Leakage Dose: The MC calculations predicted the measured dose within 0.26% of central axis dose at 1 cm depth for most profiles. The MC-calculations generally slightly over-predicted the measured mean percent leakage dose with the largest discrepancy being 0.11% of D_{max}.
- MC Analysis of Components of Out-of-Field Leakage Dose: A MC study using the LATCH bit filtering feature in EGSnrc revealed that the majority of the out-of-field leakage dose in the patient plane was deposited by electrons, though less so for high energy beams due to the increasing photon dose with increasing beam energies. Additionally, the majority of the electron leakage dose was deposited by electrons scattered from the collimation components, particularly the applicator trimmers.

8.2.2. Conclusions

- In-Field Flatness and Out-of-Field Leakage Dose for Current Elekta Electron Beams: The current Elekta collimation system produced an acceptably flat beam within the field and acceptably low leakage dose outside the field for each beam energy-applicator combination studied.
- Accuracy of MC Dose Calculation for In-Field and Out-of-Field Leakage Dose: Inside the field, the MC-calculated dose agreed with the measured dose to within 2.6%, and such differences were sufficiently small that they could be accounted for in the collimation system design process. Outside the field, the MC calculations were sufficiently accurate for use in the design process.
- Significance of Collimation-Scattered Electrons: Analysis of MC-calculated out-of-field leakage dose showed that electron dose dominated over photon dose, though photon dose became increasingly important as energy increased. The study revealed that most out-of-field electron dose came from electrons scattered from the collimation system, indicating that applicator design features which reduce this scatter dose should be of interest in the design process.

8.3. Aim 2 - Develop and Validate an Analytical Radiation Transport Code for Optimizing Trimmer Design

Aim 2: Develop an analytical electron transport model based on pencil-beam theory to use in collimation system design. The model will incorporate both a primary electron and photon component, and its accuracy will be assessed. The impetus for creating this analytical model is to evaluate new collimation designs created within the design process for both in-field flatness and out-of-field leakage dose.

8.3.1. Summary of Results

- Development of Analytical Primary Electron Dose Model: An analytical model was developed for calculating the primary electron dose at patient plane. This model was based on the work of Huizenga and Storchi (1985; 1987), who calculated the scattering moment profiles for a broad electron beam passing through a collimation level, such as a set of photon jaws. The model built upon this work by propagating the divergent beam through a series of collimation levels to the patient plane.
- Development of Analytical Photon Dose Model: An analytical model was developed for calculating the photon dose at the patient plane from bremmstrahlung photons created in the scattering foils. Because the directional distribution of emitted bremsstrahlung photons is forward peaked with respect to the electron trajectory (Hough, 1948), the angular distribution of emitted photons is governed almost entirely by the angular distribution of the electrons from which they are emitted. To determine the angular distribution of photons emitted from the scattering foils, the mean angular electron distribution within each scattering foil element was calculated by integrating the angular electron distribution over the element thickness. A ray-tracing technique was then used to project the photon angular distribution to patient plane to create a spatial distribution. Additionally, the model accounted for attenuation within the collimation system.

- Accuracy of Analytical Primary Electron Model for In-Field Dose Calculation: Within the field, the analytical primary electron model performed reasonably well. For a 7 MeV beam, the model over-predicted slightly (< 5%) the MC-calculated dose in the high-dose, shoulder region of the dose profile near the edge of the field at the patient plane. This over-prediction was likely due to the analytical model approximating the fluence as uniform at all collimation levels when calculating the scattering moment profiles, which was believed to cause an under-prediction in $\bar{\theta}_x$ for the pencil-beams near the field edge.
- Accuracy of Analytical Primary Electron Model for Out-of-Field Dose Calculation: Outside the field, the primary electron model accurately predicted the location and magnitude of the leakage bumps at the patient plane, typically within 0.2% of central axis dose at the leakage bump peak. However, due to the inaccuracy caused by the Gaussian approximation within the pencil-beam model, the analytical code under-predicted the dose between these leakage bumps by approximately 1.2% of central axis dose.
- Accuracy of Analytical Photon Model for Dose Calculation with No Collimation: The analytical photon dose model was able to predict the MC-calculated off-axis dose at the patient plane to within 0.15% of the central axis total dose at 1 cm depth for the calculation performed with no collimation.
- Accuracy of Analytical Photon Model for Dose Calculation with Collimation: When collimation was added to the calculation, the accuracy of the analytical photon dose model decreased, significantly under-predicting the MC-calculated photon dose outside the field, presumably due to neglecting bremsstrahlung created in the trimmer bars.

8.3.2. Conclusions

- Utility of Primary Electron Model for In-Field Dose Calculation in Collimation Design Process: The primary electron model was sufficiently accurate to be used in modeling the in-field dose distribution during the collimation design process. However, due to slight over-predictions in the

analytically calculated dose just inside the edge of the field, it was necessary to supplement the analytical beam flatness evaluations with MC-calculated dose profiles when determining the inner trimmer edge positions.

- Futility of Primary Electron Model for Out-of-Field Dose Calculation in Collimation Design Process: Outside the field, the analytical primary electron model was shown to significantly under-predict the leakage dose between the primary electron leakage bumps. Because of this, and finding that the primary electron leakage dose constituted only a small percentage of the total leakage dose, it was determined that the analytical primary electron dose model was not useful for evaluating out-of-field leakage dose in the design process.
- Futility of Photon Dose Model for In-Field Dose Calculation in Collimation Design Process: Inside the field, the photon dose model was ignored because (1) the photon dose at 7 MeV is small, constituting a maximum of 0.9% of total in-field dose at patient plane, and (2) the effects of ignoring the photon dose is offset by edge scatter and beam non-uniformity which preferentially increase the dose near the edge of the field and are not accounted for in the analytical model.
- Futility of Photon Dose Model for Out-of-Field Dose Calculation in Collimation Design Process: Due to the under-prediction of the bremsstrahlung dose, the analytical photon dose model was not considered useful for predicting the out-of-field dose when evaluating the leakage in the collimation system design process.

8.4. Aim 3 - Perform Material and Range Analysis to Determine the Best Trimmer Material and Thickness

Aim 3: Determine the optimal high-density material and thickness for the applicator trimmer bars, i.e. the material and range combination which produces the least amount of leakage dose while allowing the applicator to be designed with minimal weight.

8.4.1. Summary of Results

- Dependence of Collimation Thickness for Stopping Electrons in High Density Collimation Materials: Of the three materials studied, lead and tungsten were shown to produce the least

trimmer thickness for a 20 MeV beam, with thicknesses of 9.08 and 9.52 g cm^{-2}, respectively, as compared to 11.08 g cm^{-2} for copper, calculated using a MC 1% threshold method. This result is attributed to the increased radiative energy loss in these higher atomic number materials.

- Dependence of Mean Percent Leakage on Collimating Material: The MC study comparing the leakage dose from applicators made of each material revealed that tungsten produced the smallest amount of leakage dose for all beam energies, with a 20 MeV mean percent leakage dose of 1.27%, as opposed to 1.39% and 1.51% for lead and copper, respectively.

8.4.2. Conclusions

- Optimal High Density Material: Of the three materials studied, tungsten trimmers were shown to produce the least leakage dose and could be designed relatively thin compared with copper. For these reasons, tungsten was selected as the trimmer material in the collimation system design process.

8.5. Aim 4 - Determine Inner Edge Divergence Angles for Each Trimmer

Aim 4: Determine whether it is more suitable for the inner edge of each trimmer to be situated parallel to central axis or divergent such that it is emanating from the virtual source of the beam. The divergence angles that minimize out-of-field leakage dose are more suitable.

8.5.1. Summary of Results

- Reduced Leakage Dose for Diverging Trimmer Inner Edges: The applicator designed with fully-divergent inner edges (diverging from the virtual source) produced the least leakage dose. The largest leakage dose decrease was found with the 20 MeV beam, which had a total mean percent leakage dose reduction of 0.14%.
- Impact of Inner-Edge Divergence on Leakage Dose for Individual Trimmers: Designing the inner trimmer edges to be fully divergent reduced the leakage dose from electrons scattered off each trimmer, though this reduction was more significant for the upper and middle trimmers than the lower trimmer. By designing the inner edges to be fully-divergent rather than non-divergent,

mean percent leakage dose due to scatter off the upper and middle trimmers was reduced by 0.05% and 0.06% of D_{max}, respectively, as compared to 0.02% for the lower trimmer.

8.5.2. Conclusions

- Recommendations for Upper and Middle Trimmer Inner Edge Divergence: It was decided that the inner edges of the upper and middle trimmers be made fully-divergent to minimize the leakage dose due to scatter off these trimmers.
- Recommendations for Lower Trimmer Inner Edge Divergence: Because the impact of the lower trimmer inner edge divergence on the leakage dose was small, other factors were considered when selecting the lower trimmer inner edge divergence angle. To maintain constancy in the in-field dose distribution with the "open field" inserts and the custom patient Cerrobend inserts, which have non-divergent inner edges, it was decided that the lower trimmer be made with non-divergent inner edges.

8.6. Aim 5 - Determine Optimal Applicator Geometry

Aim 5: Determine the optimal thickness, shape, and position of each trimmer bar, along with the photon jaw positions for each beam energy. These specifications will be selected such that the applicator weight is minimized while meeting leakage dose and beam flatness criteria.

8.6.1. Summary of Results

A pair of initial 10x10 and 20x20 cm^2 applicators was initially designed for 6 to 20 MeV beams using the simplistic design methodology of Hogstrom (1985). Composed of tungsten, the initial designs produced 10x10 and 20x20 cm^2 trimmer weights of 7.06 and10.87 kg, respectively, well exceeding the design goals of 5.00 and 7.10 kg, respectively.

- Impact of Specifying Field Size at Isocenter: By specifying the field size of these applicators at 100 cm SSD (isocenter) rather than 95 cm SSD, the 10x10 and 20x20 cm^2 trimmer weights were reduced approximately 3% to 6.87 and 10.49 kg, respectively.

- Impact of Beveling Outer Edge of Trimmer: The outer edges of each trimmer were design to have a bevel shape, reducing the 10x10 and 20x20 cm^2 trimmer weights approximately 15% to 5.86 and 9.04 kg, respectively.
- Impact of Optimizing z-Positions of Upper and Middle Trimmers: An optimization of trimmer weights was performed by varying the upper and middle trimmer *z*-positions, which revealed that the 10x10 cm^2 applicator upper and middle trimmers should be positioned at *z*-values of 61.0 and 77.0 cm, respectively, and the 20x20 cm^2 applicator upper and middle trimmers should be positioned at *z*-values of 61.5 and 77.5 cm. Doing so reduced the 10x10 and 20x20 cm^2 applicator weights approximately 5.5% to 5.52 and 8.62 kg, respectively.
- Impact of Optimizing Trimmer Inner Edge and z-Positions: Through a combination of analytical and MC modelling, the optimum inner edge positions were determined for each trimmer, which minimized the applicator weight while ensuring acceptable in-field beam flatness. This reduced the 20x20 cm^2 applicator trimmer weight to 7.73 kg, but marginally increased the 10x10 cm^2 applicator trimmer weight to 5.87 kg, which was necessary to ensure acceptable beam flatness.
- Optimization of Photon Jaw Positions: The photon jaws were moved toward central axis for higher energy beams. This both decreased the leakage dose outside the field and adjusted the upper trimmer bevel shape, reducing the 10x10 and 20x20 cm^2 applicator weights approximately 6% to 5.43 and 7.35 kg, respectively.
- Modifications to Trimmer Thickness and Bevel Shape: In the final design step, MC calculations were performed using 20x20 cm^2 applicator models modified such that their upper, middle, and lower trimmer thicknesses and bevel shapes were adjusted by varying amounts. Based on the results of these calculations, it was decided that the upper trimmer thickness be reduced by 50% and the middle and lower trimmer bevel shapes be modified, calculated with a 20 MeV fluence matching OAR of 50%. This reduced the 10x10 and 20x20 cm^2 applicator weights approximately 31% to 3.73 and 5.09 kg, respectively.

- Evaluation of In-Field Flatness and Out-of-Field for Final Applicator Design: MC-calculations were performed to evaluate the new collimation designs, revealing that the new designs produced acceptably flat beams within the field and acceptably low leakage outside the field for all beam energies. The 10x10 cm^2 model produced mean percent leakage doses of 0.58%, 0.63%, and 1.03% of D_{max} for the nominal 7, 13, and 20 MeV beams, respectively. The 20x20 cm^2 model produced mean percent leakage doses of 0.79%, 075%, and 1.11% for the nominal 7, 13, and 20 MeV beams, respectively.

8.6.2. Conclusions

- Evaluation of Collimation System Design Process in Achieving Hypothesized Goals: The results of the collimation system design process revealed that it was possible to develop 10x10 and 20x20 cm^2 applicators with trimmer weights (3.73 and 5.09 kg, respectively) significantly less than the Varian applicator trimmer weights of the same field sizes (5.00 and 7.10 kg, respectively), while meeting criteria for patient plane leakage dose and in-field beam flatness.

8.7. Aim 6 - Construct Prototype Applicator and Evaluate Prototype Collimating System

Aim 6: Fabricate prototypes of the newly designed 10x10 and 20x20 cm^2 applicators in order to evaluate the prototype collimation system. Off-axis profiles will be measured in a water phantom to evaluate the in-field beam flatness and leakage dose of the prototype collimation system, and the prototype applicators will be weighed to determine the reduction in weight from the current clinical applicator designs. Additionally, MC calculations will be performed to evaluate the leakage dose along the side of the applicator and to investigate the effects of altering the designated photon jaw positions on the patient plane dose distribution.

8.7.1. Summary of Results

- Measured Properties of Prototype Applicators in the Patient Plane: Prototype 10x10 and 20x20 cm^2 applicators were fabricated based on the designs developed in Aim 5 with trimmers composed of lead and aluminum, rather than tungsten, to allow the trimmers to be machined with the equipment available at the LSU Physics machine shop. These 10x10 and 20x20 cm^2

prototypes weighed 5.5 and 6.8 kg, respectively, significantly less than the current clinical Elekta full applicator weights of 7.7 and 10.9 kg and the Varian full applicator weights of 6.5 and 8.6 kg, respectively. Measurements confirmed that these prototype collimation systems passed in-field beam flatness criteria specified by Hogstrom (2004) and patient plane leakage dose criteria specified by the IEC (1998) for 7, 13, and 20 MeV beams.

- MC-Calculated Dose in the Patient Plane for 6x6, 14x14 and 25x25 cm^2 Applicator Models: 6x6, 14x14, and 25x25 cm^2 applicator models were created using the same design parameters used for the 10x10 and 20x20 cm^2 prototype applicators. These models had trimmer weights of 2.79, 4.15, and 5.91 kg, respectively. MC calculations revealed that these applicator models produced acceptable in-field beam flatness and out-of-field leakage dose for the 7, 13, and 20 MeV beams.
- MC-Calculated Leakage Dose Lateral to Applicator: MC calculations revealed that the leakage dose 2 cm outside the volume contained by the 10x10 and 20x20 cm^2 applicator was less than 4.3% of D_{max} for the 7, 13, and 20 MeV beams, well below the IEC specified limit of 10.00%.
- Impact of Photon Jaw Position Changes on In-Field Beam Flatness and Leakage Dose: A MC study was performed analyzing the effect on the patient plane dose distribution of modifying the 20x20 cm^2 applicator jaw positions from those specified for each beam energy. The results revealed that moving either the in-plane or cross-plane jaw 0.5 cm (1.0 and 1.2 cm projected to isocenter for the in-plane and cross-plane jaws, respectively) towards central axis caused the 7, 13, and 20 MeV beams to fail in-field flatness criteria. The results also revealed that moving the in-plane or cross-plane jaw 0.5 cm away from central axis caused the 20 MeV beam to fail patient plane mean percent leakage dose criteria.

8.7.2. Conclusions

- Evaluation of Prototype Applicator: Fabrication and measurement validate that the prototype collimation systems designed in Aim 5 sufficiently reduced the applicator weight and produced acceptable in-field beam flatness and leakage dose, both at patient plane and along the side of the applicator, for the 7, 13, and 20 MeV beams.

- MC Evaluation of 6x6, 14x14, and 25x25 cm^2 Applicators: 6x6, 14x14, and 25x25 cm^2 applicator models designed with the same parameters used for the 10x10 and 20x20 cm^2 prototype applicator designs produced sufficient trimmer weight reduction and acceptable MC-calculated in-field beam flatness and out-of-field leakage dose.
- Importance of Photon Jaw Position: Care should be taken when adjusting the jaw positions from those specified in the collimation system design to ensure that the adjustments do not cause the beams to fail in-field flatness or out-of-field leakage dose criteria.

8.8. Overall Conclusions and Recommendations for Future Work

8.8.1. Response to Hypothesis

Within this investigation, prototype 10x10 and 20x20 cm^2 electron collimation systems were designed and fabricated with applicator trimmer weights of 3.66 and 4.95 kg, respectively, significantly less than the hypothesized goals of 5.00 and 7.10 kg. These prototypes were evaluated via both MC-calculations and beam measurements to reveal that the collimation systems met criteria for both patient plane leakage dose as specified by the IEC (1998) and in-field beam flatness as specified by Hogstrom (2004), proving the hypothesis.

8.8.2. Recommendations for New Electron Collimation System

- The new collimation system should be limited to 6 to 20 MeV electron beams.
- The applicator field sizes should be specified at isocenter, rather than 95 cm SSD, to reduce the applicator weight and comply with convention within the industry.
- The downstream surfaces of the upper, middle, and lower trimmers should be positioned at *z*-values of 66, 79, and 95 cm for all applicators.
- A unique photon jaw position should be specified for each beam based on $E_{p,0}$ and field size (decreasing off-axis position with increasing beam energy and decreasing field size). Adjustments in off-axis jaw position greater than 1 cm at isocenter should not be made. Should greater adjustments be desirable, this could be accomplished with the current design by increasing the width of only the upper trimmer bars, e.g. increasing to allow a 3 cm adjustment at isocenter,

which would increase the weight of the 20x20 cm^2 applicator by approximately 0.8 kg. If any jaw position adjustments are made, acceptable in-field flatness and leakage dose should be verified.

- Though the prototype applicator trimmers were fabricated out of a combination of lead and aluminum, it is recommended that the new applicator trimmers be made of tungsten if machining capabilities allow.
- Based on the results of this study and LeBlanc (2012), any planned changes to the collimation system should be done concurrently with the dual scattering foil system and photon jaw settings (auto-tracking system) due to their interdependence.

8.8.3. Recommendations for Additional Physics Studies

8.8.3.1. Further Investigation into Origin of Leakage from Collimation Interactions

Within this study, the LATCH bit filtering feature of EGSnrc was used on several occasions to calculate the dose at patent plane from electrons scattered from the individual collimation components. Within this process, electrons which enter the collimation component and scatter out the edge are not distinguished from electrons created by bremsstrahlung photons undergoing photoelectric, Compton, or pair production interactions within the collimation component material. Additional investigations should be performed to determine the portion of the scattered electron dose at patient plane which originates from each of these two processes.

8.8.3.2. Additional Measurements for Prototype Applicators

In addition to patient plane measurements, out-of-field leakage dose lateral to the applicator should be measured to confirm the MC results in Section 7.3.3. However, because these MC calculated lateral dose maxima were significantly lower than the IEC allowed maximum of 10% of D_{max}, this is not considered a high priority.

8.8.3.3. Assessment of In-field Flatness and Out-of-Field Leakage Dose for Agility Treatment Head

The present study and applicator designs were completed for the MLCi2 treatment head. MC calculations and measurements should be repeated for the current and newly designed 10x10 and 20x20

cm^2 applicators using the Agility treatment head to compare the in-field flatness and out-of-field leakage doses for the two treatment heads. The Agility photon jaw collimating edges, having greater area for the inner edges of the curved cross-plane collimators (the result of replacing the jaw with the MLC) and replacing the diverging inner edge of the in-plane photon jaw with a curved inner edge, could generate leakage dose exceeding IEC specified limits.

8.8.3.4. Effects of Order of Lead and Aluminum Plates for Applicator Assembly on Leakage Dose

The results from Aim 3 of our investigation revealed that modelling the trimmers out of high density materials, e.g. lead or tungsten, reduced the leakage dose due to the decreased electron scatter from the trimmers for all beam energies. However, a study by Olsson (2003) reported that positioning an aluminum plate upstream of the lead plate reduced the leakage dose from the current 10x10 cm^2 applicator with a 20 MeV beam, presumably due to a decrease in bremsstrahlung dose. This warrants further investigation.

8.8.3.5. Depth Dependence of Out-of-Field Dose

The leakage dose outside the field was evaluated in this investigation at 1 cm depth in water to be consistent with IEC specifications. However, the risk of adverse effects due to collimation leakage is dependent not only on the dose near the surface, but also at depths greater than 1 cm. Yeboah *et al.* (2010) investigated the dose at depth in water outside the field of electron beams of a Siemens Primus accelerator, showing that the dose decreased fairly linearly with depth at a rate of roughly 0.5% of D_{max} per cm. To fully analyze the effect of leakage dose of the Elekta electron collimation system, a similar study should be performed to determine the leakage dose at depth.

8.8.3.6. Impact of Out-of-Field Dose on Secondary Cancer and Future IEC Regulations

While the collimation systems designed in this study were shown to meet leakage dose acceptance criteria, the probability of these low doses causing adverse biological effects, such as a secondary cancer or alopecia (Wen *et al.*, 1989), was not investigated. Further analysis should be performed to quantify the risks of these low leakage doses. Ideally, the IEC criteria for leakage dose

should reflect these risks, as suggested by Morgan *et al.* (1993) in which a set of leakage dose limits based on a secondary cancer risk model was proposed.

References

Bethe H. and Ashkin J. 1953. *Experimental Nuclear Physics.* vol 1. (New York: John Wiley and Sons).

Cardenas C., Nitsch P., Kudchadker R., Howell R. and Kry S. 2015. An Evaluation of out-of-Field Doses for Electron Beam Applicators on Varian and Elekta Linear Accelerators. In: *AAPM Annual Meeting.* (Houston, TX

Carver R. L., Hogstrom K., Price M., LeBlanc J. and Pitcher G. 2014. Real-Time Simulator for Designing Electron Dual Scattering Foil Systems. *J App Clin Med Phys.* 15. 323-42.

Choi M. C., Purdy J. A., Gerbi B., Abrath F. G. and Glasgow G. P. 1979. Variation in Output Factor Caused by Secondary Blocking for 7-16 Mev Electron Beams. *Med Phys.* 6. 137-9.

Chow J. C. L. and Grigorov G. N. 2006. Peripheral Dose Outside Applicators in Electron Beams. *Phys Med Biol.* 51. N231.

Das K. R., Cramb J. A., Millar R. M., *et al.* 1990. Levels of Leakage Radiation from Electron Collimators of a Linear Accelerator. *Med Phys.* 17. 1058-63.

Deasy J. O., Almond P. R. and McEllistrem M. T. 1996. Measured Electron Energy and Angular Distributions from Clinical Accelerators. *Med Phys.* 23. 675-84.

Ebert M. A. and Hoban P. W. 1995a. A Model for Electron-Beam Applicator Scatter. *Med Phys.* 22. 1419-29.

Ebert M. A. and Hoban P. W. 1995b. A Monte Carlo Investigation of Electron-Beam Applicator Scatter. *Med Phys.* 22. 1431-5.

Gerbi B. J., Antolak J. A., Deibel F. C., *et al.* 2009. Recommendations for Clinical Electron Beam Dosimetry: Supplement to the Recommendations of Task Group 25. *Med Phys.* 36. 3239-79.

Giarratano J. C., Duerkes R. J. and Almond P. R. 1975. Lead Shielding Thickness for Dose Reduction of 7- to 28-Mev Electrons. *Med Phys.* 2. 336-7.

Harris G. 2012. Development and Validation of an Electron Monte Carlo Model for the Elekta Infinity Accleterator. Masters Thesis. (Baton Rouge, Louisiana: *Physics and Astronomy*. Louisiana State University).

Hogstrom K. 2004. *Principals and Practice of Radiation Oncology.* ed C A Perez, *et al.* (Philidelphia, PA.: Lippincott Williams and Wilins). pp 252-82.

Hogstrom K., Meyer J. and Melson R. 1985. Variable Electron Collimator for the Mevatron 77: Design and Dosimetry. In: *Proceedings of the 1985 Mevatron Users Conference.* (Iselin, New Jersey: Siemens Medical Systems). pp 251-75.

Hogstrom K. R. 1991a. Clinical Electron Beam Dosimetry: Basic Dosimetry Data. In: *Advances in Radiation Oncology Physics - 1990 Proceedings of the Summer School of the AAPM.* ed J Purdy (Lawrence, Kansas: American Institute of Physics). pp 390-429.

Hogstrom K. R. 1991b. *Frontiers of Radiation Therapy an Oncology.* ed J M Vaeth and J L Meyer. (San Francisco: Karger). pp 30-52.

Hogstrom K. R., Boyd R. A., Antolak J. A., *et al.* 2004. Dosimetry of a Prototype Retractable Emlc for Fixed-Beam Electron Therapy. *Med Phys.* 31. 443.

Hogstrom K. R., Boyer A. L., Shiu A. S., *et al.* 1990. Design of Metallic Electron Beam Cones for an Intraoperative Therapy Linear Accelerator. *Int J Radiat Oncol Biol Phys.* 18. 1223-32.

Hogstrom K. R., Mills M. D. and Almond P. R. 1981. Electron Beam Dose Calculations. *Phys Med Biol.* 26. 445.

Hogstrom K. R., Rosen I. I., Gelfand E., *et al.* 1980. Calculation of Pion Dose Distributions in Water. *Med Phys.* 7. 703-9.

Hough P. V. C. 1948. The Angular Distribution of Pair-Produced Electrons and Bremsstrahlung. *Phys Rev.* 74. 80-6.

Huizenga H. and Storchi P. R. M. 1987. The in-Air Scattering of Clinical Electron Beams as Produced by Accelerators with Scanning Beams and Diaphragm Collimators. *Phys Med Biol.* 32. 1011.

International Electrotechnical Commission. 1998. Medical Electrical Equipment- Part 2-1: Particular Requirements for the Safety of Electron Accelerators in the Range 1mev to 50mev. *IEC 60601-2-1*.

Kassaee A., Altschuler M. D., Ayyalsomayajula S. and Bloch P. 1994. Influence of Cone Design on the Electron Beam Characteristics on Clinical Accelerators. *Med Phys.* 21. 1671-6.

Kawrakow I., Mainegra-Hing E., Rogers D. W. O., Tessier F. and Walters B. R. B. 2011. The Egsnrc Code System: Monte Carlo Simulation of Electron and Photon Transport. *Technical Report PIRS-701*. National Research Cancil of Canada (NRCC).

Keys R. A. and Purdy J. A. 1984. Radiation Leakage from Linac Electron Applicator Assembly. *Int J Radiat Oncol Biol Phys.* 10. 713-21.

Khan F. 2003. *The Physics of Radiation Therapy.* (Philadelphia, PA: Lippincott Williams and Wilkins).

Khan F. M., Doppke K. P., Hogstrom K. R., *et al.* 1991. Clinical Electron-Beam Dosimetry: Report of Aapm Radiation Therapy Committee Task Group No. 25. *Med Phys.* 18. 73-109.

Khan F. M., Moore V. C. and Levitt S. H. 1976. Field Shaping in Electron Beam Therapy. *Br J Radiol.* 49. 883-6.

Khan F. M., Werner B. L. and Deibel F. C. 1981. Lead Shielding for Electrons. *Med Phys.* 8. 712-3.

Klein E. E., Low D. A. and Purdy J. A. 1995. Changes in Electron Beam Dosimetry with a New Scattering Foil-Applicator System on a Cl2100c. *Int J Radiat Oncol Biol Phys.* 32. 483-90.

Lax I. and Brahme A. 1980. Collimation of High Energy Electron Beams. *Acta Radiol Oncol.* 19. 199-207.

LeBlanc J. D. 2012. Design of Electron Dual Foil Scattering Systems for Elekta Infinity Radiotherapy Accelerators. Masters Thesis. (Baton Rouge, Louisiana: *Physics and Astronomy*. Louisiana State University).

McLaughlin D. 2013. Energy Spectra Comparisons for Matched Clinical Electron Beams on Elekta Linear Accelerators Using a Permanent Magnet Spectrometer. Masters Thesis. (Baton Rouge: *Physics and Astronomy*. Louisiana State University).

Meyer J. A., Palta J. R. and Hogstrom K. R. 1984. Demonstration of Relatively New Electron Dosimetry Measurement Techniques on the Mevatron 80. *Med Phys.* 11. 670-7.

Morgan H. M., Lillicrap S. C. and McKenzie A. L. 1993. Technical Note: Leakage Radiation in Radiotherapy-What Is an Acceptable Level in Electron Mode? *Br J Radiol.* 66. 548-51.

Olsson M.-L. 2003. Monte Carlo Simulations of the Elekta Sli Plus Electron Applicator System - a Base for a New Applicator Design to Reduce Radiation Leakage. Masters Thesis. (Lund, Sweden: *Department of Radiation Physics*. Lund University Hospital).

Pennington E. C., Jani S. K. and Wen B.-C. 1988. Leakage Radiation from Electron Applicators on a Medical Accelerator. *Med Phys.* 15. 763-5.

Perec A. and Kubo H. 1990. Radiation Leakage through Electron Applicators on Clinac-1800 Accelerators. *Med Phys.* 17. 715-9.

Prasad S. G., Parthasaradhi K., Bloomer W. D., *et al.* 1998. Aluminum, Copper, Tin and Lead as Shielding Materials in the Treatment of Cancer with High-Energy Electrons. *Radiat Phys and Chem.* 53. 361-6.

Purdy J. A., Choi M. C. and Feldman A. 1980. Lipowitz Metal Shielding Thickness for Dose Reduction of 6–20 Mev Electrons. *Med Phys.* 7. 251-3.

Rogers D. W. O., Walters B. and Kawrakow I. 2011. Beamnrc Users Manual. National Research Council of Canada.

Schiff L. I. 1946. Energy-Angle Distribution of Betatron Target Radiation. *Phys Rev.* 70. 87-.

Schneider A. J. 1982. Radiation Leakage from Electron Applicator Assembly on a Linear Accelerator. *Med Phys.* 9. 761-2.

Shimozato T., Okudaira K., Fuse H. and Tabushi K. 2012. Monte Carlo Simulation and Measurement of Radiation Leakage from Applicators Used in External Electron Radiotherapy. *Phys Med.* 29. 388-96.

Shiu A. S., Tung S. S., Nyerick C. E., *et al.* 1994. Comprehensive Analysis of Electron Beam Central Axis Dose for a Radiotherapy Linear Accelerator. *Med Phys.* 21. 559-66.

Storchi P. R. M. and Huizenga H. 1985. On a Numerical Approach of the Pencil Beam Model. *Phys Med Biol.* 30. 467.

Tapley N. D. 1976. *Clinical Applications of the Electron Beam.* (New York: Wiley Biomedical).

Walters B., Kawrakow I. and Rogers D. W. O. 2011. Dosxyznrc Users Manual. National Research Council of Canada.

Wen B. C., Pennington E. C., Hussey D. H. and Jani S. K. 1989. Alopecia Associated with Unexpected Leakage from Electron Cone. *Int J Radiat Oncol Biol Phys.* 16. 1637-41.

Werner B. L., Khan F. M. and Deibel F. C. 1982. A Model for Calculating Electron Beam Scattering in Treatment Planning. *Med Phys.* 9. 180-7.

Whycoff H. O., A. Allisy R. S. C. and Adams G. E. D. 1984. Radiation Dosimetry: Electron Beams with Energies between 1 and 50 Mev. *35.* (Bethesda, Maryland). ICRU.

Yeboah C., Karaotki A., Hunt D. and Holly R. 2010. Quantification and Reduction of Peripheral Dose from Leakage Radiation on Siemens Primus Accelerators in Electron Therapy Mode. *J App Clin Med Phys.* 11.

Appendix A -Supplemental Figures for Aim 2

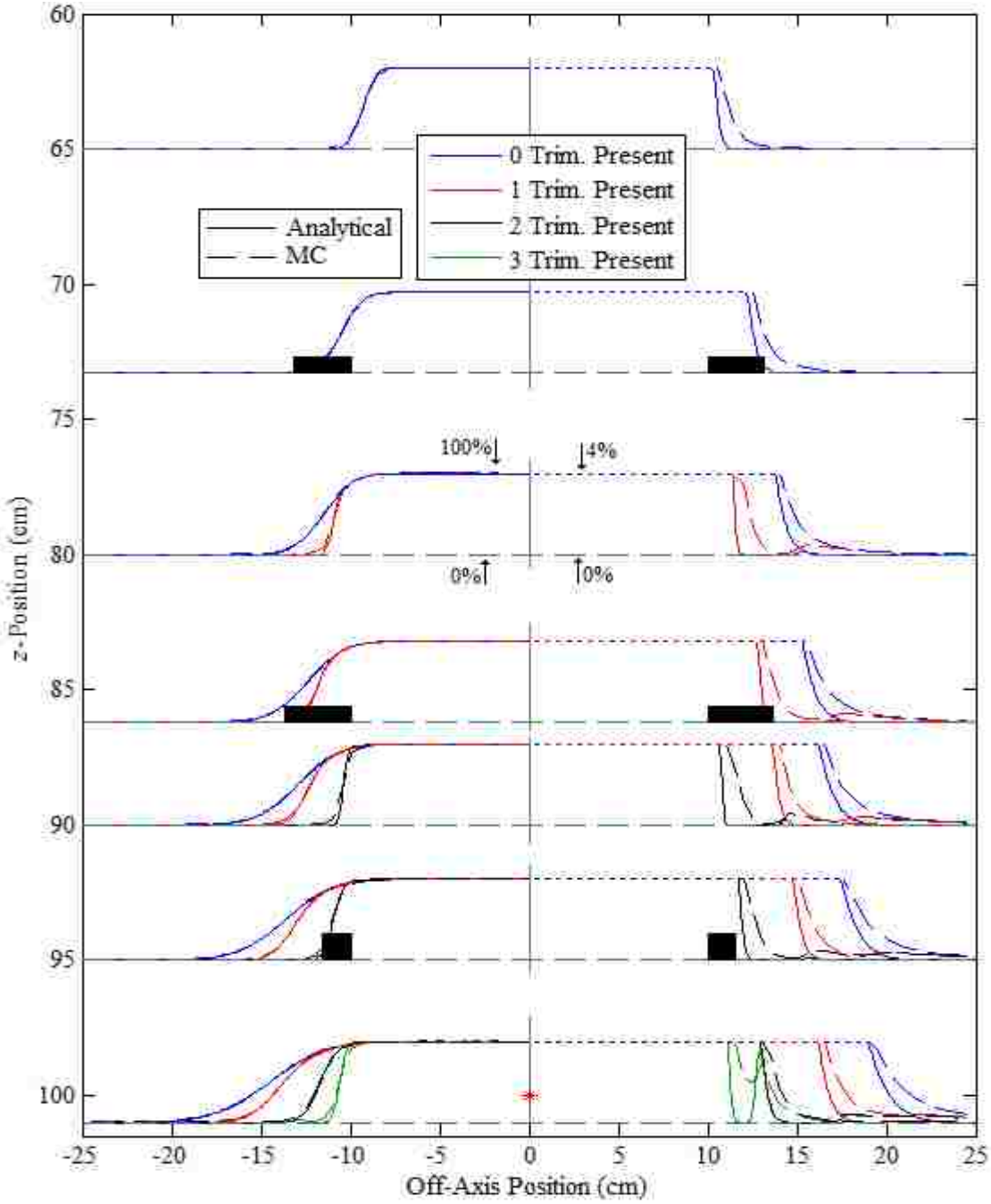

Figure A-1. Full in-plane primary electron dose profile comparisons of analytical and MC calculations for the 20x20 cm^2 applicator with a monoenergetic 7 MeV beam. The figure shows a cross-sectional view of the 20x20 cm^2 applitor with the relative dose profiles calculated at various heights. The left side of the figure (negative off-axis positions) shows plots of the full magnitude of the profiles, with the cenral axis dose (off-axis position = 0) corresponding to 100% of the dose and the dashed base line corresponding to 0%. The right side of the figure (positive off-axis positions) magnifies the same profiles showing the low dose region to more clearly see the behavior of the leakage dose. In this region, a the maximum dose plotted is 4% of central-axis dose.

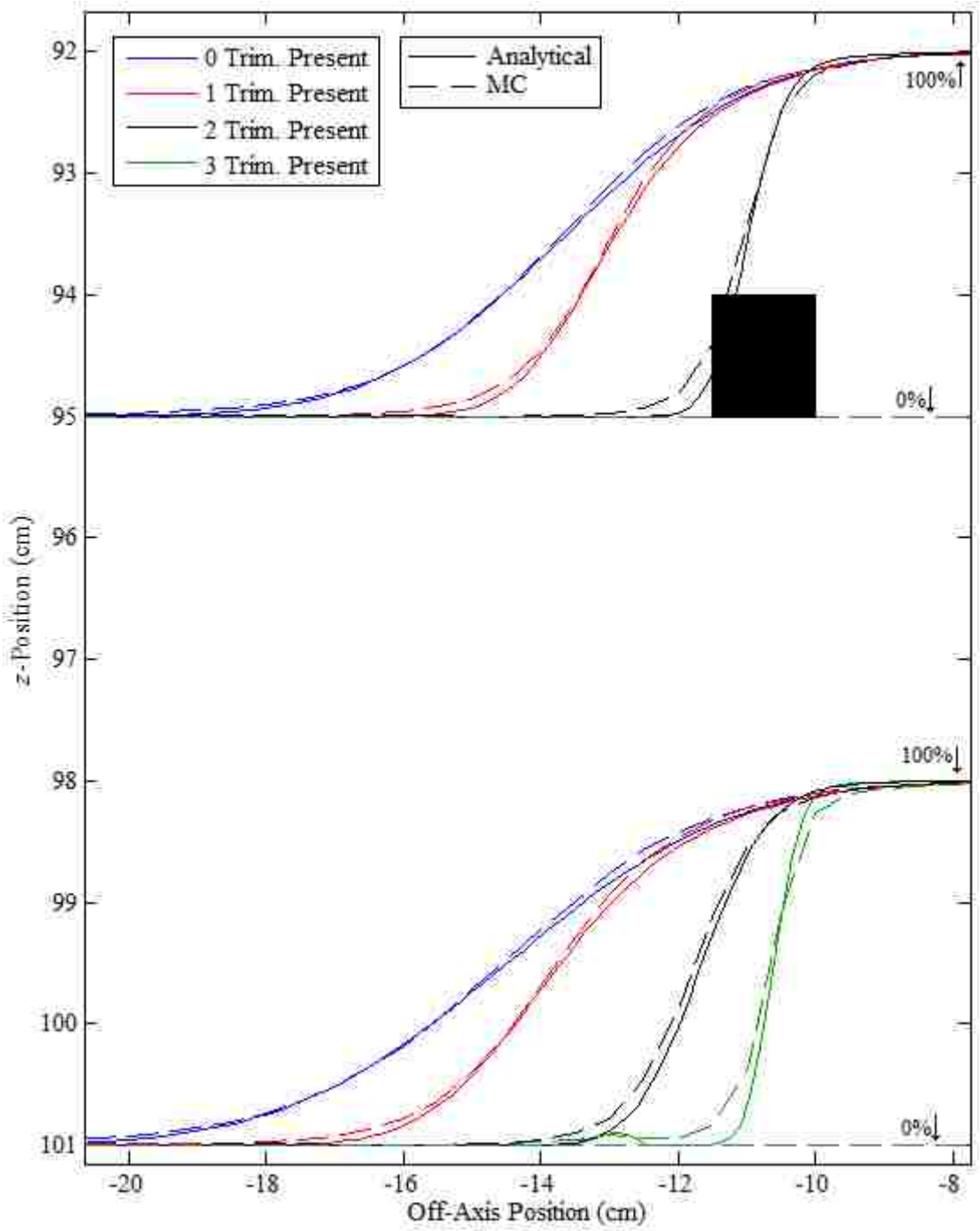

Figure A-2. In-plane primary electron dose profile comparisons of analytical and MC calculations for the 20x20 cm^2 applicator with a monoenergetic 7 MeV beam in the penumbral fall-off region. The figure shows a cross-sectional view of the 20x20 cm^2 applitor with the relative dose profiles calculated at *z*-positions of 95 and 101 cm. The plot shows the full magnitude of the dose profiles with in-field region of the plots corresponding to 100% of the central-axis dose and the dashed base line corresponding to 0%.

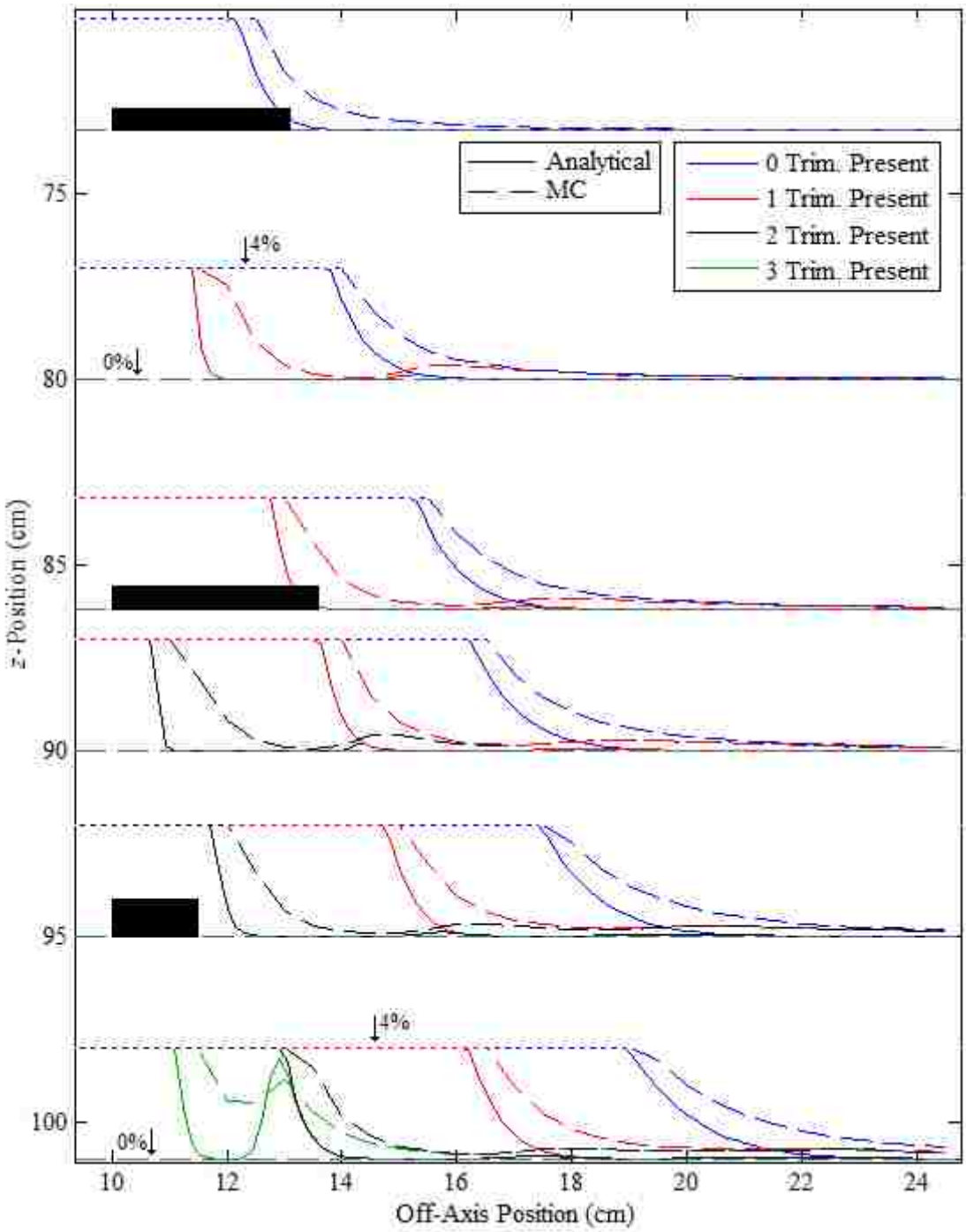

Figure A-3. In-plane primary electron dose profile comparisons of analytical and MC calculations for the 20x20 cm^2 applicator with a monoenergetic 7 MeV beam in the low dose leakage region The figure shows a cross-sectional view of the 20x20 cm^2 applitor with the relative dose profiles calculated at various heights. The plot shows the profiles magnified to highlight the low dose region with the horizontal short-dashed line corresponding to 4% of the central-axis dose and the horizontal long-dashed base line corresponding to 0%.

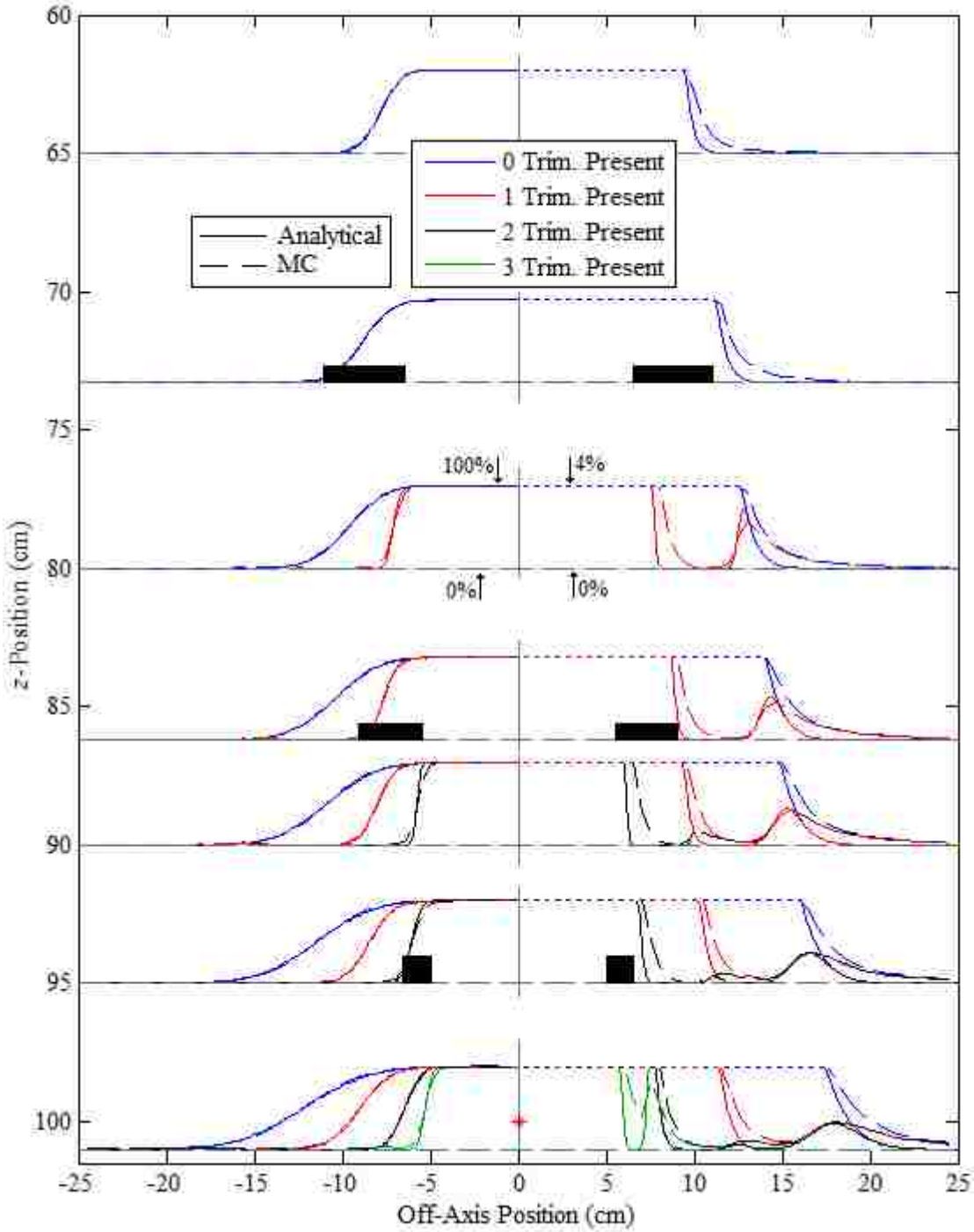

Figure A-4. Full cross-plane primary electron dose profile comparisons of analytical and MC calculations for the 10x10 cm^2 applicator with a monoenergetic 7 MeV beam. The figure shows a cross-sectional view of the 10x10 cm^2 applitor with the relative dose profiles calculated at various heights. The left side of the figure (negative off-axis positions) shows plots of the full magnitude of the profiles, with the cenral axis dose (off-axis position = 0) corresponding to 100% of the dose and the dashed base line corresponding to 0%. The right side of the figure (positive off-axis positions) magnifies the same profiles showing the low dose region to more clearly see the behavior of the leakage dose. In this region, a the maximum dose plotted is 4% of central-axis dose.

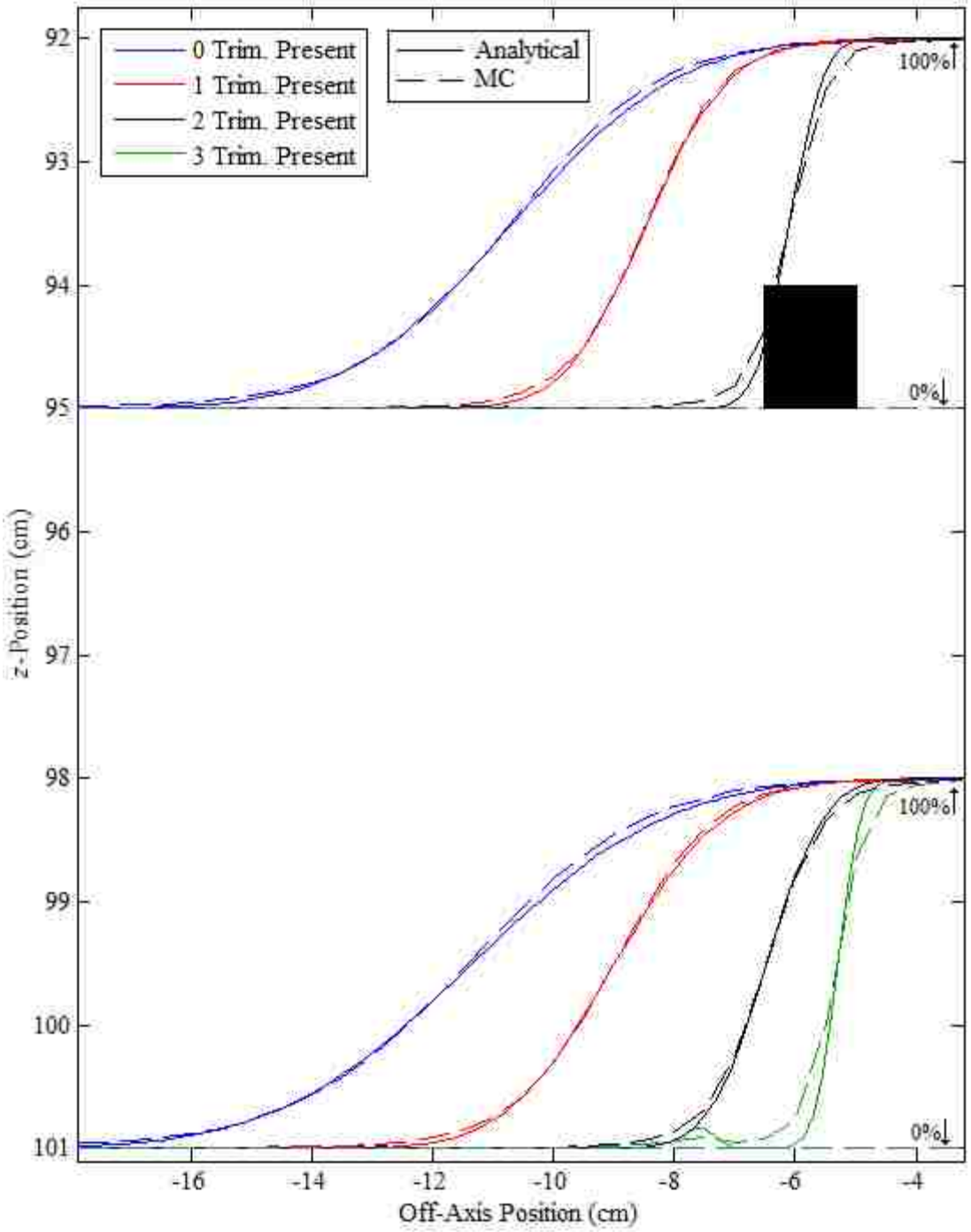

Figure A-5. Cross-plane primary electron dose profile comparisons of analytical and MC calculations for the 10x10 cm^2 applicator with a monoenergetic 7 MeV beam in the penumbral fall-off region. The figure shows a cross-sectional view of the 10x10 cm^2 applitor with the relative dose profiles calculated at *z*-positions of 95 and 101 cm. The plot shows the full magnitude of the dose profiles with in-field region of the plots corresponding to 100% of the central-axis dose and the dashed base line corresponding to 0%.

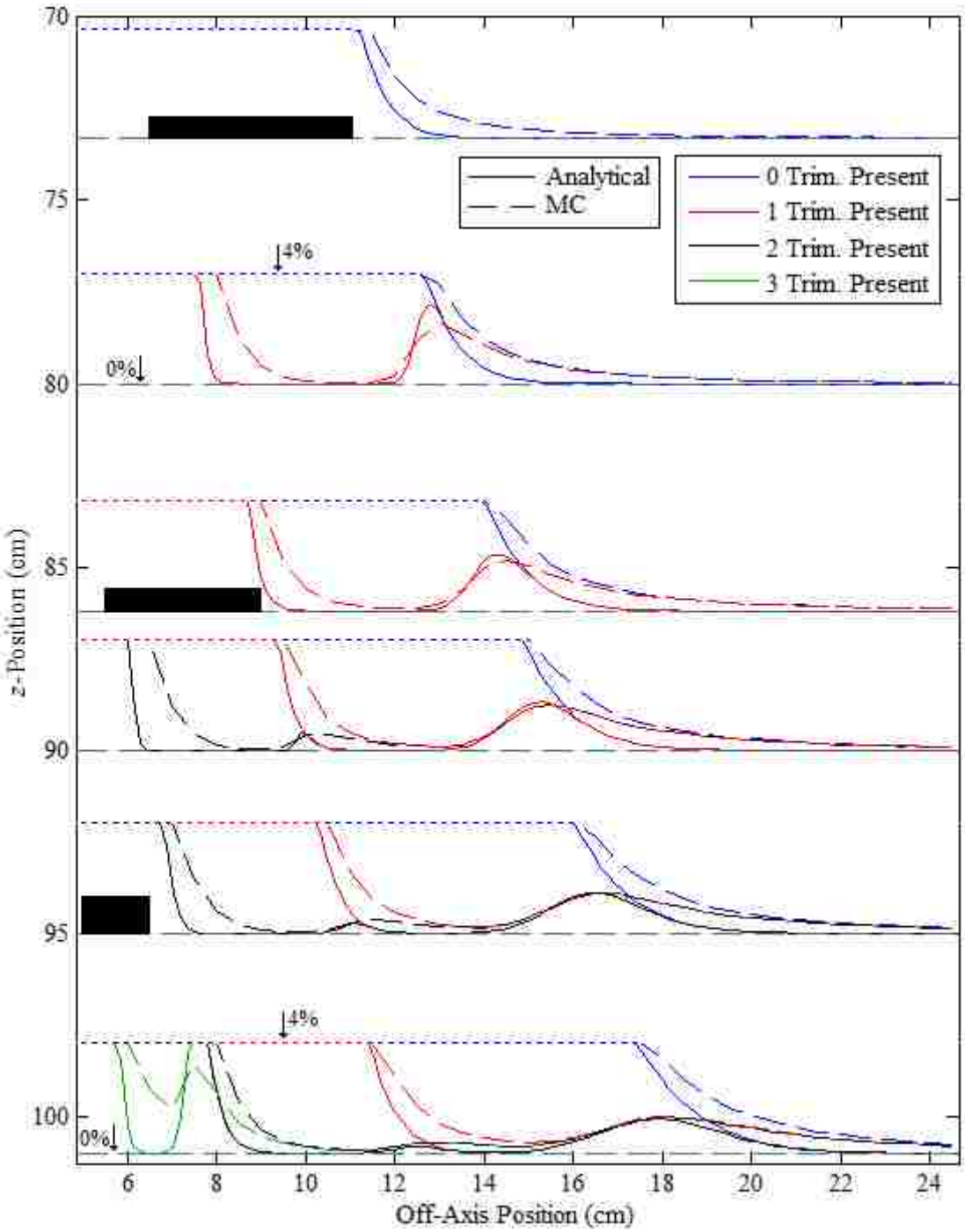

Figure A-6. Cross-plane primary electron dose profile comparisons of analytical and MC calculations for the 10x10 cm^2 applicator with a monoenergetic 7 MeV beam in the low dose leakage region The figure shows a cross-sectional view of the 10x10 cm^2 applitor with the relative dose profiles calculated at various heights. The plot shows the profiles magnified to highlight the low dose region with the horizontal short-dashed line corresponding to 4% of the central-axis dose and the horizontal long-dashed base line corresponding to 0%.

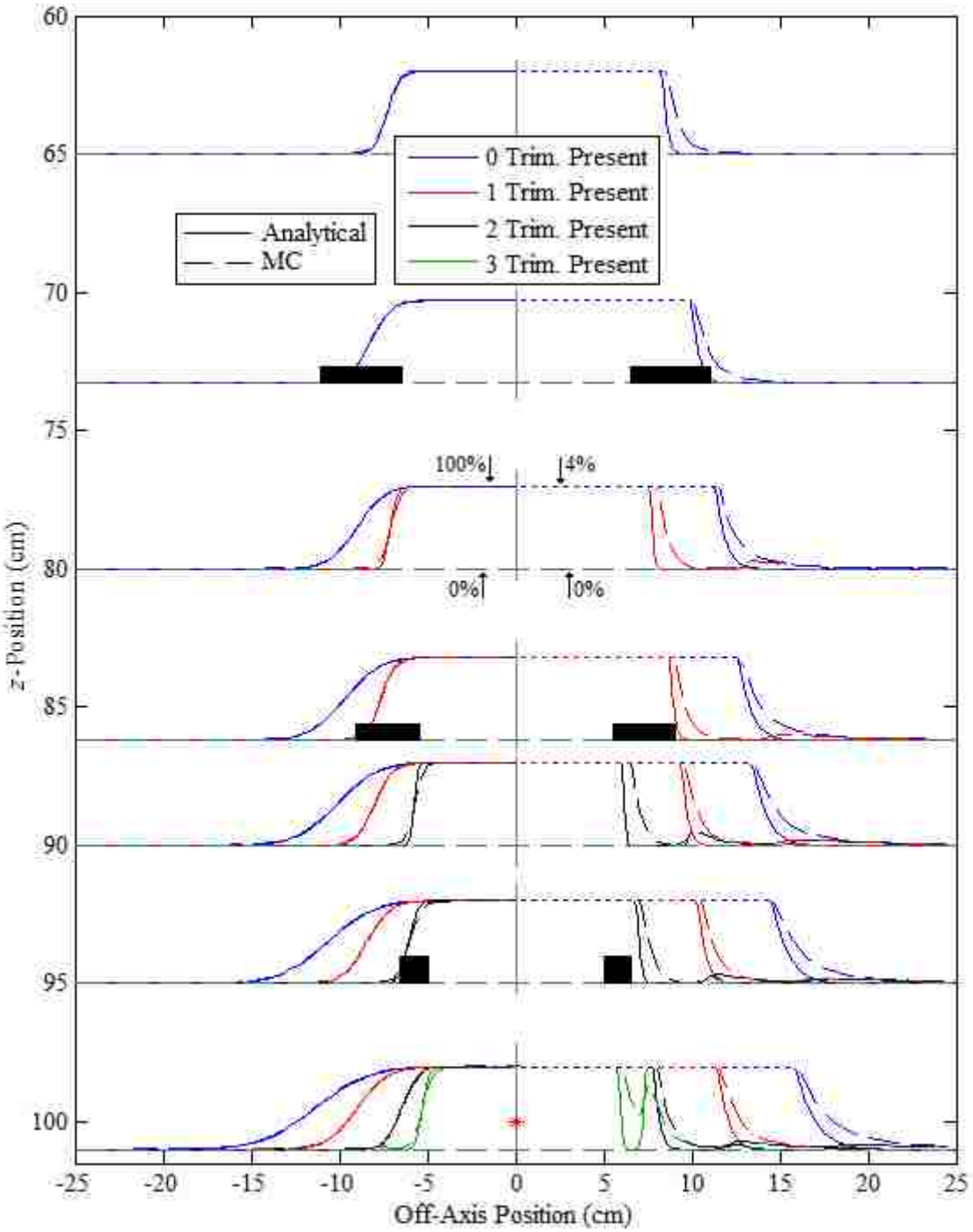

Figure A-7. Full in-plane primary electron dose profile comparisons of analytical and MC calculations for the 10x10 cm^2 applicator with a monoenergetic 7 MeV beam. The figure shows a cross-sectional view of the 10x10 cm^2 applitor with the relative dose profiles calculated at various heights. The left side of the figure (negative off-axis positions) shows plots of the full magnitude of the profiles, with the cenral axis dose (off-axis position = 0) corresponding to 100% of the dose and the dashed base line corresponding to 0%. The right side of the figure (positive off-axis positions) magnifies the same profiles showing the low dose region to more clearly see the behavior of the leakage dose. In this region, a the maximum dose plotted is 4% of central-axis dose.

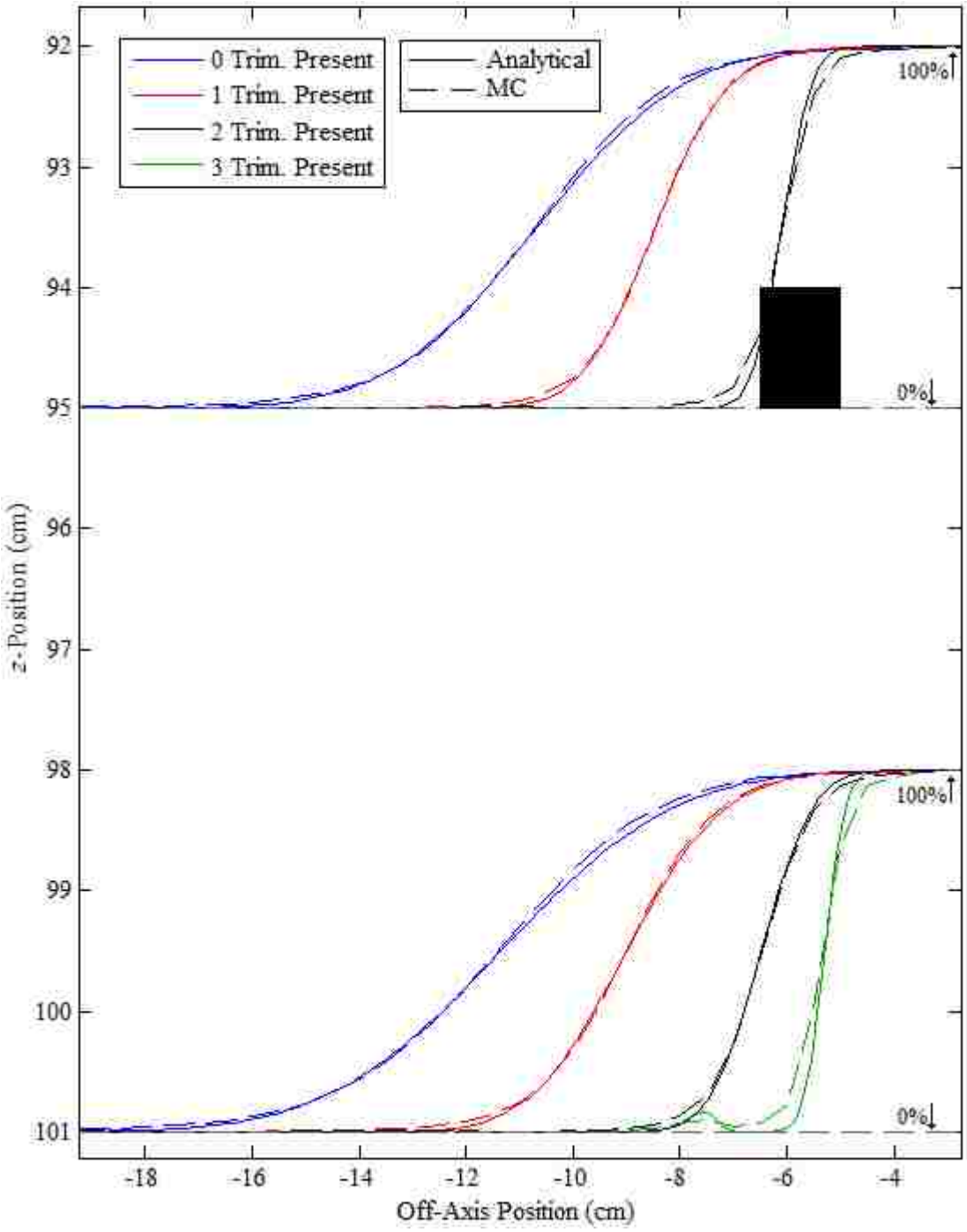

Figure A-8. In-plane primary electron dose profile comparisons of analytical and MC calculations for the 10x10 cm^2 applicator with a monoenergetic 7 MeV beam in the penumbral fall-off region. The figure shows a cross-sectional view of the 10x10 cm^2 applitor with the relative dose profiles calculated at *z*-positions of 95 and 101 cm. The plot shows the full magnitude of the dose profiles with in-field region of the plots corresponding to 100% of the central-axis dose and the dashed base line corresponding to 0%.

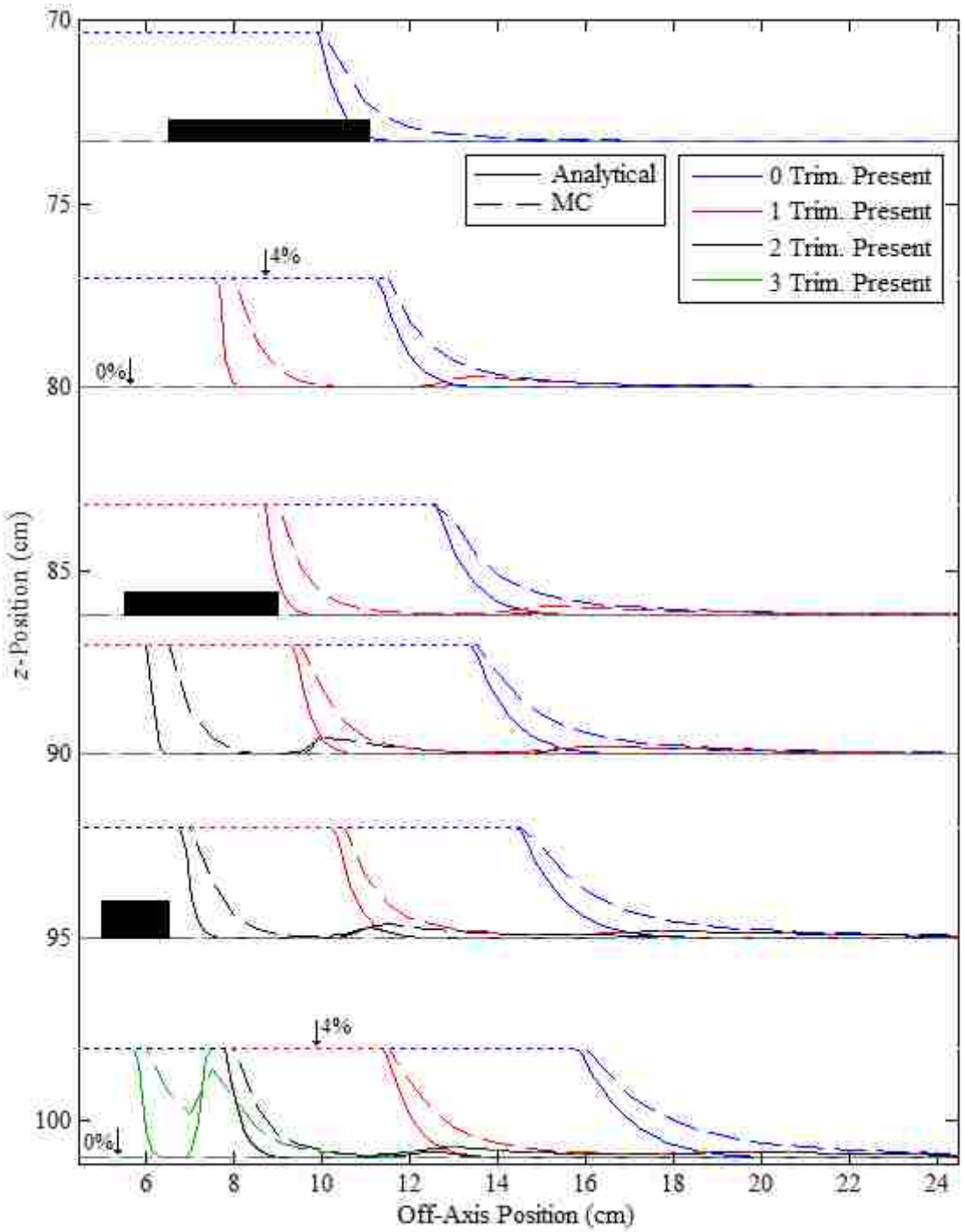

Figure A-9. In-plane primary electron dose profile comparisons of analytical and MC calculations for the 10x10 cm^2 applicator with a monoenergetic 7 MeV beam in the low dose leakage region. The figure shows a cross-sectional view of the 10x10 cm^2 applitor with the relative dose profiles calculated at various heights. The plot shows the profiles magnified to highlight the low dose region with the horizontal short-dashed line corresponding to 4% of the central-axis dose and the horizontal long-dashed base line corresponding to 0%.

Appendix B -Supplemental Figures for Aim 3

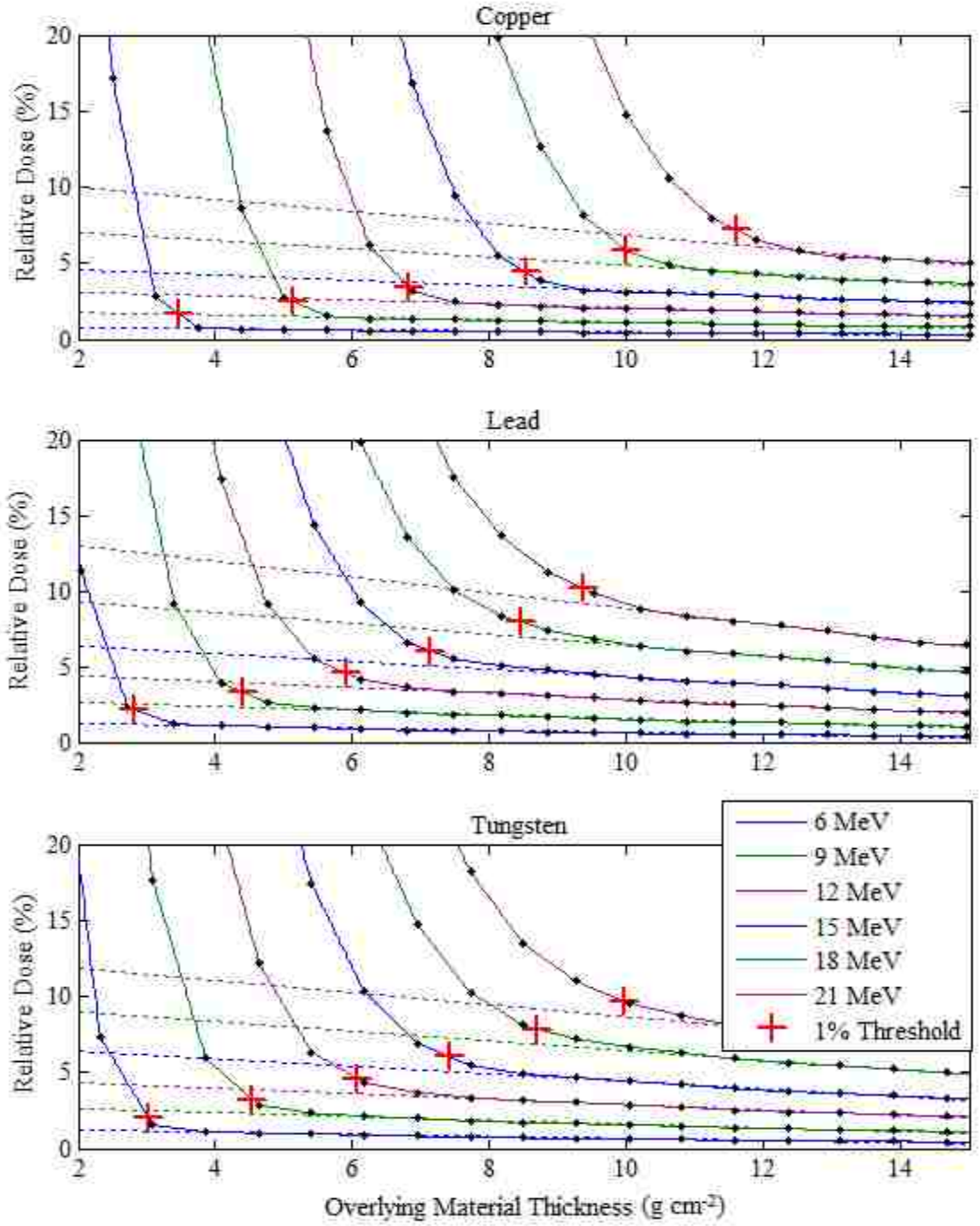

Figure B-1. Comparison of calculated relative dose (% of D_{max}) versus material thickness in the low dose region. This figure plots the relative dose calculated immediately beyond various thicknesses of material in water for various energy beams. The dose falls off to a linear photon region which is extrapolated and shown as the dashed lines. The 1% threshold marker represents where the dose diverges from this linear region by 1% of the total dose with no material present.

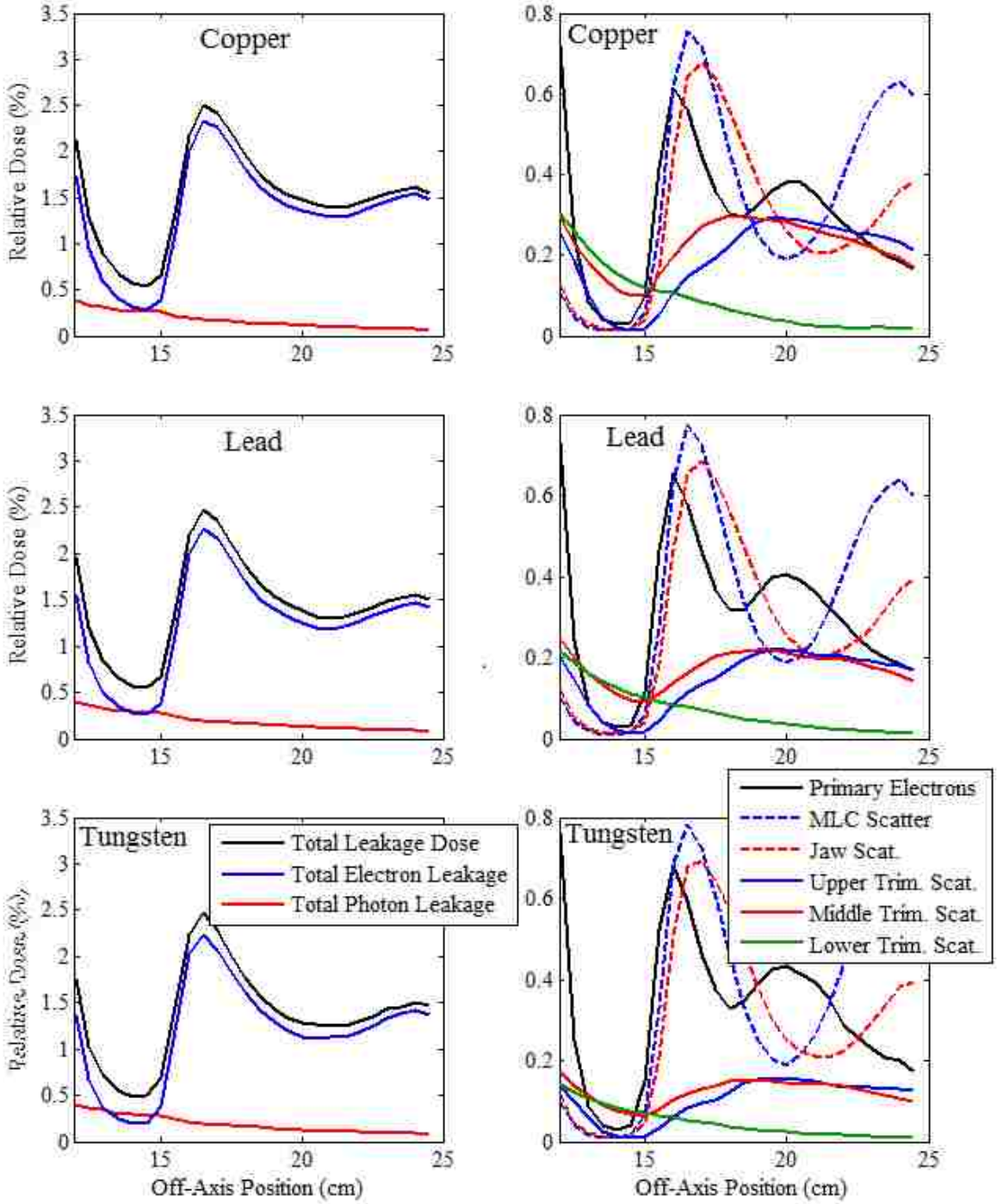

Figure B-2. Cross-plane leakage dose component profiles for copper, lead and tungsten 20x20 cm^2 applicators for the 7 MeV beam. The copper profiles are shown on the top row, lead in the middle, and tungsten profiles on the bottom row. The left column of plots shows a breakdown of the total leakage dose (black) along with the differentiated electron (blue) and photon components (red). The right column further breaks down the electron leakage dose into primary electrons and various scattered electron components.

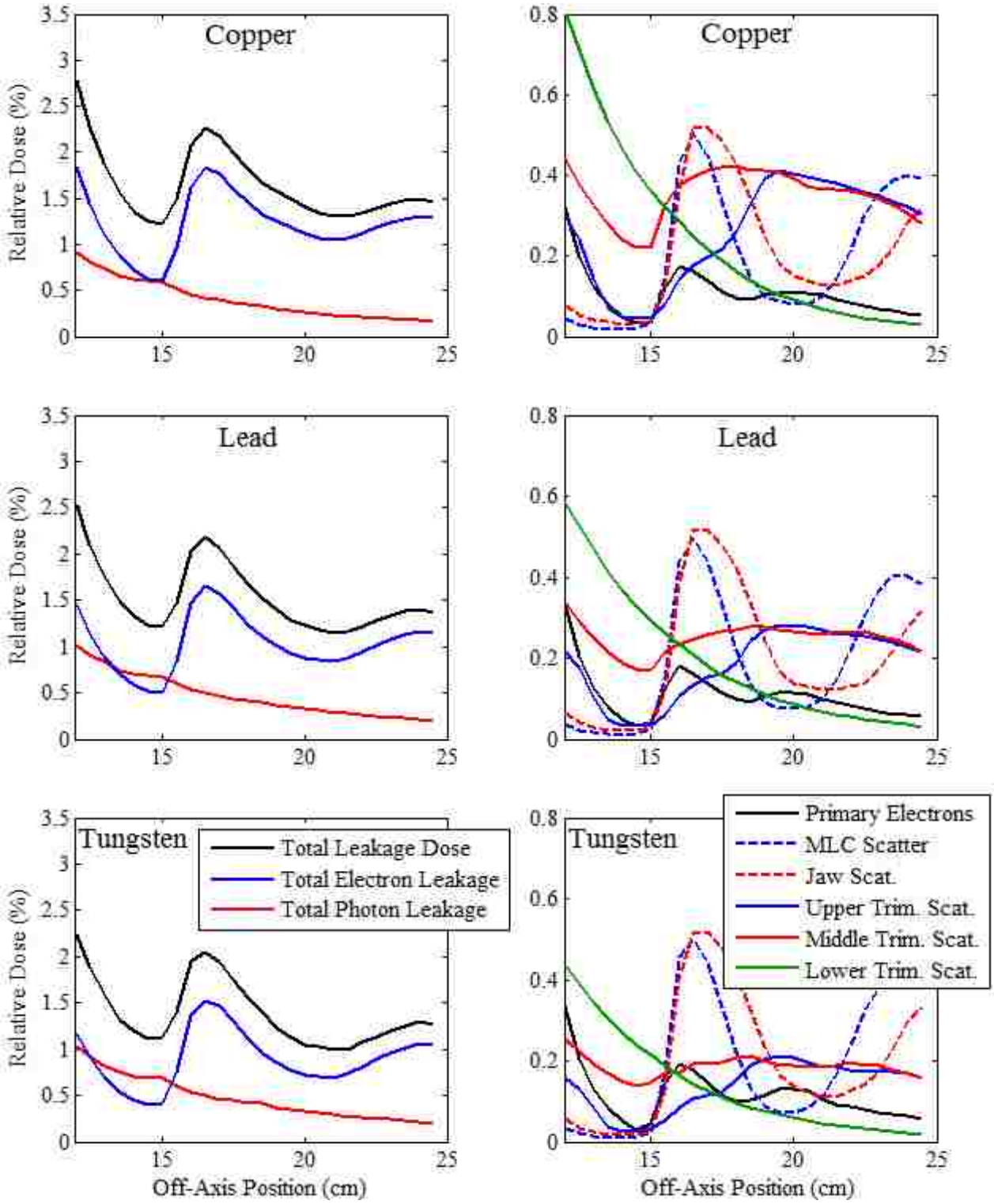

Figure B-3. Cross-plane leakage dose component profiles for copper, lead and tungsten 20x20 cm^2 applicators for the 13 MeV beam.The copper profiles are shown on the top row, lead in the middle, and tungsten profiles on the bottom row. The left column of plots shows a breakdown of the total leakage dose (black) along with the differentiated electron (blue) and photon components (red). The right column further breaks down the electron leakage dose into primary electrons and various scattered electron components.

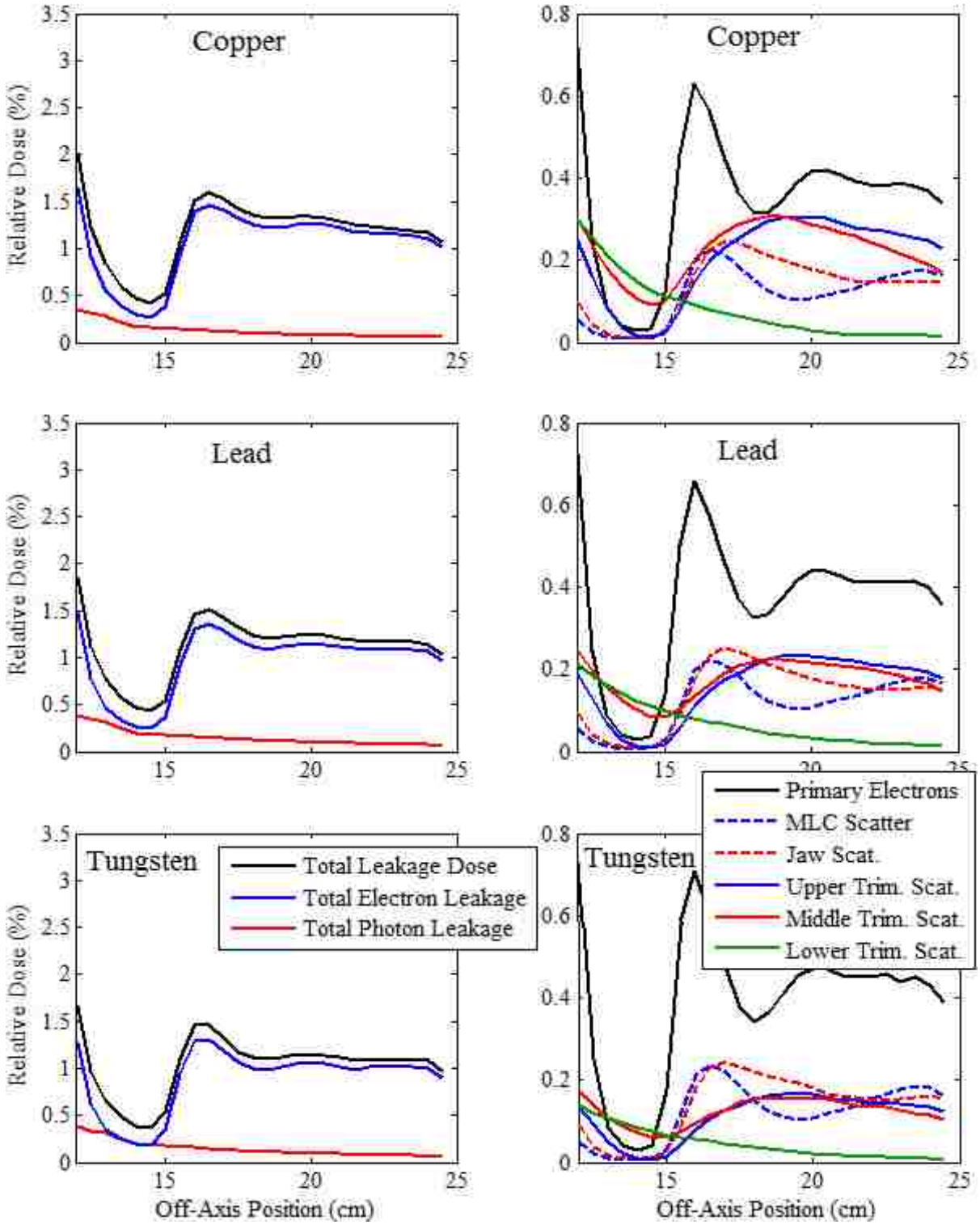

Figure B-4. In-plane leakage dose component profiles for copper, lead and tungsten 20x20 cm^2 applicators for the 7 MeV beam.The copper profiles are shown on the top row, lead in the middle, and tungsten profiles on the bottom row. The left column of plots shows a breakdown of the total leakage dose (black) along with the differentiated electron (blue) and photon components (red). The right column further breaks down the electron leakage dose into primary electrons and various scattered electron components.

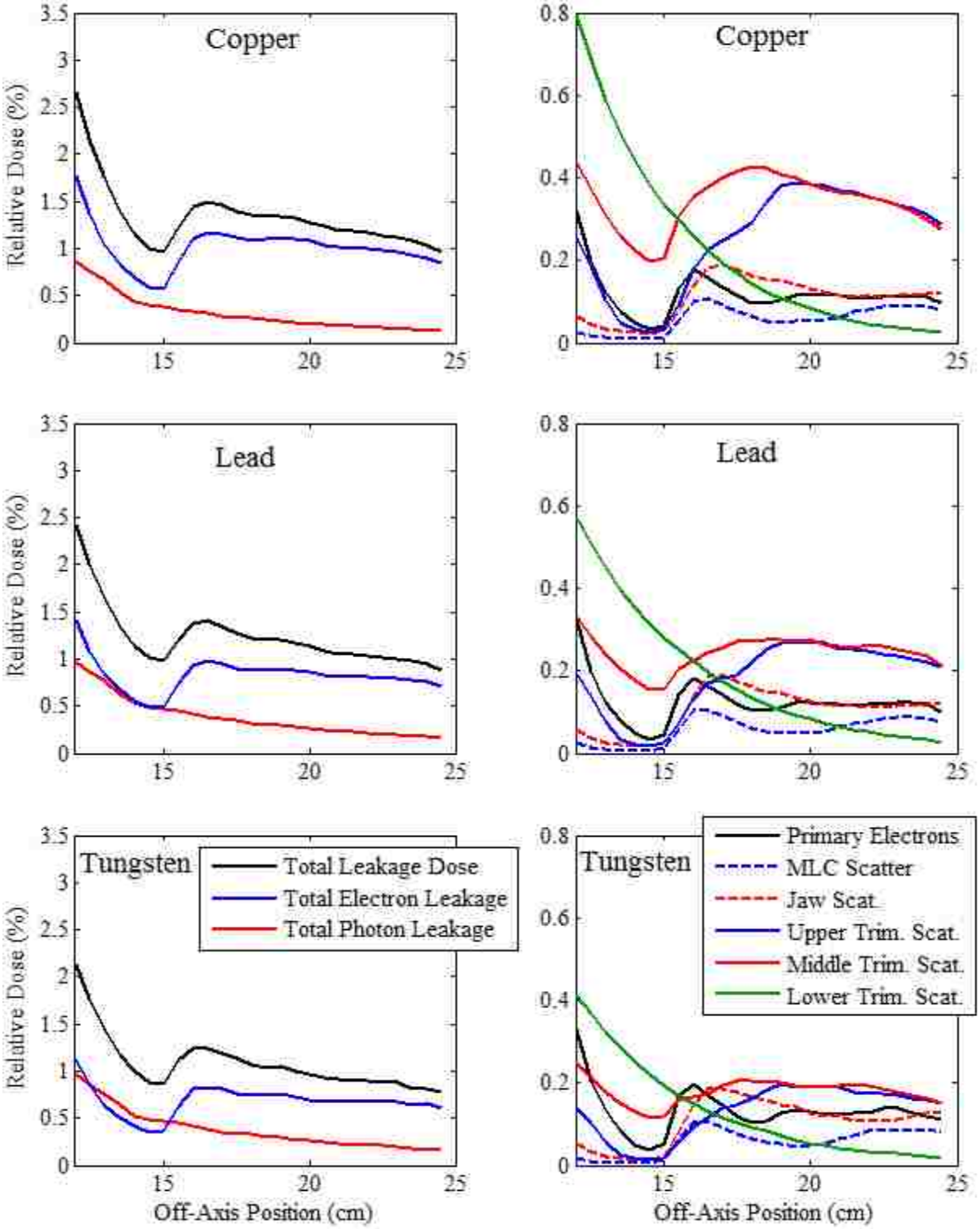

Figure B-5. In-plane leakage dose component profiles for copper, lead and tungsten 20x20 cm^2 applicators for the 13 MeV beam.The copper profiles are shown on the top row, lead in the middle, and tungsten profiles on the bottom row. The left column of plots shows a breakdown of the total leakage dose (black) along with the differentiated electron (blue) and photon components (red). The right column further breaks down the electron leakage dose into primary electrons and various scattered electron components.

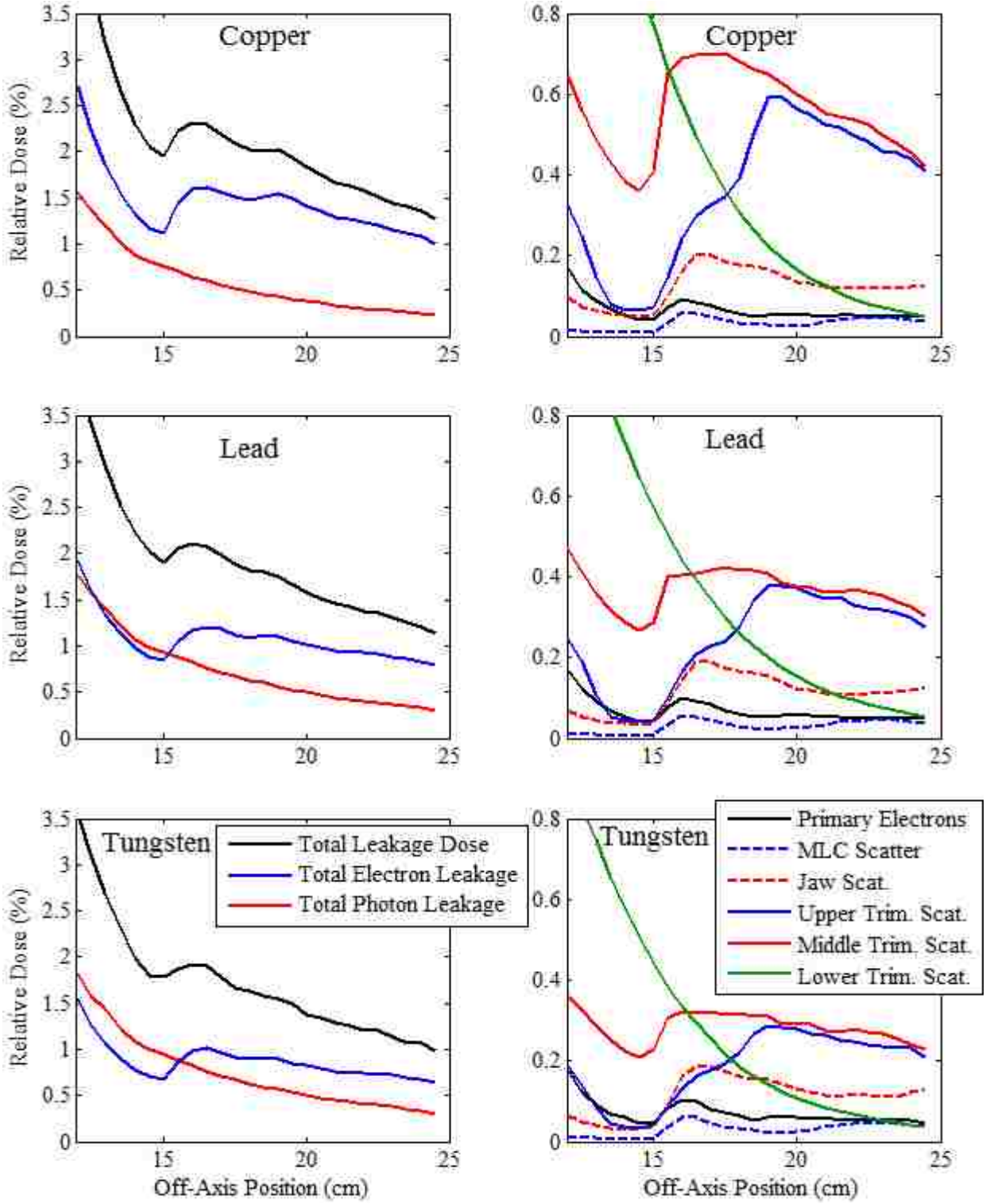

Figure B-6. In-plane leakage dose component profiles for copper, lead and tungsten 20x20 cm^2 applicators for the 20 MeV beam.The copper profiles are shown on the top row, lead in the middle, and tungsten profiles on the bottom row. The left column of plots shows a breakdown of the total leakage dose (black) along with the differentiated electron (blue) and photon components (red). The right column further breaks down the electron leakage dose into primary electrons and various scattered electron components.

Appendix C -Supplemental Figures for Aim 5

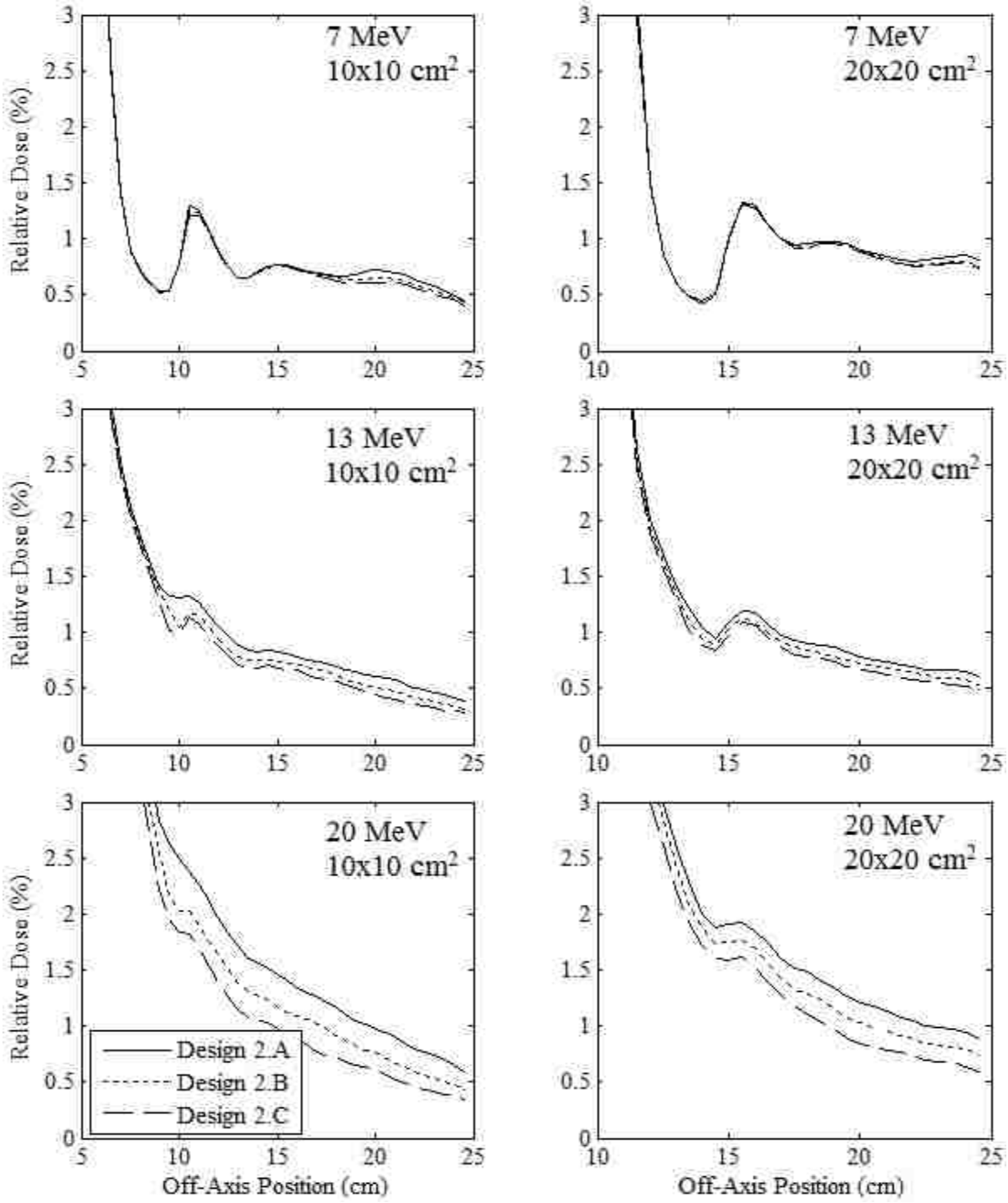

Figure C-1. In-plane total dose profiles plotted versus off-axis position in the leakage region for the analysis of jaw position variation with beam energy. The 10x10 cm^2 applicator results are shown in the left column of plots and the 20x20 cm^2 results are shown on the right for the 7 (upper row), 13 (middle row), and 20 MeV (lower row) beams. All profiles were calculated at 1 cm depth in water and normalized to central axis dose. Refer to Section 6.7.2.2. for a description of Designs 2.A, 2.B and 2.C.

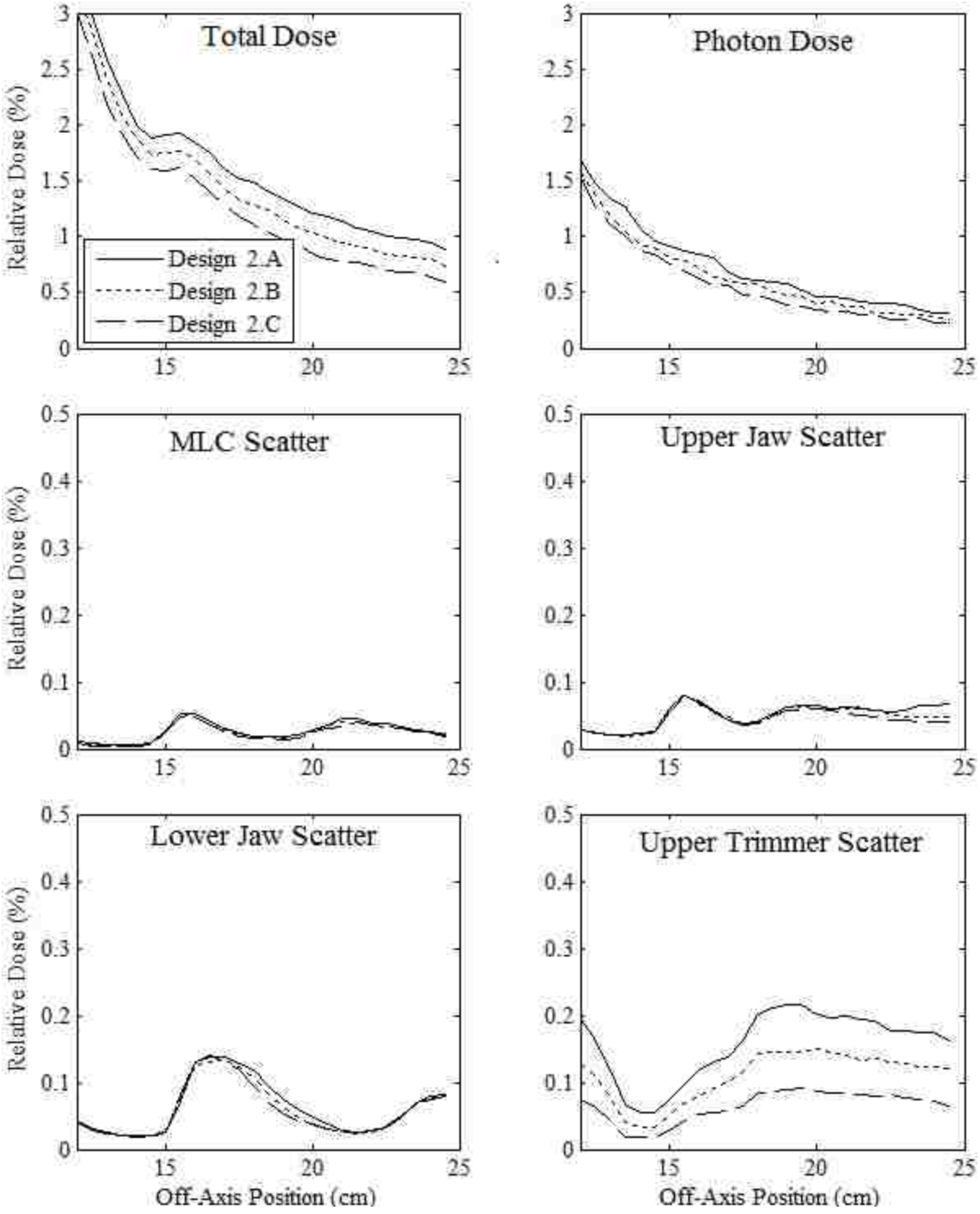

Figure C-2. In-plane leakage component profiles for analysis of jaw position variation with beam energy. All profiles were calculated at 1 cm depth in water for a 20 MeV beam with the 20x20 cm^2 applicator designs and normalized to central axis dose at the calculation depth. The range of the relative dose axis for the electron scatter dose component plots was reduced to magnify these lower dose profiles. Refer to Section 6.7.2.2. for a description of Designs 2.A, 2.B and 2.C.

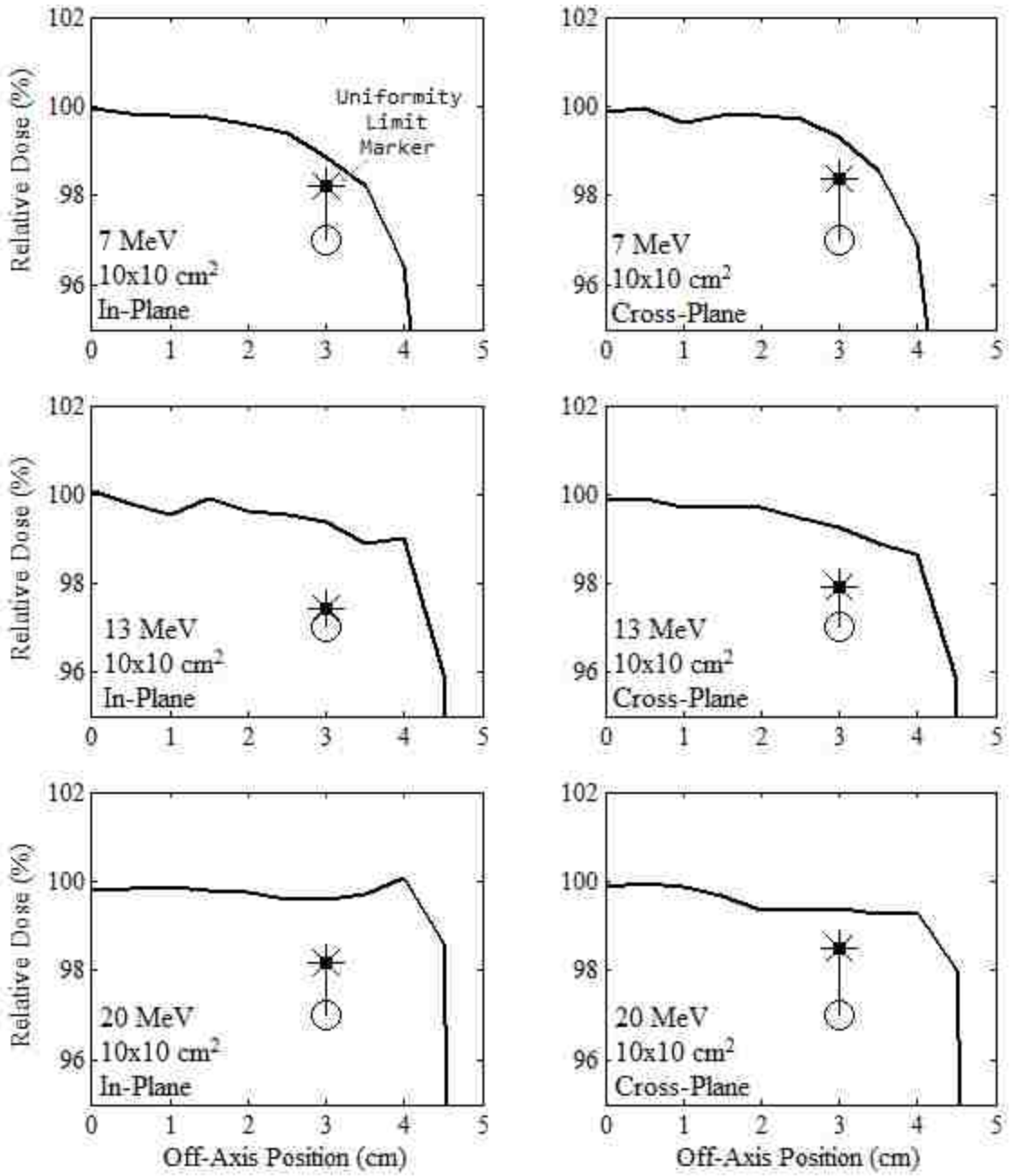

Figure C-3. In-field in-plane and cross-plane dose profiles plotted verses off-axis position for the selected 10x10 cm^2 collimation design. The in-plane applicator profiles are shown in the left column of plots and the cross-plane profiles are shown on the right for the 7 (upper row), 13 (lower row), and 20 MeV (lower row) beams. The 7 MeV dose profiles were calculated at 1 cm depth in water, and the 13 and 20 MeV dose profiles were calculated at 2 cm depth. The uniformity limit marker indicates the point at which a profile must pass above and outside in order to be considered acceptably flat. These markers are positioned at the minimally acceptable OAR at this position (97%, represented by the circular markers), plus the differences found in the MC-calculated and measured dose profiles of the current clinical collimation system at the edge of the uniformity region, plus a 1% cushion.

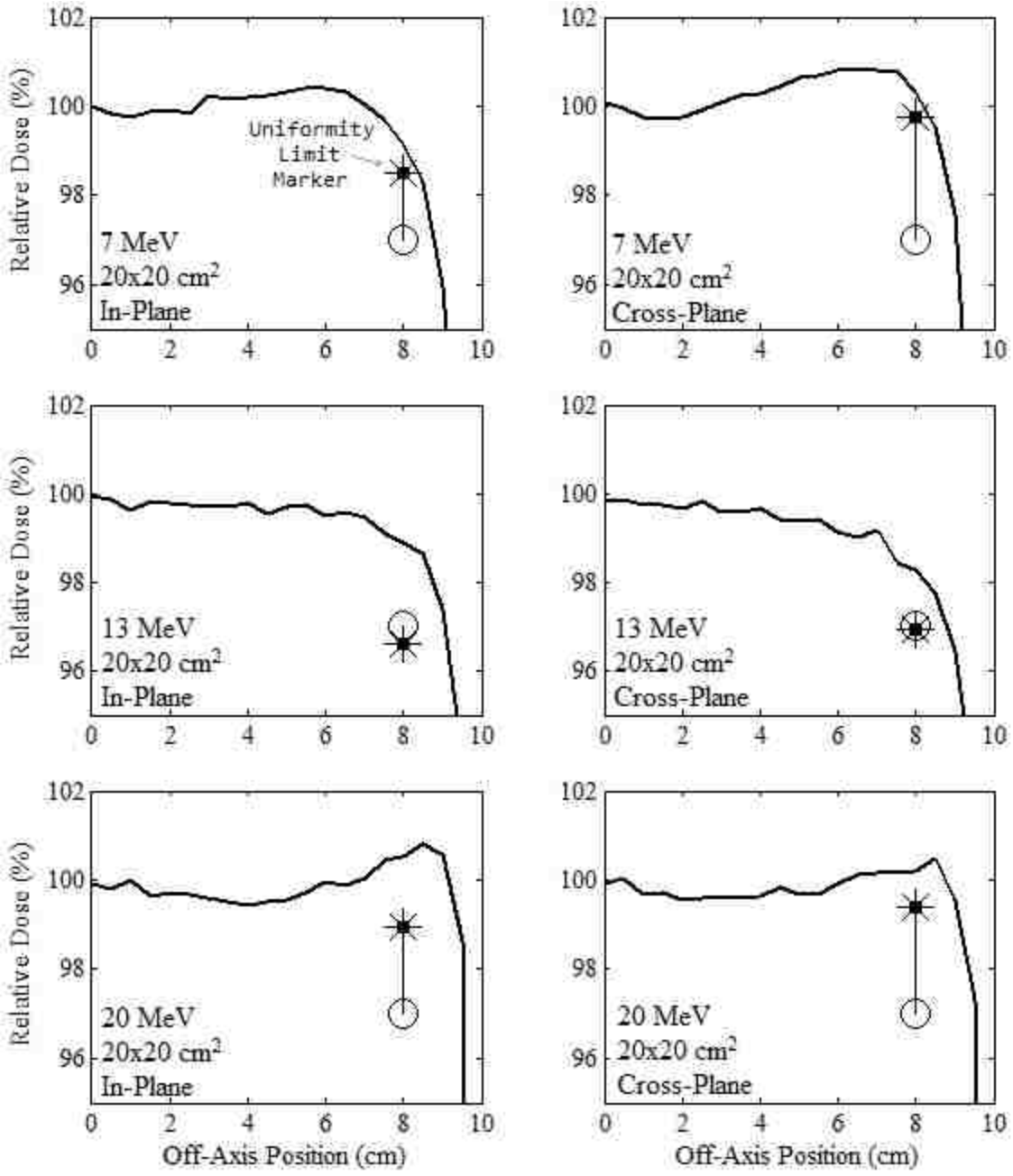

Figure C-4. In-field in-plane and cross-plane dose profiles plotted verses off-axis position for the selected 20x20 cm^2 collimation design. The in-plane applicator profiles are shown in the left column of plots and the cross-plane profiles are shown on the right for the 7 (upper row), 13 (lower row), and 20 MeV (lower row) beams. The 7 MeV dose profiles were calculated at 1 cm depth in water, and the 13 and 20 MeV dose profiles were calculated at 2 cm depth. The uniformity limit marker indicates the point at which a profile must pass above and outside in order to be considered acceptably flat. These markers are positioned at the minimally acceptable OAR at this position (97%, represented by the circular markers), plus the differences found in the MC-calculated and measured dose profiles of the current clinical collimation system at the edge of the uniformity region, plus a 1% cushion.

Appendix D - Supplemental Figures for Aim 6

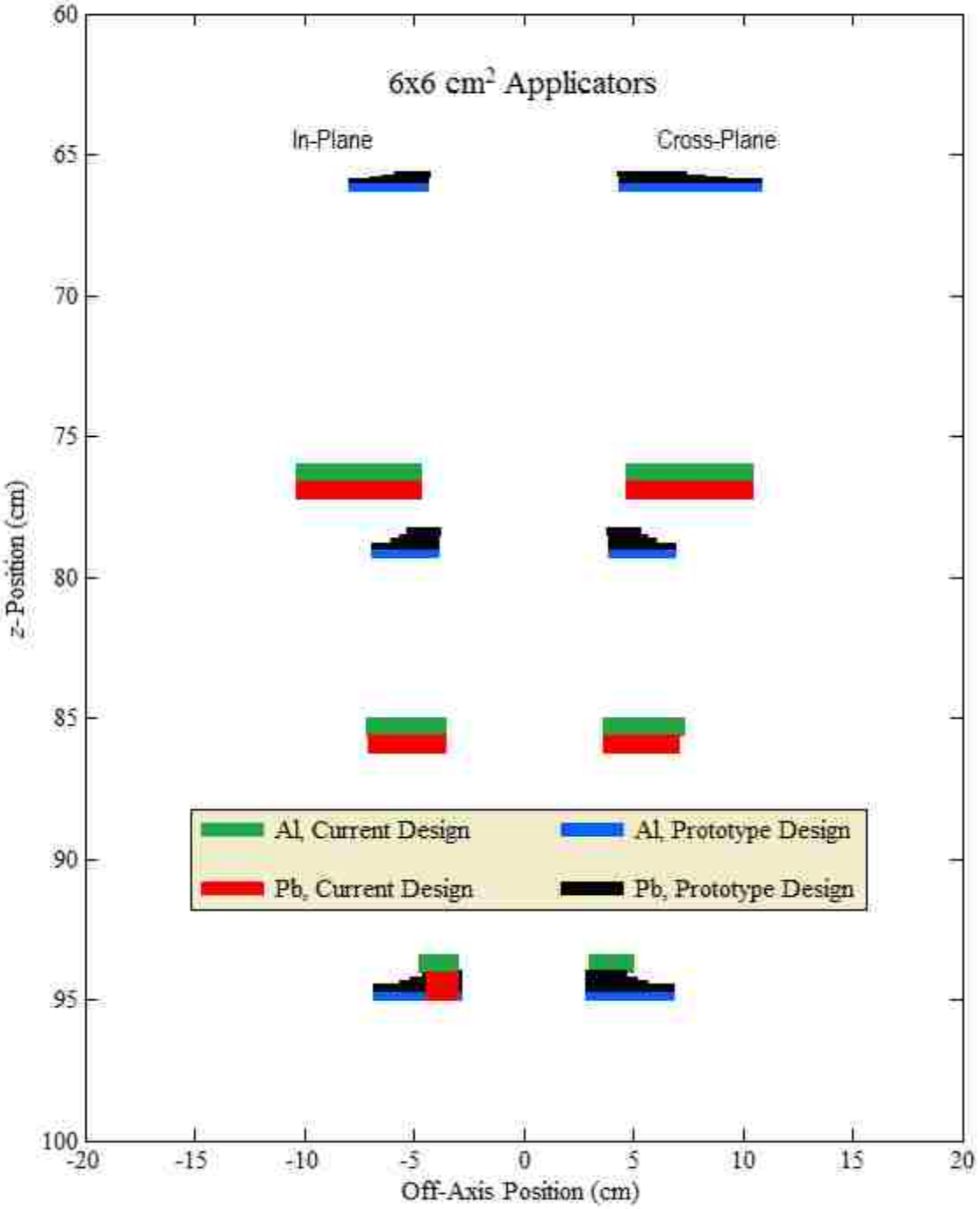

Figure D-1. Cross sectional views of the prototype and current clinical Elekta 6x6 cm^2 applicator models. The left side of the figure depicts a cross sectional view of the applicators in the in-plane dimension, and the right side of the figure depicts a cross sectional view in the cross-plane dimension. The black and blue regions demarcate the lead and aluminum plates, respectively, of the prototype design, and the red and green regions demarcate the lead and aluminum plates, respectively, of the clinical Elekta design. The current applicator is shown in the foreground on the left side of the image and the prototype model is shown in the foreground on the right.

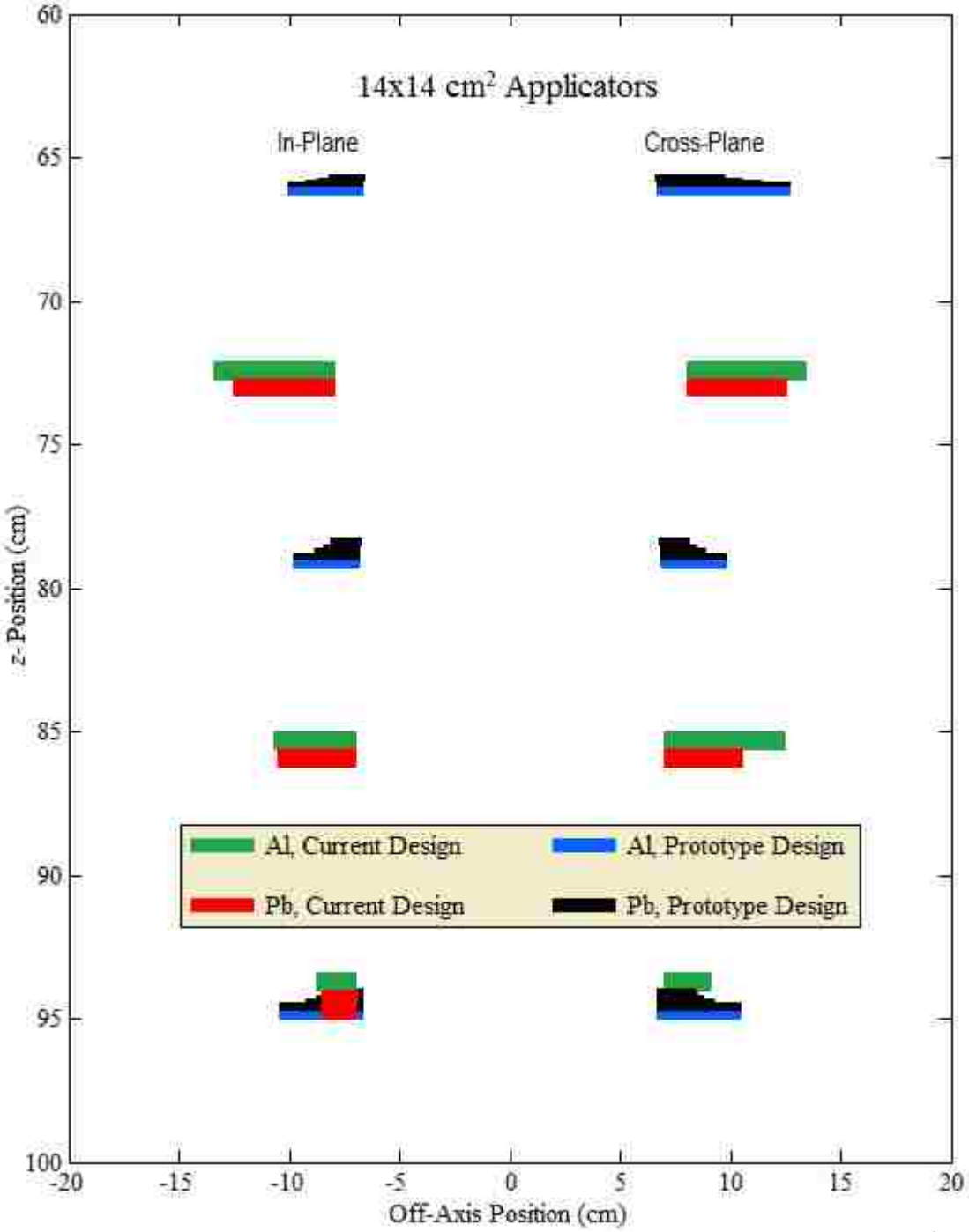

Figure D-2. Cross sectional views of the prototype and current clinical Elekta 14x14 cm^2 applicator models. The left side of the figure depicts a cross sectional view of the applicators in the in-plane dimension, and the right side of the figure depicts a cross sectional view in the cross-plane dimension. The black and blue regions demarcate the lead and aluminum plates, respectively, of the prototype design, and the red and green regions demarcate the lead and aluminum plates, respectively, of the current Elekta design. The current applicator is shown in the foreground on the left side of the image and the prototype model is shown in the foreground on the right.

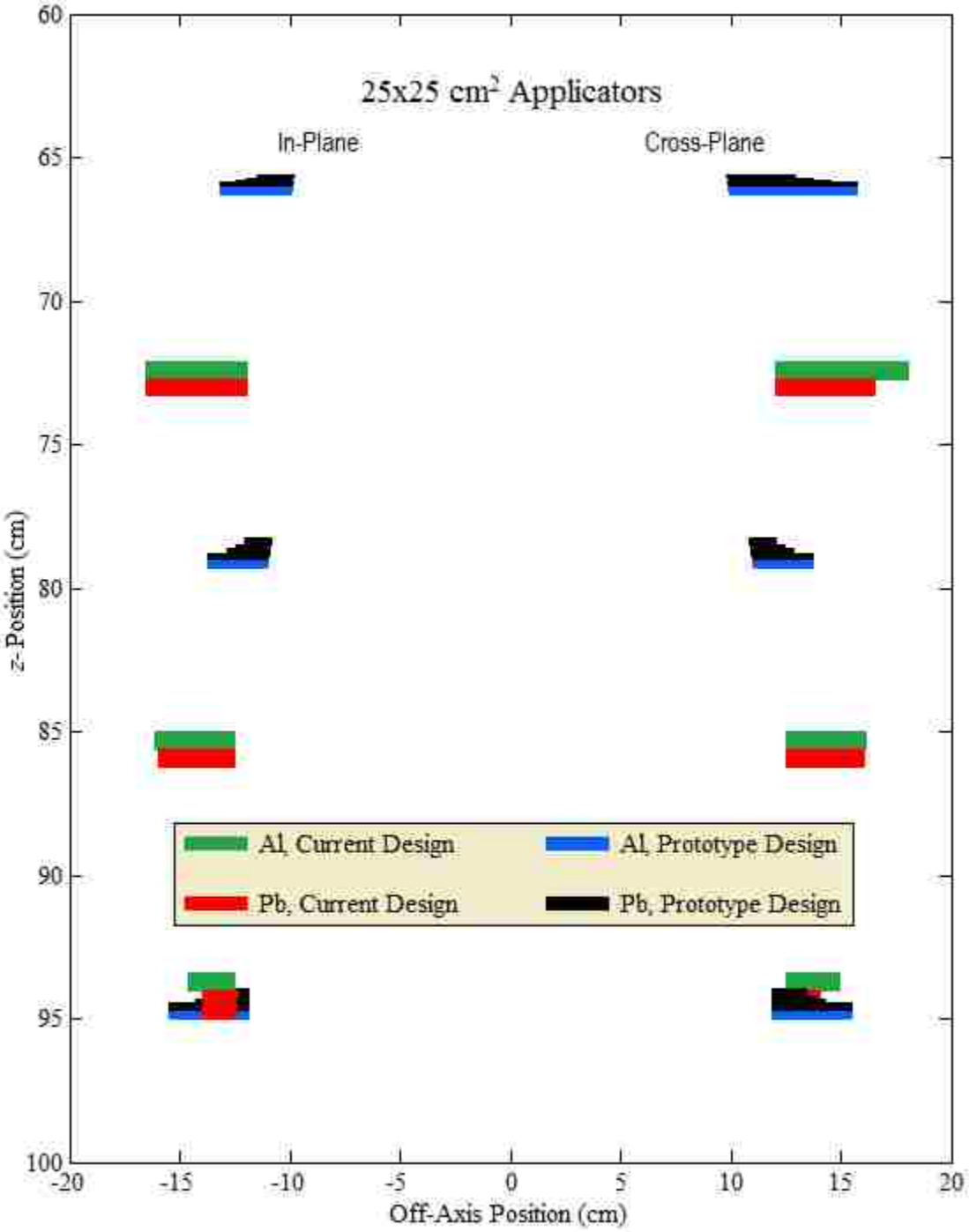

Figure D-3. Cross sectional views of the prototype and current clinical Elekta 25x25 cm^2 applicator models. The left side of the figure depicts a cross sectional view of the applicators in the in-plane dimension, and the right side of the figure depicts a cross sectional view in the cross-plane dimension. The black and blue regions demarcate the lead and aluminum plates, respectively, of the prototype design, and the red and green regions demarcate the lead and aluminum plates, respectively, of the current Elekta design. The current applicator is shown in the foreground on the left side of the image and the prototype model is shown in the foreground on the right.

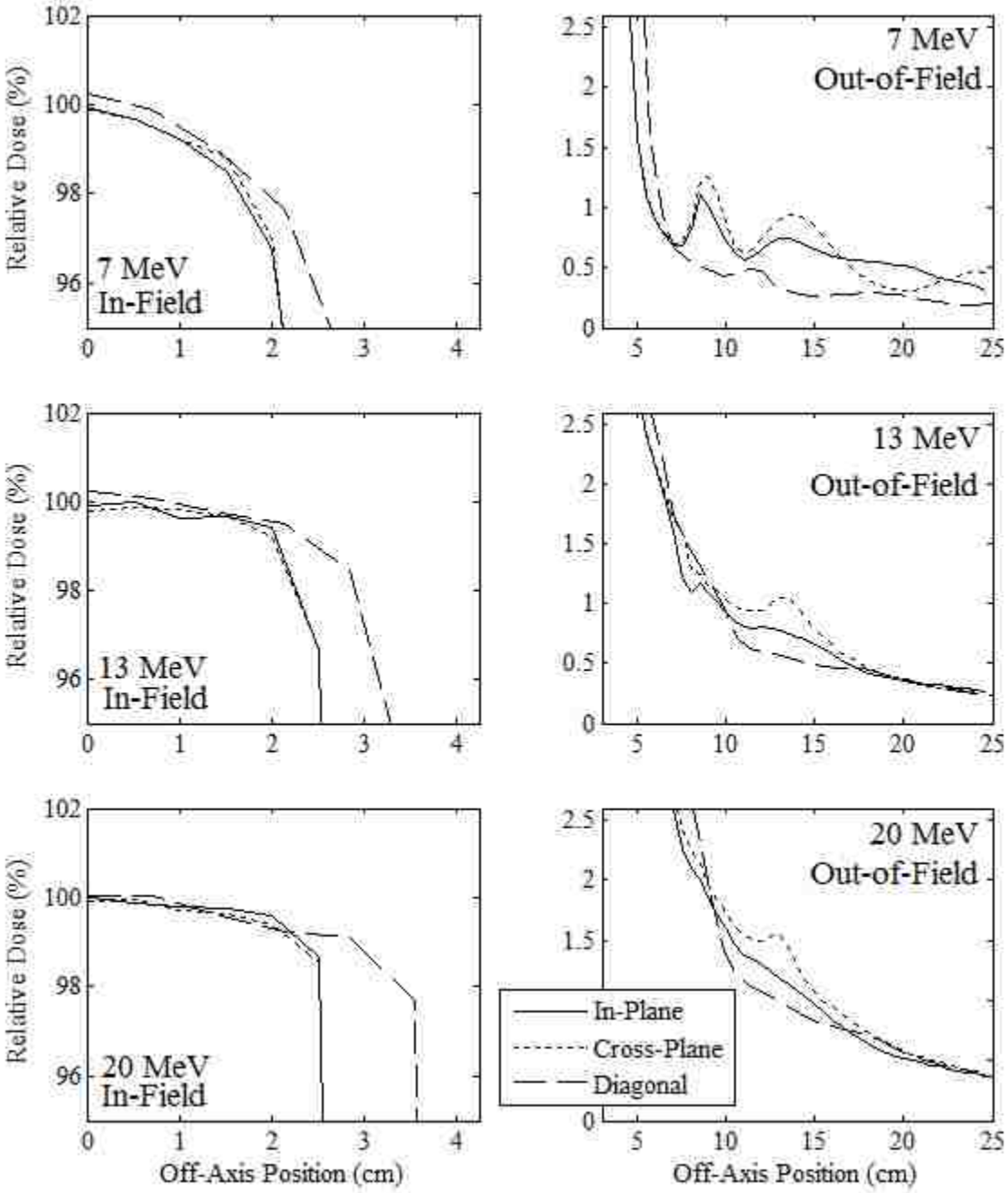

Figure D-4. MC calculated dose profiles plotted versus off-axis position for the prototype 6x6 cm^2 applicator. The in-field profiles are plotted on the left and the out-of-field profiles are plotted on the right for the 7 (upper row), 13 (middle row), and 20 MeV (lower row) beams. The 7 MeV in-field and all out-of-field profiles were calculated at 1 cm depth in water, and the 13 and 20 MeV in-field profiles were calculated at 2 cm depth.

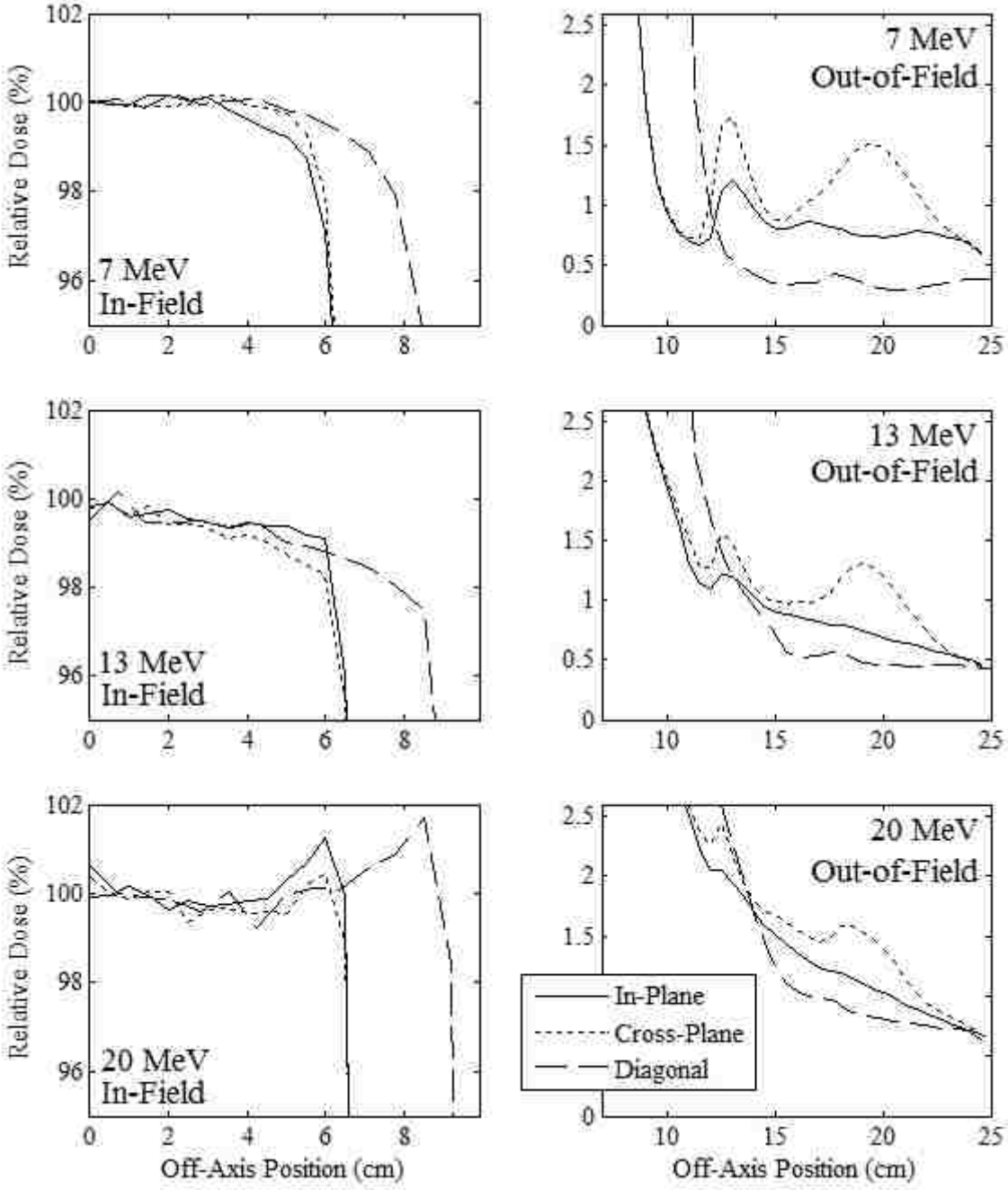

Figure D-5. MC calculated dose profiles plotted versus off-axis position for the prototype 14x14 cm^2 applicator. The in-field profiles are plotted on the left and the out-of-field profiles are plotted on the right for the 7 (upper row), 13 (middle row), and 20 MeV (lower row) beams. The 7 MeV in-field and all out-of-field profiles were calculated at 1 cm depth in water, and the 13 and 20 MeV in-field profiles were calculated at 2 cm depth.

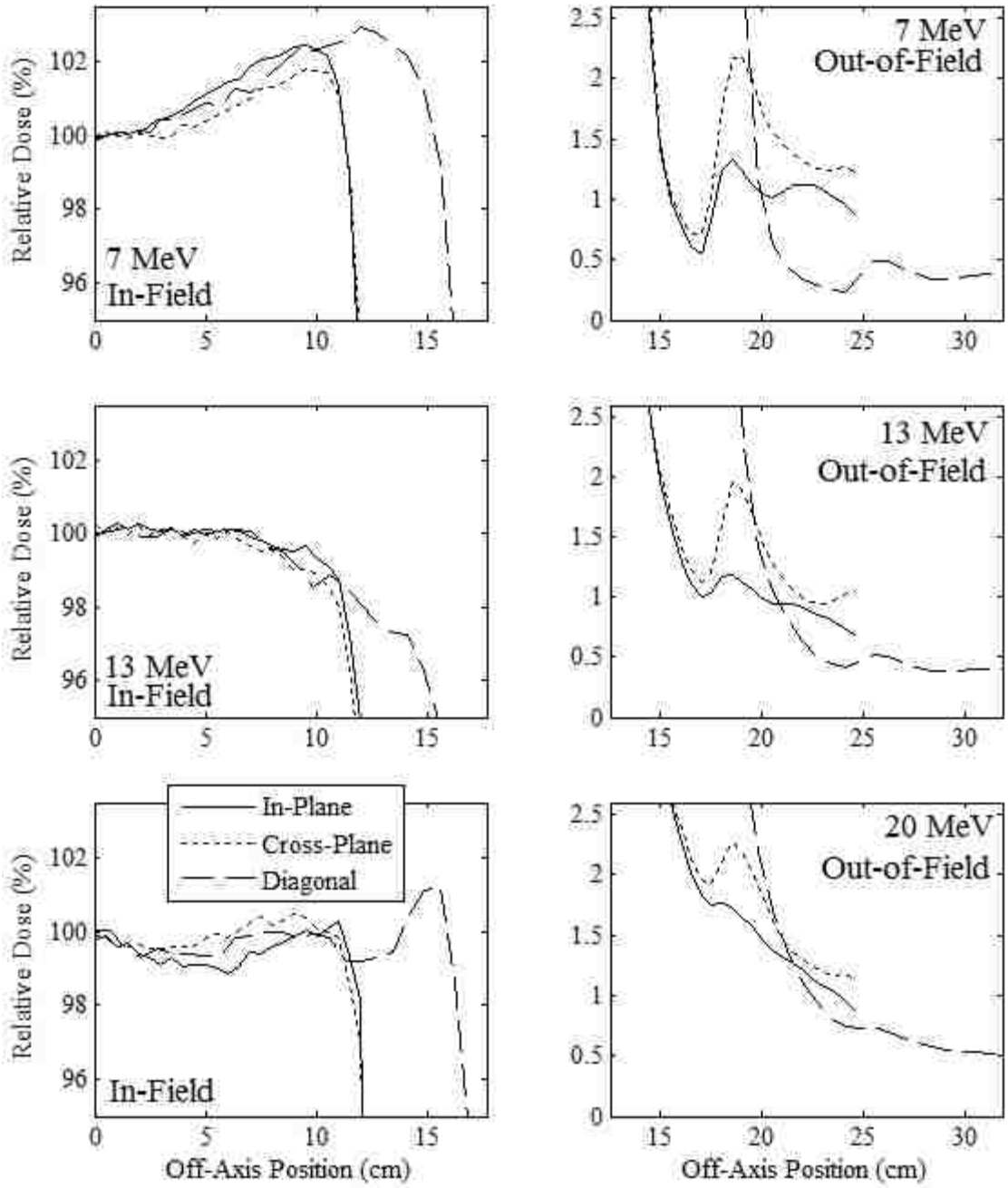

Figure D-6. MC calculated dose profiles plotted versus off-axis position for the prototype 25x25 cm^2 applicator. The in-field profiles are plotted on the left and the out-of-field profiles are plotted on the right for the 7 (upper row), 13 (middle row), and 20 MeV (lower row) beams. The 7 MeV in-field and all out-of-field profiles were calculated at 1 cm depth in water, and the 13 and 20 MeV in-field profiles were calculated at 2 cm depth.

Appendix E - Prototype Applicator Dimensions and Images

Appendix E outlines the dimensions of the prototype applicators drawn in SketchUp (Trimble Navigation, Ltd. Sunnyvale, CA). For the figures in this appendix, the X-dimension indicates the cross-plane dimension, the Y-dimension indicates the in-plane dimension, and the Z-dimension indicates the dimension parallel with central axis. . These schematics are the same as those provided to the machinists at the LSU Physics machine shop for to fabricate the 10x10 cm^2 prototype applicator.

E.1. 10x10 cm^2 Applicator

E.1.1. Full Applicator

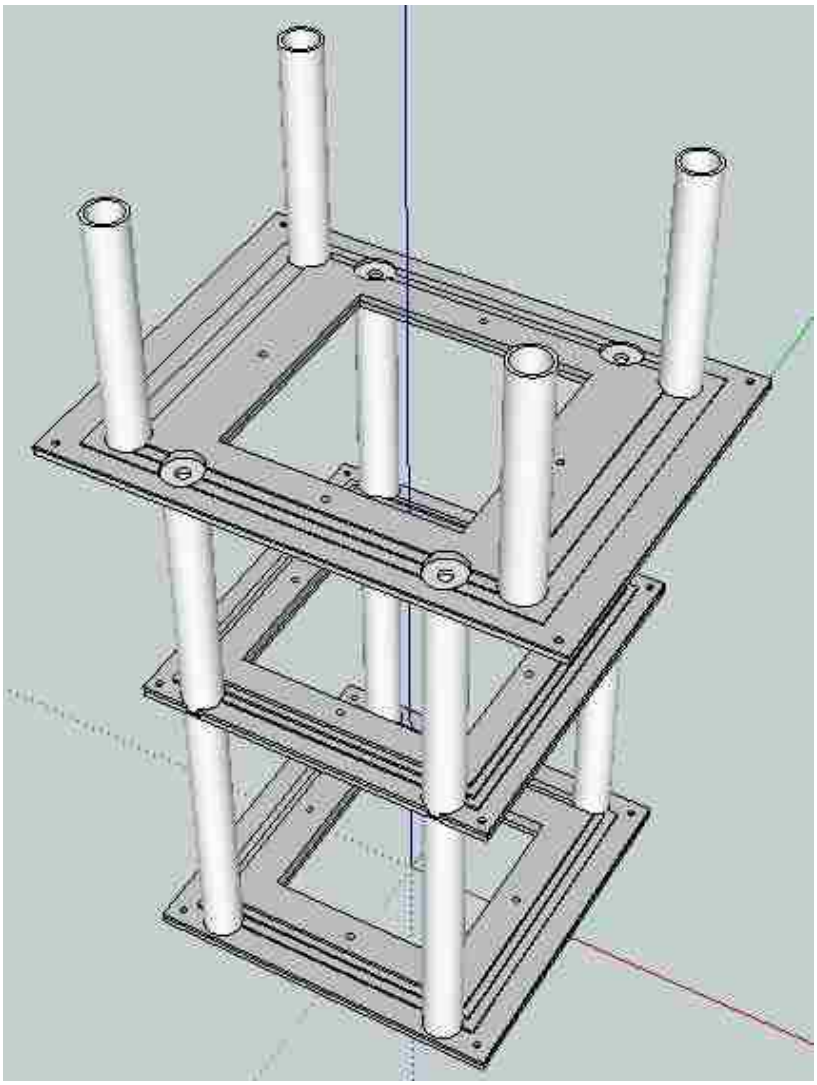

Figure E-1. Orthogonal view of the full 10x10 cm^2 applicator.

E.1.2. Upper Trimmer - Lead

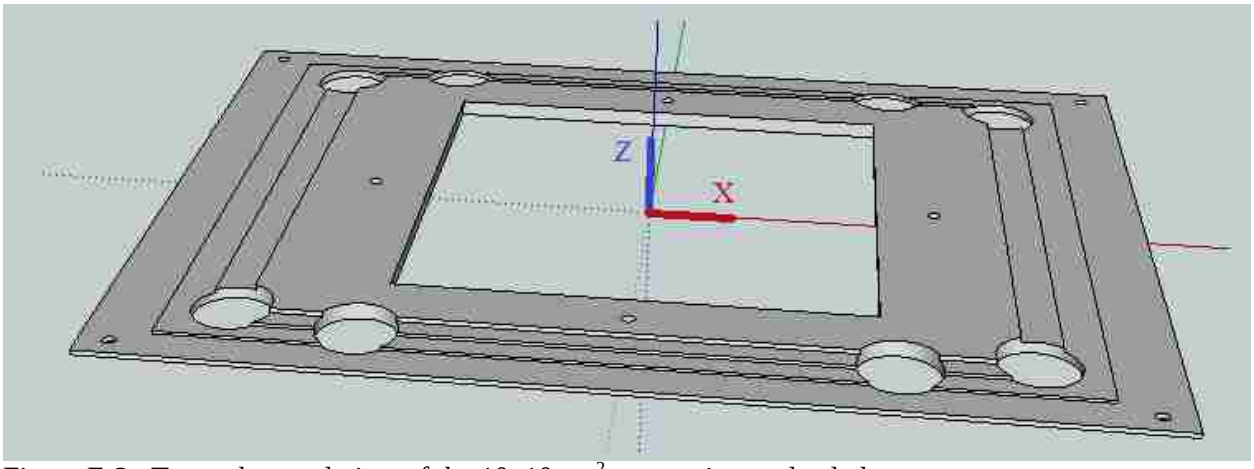

Figure E-2. Top orthogonal view of the 10x10 cm^2 upper trimmer lead plate.

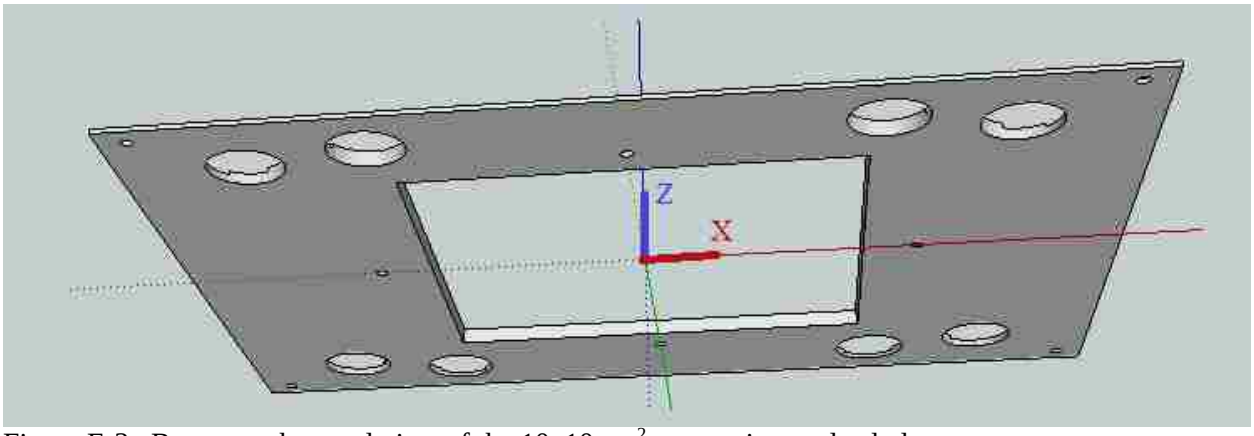

Figure E-3. Bottom orthogonal view of the 10x10 cm^2 upper trimmer lead plate.

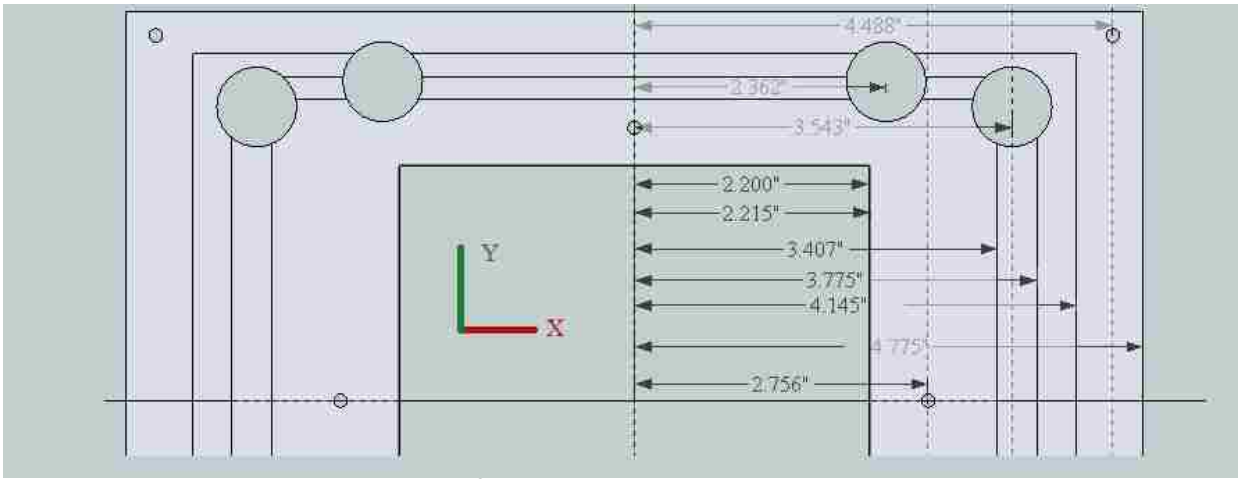

Figure E-4. Top view of the 10x10 cm^2 upper trimmer lead plate illustrating the cross-plane dimensions.

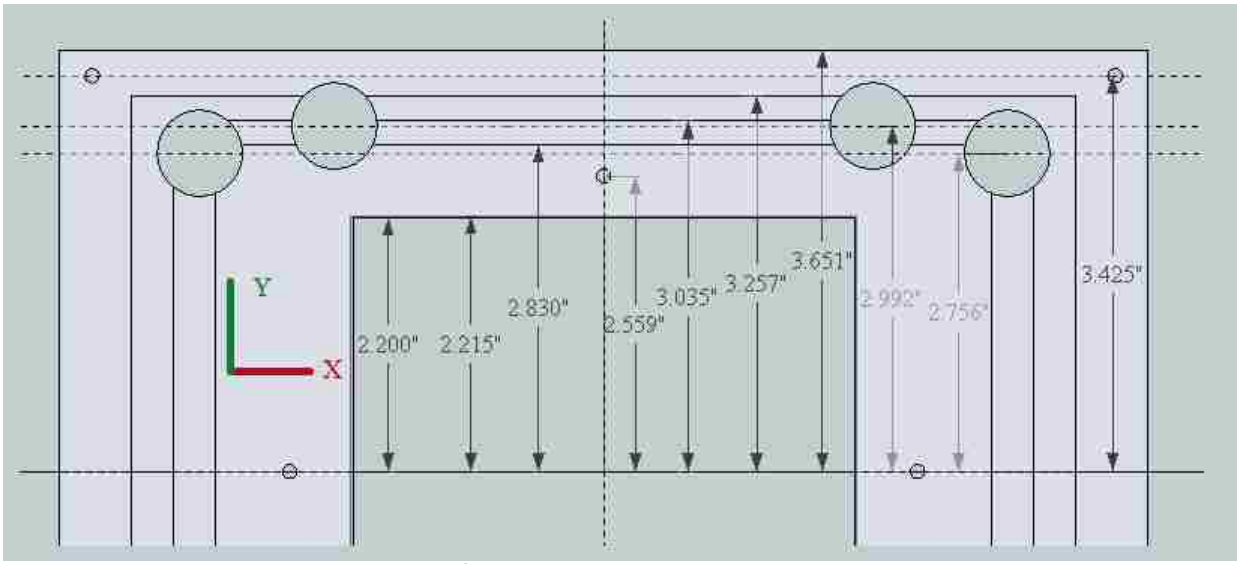

Figure E-5. Top view of the 10x10 cm^2 upper trimmer lead plate illustrating the in-plane dimensions.

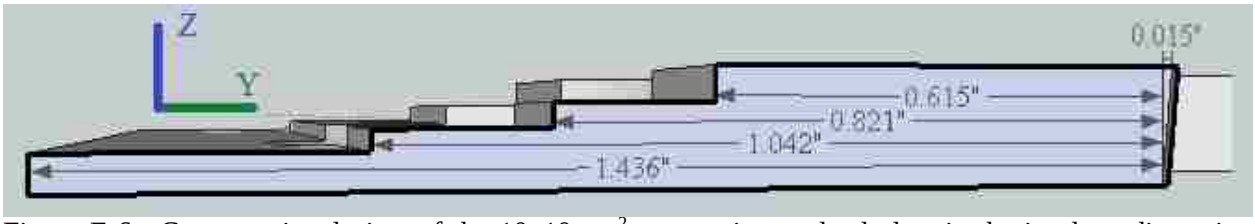

Figure E-6. Cross sectional view of the 10x10 cm^2 upper trimmer lead plate in the in-plane dimension illustrating the lateral dimensions of the plate.

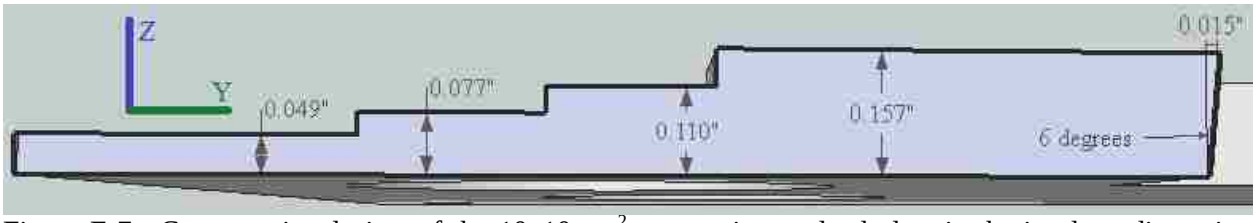

Figure E-7. Cross sectional view of the 10x10 cm^2 upper trimmer lead plate in the in-plane dimension illustrating the thickness values of the plate.

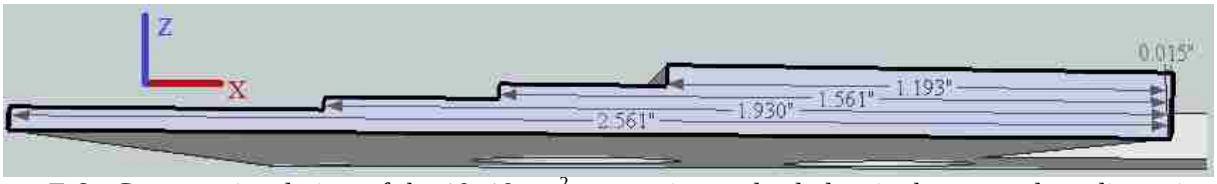

Figure E-8. Cross sectional view of the 10x10 cm^2 upper trimmer lead plate in the cross-plane dimension illustrating the lateral dimensions of the plate.

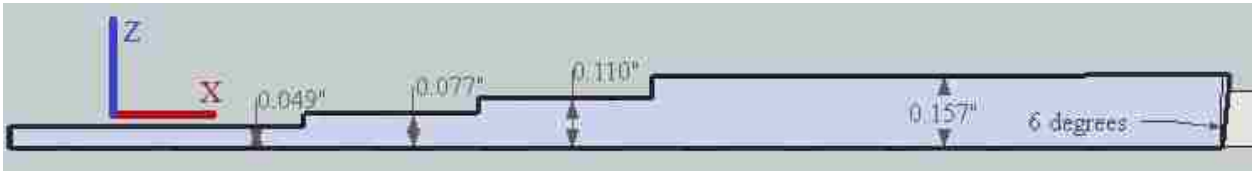

Figure E-9. Cross sectional view of the 10x10 cm^2 upper trimmer lead plate in the cross-plane dimension illustrating the thickness values of the plate.

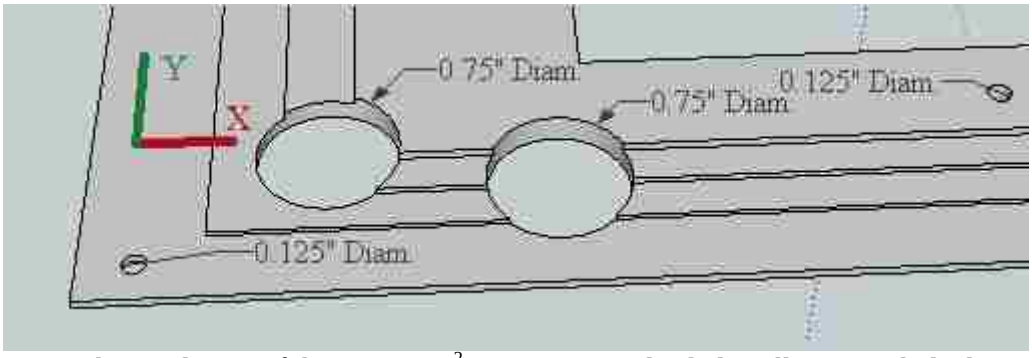

Figure E-10. Orthogonal view of the 10x10 cm^2 upper trimmer lead plate illustrating hole dimensions.

E.1.3. Middle Trimmer - Lead

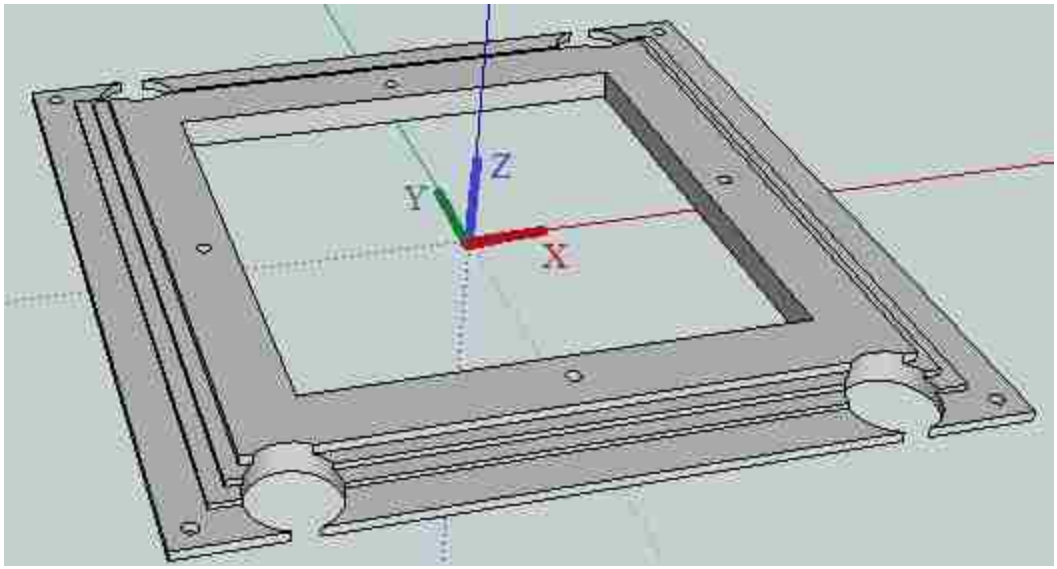

Figure E-11. Top orthogonal view of the 10x10 cm^2 middle trimmer lead plate.

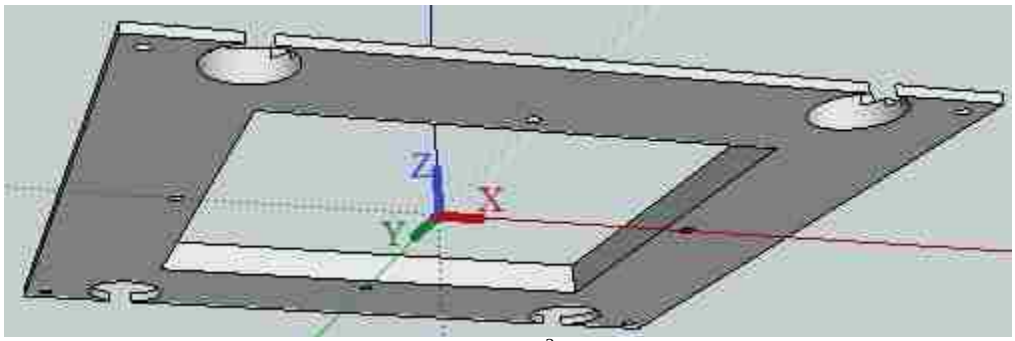

Figure E-12. Bottom orthogonal view of the 10x10 cm^2 middle trimmer lead plate.

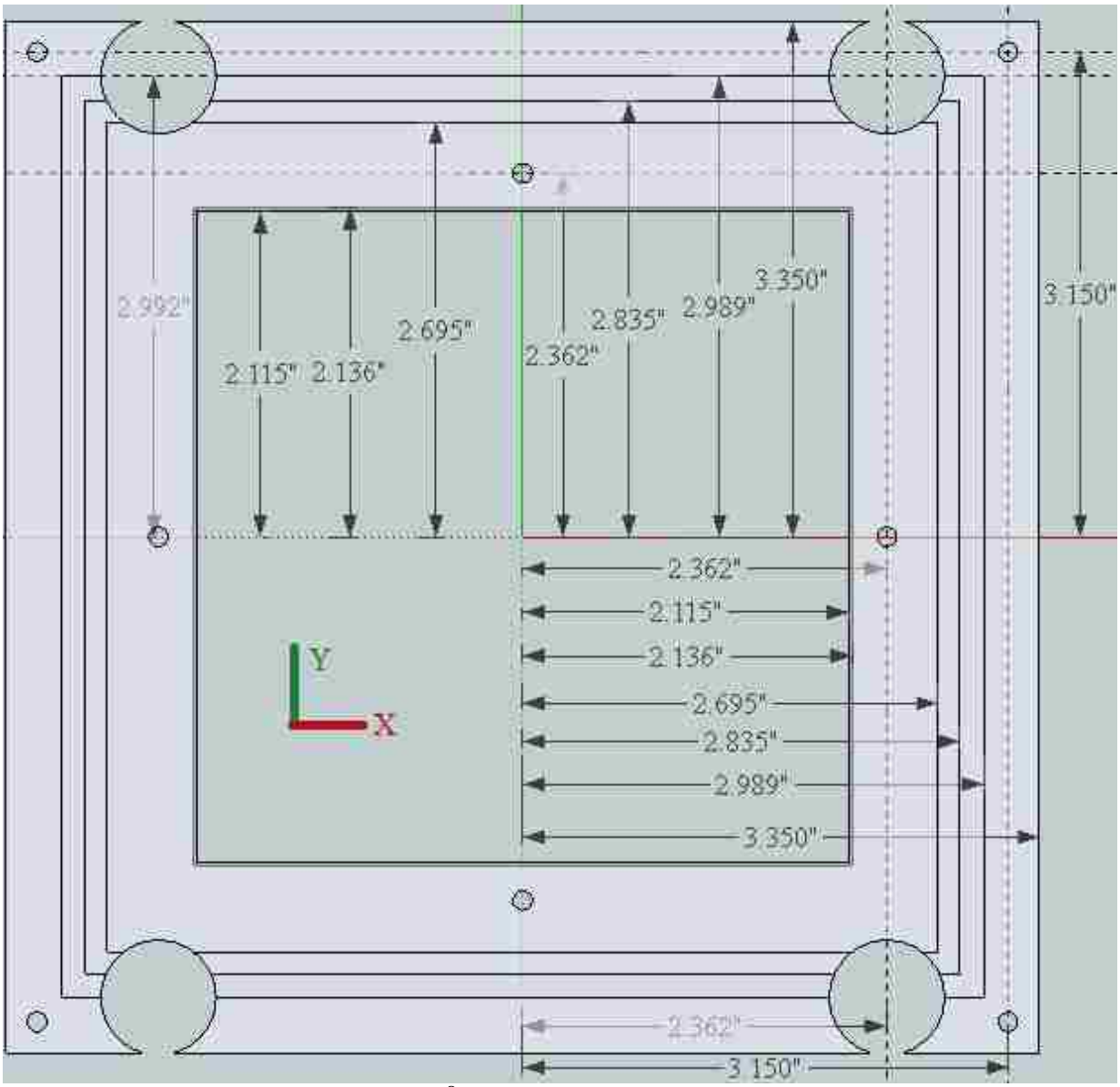

Figure E-13. Top view of the 10x10 cm^2 middle trimmer lead plate illustrating the in-plane and cross-plane dimensions. The middle trimmer is square, such that all non-hole dimensions are equal in the in-plane and cross-plane dimensions.

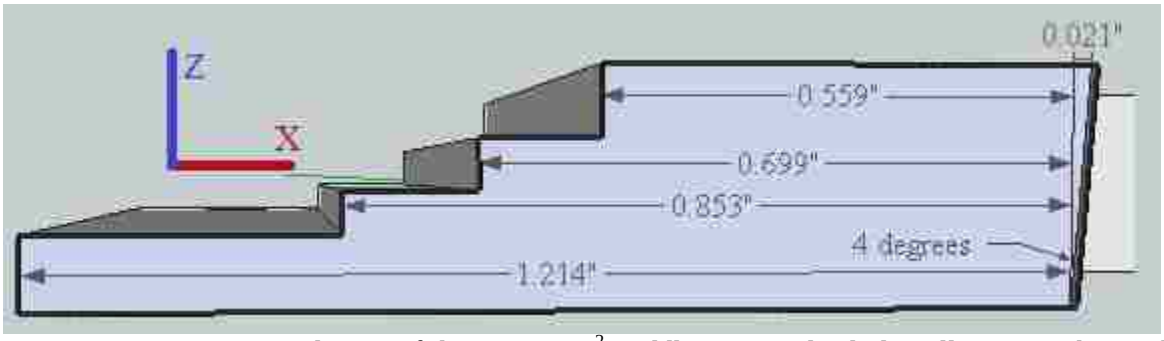

Figure E-14. Cross sectional view of the 10x10 cm^2 middle trimmer lead plate illustrating the in-plane and cross-plane lateral dimensions of the plate. The middle trimmer is square, such that all non-hole dimensions are equal in the in-plane and cross-plane dimensions.

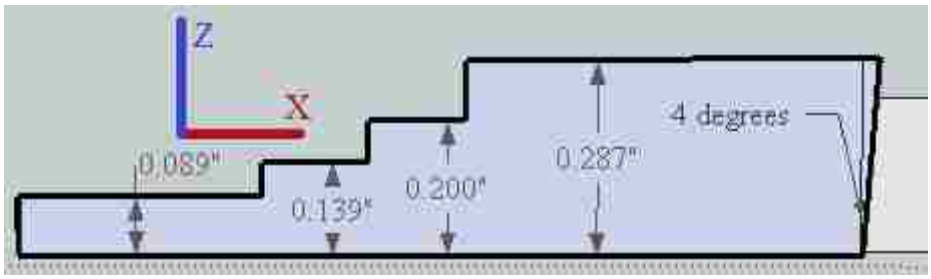

Figure E-15. Cross sectional view of the 10x10 cm^2 middle trimmer lead plate illustrating the thickness values of the plate. The middle trimmer is square, such that all non-hole dimensions are equal in the in-plane and cross-plane dimensions.

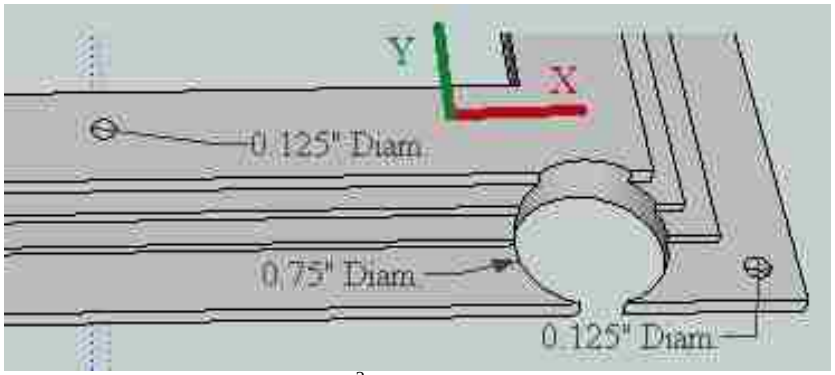

Figure E-16. Orthogonal view of the 10x10 cm^2 middle trimmer lead plate illustrating hole dimensions.

E.1.4. Lower Trimmer - Lead

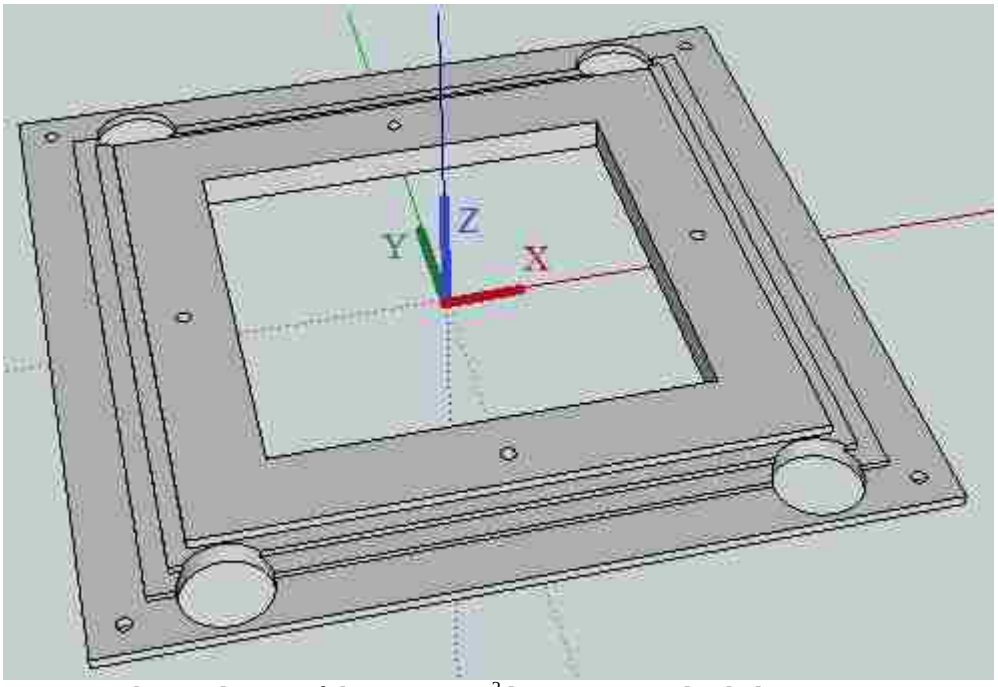

Figure E-17. Top orthogonal view of the 10x10 cm^2 lower trimmer lead plate.

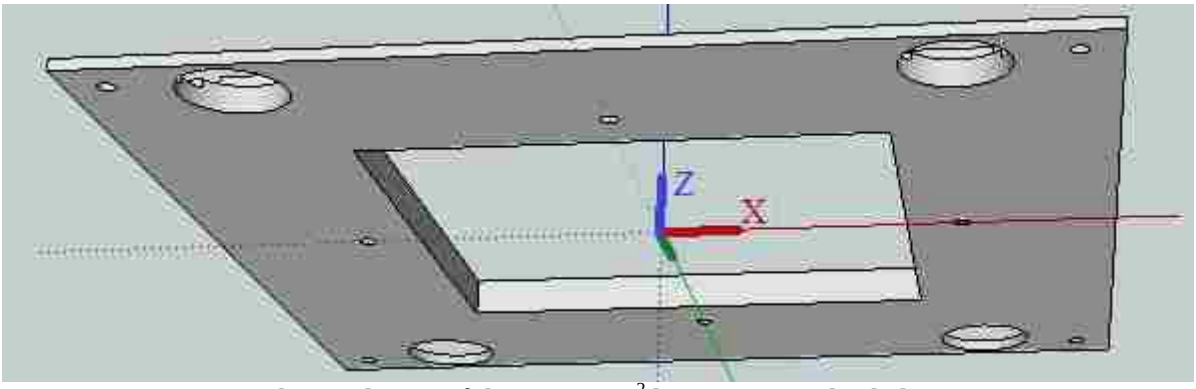

Figure E-18. Bottom orthogonal view of the 10x10 cm^2 lower trimmer lead plate.

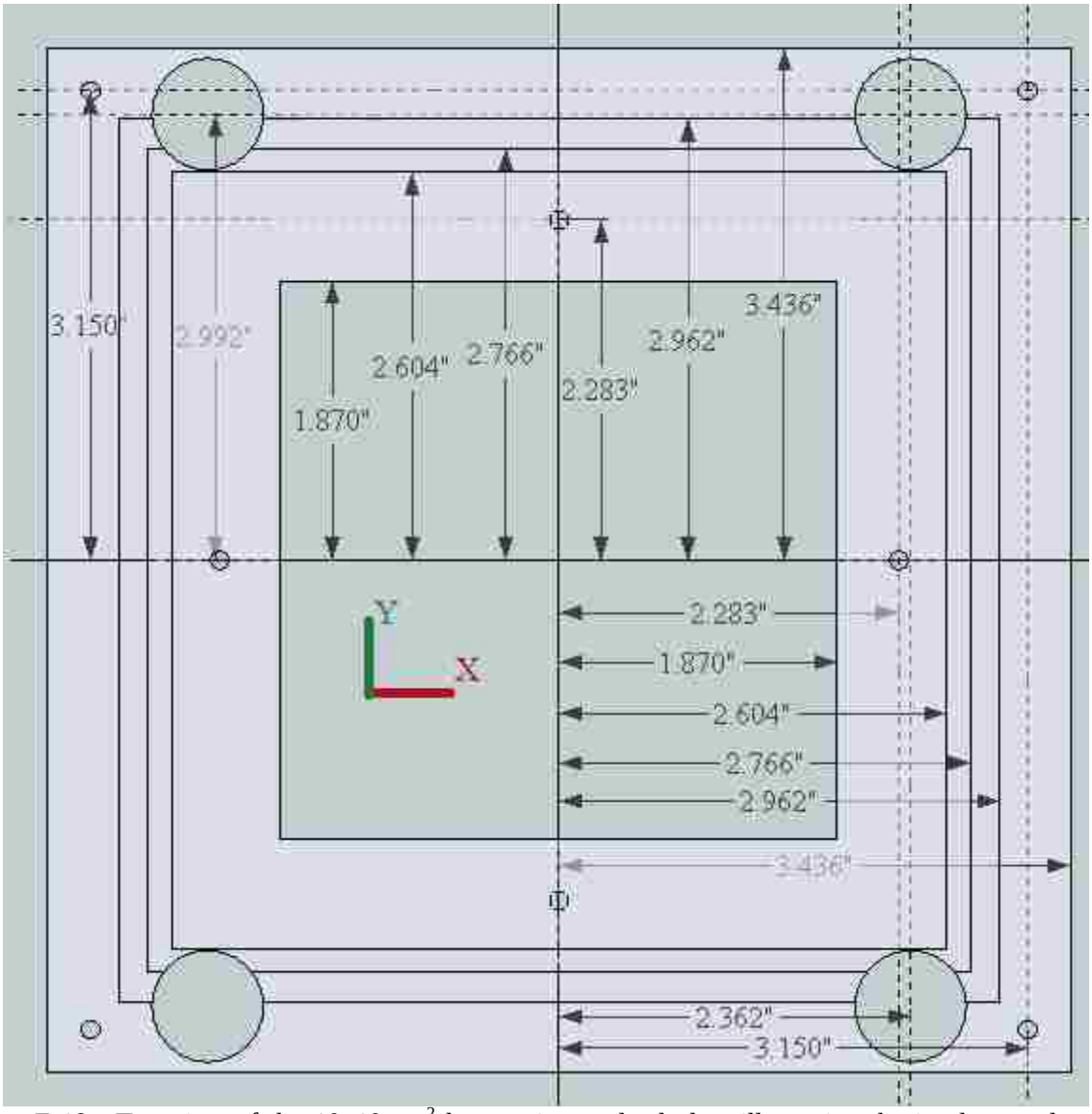

Figure E-19. Top view of the 10x10 cm^2 lower trimmer lead plate illustrating the in-plane and cross-plane dimensions. The lower trimmer is square, such that all non-hole dimensions are equal in the in-plane and cross-plane dimensions.

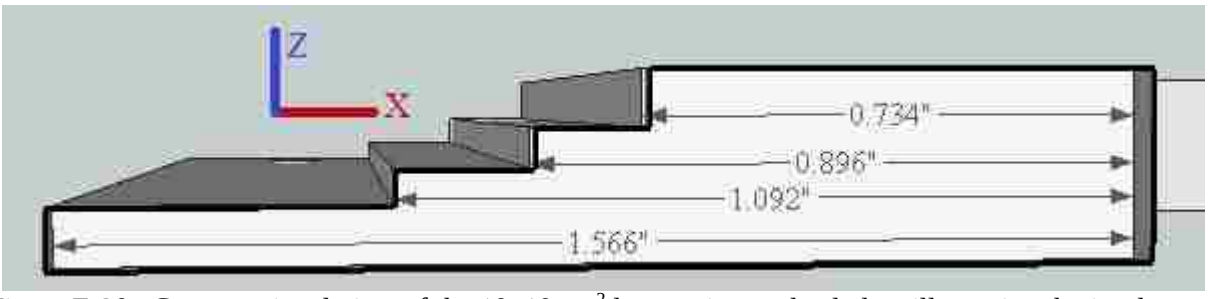

Figure E-20. Cross sectional view of the 10x10 cm^2 lower trimmer lead plate illustrating the in-plane and cross-plane lateral dimensions of the plate. The lower trimmer is square, such that all non-hole dimensions are equal in the in-plane and cross-plane dimensions.

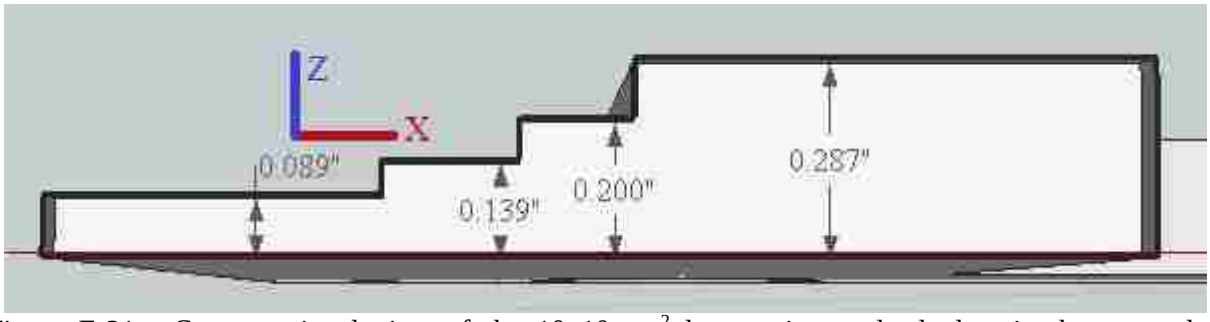

Figure E-21. Cross sectional view of the 10x10 cm^2 lower trimmer lead plate in the cross-plane dimension illustrating the thickness values of the plate. The lower trimmer is square, such that all non-hole dimensions are equal in the in-plane and cross-plane dimensions.

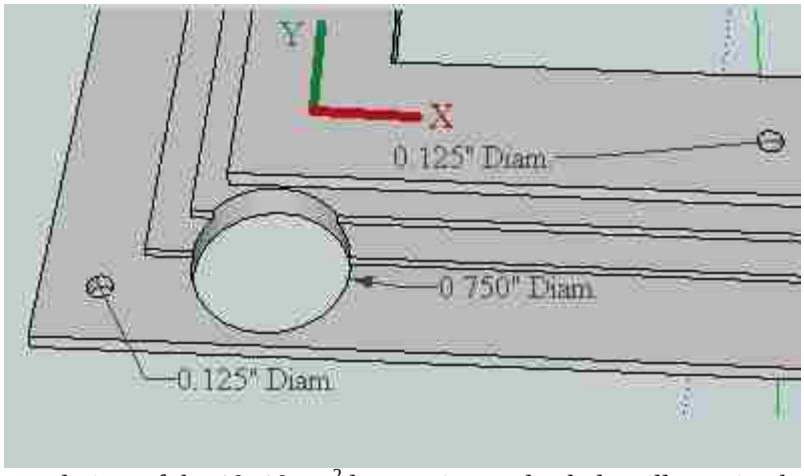

Figure E-22. Orthogonal view of the 10x10 cm^2 lower trimmer lead plate illustrating hole dimensions.

E.1.5. Upper Trimmer - Aluminum

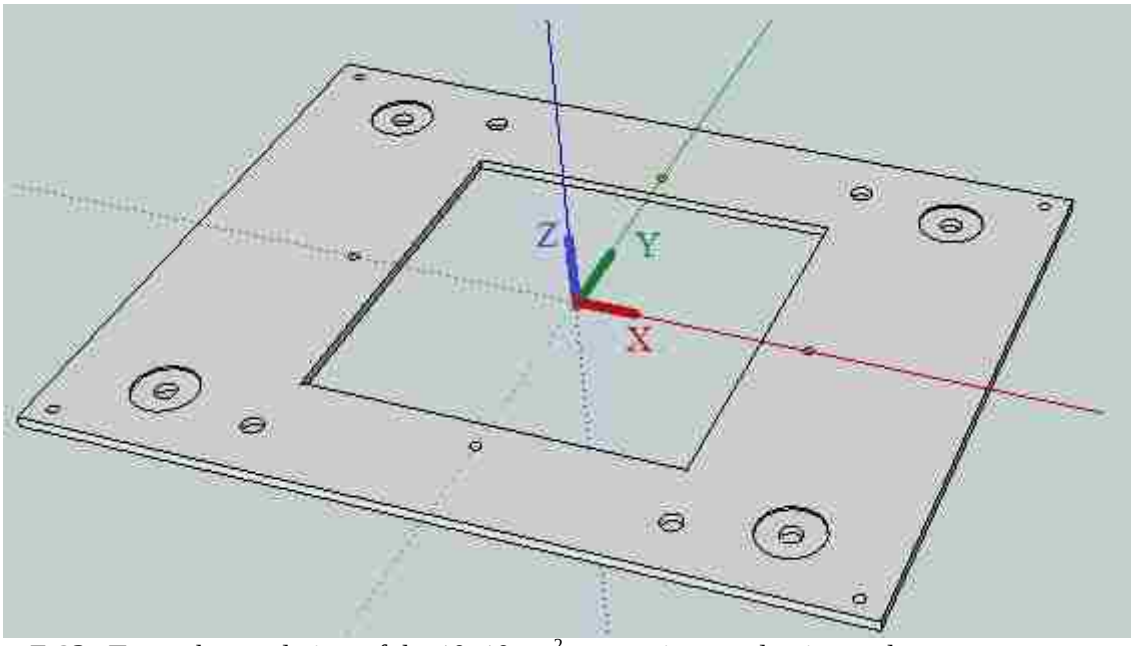

Figure E-23. Top orthogonal view of the 10x10 cm^2 upper trimmer aluminum plate.

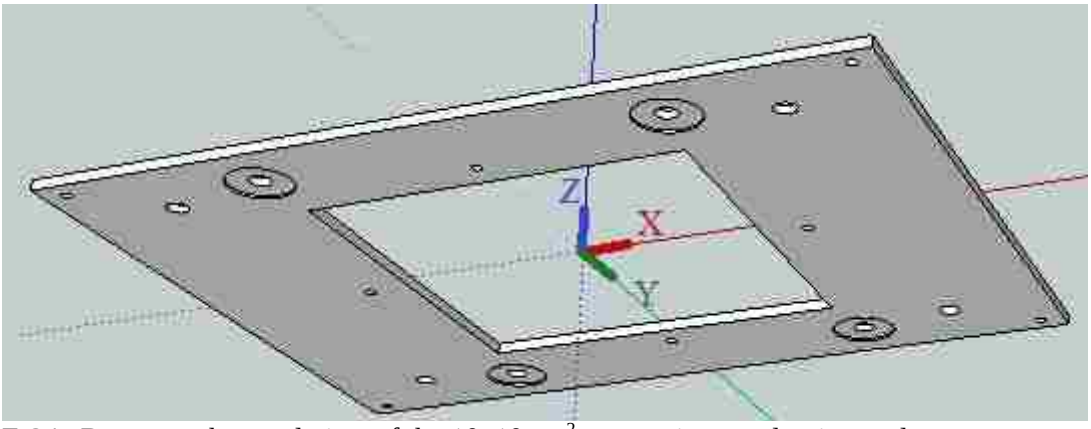

Figure E-24. Bottom orthogonal view of the 10x10 cm^2 upper trimmer aluminum plate.

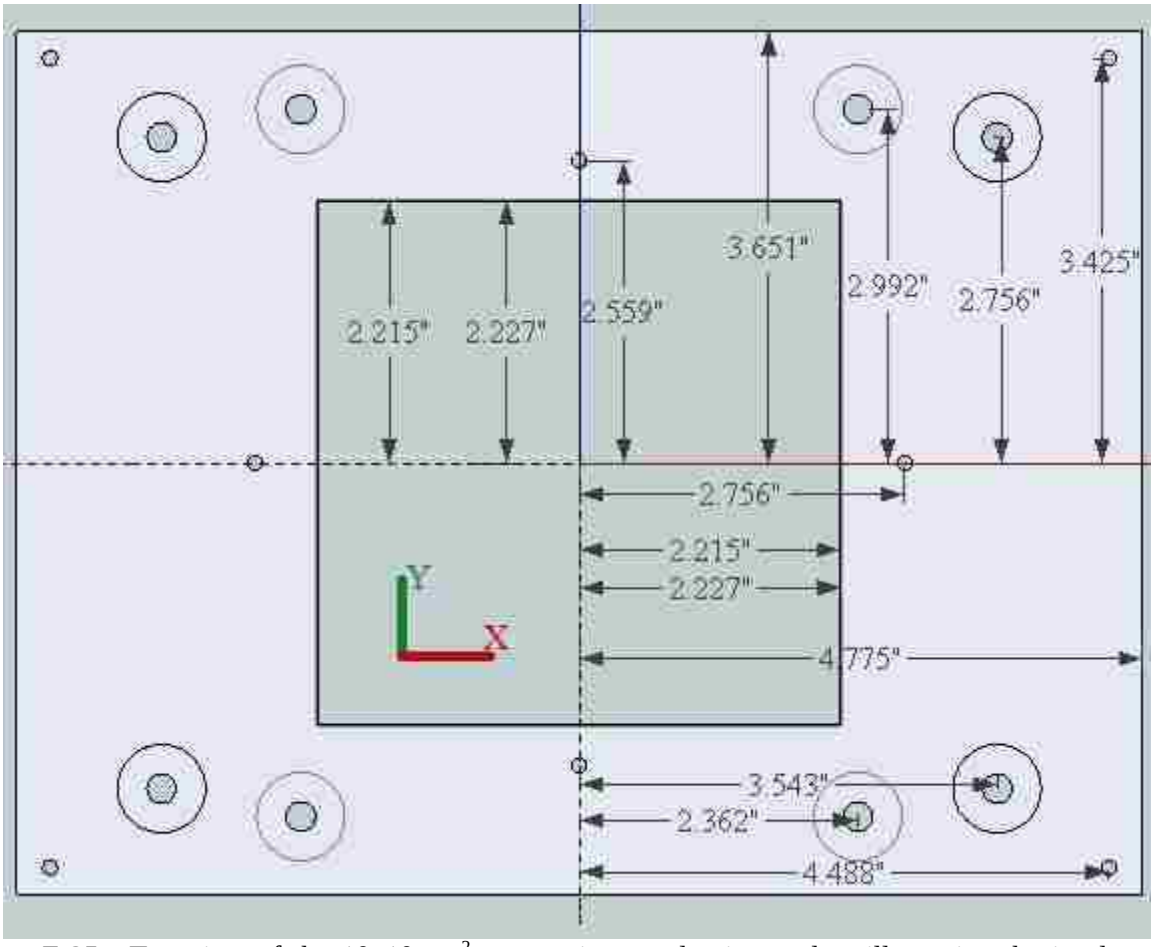

Figure E-25. Top view of the 10x10 cm^2 upper trimmer aluminum plate illustrating the in-plane and cross-plane dimensions.

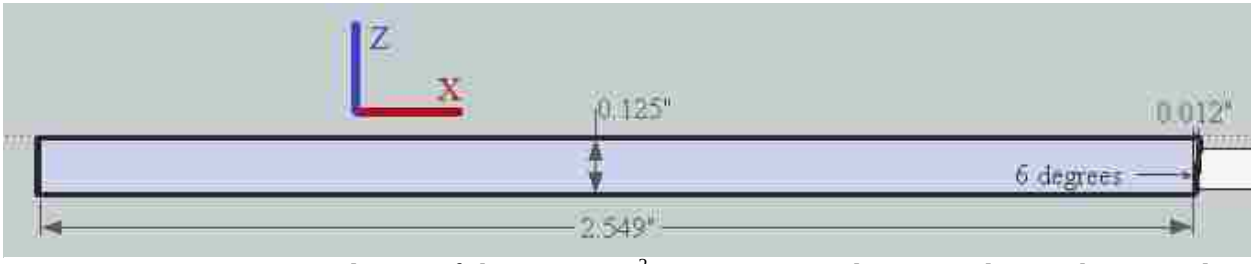

Figure E-26. Cross sectional view of the 10x10 cm^2 upper trimmer aluminum plate in the cross-plane dimension illustrating the thickness and lateral dimensions of the plate.

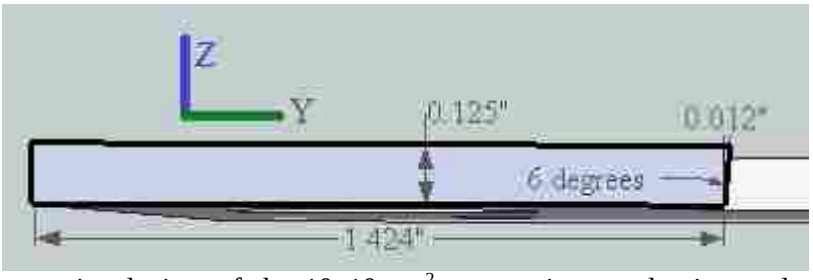

Figure E-27. Cross sectional view of the 10x10 cm^2 upper trimmer aluminum plate in the in-plane dimension illustrating the thickness and lateral dimensions of the plate.

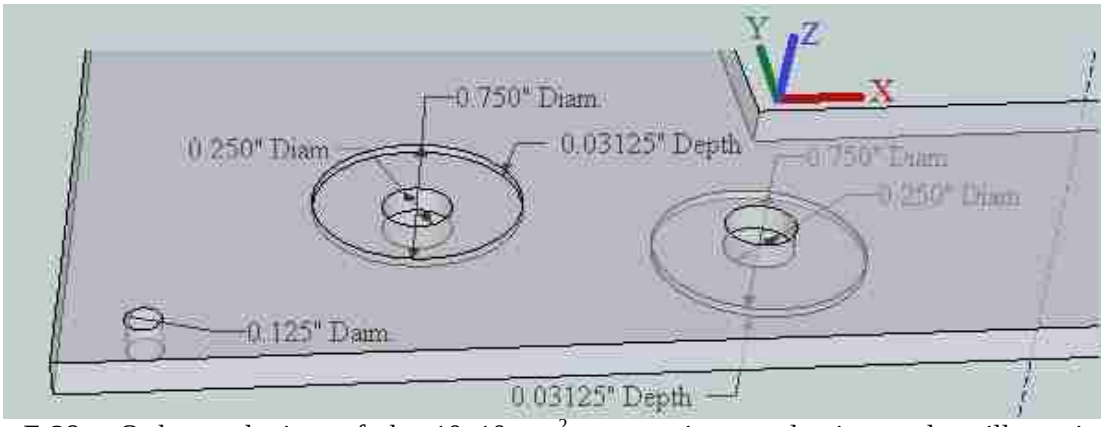

Figure E-28. Orthogonal view of the 10x10 cm^2 upper trimmer aluminum plate illustrating hole dimensions.

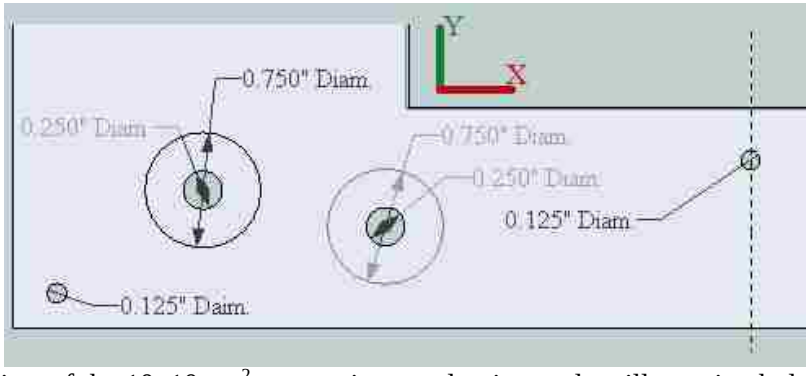

Figure E-29. Top view of the 10x10 cm^2 upper trimmer aluminum plate illustrating hole dimensions.

E.1.6. Middle Trimmer - Aluminum

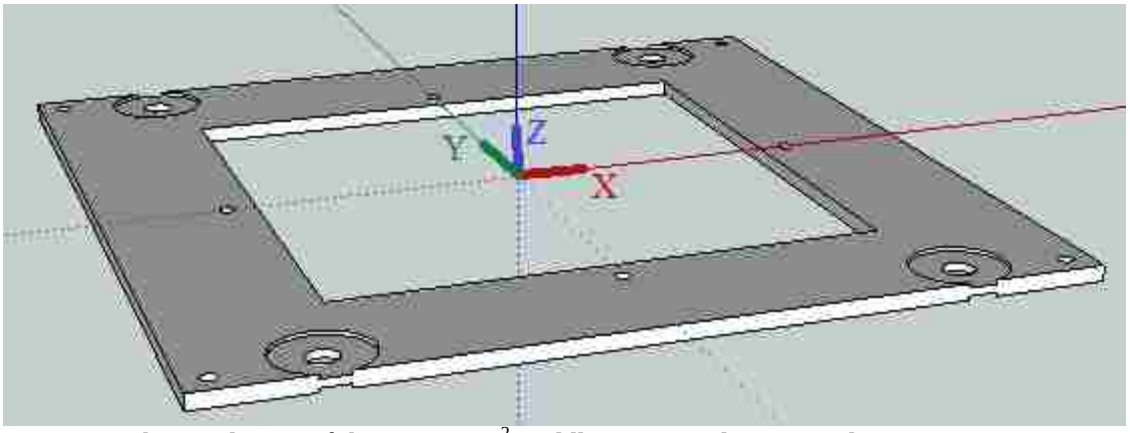

Figure E-30. Orthogonal view of the 10x10 cm^2 middle trimmer aluminum plate.

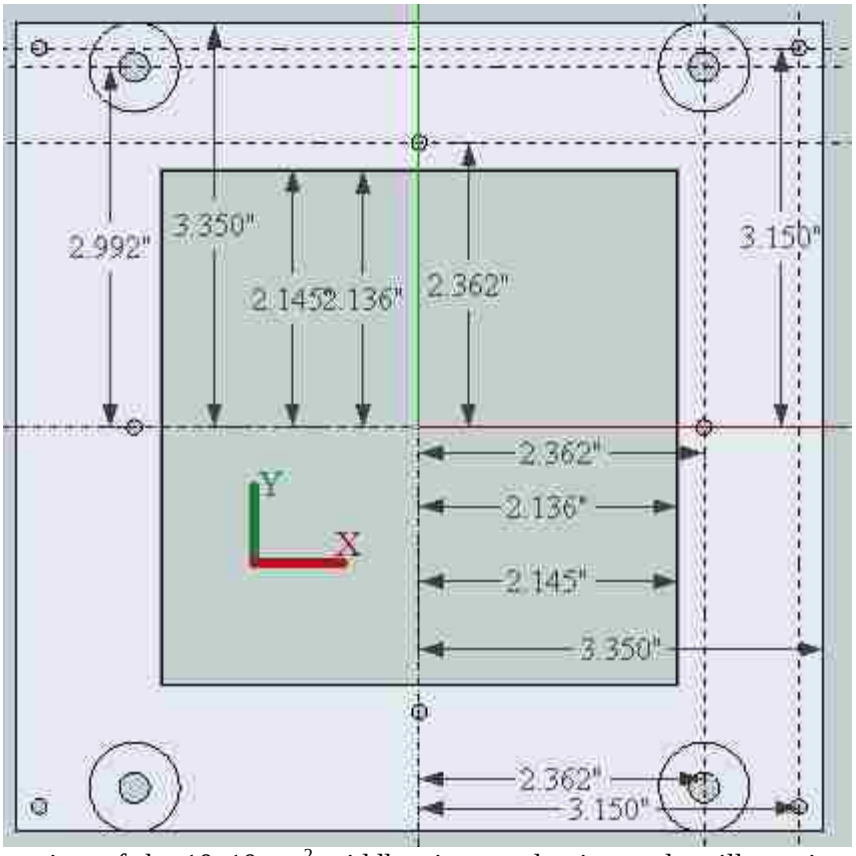

Figure E-31. Top view of the 10x10 cm^2 middle trimmer aluminum plate illustrating the in-plane and cross-plane dimensions. The middle trimmer is square, such that all non-hole dimensions are equal in the in-plane and cross-plane dimensions.

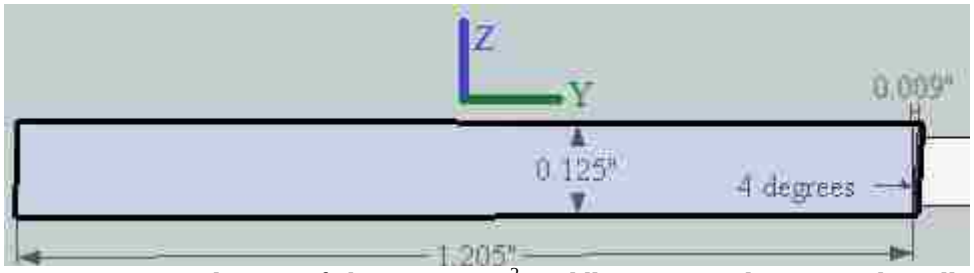

Figure E-32. Cross sectional view of the 10x10 cm^2 middle trimmer aluminum plate illustrating the thickness and lateral in-plane and cross-plane dimensions of the plate. The middle trimmer is square, such that all non-hole dimensions are equal in the in-plane and cross-plane dimensions.

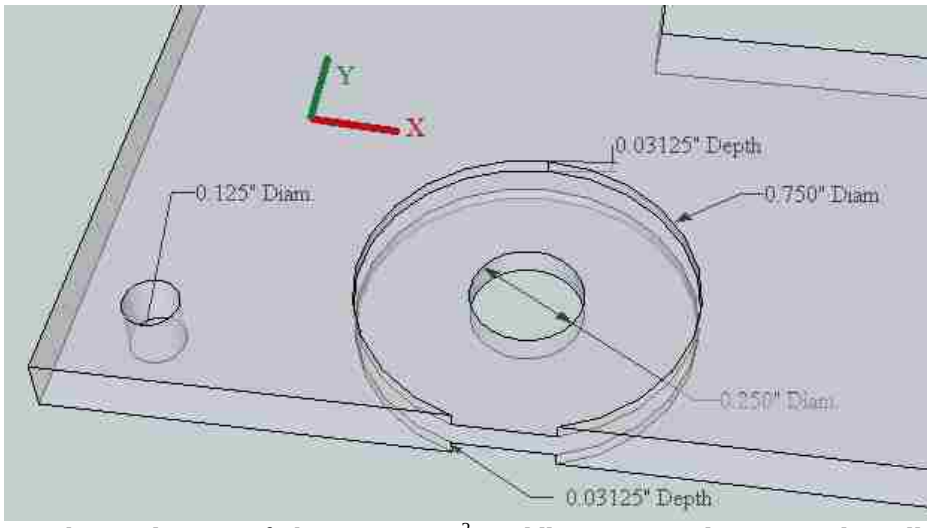

Figure E-33. Orthogonal view of the 10x10 cm^2 middle trimmer aluminum plate illustrating hole dimensions.

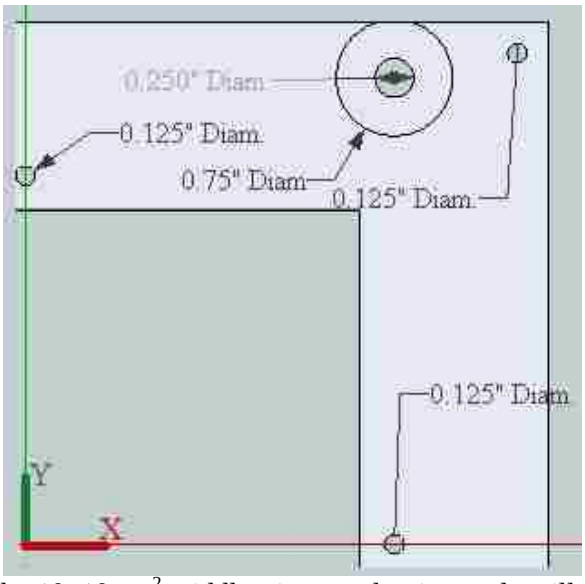

Figure E-34. Top view of the 10x10 cm^2 middle trimmer aluminum plate illustrating hole dimensions.

E.1.7. Lower Trimmer - Aluminum

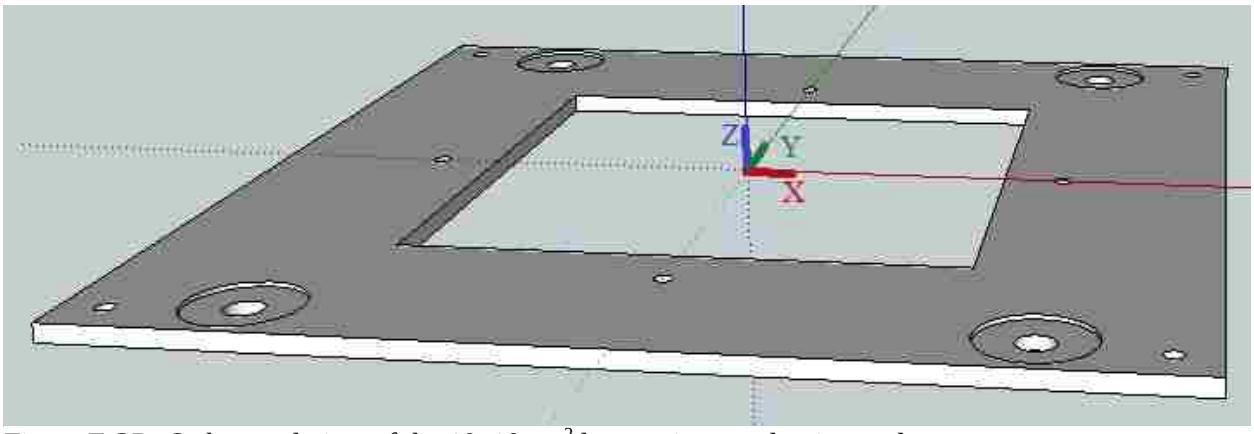

Figure E-35. Orthogonal view of the 10x10 cm^2 lower trimmer aluminum plate.

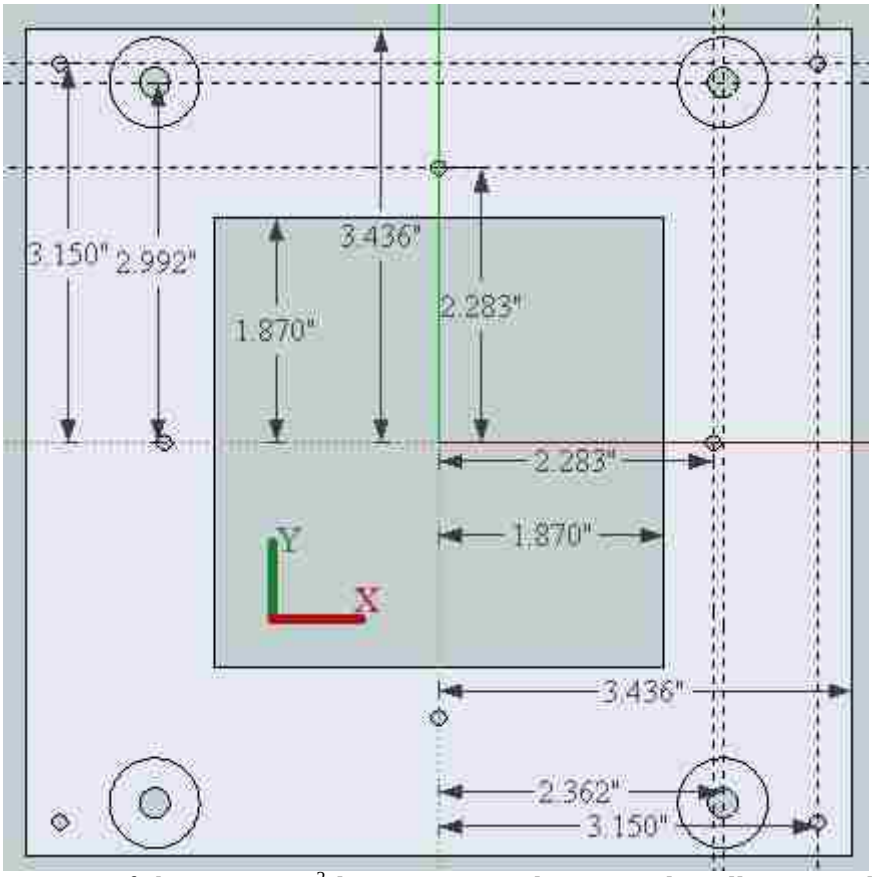

Figure E-36. Top view of the 10x10 cm^2 lower trimmer aluminum plate illustrating the in-plane and cross-plane dimensions. The lower trimmer is square, such that all non-hole dimensions are equal in the in-plane and cross-plane dimensions.

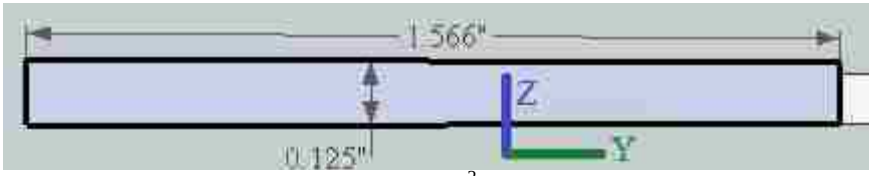

Figure E-37. Cross sectional view of the 10x10 cm^2 lower trimmer aluminum plate illustrating the thickness and lateral in-plane and cross-plane dimensions of the plate. The lower trimmer is square, such that all non-hole dimensions are equal in the in-plane and cross-plane dimensions.

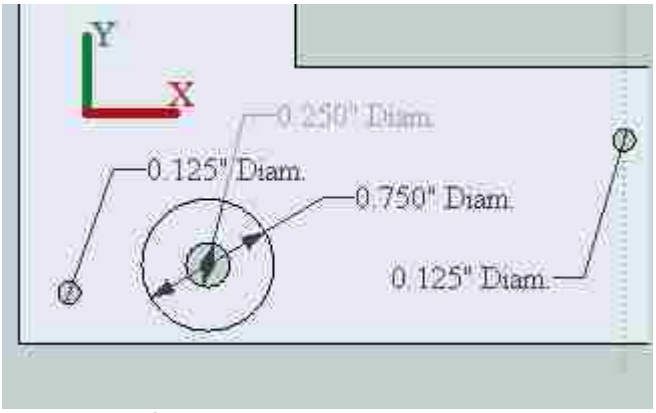

Figure E-38. Top view of the 10x10 cm^2 lower trimmer aluminum plate illustrating hole dimensions.

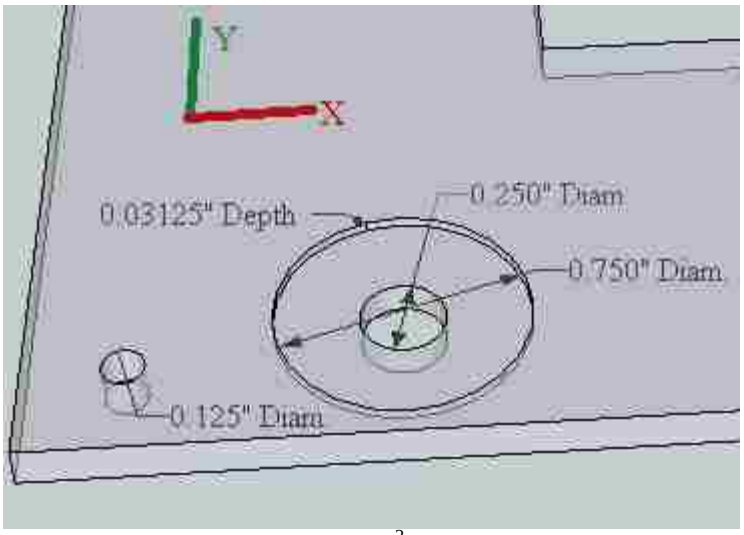

Figure E-39. Orthogonal view of the 10x10 cm^2 lower trimmer aluminum plate illustrating hole dimensions.

E.1.8. Aluminum Spacer Tubers

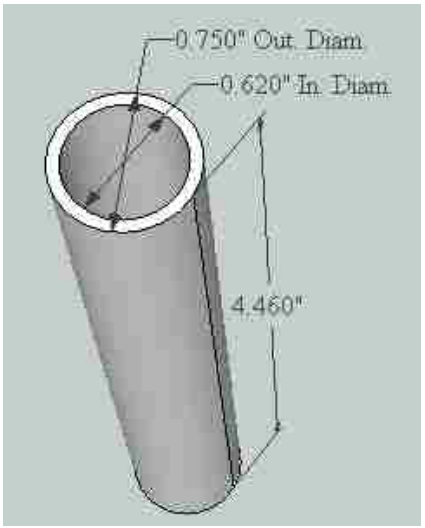

Figure E-40. Upper aluminum spacer tubes which connect the upper trimmer and the attachment plate. There are four upper aluminum spacer tubes per applicator.

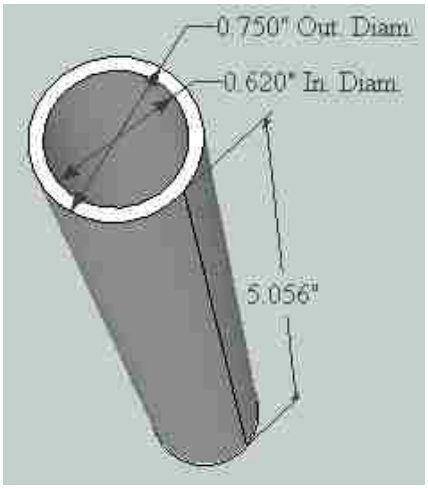

Figure E-41. Middle aluminum spacer tubes which connect the middle and upper trimmers. There are four middle aluminum spacer tubes per applicator.

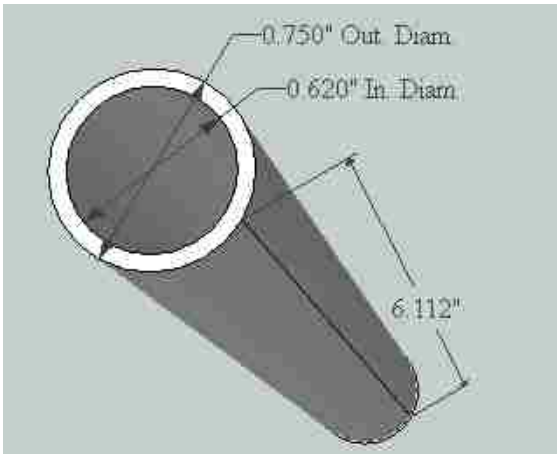

Figure E-42. Lower aluminum spacer tubes which connect the lower and middle trimmers. There are four lower aluminum spacer tubes per applicator.

E.2. 20x20 cm^2 Applicator

E.2.1. Full Applicator

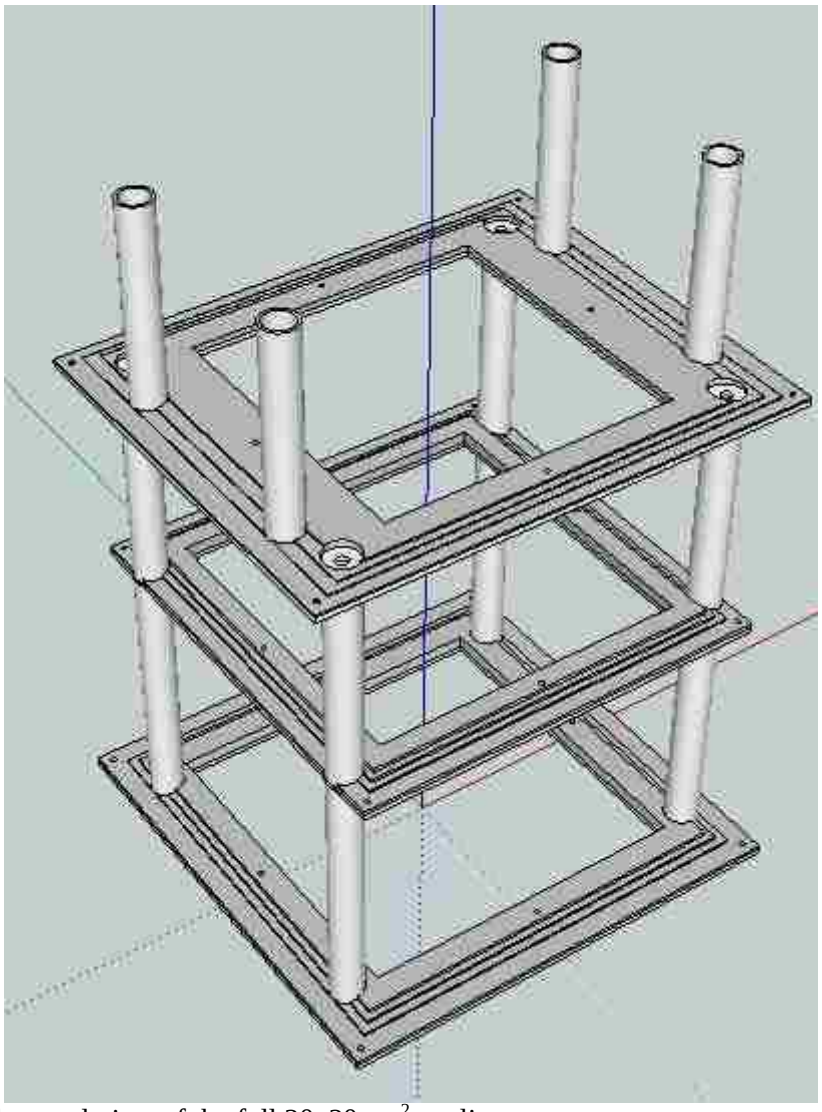

Figure E-43. Orthogonal view of the full 20x20 cm^2 applicator.

E.2.2. Upper Trimmer - Lead

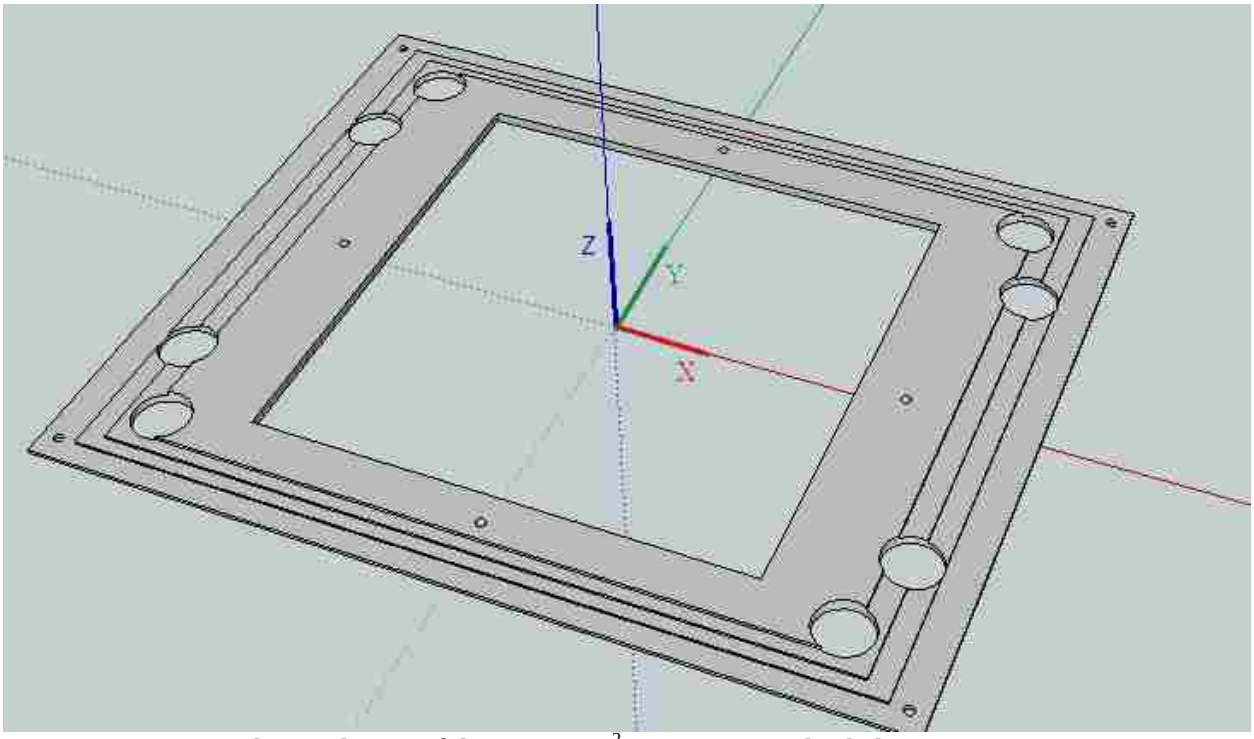

Figure E-44. Top orthogonal view of the 20x20 cm^2 upper trimmer lead plate.

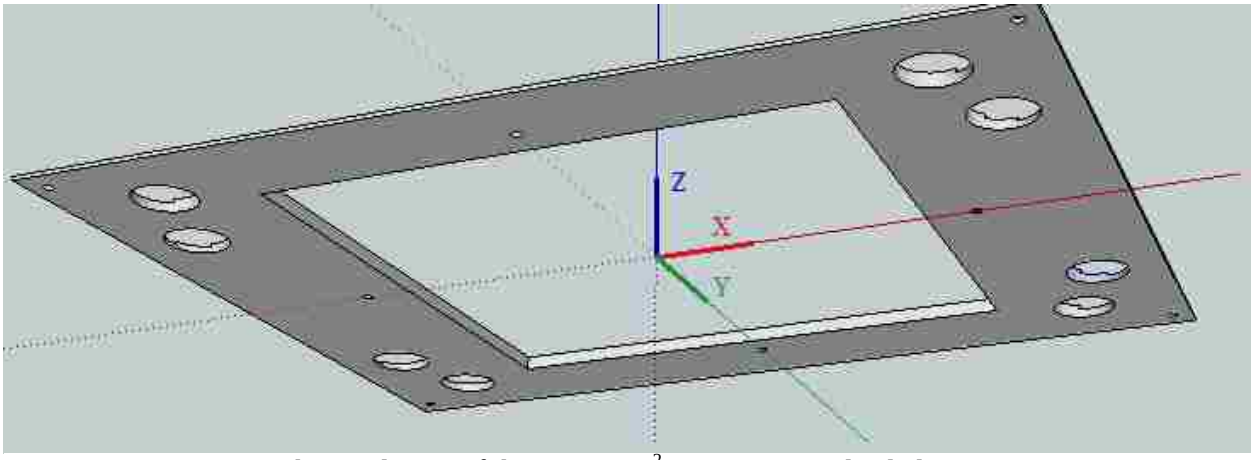

Figure E-45. Bottom orthogonal view of the 20x20 cm^2 upper trimmer lead plate.

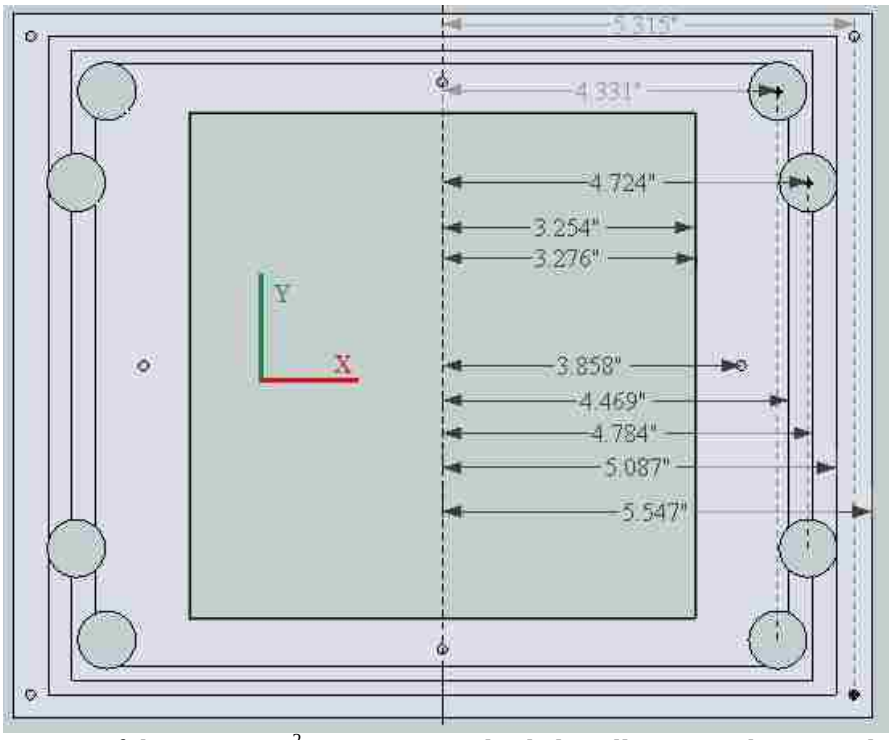

Figure E-46. Top view of the 20x20 cm^2 upper trimmer lead plate illustrating the cross-plane dimensions.

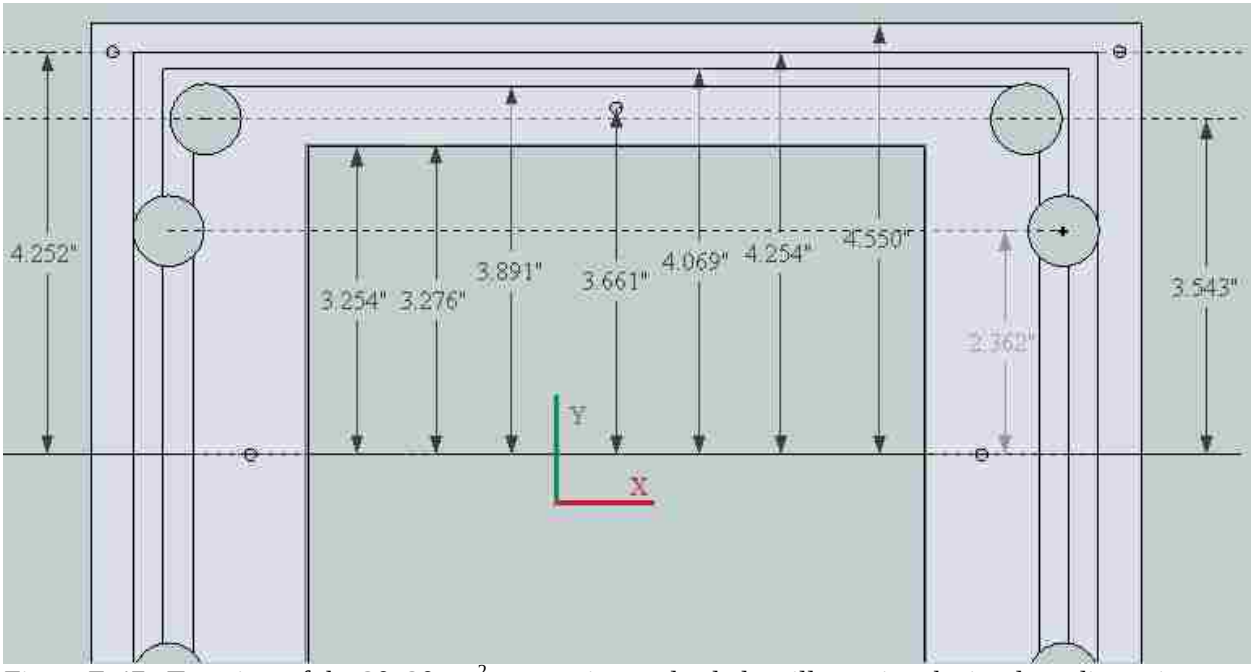

Figure E-47. Top view of the 20x20 cm^2 upper trimmer lead plate illustrating the in-plane dimensions.

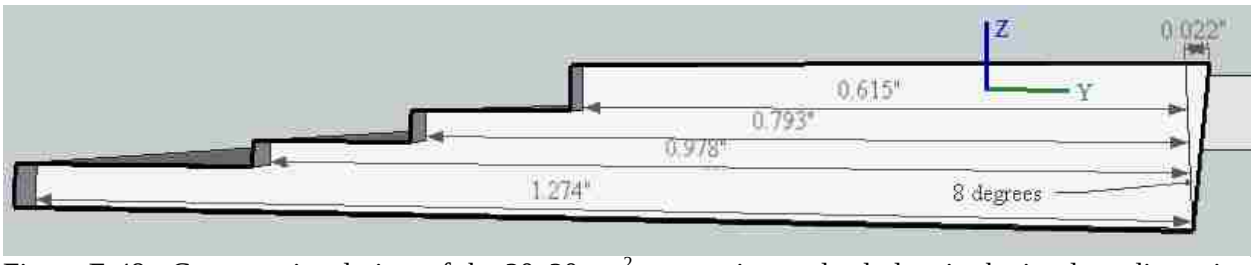

Figure E-48. Cross sectional view of the 20x20 cm^2 upper trimmer lead plate in the in-plane dimension illustrating the lateral dimensions of the plate.

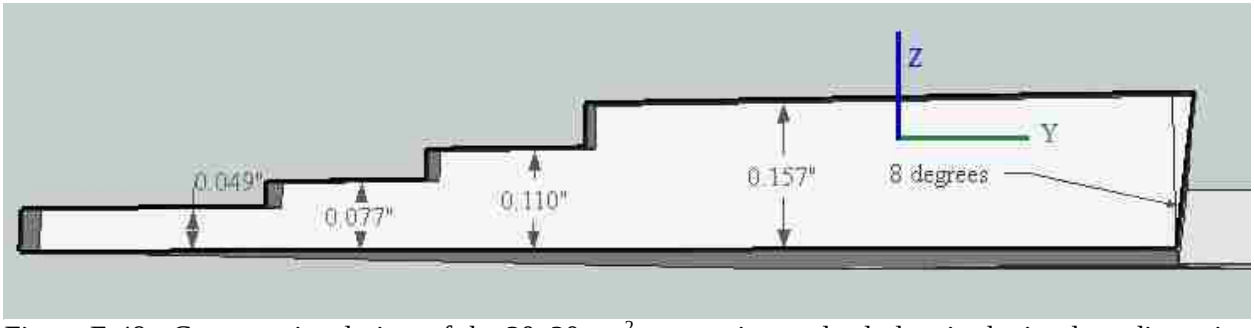

Figure E-49. Cross sectional view of the 20x20 cm^2 upper trimmer lead plate in the in-plane dimension illustrating the thickness values of the plate.

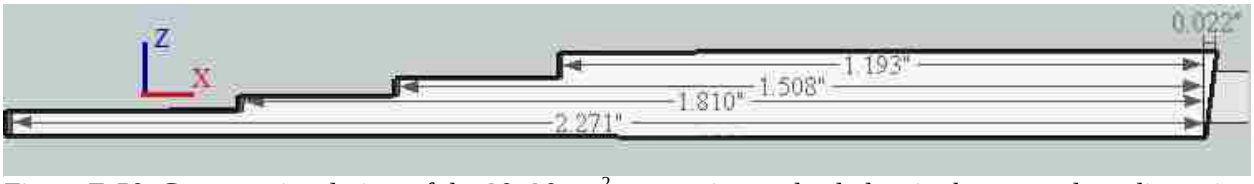

Figure E-50. Cross sectional view of the 20x20 cm^2 upper trimmer lead plate in the cross-plane dimension dimension illustrating the lateral dimensions of the plate.

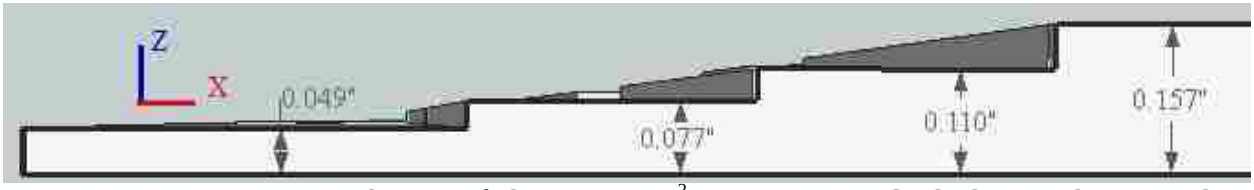

Figure E-51. Cross sectional view of the 20x20 cm^2 upper trimmer lead plate in the cross-plane dimension illustrating the thickness values of the plate.

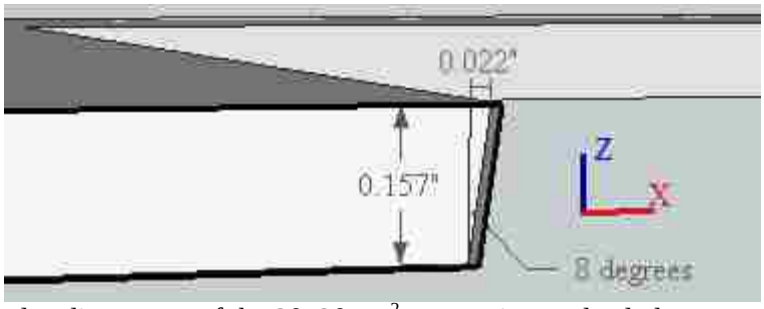

Figure E-52. Inner edge divergence of the 20x20 cm^2 upper trimmer lead plate.

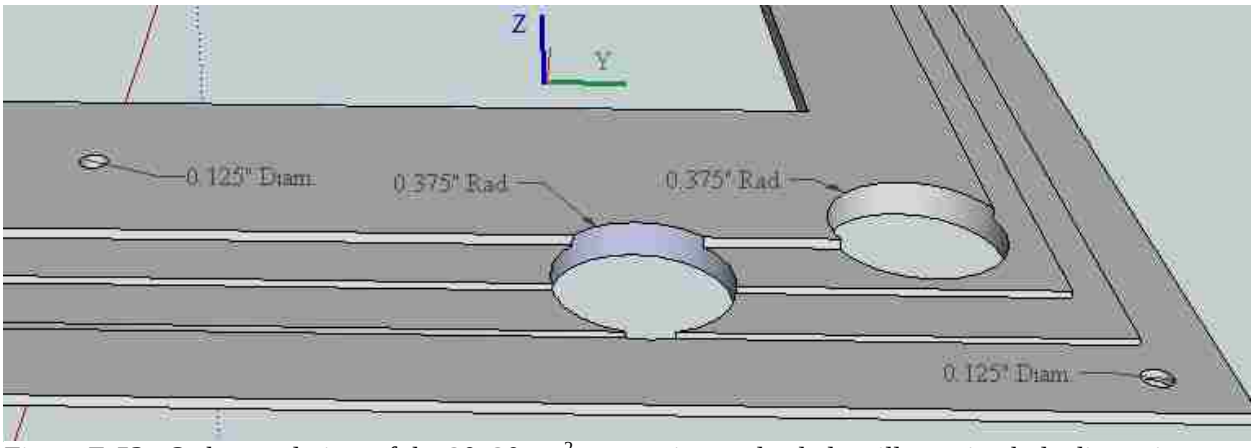

Figure E-53. Orthogonal view of the 20x20 cm^2 upper trimmer lead plate illustrating hole dimensions.

E.2.3. Middle Trimmer - Lead

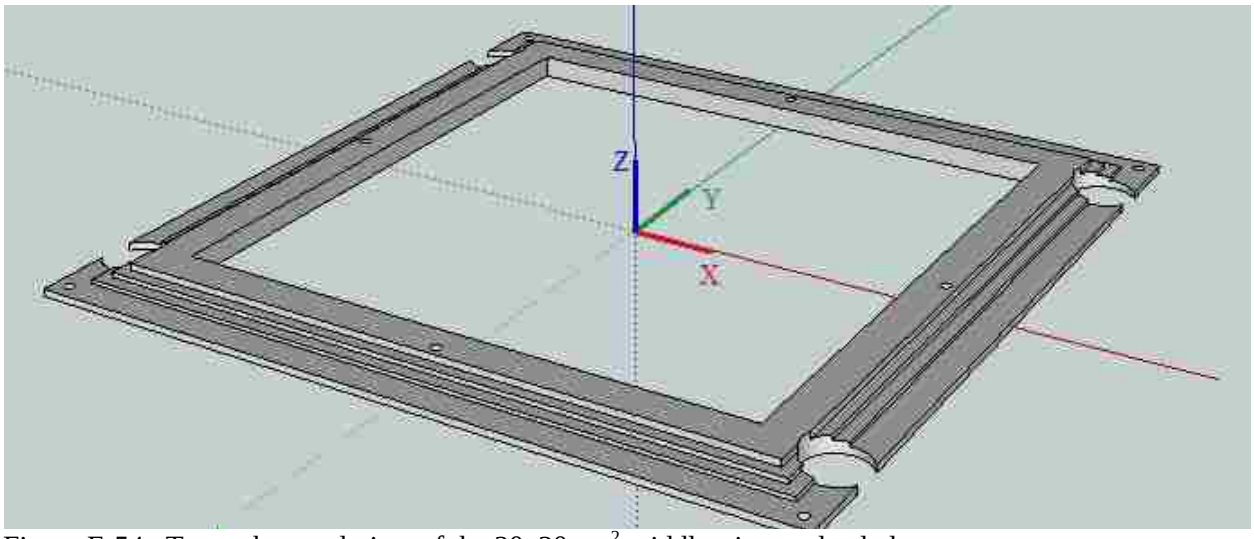

Figure E-54. Top orthogonal view of the 20x20 cm^2 middle trimmer lead plate.

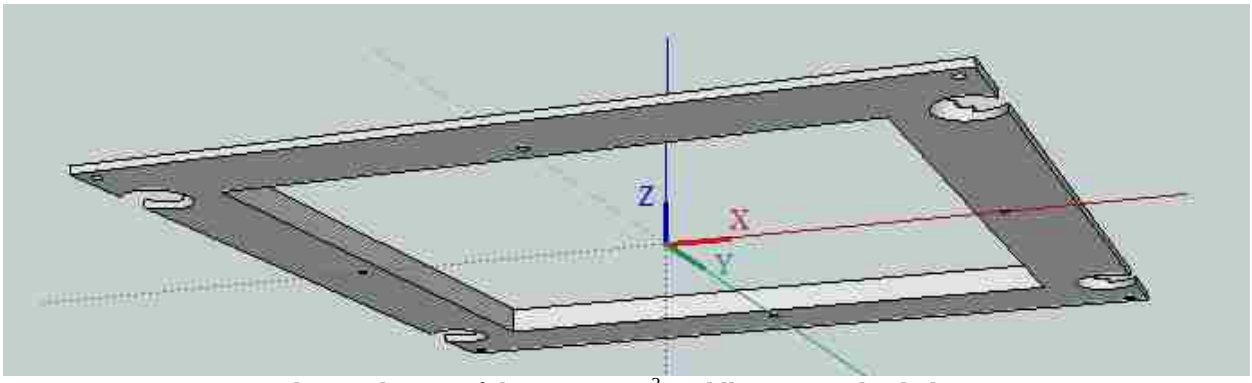

Figure E-55. Bottom orthogonal view of the 20x20 cm^2 middle trimmer lead plate.

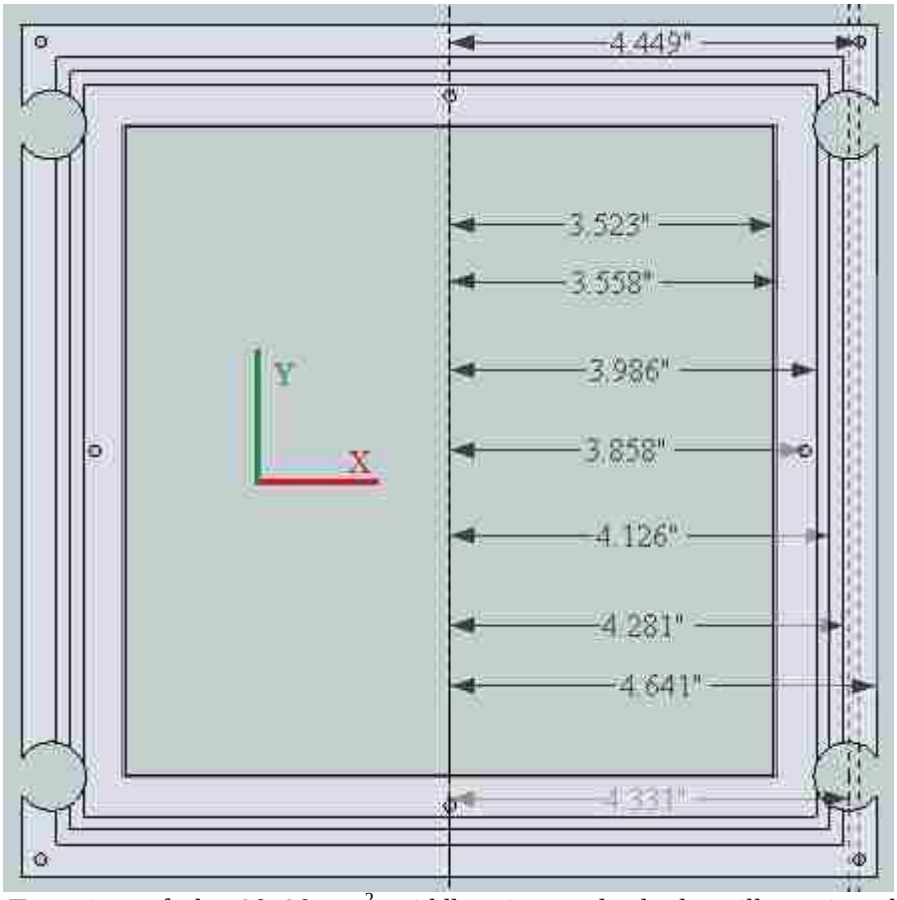

Figure E-56. Top view of the 20x20 cm^2 middle trimmer lead plate illustrating the cross-plane dimension. The middle trimmer is square, such that all non-hole dimensions are equal in the in-plane and cross-plane dimensions.

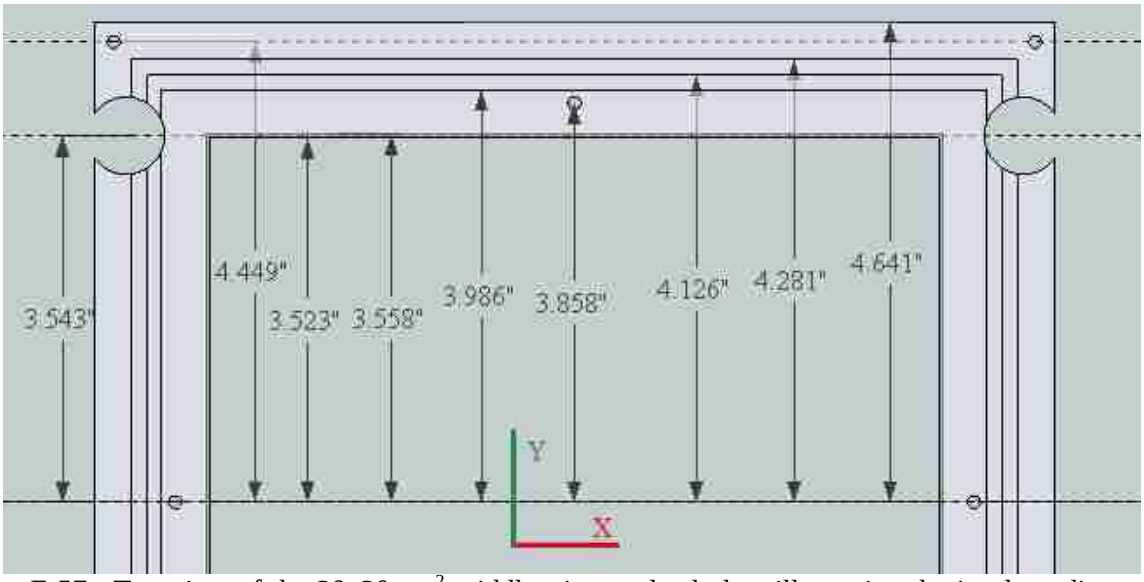

Figure E-57. Top view of the 20x20 cm^2 middle trimmer lead plate illustrating the in-plane dimension. The middle trimmer is square, such that all non-hole dimensions are equal in the in-plane and cross-plane dimensions.

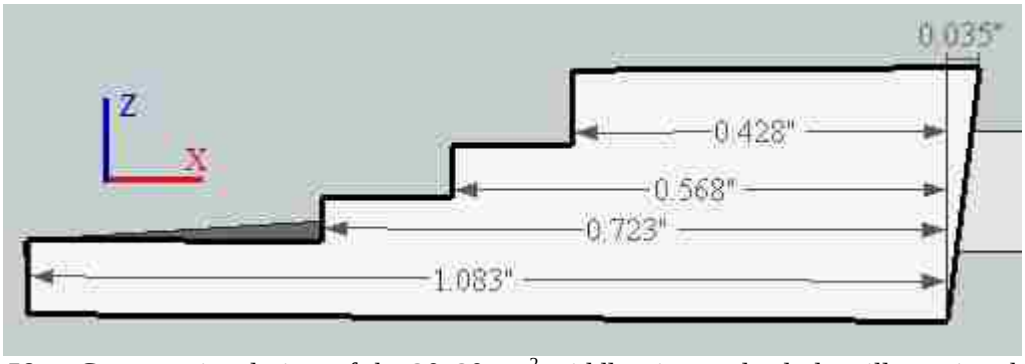

Figure E-58. . Cross sectional view of the 20x20 cm^2 middle trimmer lead plate illustrating the in-plane and cross-plane lateral dimensions of the plate. The middle trimmer is square, such that all non-hole dimensions are equal in the in-plane and cross-plane dimensions.

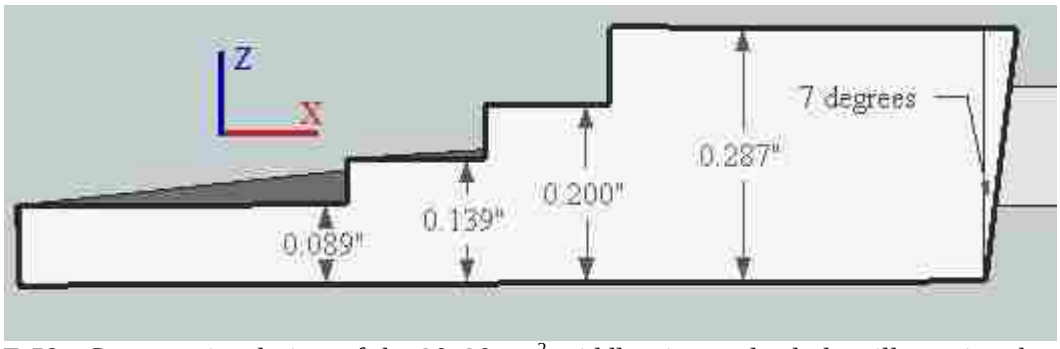

Figure E-59. Cross sectional view of the 20x20 cm^2 middle trimmer lead plate illustrating the thickness values of the plate. The middle trimmer is square, such that all non-hole dimensions are equal in the in-plane and cross-plane dimensions.

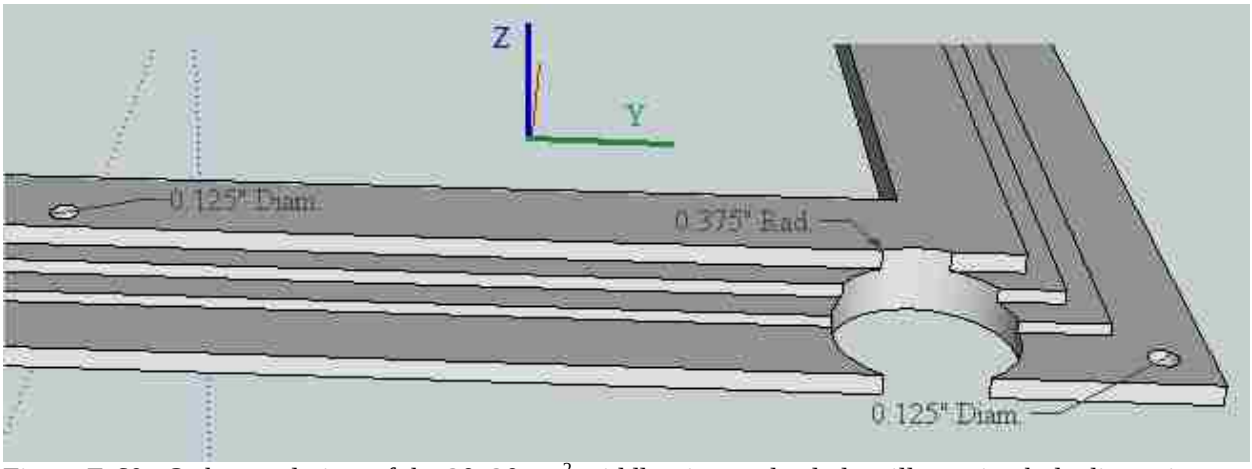

Figure E-60. Orthogonal view of the 20x20 cm^2 middle trimmer lead plate illustrating hole dimensions.

E.2.4. Lower Trimmer - Lead

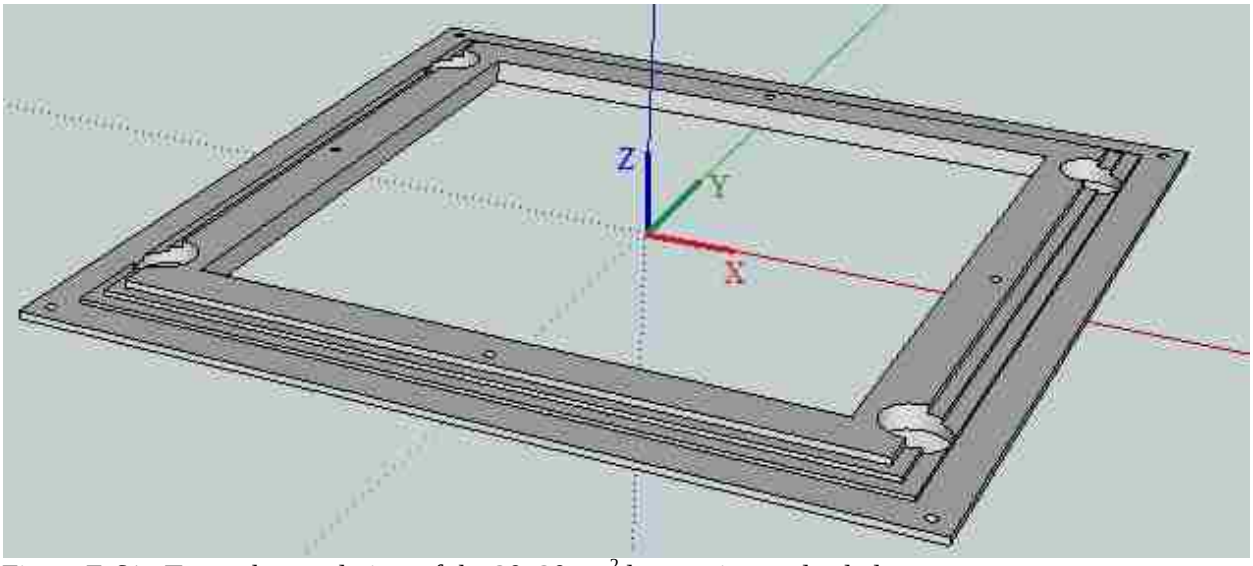

Figure E-61. Top orthogonal view of the 20x20 cm^2 lower trimmer lead plate.

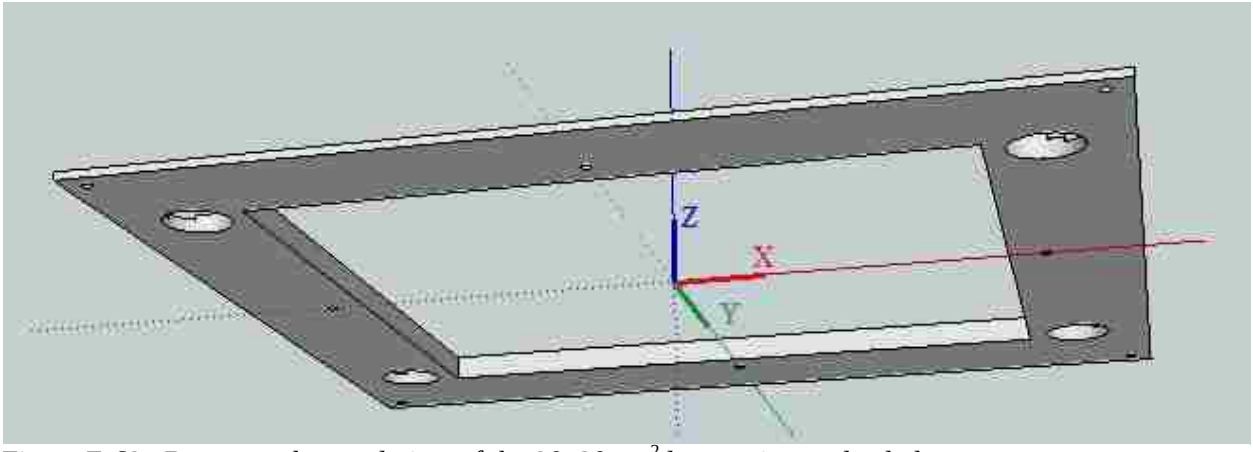

Figure E-62. Bottom orthogonal view of the 20x20 cm^2 lower trimmer lead plate.

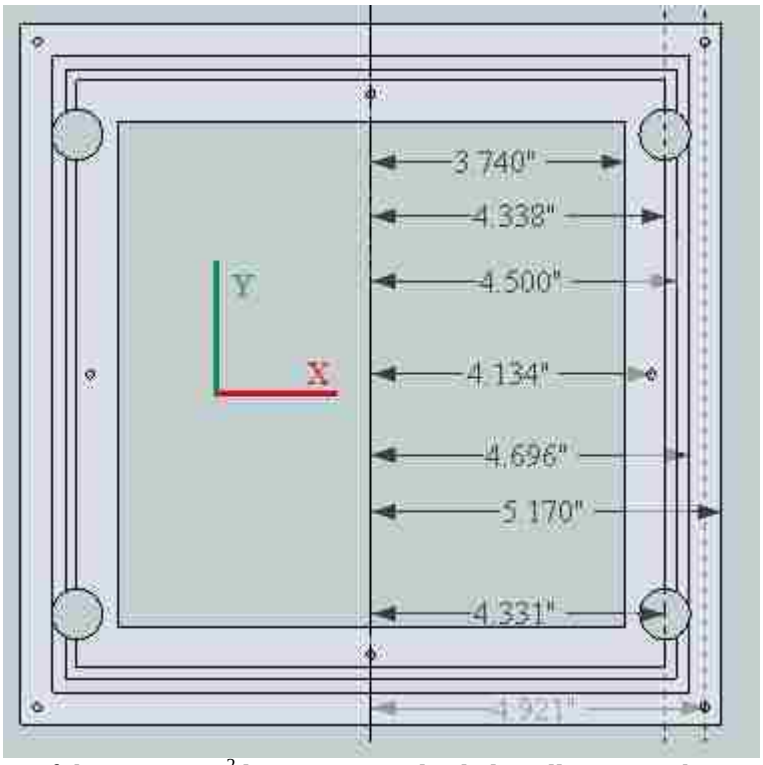

Figure E-63. Top view of the 20x20 cm^2 lower trimmer lead plate illustrating the cross-plane dimensions. The lower trimmer is square, such that all non-hole dimensions are equal in the in-plane and cross-plane dimensions.

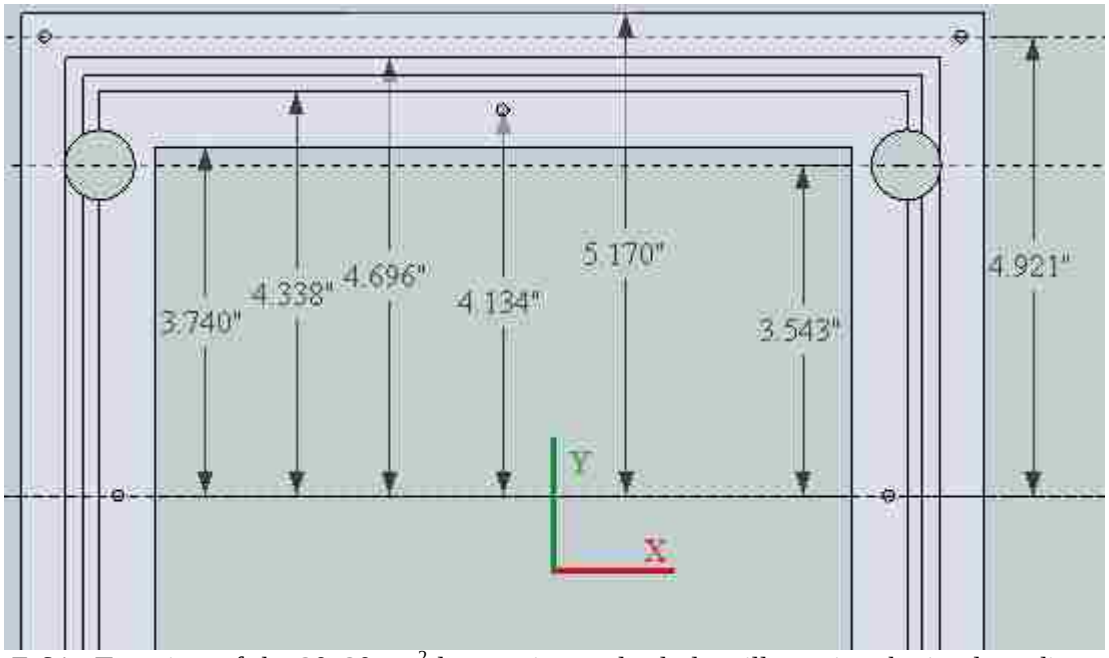

Figure E-64. Top view of the 20x20 cm^2 lower trimmer lead plate illustrating the in-plane dimensions. The lower trimmer is square, such that all non-hole dimensions are equal in the in-plane and cross-plane dimensions.

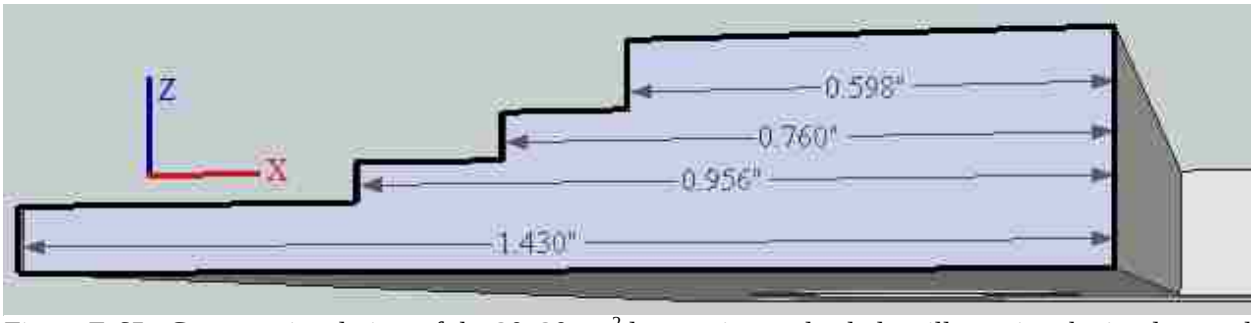

Figure E-65. Cross sectional view of the 20x20 cm^2 lower trimmer lead plate illustrating the in-plane and cross-plane lateral dimensions of the plate. The lower trimmer is square, such that all non-hole dimensions are equal in the in-plane and cross-plane dimensions.

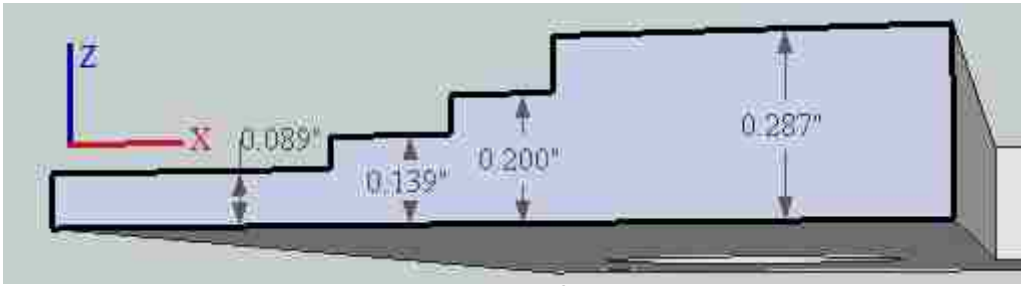

Figure E-66. Cross sectional view of the 20x20 cm^2 lower trimmer lead plate in the cross-plane dimension illustrating the thickness values of the plate. The lower trimmer is square, such that all non-hole dimensions are equal in the in-plane and cross-plane dimensions.

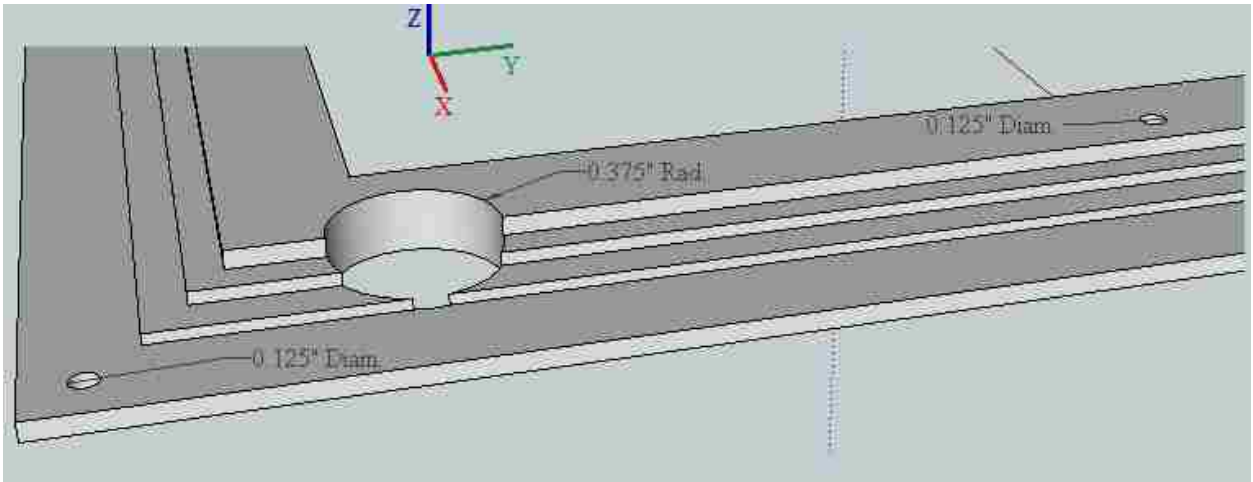

Figure E-67. Orthogonal view of the 20x20 cm^2 lower trimmer lead plate illustrating hole dimensions.

E.2.5. Upper Trimmer - Aluminum

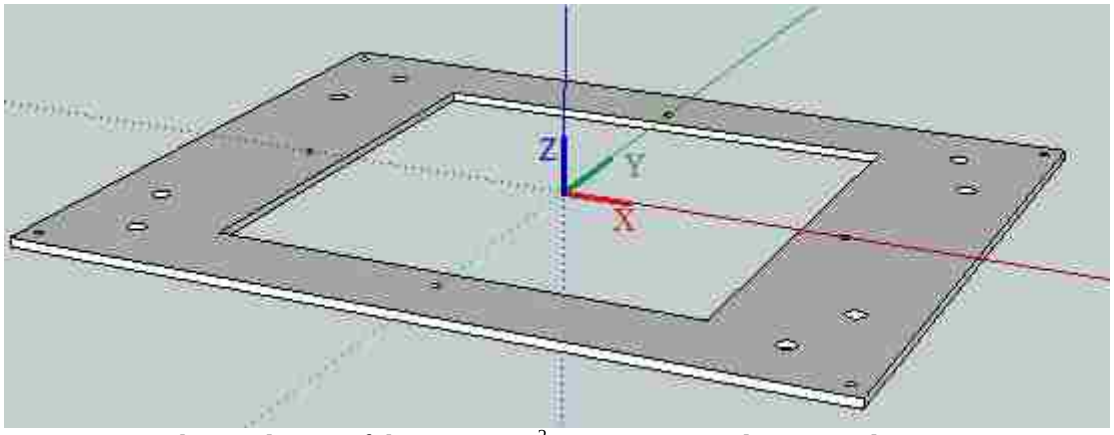

Figure E-68. Top orthogonal view of the 20x20 cm^2 upper trimmer aluminum plate.

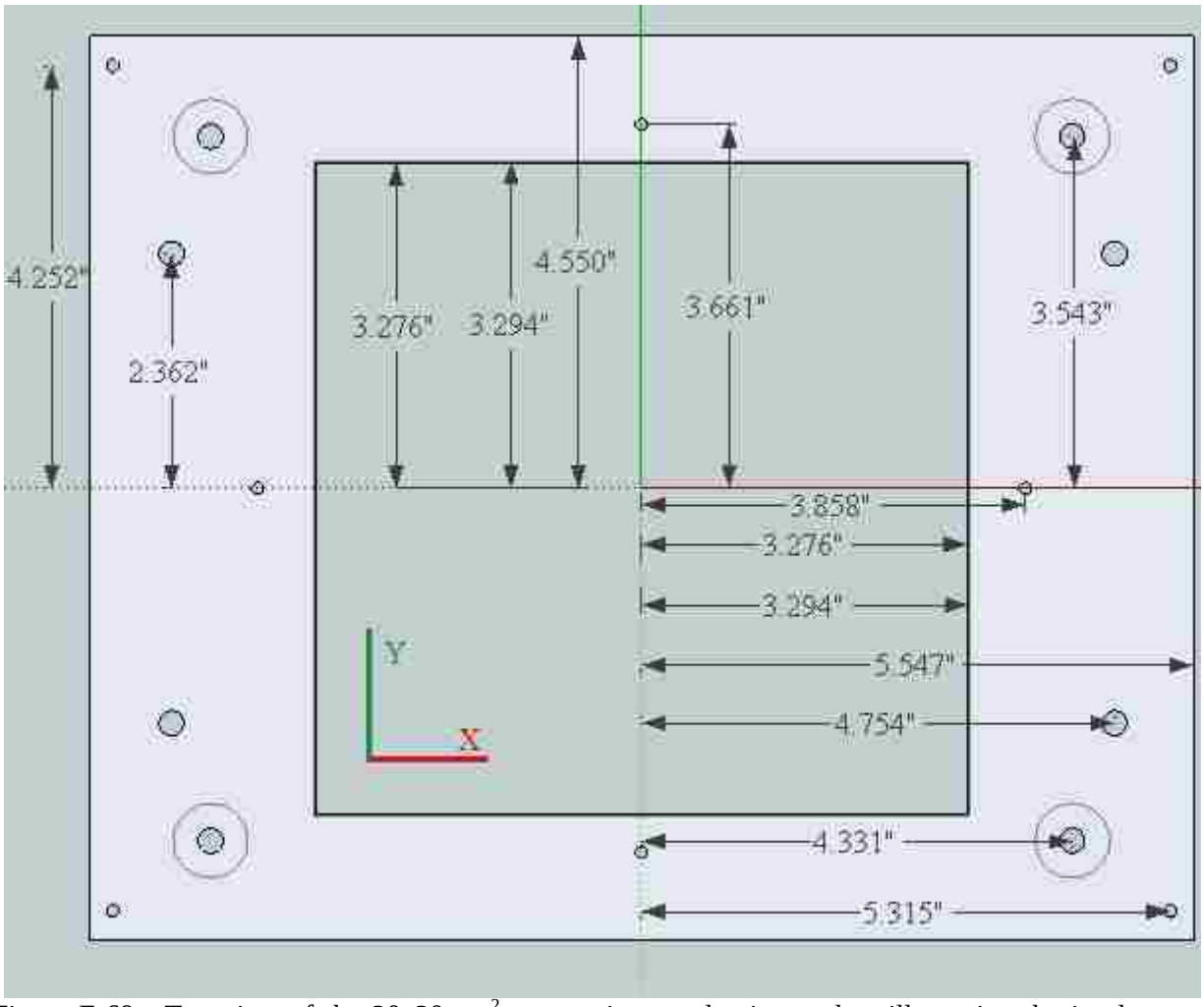

Figure E-69. Top view of the 20x20 cm^2 upper trimmer aluminum plate illustrating the in-plane and cross-plane dimensions.

Figure E-70. Cross sectional view of the 20x20 cm^2 upper trimmer aluminum plate in the cross-plane dimension illustrating the thickness and lateral dimensions of the plate.

Figure E-71. Cross sectional view of the 20x20 cm^2 upper trimmer aluminum plate in the in-plane dimension illustrating the thickness and lateral dimensions of the plate.

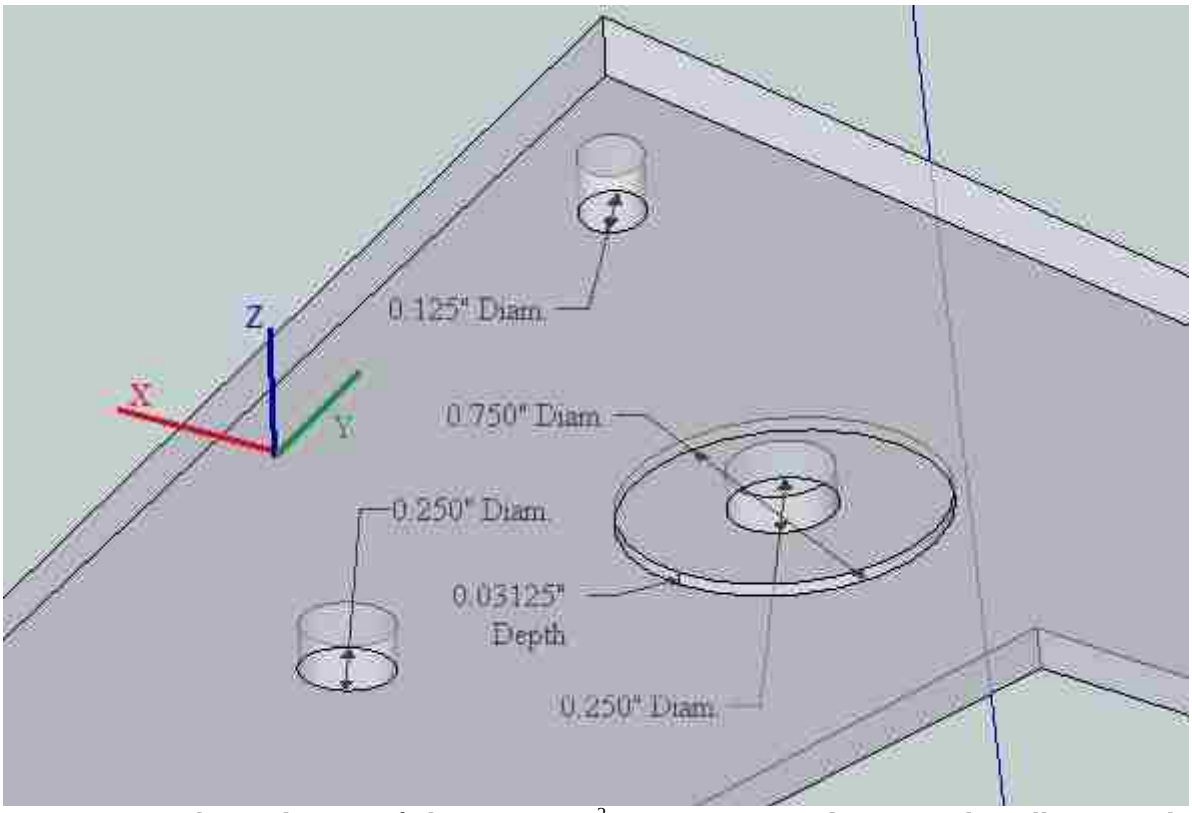

Figure E-72. Orthogonal view of the 20x20 cm^2 upper trimmer aluminum plate illustrating hole dimensions.

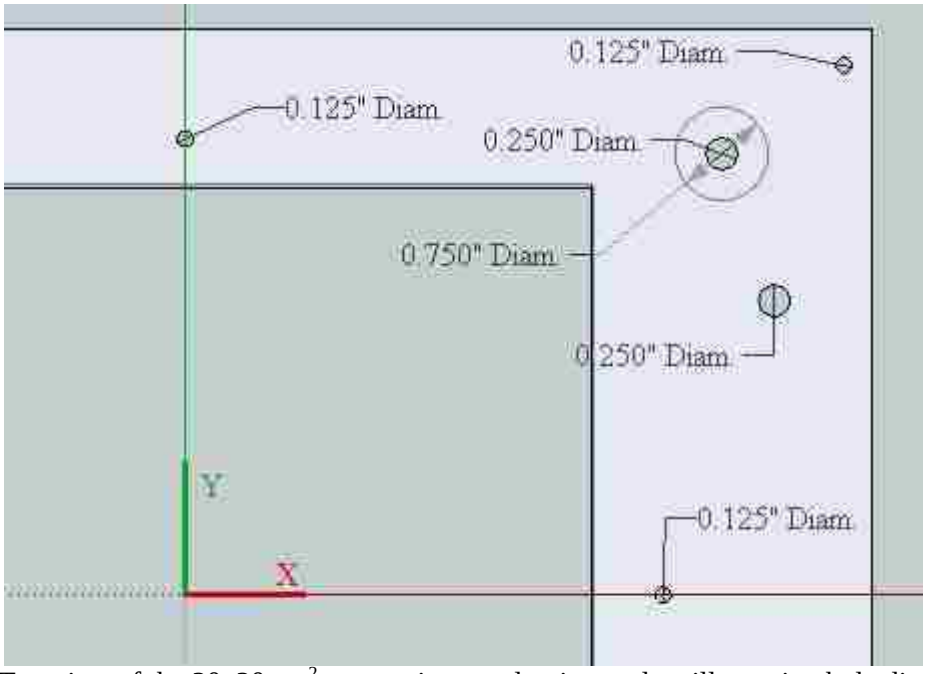

Figure E-73. Top view of the 20x20 cm^2 upper trimmer aluminum plate illustrating hole dimensions.

E.2.6. Middle Trimmer - Aluminum

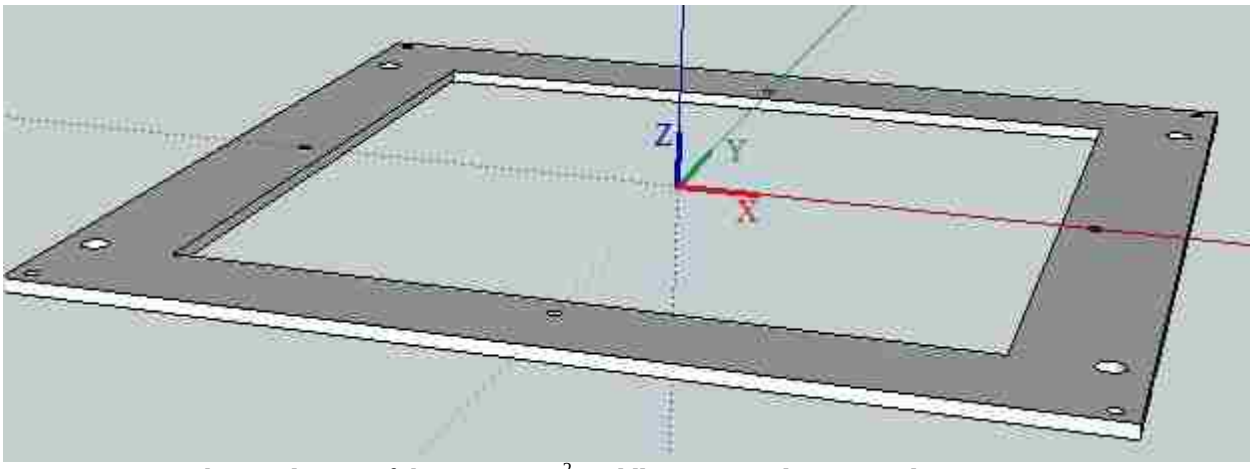

Figure E-74. Orthogonal view of the 20x20 cm^2 middle trimmer aluminum plate.

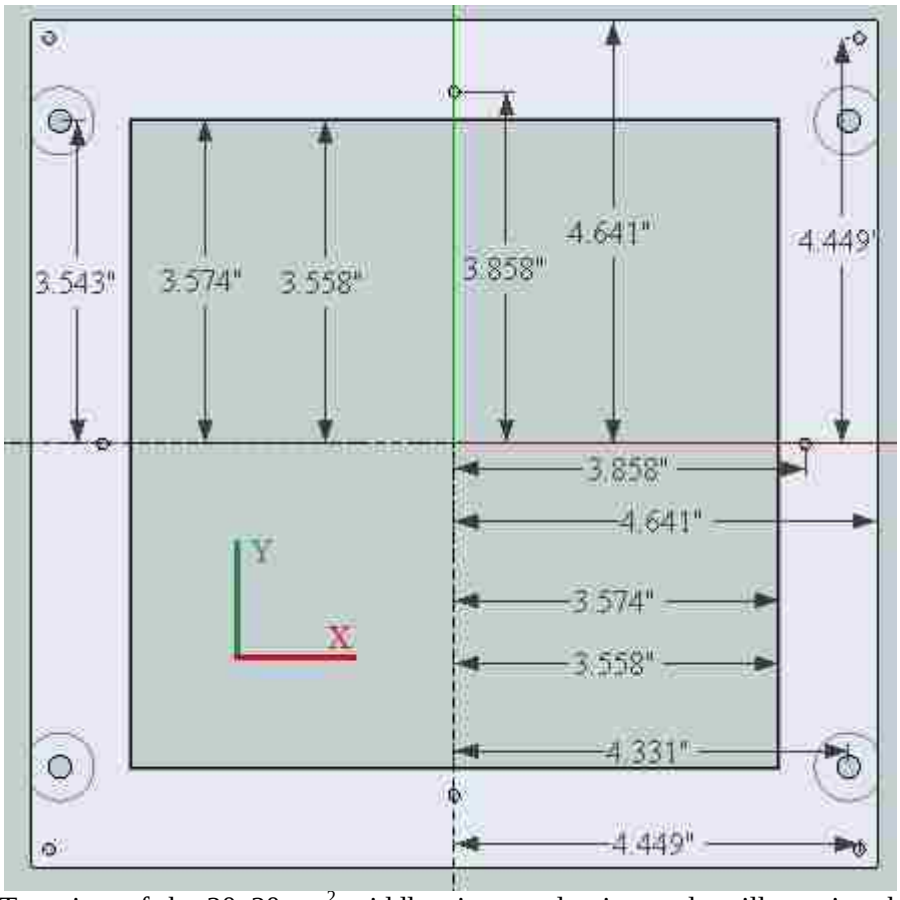

Figure E-75. Top view of the 20x20 cm^2 middle trimmer aluminum plate illustrating the in-plane and cross-plane dimensions. The middle trimmer is square, such that all non-hole dimensions are equal in the in-plane and cross-plane dimensions.

Figure E-76. Cross sectional view of the 20x20 cm^2 middle trimmer aluminum plate illustrating the thickness and lateral in-plane and cross-plane dimensions of the plate. The middle trimmer is square, such that all non-hole dimensions are equal in the in-plane and cross-plane dimensions.

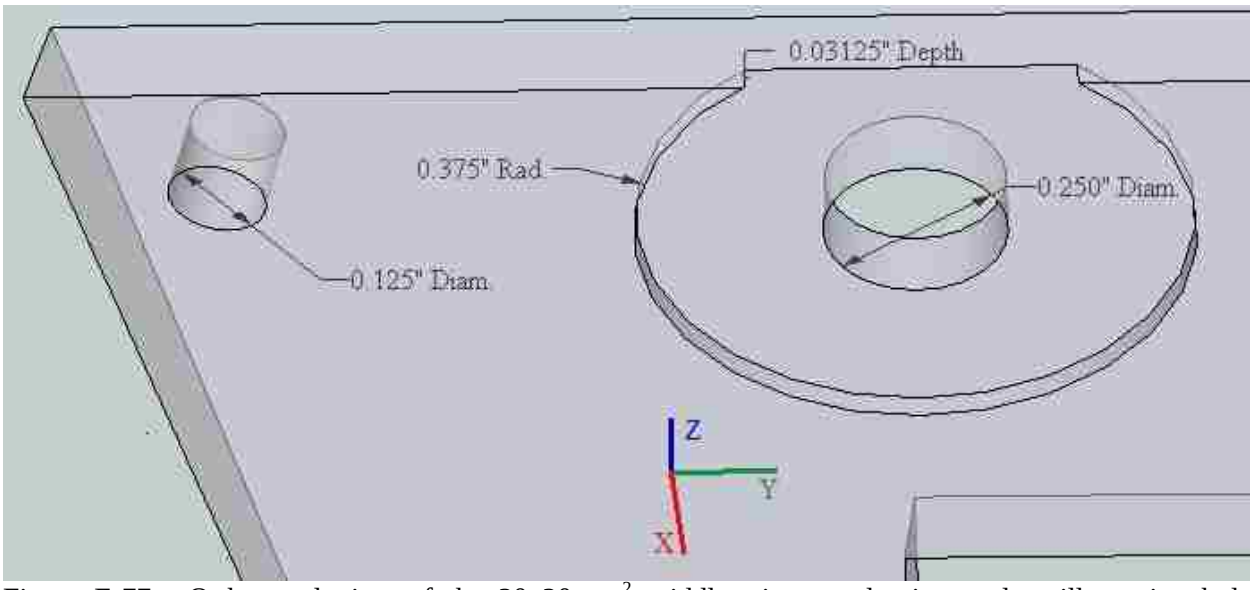

Figure E-77. Orthogonal view of the 20x20 cm^2 middle trimmer aluminum plate illustrating hole dimensions.

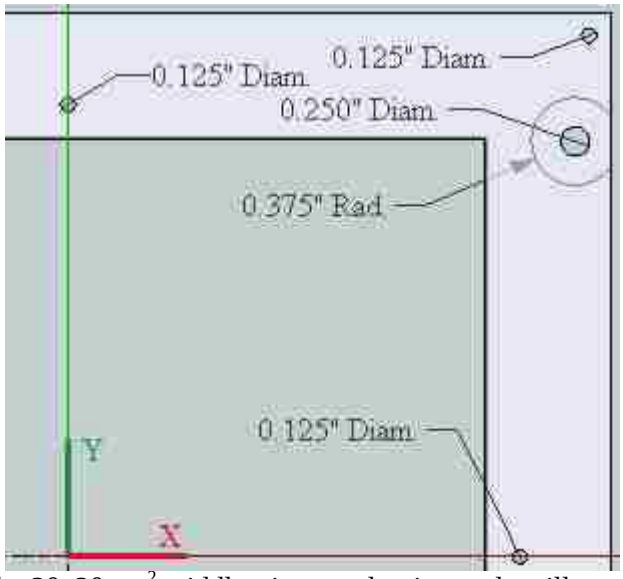

Figure E-78. Top view of the 20x20 cm^2 middle trimmer aluminum plate illustrating hole dimensions.

E.2.7. Lower Trimmer - Aluminum

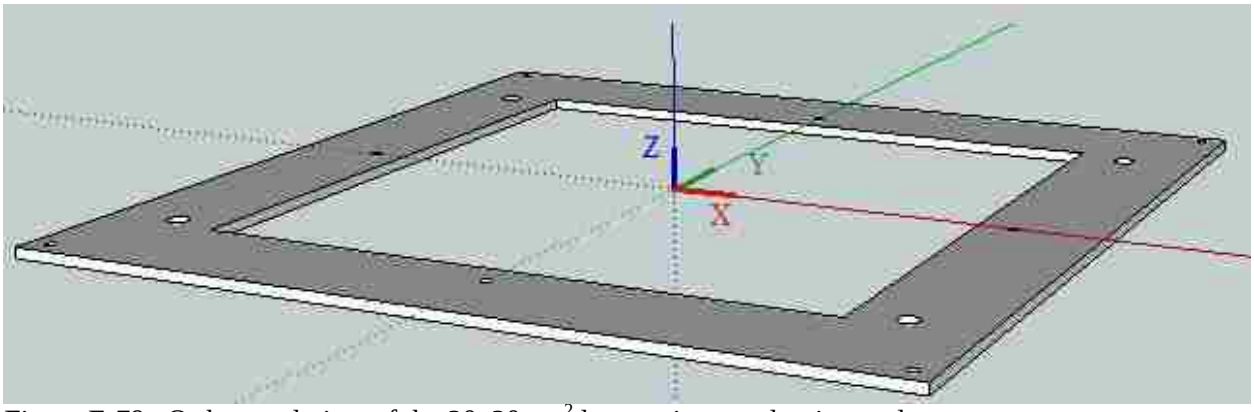

Figure E-79. Orthogonal view of the 20x20 cm^2 lower trimmer aluminum plate.

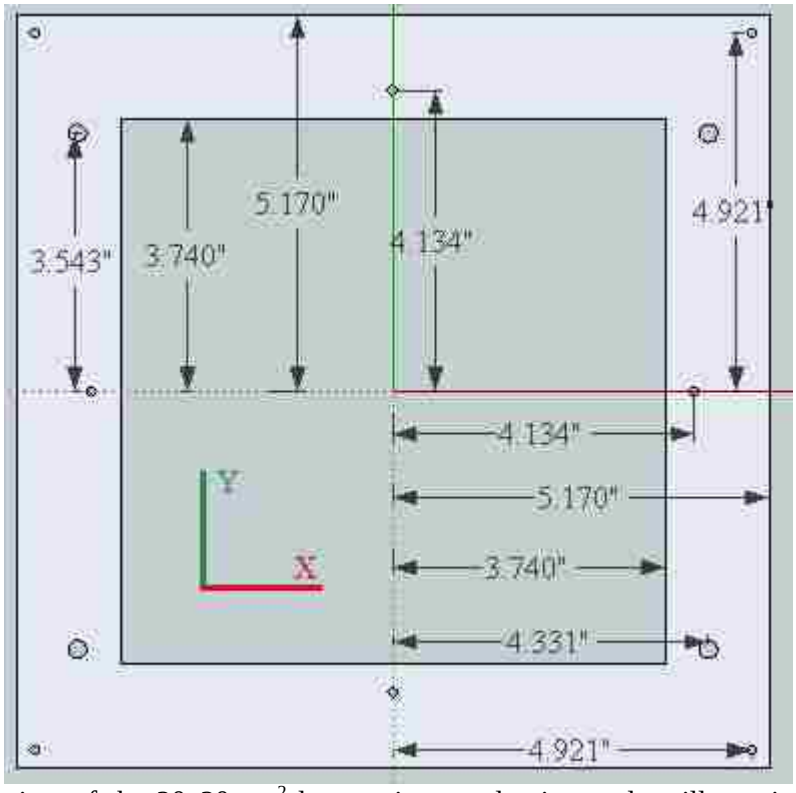

Figure E-80. Top view of the 20x20 cm^2 lower trimmer aluminum plate illustrating the in-plane and cross-plane dimensions. The lower trimmer is square, such that all non-hole dimensions are equal in the in-plane and cross-plane dimensions.

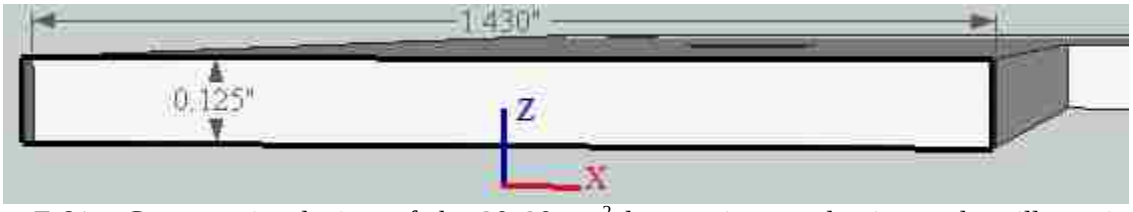

Figure E-81. Cross sectional view of the 20x20 cm^2 lower trimmer aluminum plate illustrating the thickness and lateral in-plane and cross-plane dimensions of the plate. The lower trimmer is square, such that all non-hole dimensions are equal in the in-plane and cross-plane dimensions.

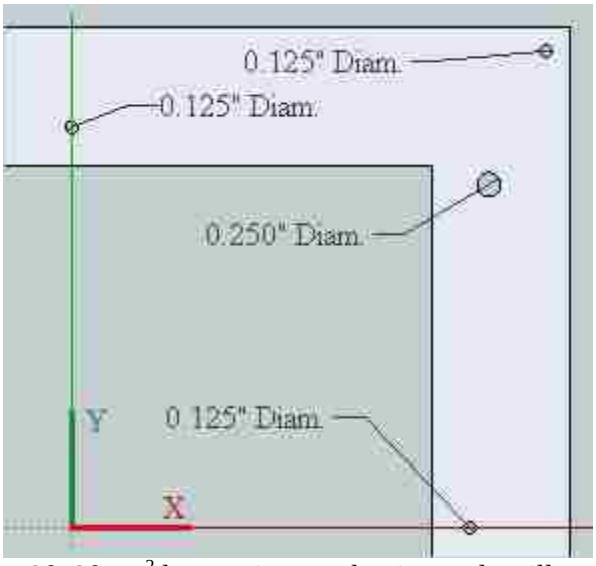

Figure E-82. Top view of the 20x20 cm^2 lower trimmer aluminum plate illustrating hole dimensions.

E.2.8. Aluminum Spacer Tubers

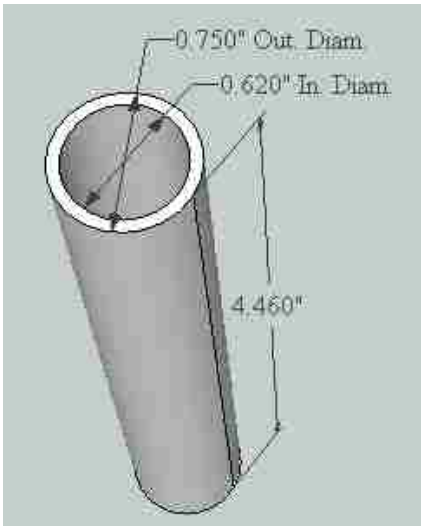

Figure E-83. Upper aluminum spacer tubes which connect the upper trimmer and the attachment plate. There are four upper aluminum spacer tubes per applicator.

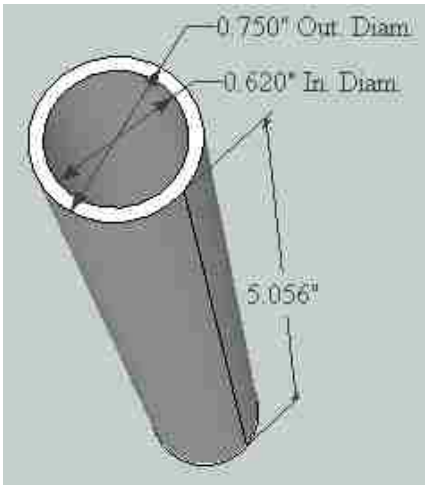

Figure E-84. Middle aluminum spacer tubes which connect the middle and upper trimmers. There are four middle aluminum spacer tubes per applicator.

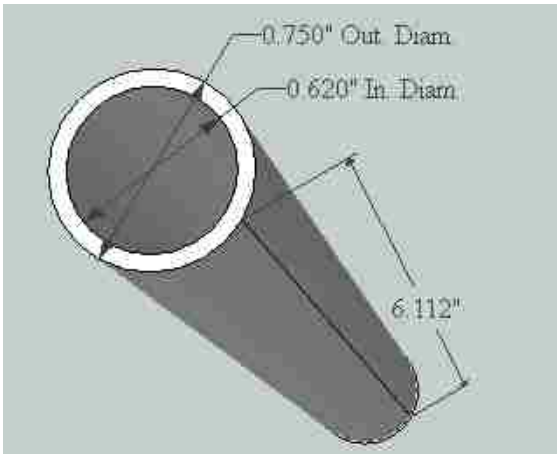

Figure E-85. Lower aluminum spacer tubes which connect the lower and middle trimmers. There are four lower aluminum spacer tubes per applicator.

Vita

Garrett Pitcher was born in Baton Rouge, LA and raised in Franklin, TN. He attended the University of Tennessee, Knoxville, where he received his Bachelor of Science in Nuclear Engineering. During this time, he discovered an interest in medical physics and began interning at Thompson Cancer Survival Center in Knoxville under the guidance of Dr. Chet Ramsey. He went on to complete his Master of Science degree in Nuclear Engineering, concentrating in medical physics. Garrett moved on to Baton Rouge where he majored in Medical Physics at LSU and began studying electron transport and electron collimation design theory under Dr. Ken Hogstrom during his first semester. Garrett plans to receive his Doctor of Philosophy in Medical Physics from LSU in the fall of 2015 and begin the Medical Physics Residency program at UF Health Cancer Center in Orlando, Florida.